



The
University
Of
Sheffield.

The Role of Carbon in the Catalytic Isomerisation-Cracking of *n*-Alkanes

By:

Amal Khalid Shehab

A thesis submitted in partial fulfilment of the requirements for the
degree of Doctor of Philosophy

The University of Sheffield
Faculty of Engineering
Department of Chemical and Biological Engineering

February 2018

Acknowledgments

First, I would like to express my sincere thanks and deep gratitude to my supervisor Dr. James McGregor for his valuable guidance, continuous support and assistance throughout this PhD project.

I am very grateful to Dr. Denis Cumming for providing access to the adsorption instrument, also I would like to thank Danlami Mustapha (Department of Chemistry/University of Glasgow), Alex James, Daniel Jackson and Neil Bramall (Department of Chemistry/University of Sheffield), and Ali Al-Shathr (Department of Chemical and Biological Engineering/University of Sheffield) for their contribution to this research.

I would like to acknowledge the assistant of the technical staff of the Department of Chemical and Biological Engineering, especially to Adrian Lumby, Andy Patrick, Mark McIntosh, Usman Younis, Oz McFarlane, James Grinham, Mark Jones, Duncan Schofield, and Keith Penny. Also, I would like to thank my colleagues of the Catalysis Group for their assistance and encouragement.

Finally, I would like to express my special thanks and sincerest gratitude to my family for their endless support and meaningful encouragements throughout my PhD study.

Abstract

The isomerisation-cracking of *n*-alkanes is one of the important processes in the refining and petrochemical industries. It is considered as a sustainable process where low value hydrocarbons are upgraded into value added products. Zeolites, and metal modified zeolites, are widely utilised as solid acid catalysts in such reactions, with metals such as platinum providing the functionality to effectively dissociate hydrogen. Catalyst deactivation by coke formation is however a crucial concern associated with hydrocarbon transformations over such catalysts. Nevertheless, recent studies have shown that these carbonaceous deposits, in addition to being implicated in catalyst deactivation, may have a beneficial or an active role in enhancing the catalytic performance. The main focus of this thesis is to understand the role of coke in the catalytic isomerisation-cracking of *n*-alkanes and to explore how a controlled pre-coking treatment can be used to enhance catalytic performance. Specifically, this thesis investigates the role of carbonaceous deposits in the isomerisation-cracking of *n*-pentane and *n*-hexadecane over the metal modified zeolite Pt/H-Beta.

Carbon laid down during *n*-pentane isomerisation over Pt/H-Beta is shown to as a catalytically beneficial species by control coking reactions and enhancing the selectivity to *iso*-pentane. These carbonaceous species are predominantly composed of polyaromatic compounds in graphitic-like structures. In *n*-hexadecane conversion over Pt/H-Beta, cracking is favoured over isomerisation and carbonaceous deposits are formed rapidly causing catalyst pore blockage. Reactions over Pt/H-Beta modified by desilication revealed that coke formation is due to the retention of reaction intermediates and/or products inside the pores, resulting in improved selectivity to *iso*-hexadecane production over the modified catalyst, with carbon deposition significantly reduced.

n-Hexadecane conversion performed over Pt/H-Beta pre-coked with *n*-pentane or toluene as paraffinic and aromatic precursors respectively, showed that selectivity to short-chained alkanes (pentane, hexane, and heptane) can be enhanced by tailored-carbon deposition. These products are highly in demand in petrochemical industry for the production of commercial fuels and solvents. Additionally, the rate of coke formation is remarkably reduced, in particular over toluene pre-coked Pt/H-Beta

where the internal sites are blocked by carbonaceous species. In general, tailored carbon deposition can be considered as a useful approach to maximise the production of short-chained hydrocarbons from heavy feedstocks and minimise the coking rate.

Table of Contents

List of figures

List of tables

1. Chapter 1: Introduction	1
1.1 Background	1
1.2 Objectives.....	2
2 Chapter 2: Literature review	5
2.1 Introduction to catalysis	5
2.2 Zeolites as a catalysts	9
2.2.1 History of zeolites	9
2.2.2 Zeolite structure and classification.....	11
2.2.3 Zeolite acidity.....	14
2.2.4 Zeolite shape selectivity.....	16
2.2.5 Zeolite Beta	17
2.3 Catalytic isomerisation-cracking of <i>n</i> -alkanes	19
2.3.1 Catalysts for <i>n</i> -alkane isomerisation-cracking	20
2.3.2 Reaction mechanism of <i>n</i> -alkane isomerisation and cracking	22
2.4 Coking and deactivation.....	26
2.4.1 The mechanism of coke formation.....	26
2.4.2 Parameters affecting the rate of coke formation	28

2.4.2.1	Influence of reactant nature	29
2.4.2.2	Influence of pore structure	29
2.4.2.3	Influence of active sites	29
2.4.2.4	Influence of operating conditions	30
2.4.3	Modes of catalyst deactivation by coke formation	30
2.4.4	Characterisation of coke deposits.....	31
2.5	The role of coke in hydrocarbon transformations	32
2.5.1	The beneficial role of coke.....	32
2.5.2	Carbonaceous deposits as an active species.....	34
3	Chapter 3: Experimental work.....	38
3.1	Introduction	38
3.2	Materials.....	38
3.3	Catalyst preparation	39
3.3.1	Zeolite modification by desilication.....	40
3.3.2	Pre-adsorption of 2,6-di-tert-butylpyridine (DTBP).....	41
3.3.3	Zeolite modification by metal loading	42
3.3.4	Silylation modification.....	44
3.4	Experimental set-ups and procedures.....	45
3.4.1	Catalytic isomerisation-cracking of <i>n</i> -pentane.....	45
3.4.1.1	Reactor set-up	45
3.4.1.2	Catalyst pelletisation.....	46

3.4.1.3	Experimental procedure	49
3.4.2	Catalytic conversion of <i>n</i> -hexadecane	50
3.4.2.1	Reactor set-up	50
3.4.2.2	Experimental procedure	52
3.4.2.3	Spent catalyst separation and cleaning	53
3.5	Analysis by gas chromatography (GC)	54
3.5.1	GC analysis of the reaction products of <i>n</i> -pentane conversion.....	56
3.5.2	GC analysis of the reaction products of <i>n</i> -hexadecane conversion	57
3.6	Calculations.....	59
3.6.1	Calculation of products composition	59
3.6.1.1	Composition of gaseous compounds	59
3.6.1.2	Composition of liquid products	60
3.6.2	Calculation of reactant conversion.....	62
3.6.3	Calculation of product selectivity	63
3.6.4	The reproducibility error calculation	63
4	Chapter 4: Characterisation techniques	66
4.1	Introduction	66
4.2	Inductively Coupled Plasma (ICP).....	66
4.3	X-ray diffraction (XRD)	67
4.4	Specific surface area using N ₂ adsorption isotherm.....	69
4.5	Temperature programmed reduction (TPR).....	73

4.6	Elemental Analysis.....	74
4.7	Thermogravimetric analysis (TGA).....	75
4.8	Temperature-programmed oxidation (TPO)	77
4.9	Raman spectroscopy.....	78
5	Chapter 5: Role and nature of coke in <i>n</i>-pentane isomerisation over Pt/H-Beta.....	85
5.1	Introduction	85
5.2	Materials and methods	88
5.3	Results and discussion	89
5.3.1	Catalyst characterisation	89
5.3.2	Catalytic activity measurements	92
5.3.2.1	Influence of reaction temperature	94
5.3.2.2	Influence of TOS	98
5.3.3	Coke characterisation	101
5.3.3.1	Thermogravimetric analysis (TGA).....	101
5.3.3.2	Elemental analysis	103
5.3.3.3	Temperature-programmed oxidation (TPO).....	103
5.3.3.4	UV-Raman spectroscopy	108
5.4	Conclusions	114
6	Chapter 6: <i>n</i>-Hexadecane isomerisation-cracking over Pt/H-Beta	117
6.1	Introduction	117

6.2	Materials and methods	119
6.3	Results and discussion	120
6.3.1	Catalyst characterisation	120
6.3.1.1	Characterisation of Pt/H-Beta.....	120
6.3.1.2	Characterisation of Pt/pre-poisoned H-Beta.....	120
6.3.1.3	Characterisation of Pt/desilicated H-Beta.....	123
6.3.2	Catalytic activity measurements	125
6.3.2.1	Influence of reaction temperature and zeolite structure.....	126
6.3.2.2	Influence of H ₂ pressure	129
6.3.2.3	Influence of TOS	131
6.3.3	Influence of catalyst surface modification	134
6.3.3.1	n-Hexadecane conversion over Pt/pre-poisoned H-Beta.....	134
6.3.3.2	n-Hexadecane conversion over Pt/desilicated H-Beta.....	135
6.3.3.3	Comparison of the performance of catalysts	137
6.3.4	Coke characterisation	138
6.3.4.1	Thermogravimetric analysis (TGA).....	138
6.3.4.2	Elemental analysis	140
6.3.4.3	Temperature-programmed oxidation (TPO).....	141
6.3.4.4	UV-Raman spectroscopy	146
6.4	Conclusions	150

7 Chapter 7: Tailored carbon deposition of Pt/H-Beta for <i>n</i>-hexadecane conversion	154
7.1 Introduction	154
7.2 Materials and methods	156
7.2.1 Catalyst preparation	156
7.2.1.1 Silylation treatment.....	156
7.2.1.2 Pre-coking of Pt/H-Beta with n-pentane.....	156
7.2.1.3 Pre-coking of Pt/H-Beta with toluene.....	157
7.2.2 Coke characterisation	159
7.2.3 Catalytic activity measurements and GC analysis	160
7.3 Results and discussion	160
7.3.1 Characterisation of the pre-treated catalysts	160
7.3.1.1 Characterisation of Pt/H-Beta after silylation.....	160
7.3.1.2 Characterisation of pre-coked Pt/H-Beta.....	162
7.3.1.2.1 Thermogravimetric analysis (TGA)	162
7.3.1.2.2 Surface area measurements	163
7.3.1.2.3 Temperature-programmed oxidation (TPO).....	163
7.3.1.2.4 UV-Raman spectroscopy.....	165
7.3.2 <i>n</i> -Hexadecane isomerisation-cracking over pre-treated catalysts	168
7.3.2.1 Catalytic activity measurements	168
7.3.2.2 Study on the selectivity to reaction products	174

7.3.3	Characterisation of pre-coked catalysts after reaction	180
7.3.3.1	Thermogravimetric analysis (TGA).....	180
7.3.3.2	UV-Raman spectroscopy	181
7.4	Conclusions	184
8	Chapter 8: Conclusions and future work	187
8.1	Conclusions	187
8.2	Future work	190

List of figures

Figure 2.1 Sequence of physical and chemical steps occurring in heterogeneous catalytic reaction (adapted from (Le Page, 1987)). The schematic drawing at the top correspond to step (i) and (v) as the mass transfer to and from the catalyst particle, and the schematic drawing at the bottom correspond to steps (ii), (iii) and (iv) which involve chemical transformation on the catalyst surface.	7
Figure 2.2 The basic building unit and the channel system of Y zeolite as an example of zeolite structure (adapted from (Weitkamp, 2000)).....	12
Figure 2.3 Pore structure of the commercial Y, ZSM-5, and Mordenite zeolites with different dimensionality (Bartholomew, 2006).....	13
Figure 2.4 The mechanism of Brønsted and Lewis acid sites formation (Bartholomew, 2006).	14
Figure 2.5 Examples for the classical zeolite shape selectivity (Degnan Jr, 2003)..	17
Figure 2.6 The three-dimensional view of zeolite Beta framework and the pore diameters in Angstroms (Baerlocher et al., 2007).....	18
Figure 2.7 Rearrangement of carbenium ions <i>via</i> PCP intermediate over solid acid (Ono, 2003).	23
Figure 2.8 Reaction pathways for the isomerisation of <i>n</i> -butane and <i>n</i> -pentane an example of <i>n</i> -alkanes isomerisation (Okuhara, 2004).....	24
Figure 2.9 Cracking modes of alkylcarbenium ions with the minimum number of carbon atoms required for each type (Soualah et al., 2010).....	25
Figure 2.10 Schematic drawing of the mechanism of coke formation from hydrocarbons over acid and bifunctional catalysts (Bauer and Karge, 2006).....	28
Figure 2.11 The proposed mechanism of <i>n</i> -butene isomerisation into <i>iso</i> -butene over coked H-FER (Andy et al., 1998).	35

Figure 2.12 The proposed mechanism of <i>n</i> -decane hydroisomerisation over tertiary carbenium ions located at TON pore mouth (Guisnet, 2002a).	36
Figure 3.1 Schematic representation of zeolite post-synthesis modification by the desilication treatment to create mesoporosity in zeolite micro-structure (adapted from (Groen et al., 2005)).	40
Figure 3.2 Poisoning of zeolite Brønsted acid sites located at the external surface by the pre-adsorption of DTBP (adapted from (Gounder et al., 2012)).	42
Figure 3.3 The preparation steps of Pt/H-Beta (adapted from (Abudawood, 2010, Yao and Yao, 2016)).	43
Figure 3.4 Schematic representation of the silylation reaction between TEOS and the surface hydroxyl groups of zeolite (Zheng et al., 2002).	44
Figure 3.5 Schematic diagram of the reactor unit employed in the catalytic conversion of <i>n</i> -pentane.	47
Figure 3.6 Schematic diagram of the system employed in the catalytic conversion of <i>n</i> -pentane.	48
Figure 3.7 Schematic drawing for the reaction system employed in <i>n</i> -hexadecane reaction.	51
Figure 3.8 Configuration of the internal parts of the batch reactor employed in <i>n</i> -hexadecane conversion.	52
Figure 3.9 The logarithmic relation between the carbon number and the RF for C8-C17 <i>n</i> -alkanes.	61
Figure 3.10 <i>n</i> -Hexadecane calibration line determined by GC analysis.	62
Figure 4.1 Schematic drawing of the scattering of X-ray from a parallel planes in a constructive interference (adapted from (Che and Védrine, 2012a)).	68
Figure 4.2 Types of adsorption isotherms (adapted from (Leofanti et al., 1998, Bekkum, 2001a)).	71

Figure 4.3 Plot of the N ₂ adsorption-desorption isotherms of a porous glass at -196 °C (adapted from (Che and Védrine, 2012a)).	72
Figure 4.4 Diagram of Rayleigh, Raman scattering, Resonance Raman, and Fluorescence emission (adapted from (Ferraro et al., 2003)).	80
Figure 4.5 (a) UV Raman spectroscopy enhancing Raman scattering intensity; (b) Raman spectra of AlPO ₄ ⁻⁵ excited at 532, 325, and 244 nm wavelength (Jin et al., 2015).	81
Figure 4.6 UV-Raman spectra of some polyaromatic hydrocarbons (Chua and Stair, 2003).	83
Figure 5.1 TGA/DTG curves for the decomposition of (a) fresh zeolite H-Beta; (b) 0.45 wt.% Pt/H-Beta before calcination; (c) 0.45 wt.% Pt/H-Beta after calcination at 320 °C in air. In all the presented analysis, air was employed as a carrier gas.	91
Figure 5.2 TPR profile of 0.45 wt.% Pt loaded on H-Beta catalyst. Inserted TPR profile of a silver oxide, used as a reference material.	92
Figure 5.3 GC/MS Chromatogram for reaction products of <i>n</i> -pentane conversion over 0.5 g Pt/H-Beta, at 300 °C, WHSV of 1.5 h ⁻¹ , H ₂ /pentane mole ratio of 3.12, and after 120 min TOS.	93
Figure 5.4 Steady state regime of <i>n</i> -pentane conversion over 0.5 g Pt/H-Beta catalyst, at 300 °C, WHSV of 1.5 h ⁻¹ , H ₂ /pentane mole ratio of 3.12, and 360 min TOS.	95
Figure 5.5 Conversion of <i>n</i> -pentane and selectivity to <i>iso</i> -pentane of the catalytic isomerisation of <i>n</i> -pentane over 0.5 g Pt/H-Beta catalyst at WHSV of 1.5 h ⁻¹ , H ₂ /pentane mole ratio of 3.12, and at 200, 250, 300, and 350 °C reaction temperatures.	95
Figure 5.6 Selectivity to different reaction products of the catalytic isomerisation of <i>n</i> -pentane over 0.5 g Pt/H-Beta catalyst at WHSV of 1.5 h ⁻¹ , H ₂ /pentane mole ratio of 3.12, and at 250, 300, and 350 °C reaction temperatures.	97

Figure 5.7 <i>n</i> -Pentane conversion and the selectivity to reaction products as a function of TOS for <i>n</i> - pentane conversion over 0.5 g Pt/H-Beta at 300 °C, WHSV of 1.5 h ⁻¹ , and H ₂ /pentane mole ratio of 3.12. The same data are presnted in Figure 5.4.	98
Figure 5.8 <i>n</i> -Pentane conversion and selectivity to <i>iso</i> -pentane as a function of TOS over 0.5 g Pt/H-Beta at 300 °C, WHSV of 1.5 h ⁻¹ , and H ₂ /pentane mole ratio of 3.12.	100
Figure 5.9 TPO fitted profile of the spent catalyst samples after <i>n</i> -pentane conversion over 0.5 g of 0.45 wt.% Pt/H-Beta at 300 °C, WHSV of 1.5 h ⁻¹ , H ₂ /pentane mole ratio of 3.12, and at 1, 6, 92 h TOS.	104
Figure 5.10 TPO profiles after baseline subtraction and peak deconvolution using Gaussian function for the spent catalyst samples of <i>n</i> -pentane conversion over 0.5 g Pt/H-Beta at 300 °C, WHSV of 1.5 h ⁻¹ , H ₂ /pentane mole ratio of 3.12, and after (a) 1 h; (b) 6 h; and (c) 4 days TOS. The temperature shown in brackets corresponds to centre of the oxidation peak.	106
Figure 5.11 UV-Raman spectra of the spent catalyst samples of <i>n</i> -pentane conversion over 0.5 g Pt/H-Beta at 300 °C, WHSV of 1.5 h ⁻¹ , H ₂ /pentane mole ratio of 3.12, and after different stages of reaction.	109
Figure 5.12 UV-Raman spectra of spent Pt/H-Beta of <i>n</i> -pentane conversion over at 300 °C, WHSV of 1.5 h ⁻¹ , H ₂ /pentane mole ratio of 3.12, and after (a) 1 h; (b) 6 h; and (c); 4 days TOS.	111
Figure 6.1 TGA/DTG curves for the decomposition of (a) fresh H-Beta zeolite; (b) pre-poisoned H-Beta; (c) Pt/pre-poisoned H-Beta before calcination; (d) Pt/pre-poisoned H-Beta after calcination in air at 320 °C.	122
Figure 6.2 XRD patterns of the fresh and the desilicated H-Beta samples.	123
Figure 6.3 N ₂ adsorption-desorption isotherms of fresh and desilicated H-Beta zeolite.	124
Figure 6.4 GC/FID Chromatogram for reaction products of <i>n</i> -hexadecane conversion over 0.5 g of 0.45 wt.% Pt/H-Beta at 300 °C, 50 bar H ₂ , and after 30 min TOS.	126

Figure 6.5 Influence of reaction temperature on (a) overall <i>n</i> -hexadecane conversion; and (b) hexadecane isomerisation degree, over 0.5g of the commercial ZSM-5 and H-Beta zeolites at 200, 250,300 °C reaction temperatures, 30 bar He, and 120 min TOS. Isomerisation degree was determined as $iso-C16/(iso-C16 + n-C16 \text{ unreacted})$ (Christensen et al., 2004).....	128
Figure 6.6 <i>n</i> -Hexadecane conversion and selectivity to reaction products as a function of H ₂ pressure over 0.5 g of 0.45 wt.% Pt/H-Beta at 300 °C and 120 min TOS. ...	129
Figure 6.7 <i>n</i> -Hexadecane conversion and selectivity to reaction products as a function of TOS over 0.5 g of 0.45 wt.% Pt/H-Beta at 300 °C and 50 bar H ₂	131
Figure 6.8 Pressure of H ₂ consumed <i>versus</i> TOS in <i>n</i> -hexadecane conversion over 0.5 g of 0.45 wt.% Pt/H-Beta at 300 °C and 50 bar H ₂	132
Figure 6.9 The selectivity to different reaction products in liquid-phase produced from <i>n</i> -hexadecane conversion over 0.5 g of 0.45 wt.% Pt/H-Beta at 300 °C, 50 bar H ₂ , and after 30 and 240 min TOS.	133
Figure 6.10 Selectivity to reaction products, and the total conversion of <i>n</i> -hexadecane over 0.5 g of the fresh and the pre-poisoned Pt/H-Beta with DTBP at 300 °C, 50 bar H ₂ , and 30 min TOS.	135
Figure 6.11 Selectivity to reaction products, and the total conversion of <i>n</i> -hexadecane over 0.5 g of the fresh, pre-poisoned, and desilicated Pt/H-Beta at 300 °C, 50 bar H ₂ , and 30 min TOS.	136
Figure 6.12 TPO fitted profile of the spent catalyst samples after <i>n</i> -hexadecane conversion over 0.5 g of 0.45 wt.% Pt/H-Beta at 300 °C, 50 bar H ₂ , and at 30, 60, 120, and 240 min TOS.	141
Figure 6.13 TPO profiles after baseline subtraction and peak deconvolution using Gaussian function of the spent catalyst samples of <i>n</i> -hexadecane conversion over 0.5 g of 0.45 wt.% Pt/H-Beta at 300 °C, 50 bar H ₂ , and after (a) 30 min; (b) 240 min TOS. The temperature shown in brackets corresponds to centre of the oxidation peak. ..	142

Figure 6.14 TPO profiles of spent catalysts of <i>n</i> -hexadecane conversion over 0.5 g of (a) 0.45 wt.% Pt/pre-poisoned H-Beta; (b) 0.45 wt.% Pt/desilicated H-Beta, at 300 °C, 50 bar H ₂ , and 30 min TOS. Fitting was performed using Gaussian function after baseline subtraction.	145
Figure 6.15 UV-Raman spectra of spent 0.45 wt.% Pt/H-Beta of <i>n</i> -hexadecane conversion at 300 °C, 50 bar H ₂ , and after (a) 30 min; (b) 240 min. Deconvolution performed after baseline subtraction and curve fitting using Voigt function.	147
Figure 6.16 UV-Raman spectra of spent catalyst of <i>n</i> -hexadecane conversion over (a) 0.45 wt.% Pt/pre-poisoned H-Beta; (b) 0.45wt.% Pt/desilicated H-Beta, at 300 °C, 50 bar H ₂ , and 30 min TOS. Deconvolution was performed after baseline subtraction and curve fitting using Voigt function.	149
Figure 7.1 Ampoules used in the preparation of pre-coked Pt/H-Beta with toluene (a) before pre-coking; (b) after pre-coking at 650 °C.....	159
Figure 7.2 TG/DTG analysis for the decomposition of (a) fresh Pt/ H-Beta; (b) TEOS loaded on Pt/H-Beta, using N ₂ a carrier gas.....	161
Figure 7.3 TPO profile of pre-coked Pt/H-Beta at 650 °C using toluene as a coke precursor.....	164
Figure 7.4 UV-Raman spectra of the pre-coked 0.45 wt.% Pt/H-Beta with (a) toluene liquid adsorption /6 h; (b) toluene vapour adsorption /12 h. Deconvolution was performed after baseline subtraction and curve fitting using Voigt function.	167
Figure 7.5 Selectivity and conversion profile of <i>n</i> -hexadecane conversion over 0.5 g of fresh and pre-treated Pt/H-Beta at 300 °C, 50 bar H ₂ , and 30 min TOS.	169
Figure 7.6 Selectivity to different liquid products of <i>n</i> -hexadecane conversion at 300 °C, 50 bar H ₂ , and 30 min TOS over 0.5 g of fresh and pre-treated Pt/H-Beta.	179
Figure 7.7 UV-Raman spectra of spent pre-treated Pt/H-Beta of <i>n</i> -hexadecane conversion at 300 °C, 50 bar H ₂ , and after 30 min TOS. (a) Spent <i>n</i> -pentane pre-coked	

Pt/H-Beta, (b) Spent toluene pre-coked Pt/H-Beta (liquid adsorption /6 h), (c) Silylated Pt/H-Beta.....	183
---	-----

List of tables

Table 3.1 Specifications of gases employed.	38
Table 3.2 Names and specifications of chemicals and zeolites used in this work.	39
Table 3.3 GC/FID method conditions used in the analysis of <i>n</i> -pentane reaction products.	57
Table 3.4 Conditions of the GC/FID method employed in the analysis of headspace gases following <i>n</i> -hexadecane conversion.	57
Table 3.5 Conditions of the GC/FID method employed in the analysis of liquid products following <i>n</i> -hexadecane conversion.	58
Table 3.6 Experimentally determined chromatographic RF for C5-C18 <i>n</i> -alkanes. .	61
Table 4.1 Type and characteristics of adsorption isotherms (adapted from (Bekum, 2001a)).	71
Table 4.2 Raman bands for carbonaceous materials (Sadezky et al., 2005).	82
Table 5.1 Coke content percent of the spent 0.45 wt.% Pt/H-Beta catalysts in <i>n</i> -pentane conversion at 300 °C, WHSV of 1.53h ⁻¹ , H ₂ /pentane mole ratio of 3.12, and at different TOS. The measurement was repeated three times for each sample and the standard deviation from the mean value was calculated.	102
Table 5.2 Elemental analysis data showing the wt.% of C and H and the H/C mass ratio after different stages of <i>n</i> -pentane conversion over 0.5 g Pt/H-Beta at 300 °C, WHSV of 1.53h ⁻¹ , and H ₂ /pentane mole ratio of 3.12.	103
Table 5.3 The peak area of different types of coke resulted from the deconvolution of the TPO profile shown in Figure 5.10.	107

Table 5.4 The expected structure, location, and bounding strength of the carbon species presented in the deconvoluted peaks A, B, C, and D of TPO profile of <i>n</i> -pentane isomerisation over 0.45 wt.% Pt/H-Beta.	108
Table 5.5 Typical wave number and assignment of Raman bands derived from the literature.	112
Table 6.1 Surface area data of fresh and desilicated H-Beta zeolite.....	125
Table 6.2 Coke content percent of the spent 0.45 wt.% Pt/H-Beta catalysts in <i>n</i> -hexadecane conversion at 300 °C, 50 bar H ₂ , and at increasing TOS. Analysis was repeated three times for each sample and the standard deviation from the mean value was calculated.	139
Table 6.3 Coke percent formed over the fresh and modified Pt/H-Beta catalysts in <i>n</i> -hexadecane conversion at 300 °C, 50 bar H ₂ , and 30 min TOS. All samples were repeated three times and the standard deviation from the mean value was calculated.	140
Table 6.4 Elemental analysis data showing the wt.% of C and H, and the H/C mass ratio of coke deposits after <i>n</i> -hexadecane conversion over 0.5 g of 0.45 wt.% Pt/H-Beta at 300 °C, 50 bar H ₂ , and at increasing TOS.	140
Table 6.5 Elemental analysis data of the coke formed over the unmodified and modified Pt/H-Beta catalysts during <i>n</i> -hexadecane conversion at 300 °C, 50 bar H ₂ , and 30 min TOS.	141
Table 6.6 Peak areas of the resolved peaks of TPO profiles shown in Figure 6.13.	144
Table 6.7 Peak areas of the resolved peaks of TPO profiles shown in Figure 6.14.	144
Table 6.8 D1/G and D1/D3 area ratios of the carbonaceous deposits accumulated over the fresh and the modified Pt/H-Beta catalysts of <i>n</i> -hexadecane conversion at 300 °C, 50 bar H ₂ , and 30 min TOS.	148

Table 7.1 Coke content in wt.% formed over Pt/H-Beta after pre-coking with <i>n</i> -pentane and toluene. The analysis was repeated three times for each sample and the standard deviation from the mean value was determined.	162
Table 7.2 BET Surface area of Pt/H-Beta before and after pre-coking treatments with <i>n</i> -pentane and toluene.	163
Table 7.3 Integrated peak areas of the pronounced peaks of TPO profiles shown in Figure 7.3.	165
Table 7.4 Position of the Raman bands, D1/G and D1/D3 ratios of the Raman spectra of pre-coked Pt/H-Beta. The results involve a degree of uncertainty due to the noisy Raman signal.	166
Table 7.5 The influence of catalyst modification by pre-coking and silylation on the performance of Pt/H-Beta during <i>n</i> -hexadecane conversion at 300 °C, 50 bar H ₂ , and 30 min TOS. Treatment (iv) by toluene (vapour adsorption /12 h) is not shown as it resulted in total deactivation of the catalyst for the studied reaction.	174
Table 7.6 Total selectivity to cracking products and the selectivity to pentane, hexane, and heptane obtained in <i>n</i> -hexadecane conversion over 0.5 g of fresh and pre-treated Pt/H-Beta, at 300 °C, 50 bar H ₂ , and 30 min TOS.	175
Table 7.7 Coke content percent formed over the fresh and the pre-coked Pt/H-Beta before and after <i>n</i> -hexadecane conversion at 300 °C, 50 bar H ₂ , and 30 min TOS. The net coke was calculated as the percentage of total coke minus the percentage of the initial coke. All samples were repeated three times and the standard deviation from the mean value was calculated.	180

Chapter 1

Introduction

1. Chapter 1: Introduction

1.1 Background

Several commercial processes in the modern refining and petrochemical industries utilise zeolites as solid acid catalysts. For instance, in the catalytic cracking process, the carbon-carbon bond of a hydrocarbon molecule breakdown on zeolite acid site to produce smaller molecules. This is applied in the conversion of the high-boiling point, long-chain hydrocarbons into lower boiling-point, shorter-chain products. Furthermore, in the isomerisation process, a linear hydrocarbon molecule is rearranged on zeolite acid site into another molecule, which has exactly the same number of atoms but in a different structure, such as the isomerisation of *n*-pentane and *n*-hexane into *iso*-pentane and *iso*-hexane applied in the production of gasoline with a high octane number. This is a reflection of the significant acidity and the unique sieving properties of zeolites (Clark, 2000, Guisnet et al., 2009). However, in most of these transformations, there is a progressive decrease of the zeolite efficiency with time-on-stream; this phenomenon is called “deactivation”. Coke formation is often responsible for the deactivation of zeolite catalysts either by active site poisoning or pore blockage (Karge, 1991, Bartholomew, 2001, Guisnet and Magnoux, 1997).

The catalytic activity of zeolite-based catalysts can be restored through the regeneration process. The removal of coke deposits using this oxidative treatment is therefore of considerable technological and economic importance in industrial processes. However, the high oxidation temperature required for this treatment may have harmful effects on the catalyst, such as loss of active sites and sintering of any supported metals; in addition to the high energy cost associated with this treatment (Menon, 1990, Guisnet and Magnoux, 1997).

It is generally accepted that carbonaceous overlayers, in addition to their negative influence in catalyst deactivation, can play a positive role in enhancing the catalytic performance in several reaction systems (Guisnet, 2002a, Jackson et al., 1981, Menon, 1990). Thus, certain carbonaceous species may have a “beneficial” effect by deactivating the non-selective acid sites and/or improving zeolite-sieving properties, or contributing as a partner in the reaction itself as “catalytically active coke” (Bauer

and Karge, 2006). Therefore, the deliberate formation of beneficial and/or catalytically active coke to enhance catalytic activity or selectivity is a subject of increasing interest in the studies of hydrocarbon transformations. In this context, it is worth mentioning the isomerisation-cracking of *n*-alkanes, one of the most important commercial processes in upgrading refinery and petrochemical feed streams. Bifunctional catalysts typically are employed in this process, consisting of metallic sites such as platinum for hydrogenation/dehydrogenation function, and an acidic support such a zeolite, for carbon-carbon bond rearrangement (Ertl et al., 2008). It is widely known that these catalysts typically experience deactivation by coking due to the presence of olefinic-reaction intermediates which can be precursors for the formation of carbonaceous deposits (Regali et al., 2013).

Based on this concept, this research aims to explore the relationship between the carbonaceous deposits accumulated on the catalyst surface and the catalyst performance during the isomerisation-cracking of *n*-alkanes, in particular, to understand mechanisms of deactivation and to establish whether particular terms of carbonaceous materials can enhance the catalyst activity and/or selectivity and reduce coke formation. This will be investigated through the controlled deposition of carbonaceous material on the catalyst surface using different coke precursors. This work will lead to an advance in understanding of the mechanism behind coke formation, which can in turn lead to the control of carbon deposition thereby extending catalyst lifetime.

1.2 Objectives

The over-arching aim of this work is to study the role and nature of coke in isomerisation-cracking of *n*-alkanes over Pt/H-Beta. This comprises:

- i. the isomerisation-cracking of *n*-pentane as a representative short-chained *n*-alkane; and
- ii. the isomerisation-cracking of *n*-hexadecane as exemplar long-chained *n*-alkane

Within these two headings, a number of discrete objectives have been identified, namely:

- To investigate the influence of reaction conditions on the performance of Pt/H-Beta in *n*-pentane conversion.
- To identify different reaction stages during the isomerisation-cracking of *n*-pentane with time-on-stream.
- To study the chemical nature, structure, and the quantity of carbonaceous deposits formed during *n*-pentane conversion at different stages of reaction.
- To explore the role of coke formed during *n*-pentane conversion on the catalytic performance of Pt/H-Beta.
- To investigate the influence of reaction conditions (temperature and hydrogen pressure) on the performance of Pt/H-Beta in *n*-hexadecane conversion.
- To investigate the reasons behind coke formation during *n*-hexadecane conversion.
- To study the influence of catalyst surface modification by desilication treatment and selective poisoning of acid sites on the catalytic performance.
- To characterise carbonaceous deposits formed over Pt/H-Beta during *n*-hexadecane conversion.
- To carry out the controlled deposition of carbonaceous materials originating from different precursor molecules (light alkanes and aromatics) to produce pre-coked Pt/H-Beta catalysts suitable for *n*-hexadecane conversion.
- To characterise the pre-coked catalysts and study the influence of deposited carbon upon catalytic performance in *n*-hexadecane conversion.
- To explore the relationship between the nature, structure, location of carbon deposition formed in the controlled pre-coking treatment of Pt/H-Beta and the catalytic performance in *n*-hexadecane conversion.

Chapter 2

Literature review

2 Chapter 2: Literature review

2.1 Introduction to catalysis

The term “catalysis” was introduced for the first time by the Swedish chemist Berzelius in 1836 to explain the decomposition and the transformation of substances. Later, Ostwald in 1895 introduced the definition of a catalyst as “*a material that accelerates a chemical reaction without affecting the position of the equilibrium*” (Bond, 1974, Satterfield, 1980, Hagen, 2006).

Catalysis can be classified as homogenous when the catalyst is soluble in the reaction medium, heterogeneous when the catalyst phase is different from the phase of reactants, and biological when the catalyst is in the form of enzymes (Le Page, 1987, Smith and Notheisz, 2006). Heterogeneous catalysts are of crucial importance in chemical industries due to the fact that 90% of the chemical and petrochemical processes in the world are catalysed heterogeneously (Thomas, 1996, Ertl et al., 2008). In most instances of heterogeneous catalysis, the catalyst is in a solid phase and the reactants are in liquid or gas phase (Hagen, 2006).

During the last century, heterogeneous catalysis technology played an essential role in the development of the world economy through the manufacturing of a wide range of products such as fuels, plastics, food products, and fertilizers. In addition, heterogeneous catalysis offers promising applications in reducing pollution and environment control (Bartholomew, 2006).

The typical components of a heterogeneous catalyst are the metal, the support, and the promoter. The metal or metal oxide or sulphide is often dispersed on the surface of a support material, the active sites of these metals or metal oxides are capable of catalysing different reactions. The support is usually a material with a high surface area and high thermal stability that carrying the metal and may also participate in the reaction. Examples include zeolites, activated carbon, and transition metal oxides. The promoters are usually transition metal oxides that are dispersed in small amounts on the catalyst surface to enhance the catalytic activity of some catalysts (Bartholomew, 2006).

Advantages of heterogeneous catalysts in industry

Most the large-scale industrial processes are conducted heterogeneously because of the considerable advantages of solid catalysts in comparison to homogenous ones (Clark, 2000, Hattori, 2010). The main engineering advantages are:

- i. Heterogeneous catalysts can be easily separated from the products without expensive cost.
- ii. Reduced corrosion problems in which the solid catalysts are rarely corrosive.
- iii. Heterogeneous catalysis can be performed over a wide range of reaction conditions (temperature and pressure).
- iv. Less disposal problems where heterogeneous catalysts can be regenerated and reused for longer periods.

The contact mechanism over heterogeneous catalyst

The chemical reaction over the surface of a heterogeneous catalyst takes place in a five consecutive physical and chemical steps as shown in Figure 2.1, each step has an influence on the overall rate of reaction and any one of them could be the rate determining step (Satterfield, 1980, Hagen, 2006, Le Page, 1987). These steps are:

- i. Diffusion of the reactant from the bulk to the catalyst surface.
- ii. Adsorption of the reactant on the catalyst surface.
- iii. Reaction over the catalyst surface through the active sites.
- iv. Desorption of the products from the catalyst.
- v. Diffusion of the products to the surrounding media.

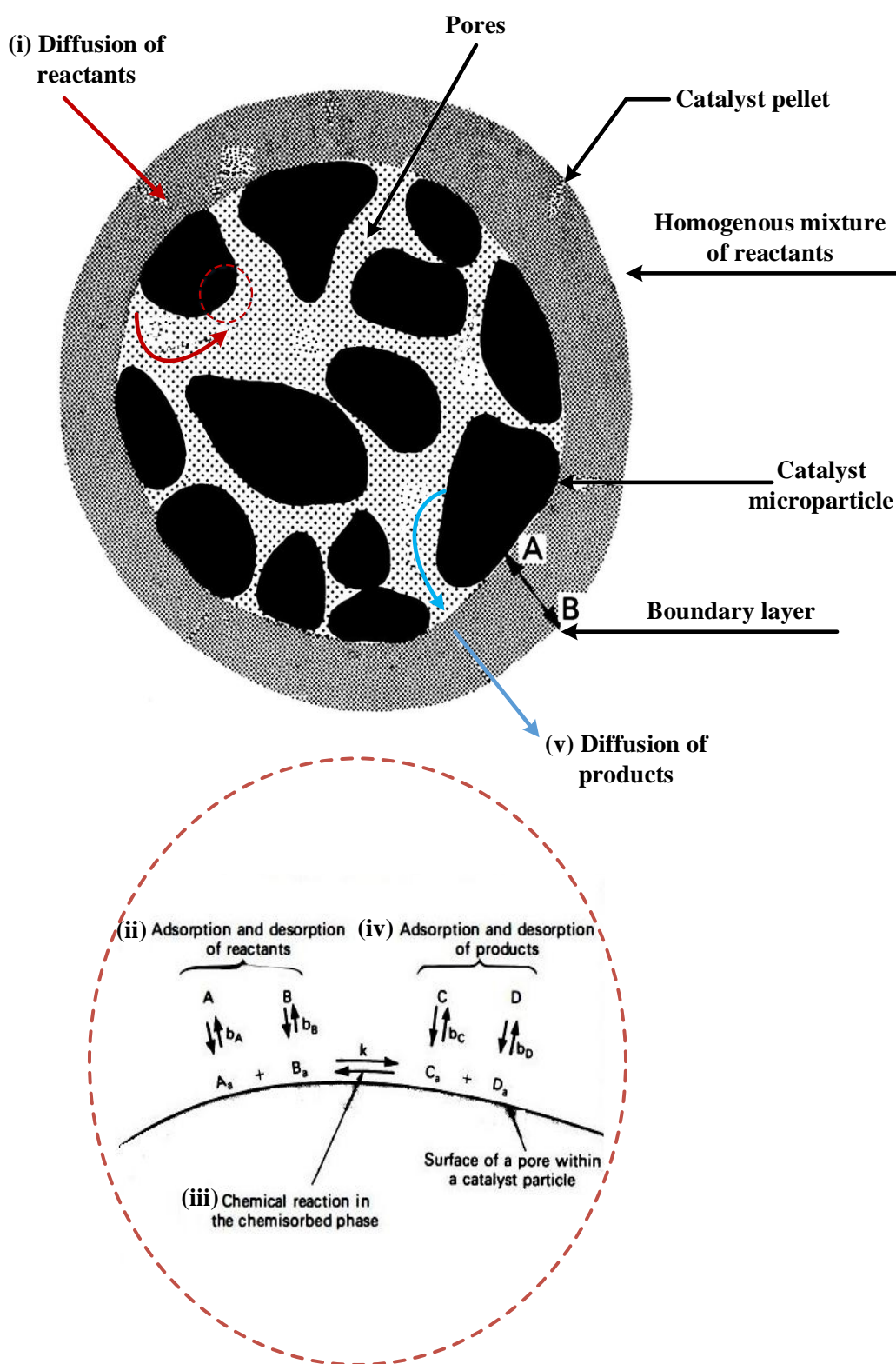


Figure 2.1 Sequence of physical and chemical steps occurring in heterogeneous catalytic reaction (adapted from (Le Page, 1987)). The schematic drawing at the top correspond to step (i) and (v) as the mass transfer to and from the catalyst particle, and the schematic drawing at the bottom correspond to steps (ii), (iii) and (iv) which involve chemical transformation on the catalyst surface.

Heterogeneous catalyst deactivation

Catalyst deactivation is one of the major problems associated with the operation of heterogeneous catalysts. It often occurs simultaneously with the main reaction. Although deactivation is unavoidable, it can be slowed down and some of its consequences can be reduced. The deactivation process is both of chemical and physical nature and can occur by a number of different mechanisms. These are commonly divided into four main classes, namely fouling and coking, poisoning, sintering, and phase transformation. These mechanisms can occur separately or in combination, however, in any case the result is the loss of catalyst activity (Satterfield, 1980, Butt, 1988, Forzatti and Lietti, 1999).

A brief description regarding the deactivation mechanisms is given below:

- i. Fouling and coking: these terms are usually used to describe the physical blockage of the catalyst pores by simple deposits such as dust or fine powder (fouling) or by the accumulation of the carbonaceous deposits (coking). The catalytic conversion of hydrocarbons is often combined with side reactions that consequently lead to coke formation. These carbonaceous deposits usually result in catalyst deactivation by covering the active sites and/or pore blockage. In this type of deactivation, the catalyst can be restored by a regeneration process through coke oxidation (Forzatti and Lietti, 1999, Satterfield, 1980, Guisnet, 2011).
- ii. Poisoning: this is the reduction of catalyst activity by strong chemisorption of impurities presented in the feed stream. Poisoning can be either “reversible”, in which the catalyst can be regenerated by the removal of the impurities from the reactant stream, or “irreversible” when irreversible damage of the catalyst occurs (Forzatti and Lietti, 1999). However, in some catalytic processes, a deliberate addition of poisons is needed to improve the selectivity to the desired product, e.g. pre-treating reforming catalysts with low concentrations of sulphur compounds to limit the high hydrocracking activity of the catalyst (Guisnet, 2011).

- iii. Sintering: this is an irreversible physical process, usually can occur at high operation temperatures over supported metal catalysts. The active component is usually present on the catalyst surface in the form of small particles. These particles may move and when two particles come into contact, they may merge to form larger particles leading to a loss in the active surface area and consequently lower catalytic activity (Stoltze, 2007).
- iv. Solid state transformation: this can be considered as an extreme form of sintering that occurs at high temperatures causing the loss or the transformation of the active components from one form to another with lower activity such as the decomposition of metal oxide complex, the volatilisation of particular element, or the alloying of metal crystals with the support (Satterfield, 1980, Forzatti and Lietti, 1999).

2.2 Zeolites as a catalysts

Zeolites are crystalline microporous materials with a framework of aluminium and silicon oxides. This section covers the fundamentals of zeolite materials with a brief introduction into their history and structures. In addition, the most important parameters of zeolites as solid acids such as acidity and shape-selectivity are briefly discussed.

2.2.1 History of zeolites

The history of zeolites started with the discovery of the mineral “stilbite” by the Swedish mineralogist Cronsted more than 250 years ago. The term “zeolite” was derived from two Greek words “zeo” and “lithos”, which mean, “to boil” and “stone” because water adsorbed by the zeolite is desorbed as steam when it is subjected to a high temperature. There are several types of the naturally accruing zeolites such as faujasite, mordenite, offretite, erionite and chabazite which have extensive applications in catalysis (Guisnet, 2002b, Bond, 1974).

Studies on the fundamental properties of zeolites originated with Damour in 1840 who observed that zeolites could undergo reversible dehydration without changes in the apparent transparency and morphology of the crystal. After that, in 1858 Eichhorn

illustrated the reversibility of ion exchange on zeolite minerals (Bekkum, 2001b). In 1930 Taylor and Pauling determined the first crystal structure of zeolites. Later, McBain in 1932 established, for the first time, the term “molecular sieve” to describe porous solid materials which have the ability to act as sieves on a molecular scale (Kulprathipanja, 2010). A few years later, the pioneering work in zeolite adsorption and synthesis was presented by Barrer in 1945 when he established the first classification of zeolites according to molecular size. This was followed by his work in adsorption and synthesis which paved the way for the era of synthetic zeolites (Kulprathipanja, 2010, Guisnet, 2002b, Bond, 1974).

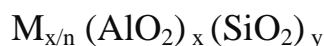
Between 1949 and 1954, Robert M. Milton, considered to be the grandfather of zeolite science and technology, discovered the synthesis of zeolites. His work started with the synthesis of chabazite followed by the synthesis of zeolites A, X, and Y. The new synthetic zeolites were introduced by Union Carbide Corporation as commercial synthetic zeolites and rapidly found application in industry. Zeolite A was used successfully for many commercial applications such as an adsorbent in the drying of refrigerant and natural gas in 1955, and as molecular sieves for *iso*-butane separation in 1959, and for ion exchange in detergent industry in 1974. Zeolites X and Y were introduced as catalysts in the isomerisation processes of hydrocarbons in 1959. The landmark event was the introduction of zeolite Y in fluid catalytic cracking of heavy petroleum distillates in 1962, which is considered one of the most important processes in hydrocarbon industries. Afterwards, between 1967 and 1969, Mobil Oil Company reported the synthesis of the high silica zeolites Beta and ZSM-5. These have wide commercial applications in industry in areas such as dewaxing and xylene isomerization and production (Kulprathipanja, 2010, Guisnet, 2002b, Rabo and Schoonover, 2001, Weitkamp, 2000).

Today, more than 40 natural zeolites have been discovered and more than 130 zeolites have been synthesised by creative zeolite chemists. In addition, great progress has been made in understanding the mechanism of organic molecule transformation into zeolites, which has a large impact on the development of refining, the petrochemical industry, and the clean synthesis of fine chemicals (Guisnet, 2002b).

Nowadays, the industrial application of zeolites as catalysts depends largely on synthetic zeolites due to their particular ion exchange properties, high and adjustable acidity, sharply defined pore size, very high surface area, good thermal stability, and shape selectivity, which is considered as a unique feature of zeolites. In contrast, natural zeolites have limited applications because nature cannot optimise their properties for catalytic applications owing to their varied chemical composition and the presence of undesirable impurities (Chen, 1994, Thomas, 1996).

2.2.2 Zeolite structure and classification

The structure of a zeolite consists of a three dimensional framework of alumina (AlO_4)⁵⁻ and silica (SiO_4)⁴⁻ tetrahedral units. Each tetrahedron consists of a silicon or aluminium atom in the centre, sharing the oxygen atoms with other units at the corners (TO_4 , T = Si or Al) which form the basic building unit (BBU) of zeolite structure. Since silicon has a valence of four and aluminium has a valence of three, one excess negative charge for each aluminium atoms needs to be balanced. Thus to keep the electrical neutrality, a positive cation such as (Na^+ , Mg^{2+} , Ca^{2+} , K^+) or H^+ can be used as a charge counter-balance, giving the zeolite ion exchange capability. The structure of a zeolite can be represented by the following general formula:



Where n is the valence of cation M, $x+y$ is the total number of tetrahedral per unit cell, y/x is the atomic Si/Al ratio varying from minimal value of 1 to infinite (Bond, 1974, Satterfield, 1980, E.M. Flanigen, 1991, Kulprathipanja, 2010). However, according to Löwenstein's rule, it is not possible to have two neighbouring aluminium tetrahedral *i.e.* the bridge Al-O-Al are prohibited or y/x is always ≥ 1 (Weitkamp, 2000).

The three dimensional framework of a zeolite is formed by connecting massive number of BBU in a lattice as shown in Figure 2.2. This framework contains uniform channels (interconnected or not) and/or cages with dimensions from approximately 0.2 to 1 nm. These voids accommodate water and the cations that compensate the framework negative charge (Kulprathipanja, 2010).

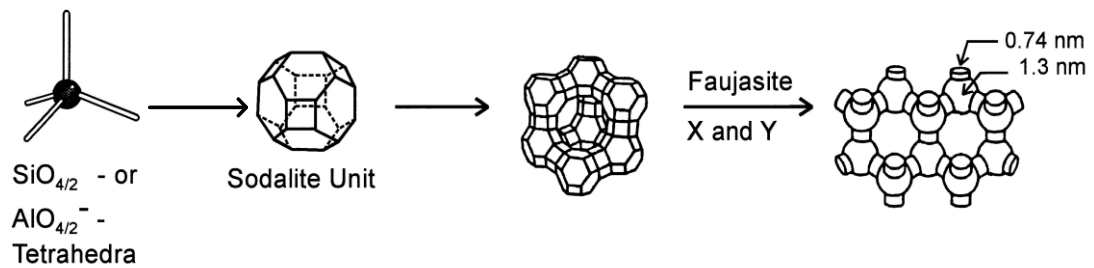


Figure 2.2 The basic building unit and the channel system of Y zeolite as an example of zeolite structure (adapted from (Weitkamp, 2000)).

The description of zeolite structure is often related to the size of pore openings and the dimensionality of the channels system. The pore openings are determined depending on several factors such as the number of tetrahedral units, the shape of the pore (circular, elliptic, teardrop shape), and the concentration and the nature of the cations that exist in or at the pore mouth (Chen, 1994). Zeolite pores may be arranged in one, two, or three dimensions leading to D1, D2, and D3 structures respectively as shown in Figure 2.3. In addition, the pore size can be increased by ion exchange with different ions; a good example for that is zeolite A which has different aperture sizes of 3, 3.8, and 4.3 Å which corresponds to K^+ , Na^+ , and Ca^+ ions respectively. This zeolite is usually used as a drying agent with the familiar industrial names 3A, 4A, and 5A (Bartholomew, 2006).

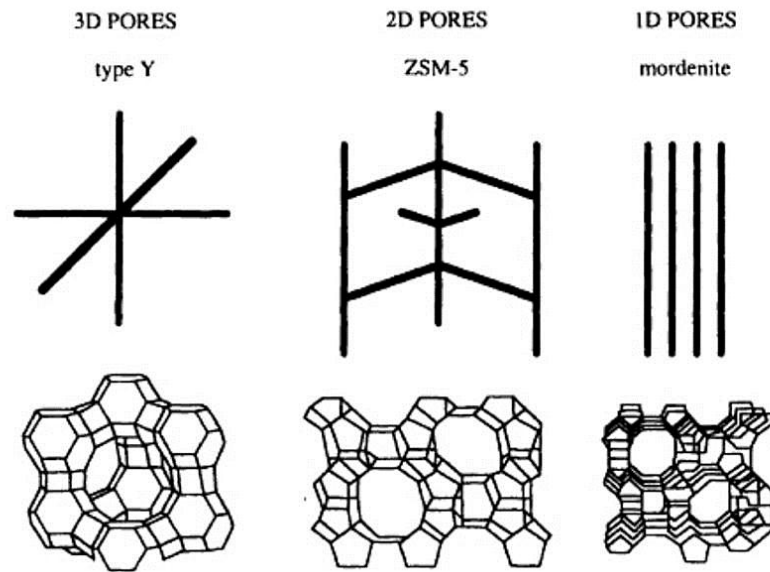


Figure 2.3 Pore structure of the commercial Y, ZSM-5, and Mordenite zeolites with different dimensionality (Bartholomew, 2006).

Most zeolites are classified according to their pore diameter and the number of oxygen atoms at the pore (Guisnet, 2002b):

- Small pore zeolites: eight-member ring pore apertures (8 MR) with free diameters of 0.30 - 0.45 nm, e.g. LTA (Linde Type A), ERI (Erionite).
- Medium pore zeolites: ten-member ring pore apertures (10 MR) with free diameters of 0.45 - 0.60 nm, e.g. MFI (ZSM-5), FER (Ferrierite).
- Large pore zeolites: twelve-member ring pore apertures (12 MR) with free diameter of 0.6 - 0.8 nm, e.g. FAU (Faujasite (X, Y)), MOR (Mordenite), BEA (Beta).

Furthermore, the International Union of Pure and Applied Chemistry (IUPAC) classifies zeolites and other porous materials according to their pore diameter (d_p) such that, micropores: $2.0 \text{ nm} \geq d_p$, mesopores: $2.0 \text{ nm} < d_p \leq 50 \text{ nm}$, and macropores: $d_p > 50 \text{ nm}$, Zeolites are then considered as a typical microporous material (Weitkamp, 2000, E.M. Flanigen, 1991).

2.2.3 Zeolite acidity

Zeolites are often used as acid catalysts; this acidity is mainly attributed to the presence of Brønsted and Lewis acid sites on the zeolite surface which play an important role in catalysing several hydrocarbon reactions such as isomerisation and cracking. The mechanism of acid site generation is shown in Figure 2.4. Brønsted sites are formed when the negatively charged aluminium framework is balanced by a proton (H^+). If a dehydroxylation takes place, the protonic sites are converted to Lewis acid sites. Brønsted acid sites can donate a proton to other chemical species, while Lewis acid sites can accept an electron pair from other species (Hattori, 2010, Bartholomew, 2006, Satterfield, 1980).

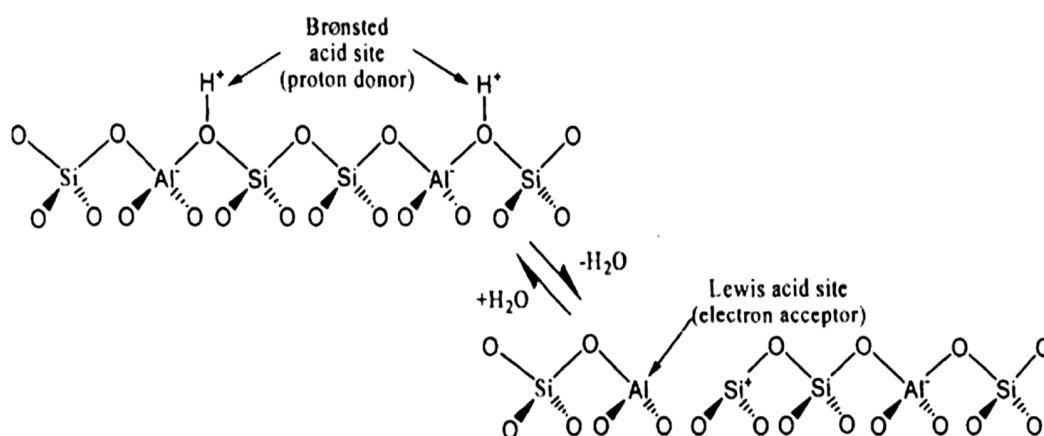
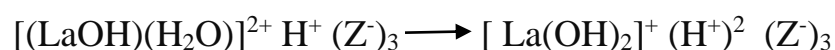
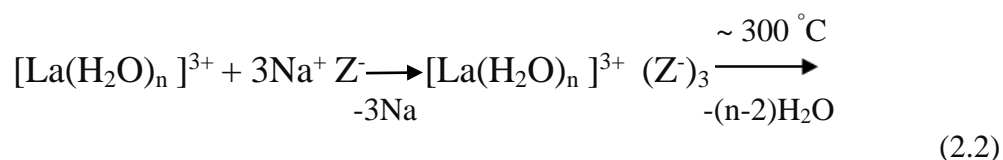
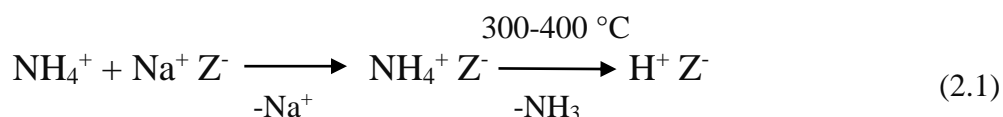


Figure 2.4 The mechanism of Brønsted and Lewis acid sites formation (Bartholomew, 2006).

Brønsted acid sites can be generated either by treating the ion exchanged framework with ammonium salt in an aqueous solution followed by calcination at high temperatures (300 – 400 °C) to remove the ammonia, leaving the framework with H^+ ions as shown in Equation 2.1, or by aqueous ion exchange with the salt of a multi-valent metal cation (e.g. Mg^{2+} , Ca^{2+} , La^{3+}) followed by thermal dehydration as illustrated in Equation 2.2. It is worth mentioning that direct ion exchange with mineral acids often leads to undesired results such as framework dealumination or, in the case of aluminium-rich zeolites, a total framework collapse (Weitkamp, 2000).



where Z^- represent the negatively charged framework.

It is clear from Equation 2.2 that two Brønsted acid sites can be formed per La ion introduced, this process is usually called the Hirschler-Plank scheme (Weitkamp, 2000).

To describe zeolite acidity precisely, a distinction must be made between several variables such as the nature of acid sites (Brønsted or Lewis), the density or concentration of these sites, and their strength and distribution (Haw, 2002). Brønsted acid sites have the major influence on catalysis; it has been reported that most hydrocarbon reactions are catalysed by Brønsted acid sites only and it is doubtful if Lewis sites play a significant role in catalysing such reactions. However, it is also mentioned that the strength of Brønsted acid sites might be enhanced by a neighbouring Lewis acid site, thus Lewis acid sites may have an indirect impact on the reaction (Guisnet, 2002b, Weitkamp, 2000).

Brønsted acidity strength is always associated with the framework Si/Al ratio, which reflects the number of Al-atoms in the framework. Therefore, the Si/Al ratio is proportionally inverse with Brønsted acid sites density (Corma, 2003). The acid strength of a zeolite plays a major role in the selection of zeolite to catalyse a specific reaction, not only because it controls the reaction pathway, but also it limits the reaction conditions, in particular the reaction temperature needed to reach the required activity the higher the acidity the lower the temperature. It is widely known that

cracking is the reaction that requires the strongest acidity among hydrocarbon conversion processes while moderate acidity is required to catalyse skeletal isomerisation, and weak acidity for double bond isomerisation (Kulprathipanja, 2010).

2.2.4 Zeolite shape selectivity

Shape selectivity is a fundamental and unique property of zeolites, therefore, it has been extensively used to separate molecules with different sizes and shapes depending on zeolite pore diameter and structure as well as on the dimensions of the diffusing molecules. Zeolite shape selectivity can be defined as a geometric restriction that can control the diffusion of reactants in or products out, and/or the formation of transition state intermediates inside the pores or the channels. Based on that definition, three main categories of shape selectivity have been identified and described in the literature (Guisnet, 2002b, Bartholomew, 2006, Marcilly, 2000, Degnan Jr, 2003):

- i. Reactant shape selectivity: this occurs when zeolite pores allow the reactant molecules with dimensions lower than the pore size to penetrate through the channel system whereas bulkier molecules are hindered from accessing the internal active sites, thus leaving the reactor without conversion. A good example for this selectivity is the exclusion of multiply branched paraffin in catalytic dewaxing of waxy lube fractions over zeolite ZSM-5 as shown in Figure 2.5 (A).
- ii. Product shape selectivity: this is also based on the principle of size exclusion in which only product molecule that has a certain size less than the zeolite pore dimensions can diffuse out of zeolite framework while larger molecules produced inside the channel system cannot diffuse unless converted to smaller molecules which can escape from the pores. Figure 2.5 (B), shows the selective toluene disproportionation to produce p-xylene over ZSM-5 zeolite as an example of this kind of shape selectivity.
- iii. Restricted transition state shape selectivity: this occurs when the space around the active sites inside the pore limits or prevents the formation of reaction intermediate larger than the size of the desired products molecules. A useful

example of this type of shape selectivity is the alkylation of aromatics as illustrated in Figure 2.5 (C).

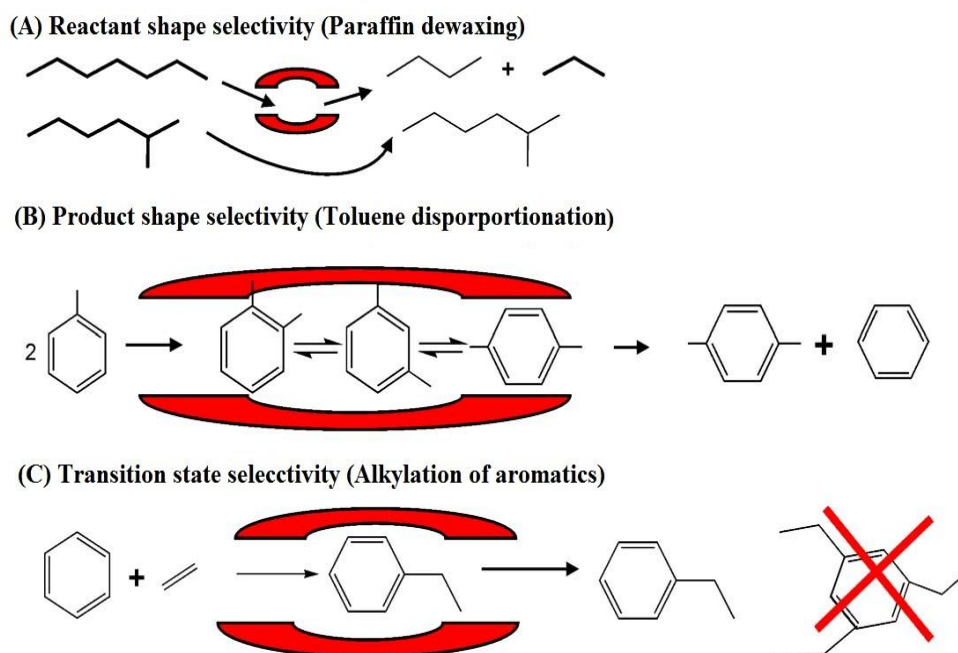


Figure 2.5 Examples for the classical zeolite shape selectivity (Degnan Jr, 2003).

2.2.5 Zeolite Beta

Zeolite Beta is a high-silica, large pore zeolite having a three-dimensional, 12-membered rings interconnected channel system. The large channels with pore openings of 0.66×0.67 nm and the medium channels with pore openings of 0.56×0.56 nm are interconnected by cages (Liu et al., 1991, Eapen et al., 1994, Busca, 2014).

Figure 2.6 shows the typical three-dimensional structure and pore openings for zeolite Beta.

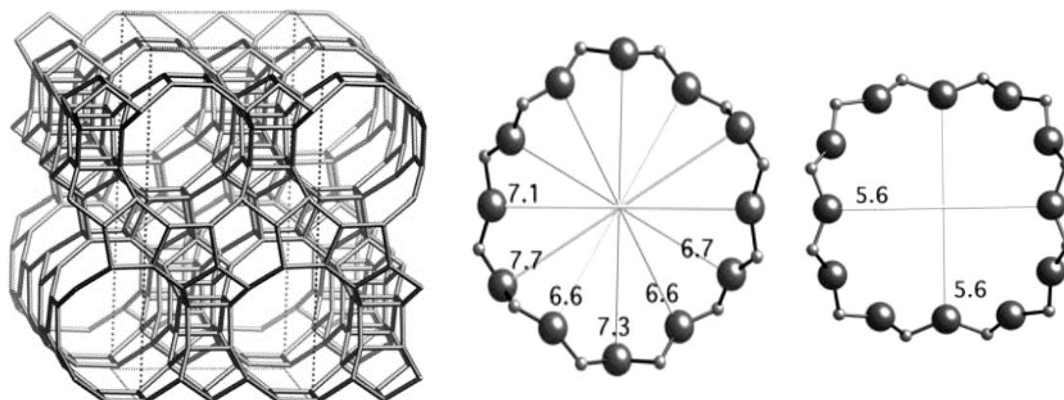


Figure 2.6 The three-dimensional view of zeolite Beta framework and the pore diameters in Angstroms (Baerlocher et al., 2007).

Zeolite Beta was synthesised for the first time at Mobil Research and Development Laboratories (Higgins et al., 1988). It has a high Si/Al ratio ranging from five to infinity (Busca, 2014). This siliceous nature gives zeolite Beta high thermal and hydrothermal stabilities, which are of crucial importance for practical applications (Liu et al., 1991, Halgeri and Das, 1999). In addition, the small crystal size (20-50 nm) provides the zeolite with a shorter diffusional path, thus in a certain catalytic reaction, reactant and product molecules can diffuse easily through zeolite pores without significant diffusion limitations (Simon-Masseron et al., 2007). These unique features of zeolite Beta makes it an efficient catalyst for many important reactions of hydrocarbons such as the alkylation of *iso*-butane with 2-butene (De Jong et al., 1996), the production of cumene through the alkylation of benzene with propene (Perego and Ingallina, 2002), the isomerisation and cracking of heavy paraffins (Bauer et al., 2014, Taylor and Petty, 1994), *etc.*

Finally, zeolite Beta containing catalysts can be completely regenerated by coke oxidation. This is usually required every 2-3 years in commercial industrial applications (Busca, 2014).

2.3 Catalytic isomerisation-cracking of *n*-alkanes

One of the important objectives in petroleum and petrochemical industries is the conversion of *n*-paraffins into their branched isomers through skeletal isomerisation, either to upgrade their quality as finished products or to produce starting materials for other petrochemical processes. The conversion of light linear alkanes such as *n*-pentane and *n*-hexane into their branched forms is of essential importance in the improvement of the octane quality of the gasoline pool. The research octane numbers (RON) of linear pentane and hexane are 61.7 and 24.8 respectively, whereas their corresponding isomers have a RON of 92.3 and 103.6 respectively (Ono, 2003, Deldari, 2005, López et al., 2010). Furthermore, the isomerisation of light linear alkanes also has importance in industrial scale, such as the conversion of *n*-butane into *iso*-butane which is used after dehydrogenation to *iso*-butene in the synthesis of methyl tert-butyl ether (MTBE), one of the chemical additives used to improve gasoline octane number (Caeiro et al., 2006, Miyaji et al., 2002, Ono, 2003).

Skeletal isomerisation of higher alkanes such as C7-C15 is the basis for the production of diesel fuel with high cetane number and good cold flow behaviour. Moreover, the mono-branched isomers produced from the conversion of waxy paraffins heavier than C15 are the desired products for the manufacturing of commercial products such as jet fuels and lubricants with low pour and freezing points (Ertl et al., 2008, Deldari, 2005, Taylor and Petty, 1994).

Catalytic isomerisation process usually take place in the presence of hydrogen, and are referred to as hydroisomerisation process. The hydrogen atmosphere is necessary to reduce coke build-up on the catalyst but hydrogen consumption is negligible (Deldari, 2005).

Both skeletal isomerisation and cracking are acid-catalysed reactions, therefore, the isomerisation reaction is always accompanied by a cracking reaction (Deldari, 2005, Busto et al., 2011). The term hydroisomerisation is used to indicate a situation where isomerisation dominates over hydrocracking, while the term hydrocracking is used to describe the opposite situation (Calemma et al., 2000).

2.3.1 Catalysts for *n*-alkane isomerisation-cracking

The acid catalysts that were extensively applied in the early industrial isomerisation process were the Friedel-Crafts catalysts. These monofunctional acidic catalysts consist of aluminium chloride in combination with additives such as HCl and SbCl₃. This catalyst is highly active even at low reaction temperature (27-117 °C). However, it suffers from several drawbacks such as corrosion problems, the need to supply fresh acid to compensate the loss of acidity, and the disposal of the used catalysts. Therefore, the industrial processes employing this catalyst no longer exist and have been replaced by bifunctional catalyst processes (Ertl et al., 2008, Ono, 2003, Akhmedov and Al-Khowaiter, 2007).

Bifunctional catalysts are considered as typical catalysts for the alkane isomerisation-cracking process. They consist of metallic sites for hydrogenation-dehydrogenation, and acidic sites for the skeletal isomerisation and cracking. Numerous materials have been used as an acidic support for this catalyst such as alumina, amorphous silica-alumina, zeolites, and sulphated zirconia. The metals most commonly used are small amounts of noble metals such as Pd and Pt or bimetallic systems such as Ni/Co, Ni/W, Ni/Mo, W/Mo in the sulphide form. However, catalysts loaded with a noble metal show considerable activity and higher selectivity to isomerisation than those loaded with non-noble metals (Calemma et al., 2000, Deldari, 2005, Akhmedov and Al-Khowaiter, 2007).

Since the isomerisation is favoured at lower reaction temperatures, the ideal catalyst for this process should provide a sufficient activity to operate at low temperatures (Rase, 2000, Ertl et al., 2008).

The commercial catalysts used for the isomerisation of Light Straight Run (LSR) gasoline fraction are Pt-loaded chlorinated alumina and Pt-supported H-mordenite (Chica and Corma, 1999, Rase, 2000). Platinum-supported chlorinated alumina catalysts have been used due to their activity for isomerisation at low reaction temperatures, (97-197 °C). Nevertheless, this catalyst suffers from disadvantages that limit its use e.g. the need for a continuous supply of chlorine during the operation to maintain the acidity of the catalyst. This leads to several corrosion and environmental

problems in addition to its sensitivity to trace impurities in the feed such as water and sulphur. In contrast, zeolites exhibit higher acidity, good stability, and the ability to withstand feedstock contaminants. This makes zeolites the ideal alternative to replace chlorinated alumina in isomerisation-cracking processes (Bekkum, 2001b, Ono, 2003).

In recent decades, it has been found that sulphated zirconia (SZ) was an active material for the isomerisation of short alkanes including *n*-butane and *n*-pentane (Matsushashi et al., 1999, Yang et al., 2002). The acidity of this material was found to be 10^4 times stronger than concentrated sulfuric acid, therefore, it was considered as a “superacid” (Adeeva et al., 1998). The isomerisation of light naphtha over Pt/SZ was developed by Cosmo Oil Ltd. and Mitsubishi Heavy Industries Ltd., and commercialised by UOP LLC (Universal Oil Products) (Kimura, 2003, Ono, 2003, Akhmedov and Al-Khowaiter, 2007, Okuhara, 2004). The catalyst has the advantage of lower operation temperature compared with zeolite-based catalysts, however, the selectivity to isomerisation over that catalyst was limited for the isomerisation of small alkanes due to the extensive cracking of the produced *iso*-alkanes of hydrocarbons higher than C7 (Iglesia et al., 1993). The main disadvantage of that catalyst is the rapid deactivation as a result of coke formation in addition to the reduction of the sulphide species under the employed reaction conditions and the poisoning of the catalyst with sulphur (Akhmedov and Al-Khowaiter, 2007).

Later, it was found that Pt-supported tungstated zirconia (Pt/WZ) is more stable and selective to alkane isomerisation than Pt/SZ (Arribas et al., 2000, Akhmedov and Al-Khowaiter, 2007). This catalyst is more resistant to deactivation because sulphide species are not contained in this catalyst (Ono, 2003). Pt/WZ was found to be a promising catalyst for the conversion of waxy normal paraffin to middle distillate, in particular the heavy paraffin produced from the commercial Fischer-Tropsch processes (Zhang et al., 2001, Martínez et al., 2006). However, zirconia based catalysts are not commercialised at the present time due to the low surface area of these catalyst (Akhmedov and Al-Khowaiter, 2007).

In addition to amorphous oxides (Al_2O_3 , $\text{SiO}_2\text{-Al}_2\text{O}_3$, SZ) and zeolites (Y, Beta, Mordenite, ZSM-5, ZSM-22), other materials were used as solid acids in bifunctional catalysts of the conversion of *n*-alkanes such as silicoaluminophosphates (SAPO-11, SAPO-31, SAPO-41) and mesoporous materials (MCM-41, AIMCM-41) (Deldari, 2005).

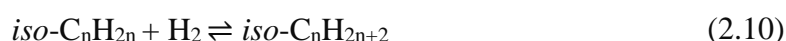
2.3.2 Reaction mechanism of *n*-alkane isomerisation and cracking

n-Alkane conversion can be conducted over acid catalysts (homogenous or heterogeneous) and over heterogeneous bifunctional catalysts *via* the formation of carbenium ions as reaction intermediates. The isomerisation of alkanes over acid catalysts and in the absence of hydrogen occurs when the *n*-alkane molecule is protonated over Brønsted acid sites to form a carbenium ion. The produced carbenium ion undergoes skeletal rearrangement to the corresponding isomer and then reacts with a new alkane molecule (hydrate transfer reaction) to produce isomerised alkane and new alkylcarbenium ion as illustrated in the reactions shown in Equations 2.3, 2.4, and 2.5 (Ono, 2003, Akhmedov and Al-Khowaiter, 2007).



For bifunctional catalysts, the mechanism involves dehydrogenation of the *n*-alkane molecule on the metallic sites to form the corresponding *n*-alkene. Thereafter, the alkene is transported to the acid sites and protonated to form a carbenium ion, which can either undergo structural rearrangement followed by deprotonation on the acidic sites and hydrogenation on the metallic sites and then desorbed as the isomer, or cracked through β -scission into a smaller carbenium ion and an alkene producing cracked products after hydrogenation (Blomsma et al., 1995, Bekkum, 2001b, Ono, 2003, Akhmedov and Al-Khowaiter, 2007).

The reactions involved over the bifunctional catalyst are illustrated in Equations 2.6-2.10:



The skeletal rearrangement of alkanes over solid acid catalysts can proceed through two possible reaction pathways: the monomolecular mechanism and the bimolecular mechanism. The monomolecular mechanism *via* the formation of the protonated cyclopropane (PCP) intermediate is more accepted for alkanes larger than *n*-butane since the transformation of the PCP into a secondary carbenium ion does not require very high energy, therefore, this rearrangement can take place on moderate acid strength and at low temperatures. The mechanism of PCP formation as a reaction intermediate is shown in Figure 2.7.

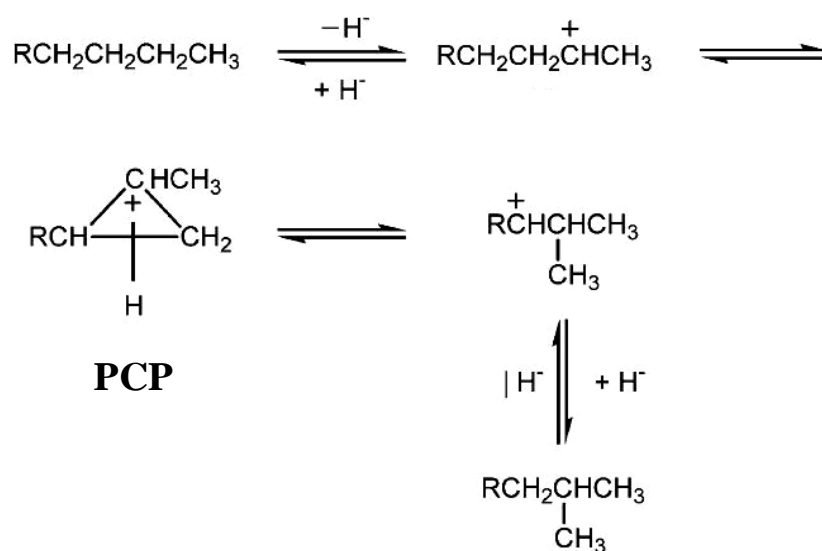


Figure 2.7 Rearrangement of carbenium ions *via* PCP intermediate over solid acid (Ono, 2003).

In contrast, the bimolecular mechanism is more likely expected in case of *n*-butane isomerisation since the monomolecular reaction involves the conversion of the secondary to primary carbenium ion, which is energetically not feasible when the energy level of the primary carbenium ion is higher than the secondary carbenium ion. The bimolecular mechanism of *n*-butane involves the oligomerisation of *n*-butene and the carbenium ion to form a C8 carbenium ion, thereafter, the newly carbenium ion is cracked to produce *iso*-butane and cracking products such as propane and pentane (Miyaji et al., 2002, Okuhara, 2004, Akhmedov and Al-Khowaiter, 2007). A scheme of the possible reaction pathways of *n*-alkanes isomerisation is shown in Figure 2.8.

For *n*-heptane and higher alkanes, it has been reported that the monomolecular mechanism is dominant and the oligomerisation-cracking takes place through β -scission of the carbenium ion to produce a lower alkene and a new carbenium fragment with different carbon number as shown in Figure 2.9 (Blomsma et al., 1995, Ono, 2003, Okuhara, 2004, Soualah et al., 2010, Weitkamp et al., 1983, Martens et al., 1991). In addition, the cracking rate increase with increasing the degree of branching, therefore, to enhance isomerisation, multi-branched paraffins must be reduced (Calemma et al., 2000, Deldari, 2005).

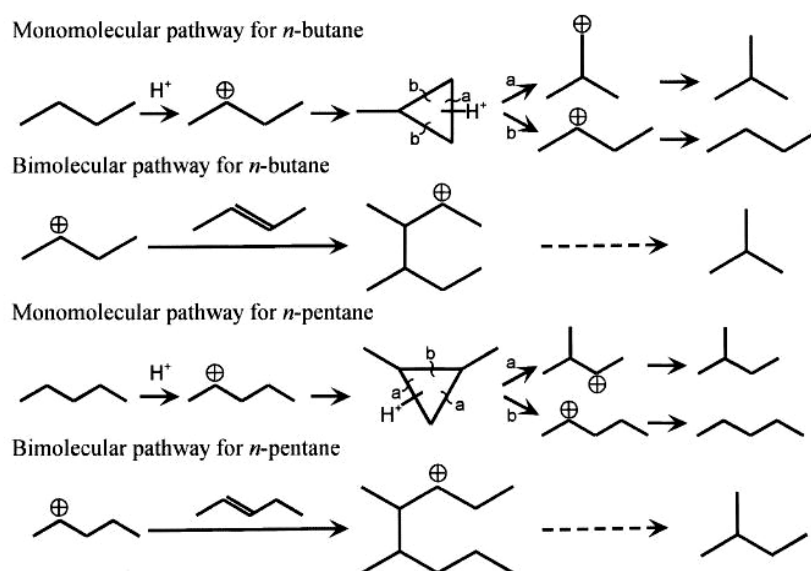


Figure 2.8 Reaction pathways for the isomerisation of *n*-butane and *n*-pentane an example of *n*-alkanes isomerisation (Okuhara, 2004).

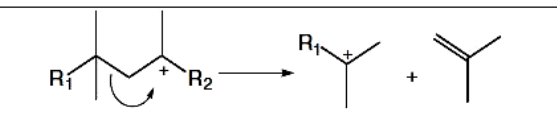
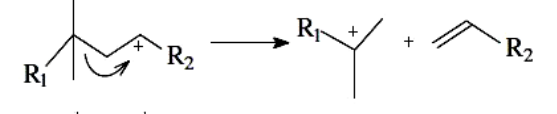
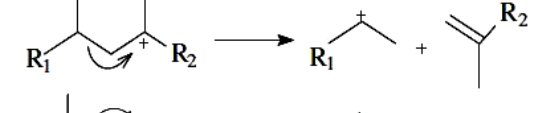
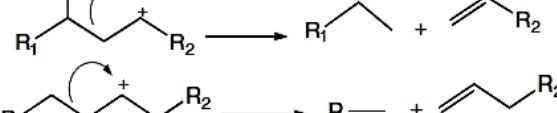
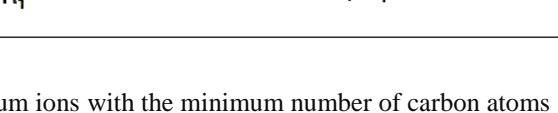
type	minimum carbon number	ions involved	rearrangement
A	≥ 8	tert \rightarrow tert	
B1	≥ 7	sec \rightarrow tert	
B2	≥ 6	tert \rightarrow sec	
C	≥ 5	sec \rightarrow sec	
D	≥ 4	sec \rightarrow prim	

Figure 2.9 Cracking modes of alkylcarbenium ions with the minimum number of carbon atoms required for each type (Soualah et al., 2010).

The rate of cracking of the tertiary carbenium ion is faster than the secondary carbenium ion, and the cracking rate of the secondary carbenium ion is faster than the primary carbenium ion (Akhmedov and Al-Khowaiter, 2007). In addition, it has been found that the isomerisation of *n*-pentane and *n*-hexane involves a very slow C type cracking (involving β -scission of secondary into secondary alkylcarbenium ions), whereas with *n*-heptane B type cracking appeared (involving β -scission of secondary into primary alkylcarbenium ions). For longer hydrocarbon chain, A cracking (involving β -scission of tertiary into tertiary alkylcarbenium ions) was found to be 50 times faster than B cracking (involving β -scission of tertiary into secondary alkylcarbenium ions) and 10,000 times faster than C cracking (Alvarez et al., 1996). Therefore, with increasing the hydrocarbon chain length the isomerisation selectivity decreased and the rate of the cracking reaction became more rapid (Calemma et al., 2000, Akhmedov and Al-Khowaiter, 2007).

2.4 Coking and deactivation

The term “coke” in heterogeneous catalysis refers to a mixture of heavy, low hydrogen content and non-volatile compounds that form on a catalyst surface as by-products during organic reactions. This material is strongly adsorbed on the catalyst surface causing catalyst deactivation by poisoning the active sites and/or pore blockage (Chen and Manos, 2004, Guisnet and Magnoux, 2001). Although the catalyst can be regenerated by coke oxidation, complete catalytic activity cannot be recovered due to some secondary effects such as the extreme regeneration conditions and the presence of water (Guisnet and Magnoux, 2001). Generally, the term “coke” is used to describe the carbonaceous deposits that remain at the catalyst surface and are removed by oxidation, and the term “coke precursor” is used to refer to the intermediate components that form coke in subsequent stages and can be removed from the catalyst by volatilisation in an inert gas (Chen and Manos, 2004).

Minimising the need for catalyst regeneration is an important economic objective in any industrial process, therefore, great efforts have been made to reduce deactivation by coking (Guisnet and Magnoux, 2001). It is important to know the main features of coke such as mechanisms of coke formation, parameters affects the rate of coking, coke characterisation, and the modes of catalyst deactivation by coke formation.

2.4.1 The mechanism of coke formation

The formation of carbonaceous deposits during hydrocarbon transformations over zeolites involves a complex series of reactions. These reactions most often include oligomerisation, cyclisation of the oligomers (rearrangement reactions), hydrogen transfer into monoaromatics (dehydrogenation), and alkylation of the monoaromatics followed by cyclisation and hydrogen transfer to produce bi- and tri-aromatics *etc.* (Guisnet and Magnoux, 1989). However, the heavy by-products of the reaction can be considered as “coke” only if they are irreversibly retained in the zeolite under reaction conditions (Guisnet and Magnoux, 1992).

The formation of coke can occur (i) in parallel with the desired reaction (competitive mode), (ii) consecutive to the desired reaction (successive mode), or (iii) from a combination of both modes (Guisnet and Magnoux, 1992).

Several parameters can affect the method of coke formation as shown in Section 2.4.2, however, there is a general agreement that coke formation modes depend strongly on reaction temperature. Guisnet and Magnoux, classified coke formed over zeolites and noble metal supported zeolites into two types: low temperature coke usually formed at reaction temperatures lower than 200 °C, which is non-polyaromatic in nature, results from oligomerisation and cyclisation of oligomers, and is depending largely on the type of reactants. The other type is high temperature coke formed at reaction temperatures greater than 350 °C. This is a highly ordered polyaromatic coke formed through hydrogen transfer reactions (dehydrogenation) in addition to oligomerisation and cyclisation reactions, and its formation is determined by the shape and size of zeolite pores (Guisnet and Magnoux, 2001, Guisnet et al., 2009).

A similar classification was established by Bauer and Karge (Bauer and Karge, 2006), where coke was classified into “coke-type I” that formed at low temperatures and results from condensation, oligomerisation and alkylation reactions of reactant and/or intermediate molecules, and “coke-type II” formed at higher reaction temperatures where reaction steps that required high activation energies are involved, e.g. cyclisation, cracking and hydrogen transfer. Figure 2.10 shows a scheme of the proposed mechanism of coke formation.

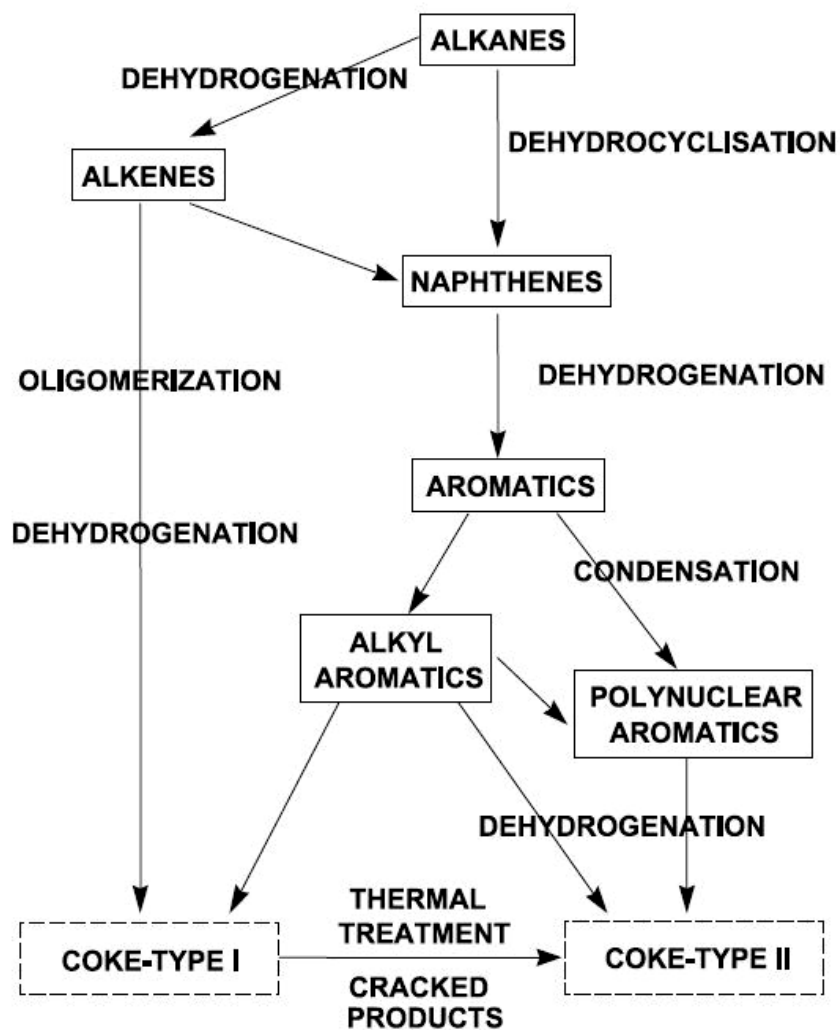


Figure 2.10 Schematic drawing of the mechanism of coke formation from hydrocarbons over acid and bifunctional catalysts (Bauer and Karge, 2006).

2.4.2 Parameters affecting the rate of coke formation

The rate of coke formation is affected by the same parameters that affect the rate of the catalytic reaction itself including: the nature of reactants, catalyst pore structure, catalytic activity, and operating conditions (Guisnet and Magnoux, 1997). In this section, the influence of each parameter is briefly discussed.

2.4.2.1 Influence of reactant nature

It is generally believed that some hydrocarbons such as alkenes and polyaromatics, have a tendency to form coke more rapidly than others such as alkanes or monoaromatics (Guisnet and Magnoux, 1997). The fast rate of coke formation from alkenes is due to their high reactivity, thus these reactive molecules can easily undergo condensation reactions and form bulkier, and polar molecules that are trapped inside zeolite pores. Polyaromatic compounds are not as reactive as alkenes, but their retention inside the zeolite pores is attributed to their bulky size; this allows for longer residence time inside zeolite pores and longer contact with the active sites, and consequently the formation of heavier molecules, which cannot diffuse from zeolite pores (Guisnet et al., 2009).

2.4.2.2 Influence of pore structure

Coking is a shape selective reaction (Rollmann, 1977, Karge, 1991), therefore, zeolite pore structure plays a significant role in determining the size and the shape of coke molecules and the rate of coke formation. Consequently, the shape of coke molecules is determined by the shape of cages, channels and channel intersections of zeolite, while the maximum size of coke molecules that can be trapped inside the pores is intermediate between the size of the cages or channel intersection and the size of pore apertures (Guisnet and Magnoux, 2001, Magnoux et al., 1989). Therefore, the coking rate is increased when the steric constraints are large enough to allow for the formation of coke intermediates, and when the diffusion of these intermediates through the pore aperture is slow (Bauer and Karge, 2006, Guisnet and Magnoux, 1989).

2.4.2.3 Influence of active sites

The strength and the density of zeolite active sites have a strong influence on the rate of coke formation. This is because coke forms favourably on the strongest acid sites causing their deactivation (Brillis and Manos, 2003). Therefore, the high strength of the acid sites can result in faster chemical steps hence a faster coking rate. Likewise, the high density of the acid sites leads to an increased probability of condensation reactions of reactant molecules and thereby a faster coking rate (Guisnet et al., 2009).

2.4.2.4 Influence of operating conditions

There is direct relation between the rate of reaction and reaction temperature, as described through the Arrhenius equation. Therefore, it is expected that the rate of coke formation increase with increasing reaction temperature. On the other hand, high temperatures increase the desorption rate of coke intermediates, therefore, it is widely accepted that the retention of coke inside the pores at high temperature is due to pore blockage; while at low temperature is attributed to the strong adsorption of coke molecules (Brillis and Manos, 2003). Moreover, increasing reactant pressure can lead to an increase in the rate of coking (Guisnet and Magnoux, 1997).

2.4.3 Modes of catalyst deactivation by coke formation

It is generally accepted that coke deposits may deactivate the catalyst either by poisoning (covering) the active sites, or by pore blocking (Forzatti and Lietti, 1999, Guisnet et al., 2009). However, the deactivating effect as a result of coke formation is more pronounced when deactivation is due to pore blockage than when it is due to active site poisoning (Guisnet and Magnoux, 1989, Rombi et al., 1999). In this case, one active site can be deactivated per coke molecule, whereas, pore blockage by a single coke molecule can limit or prevent reactant molecules from accessing all the active sites located inside the blocked pore (Guisnet et al., 2009).

Coke can be accumulated within catalyst pores in three modes: uniform surface deposition (Richardson et al., 1996), pore-mouth plugging (Muegge and Massoth, 1991, Wang, 2007, Zhao, 2008) and bulk-phase plugging (Richardson et al., 1996, Zhao, 2008, Zhang et al., 2005). Each mode has different influence on the diffusivity of reactants and consequently, on the catalytic activity. In uniform surface deposition, it has been suggested that coke deposits are distributed uniformly through the catalyst micropores system, however, pore channels are expected to narrow to smaller sizes which consequently leads to lower diffusion rate and more likely to lower catalytic activity (Richardson et al., 1996).

The pore-mouth plugging mode assumes the accumulation of coke deposits near the pore mouths, thus limiting reactant molecules from accessing the active sites inside

the micropores thereby causing lower diffusion rates but without complete blockage. In this mode very few of the active sites are covered by coke and the catalytic activity would be proportional to the number of the accessible active sites (Muegge and Massoth, 1991, Wang, 2007).

The bulk-phase plugging mode involves the two previous coke deposition modes, however, larger amounts of coke formed on the catalyst outer surface causing complete pore blockage (Zhang et al., 2005, Zhao, 2008).

2.4.4 Characterisation of coke deposits

The characterisation of coke deposits is considered the key to understanding the mechanism behind coke formation (Guisnet and Magnoux, 2001). Several techniques have been developed to characterise carbonaceous deposits, however, a single technique cannot provide clear information about coke composition. Therefore, the multi-technique approach is widely used to understand coking and deactivation. A number of spectroscopic techniques have been utilised for catalytic coke characterisation such as infrared (IR) spectroscopy, Laser Raman spectroscopy, ultraviolet-visible (UV-Vis) spectroscopy and nuclear magnetic resonance (NMR) spectroscopy. These techniques are non-destructive and can provide different information about coke such as the nature of the interaction between the coke molecules and the active sites (Guisnet et al., 2009, Karge, 1991). However, these spectroscopic techniques cannot provide information regarding coke thermal reactivity; therefore, temperature programmed techniques are usually used to explore coke reactivity, structure and location (Querini and Fung, 1997).

Generally, coke characterisation approaches can be classified into two categories: *ex situ* (post-reaction) characterisation and *in situ* characterisation. *Ex situ* approach is relatively easier to perform, lower cost, least sophisticated instrumentation can be used, and generally requires less time to achieve the characterisation. Although this approach yields interesting information, it may not provide direct insight into the processes of coke formation during the reaction (Wulfers and Jentoft, 2013). In contrast, the *in situ* characterisation enables the catalyst scientist to identify and understand the important steps, e.g., the formation of important reaction intermediates

and active sites, and stages in a catalyst's lifetime, such as activation/deactivation. However, this approach requires developed characterisation techniques as well as the design and construction of appropriate *in situ* cells and reactors (Beale et al., 2015).

Guisnet and Magnoux, established an *ex situ* method for the identification of the chemical species presented in coke formed over zeolite. This method involves the separation of coke from the spent zeolite by the digestion of the zeolite framework in hydrofluoric acid (HF), followed by the extraction of the soluble coke by dichloromethane (CH₂Cl₂). The soluble coke is then analysed by gas chromatography-mass spectrometry (GC-MS) and the insoluble coke is characterised using spectroscopic techniques (Guisnet and Magnoux, 1989).

2.5 The role of coke in hydrocarbon transformations

It is widely known that catalyst deactivation caused by coke deposition is harmful and expensive for the industry, therefore, great efforts have been made to reduce the consequences of this problem. Nevertheless, coke can sometimes play a beneficial or active role in enhancing catalyst performance (Menon, 1990).

2.5.1 The beneficial role of coke

Zeolite shape selectivity depends on zeolite pore size and structure, which can be influenced by coke deposition. The modification in zeolite pores by coke deposits can sometimes lead to an improvement in zeolite shape selectivity by limiting the diffusivity of some reactant and product molecules through zeolite pores (Chen et al., 1997a, Guisnet, 2002a). Coke can enhance product selectivity of several hydrocarbon transformations, through the deactivation of the non-selective acid sites and/or improving zeolite sieving properties by the alteration in pores dimensions (Guisnet, 2002b, Guisnet, 2002a). This will be named hereafter as "beneficial role". A good example about the beneficial role of coke is the skeletal isomerisation of *n*-butene to *iso*-butene over ferrierite zeolite, it has been reported that the aged catalyst exhibits higher selectivity toward *iso*-butene than the fresh one and consequently lower cracking and oligomerisation by-products are observed over an aged catalyst. This improvement in *iso*-butene selectivity was ascribed to the formation of carbonaceous

deposits that deactivate the acid sites responsible for the cracking reactions in addition to the modification of zeolite pore dimensions (Van Donk et al., 2001).

Several studies in the literature have been performed to investigate the role of carbonaceous deposits in hydrocarbons transformations over different zeolites. However, the majority of these studies focused on the conversion of hydrocarbons lighter than C5 which is not necessarily directly applicable to heavier hydrocarbons. One of these studies investigated the role of coke deposited over ferrierite zeolite in the skeletal isomerisation of 1-butene by utilising propene as a pre-coking agent. Propene was selected as it is a small molecule, which allows for the formation of internal coke inside ferrierite pores without causing pore blockage. It has been found that even a small weight loading (0.8 wt.%) of carbonaceous deposits within the inner pores of ferrierite zeolite was sufficient to modify the pore structure of the zeolite, leading to a noticeable enhancement of the selectivity to *iso*-butene in comparison to the fresh zeolite (Seo et al., 1996).

Another study carried out by Villegas *et al.* focused on the deactivation behaviour of ZSM-5 and Beta zeolites during the isomerization of *n*-butane. The study showed that most of the coke deposits were formed during the first 70 min on stream causing a decrease on *n*-butane conversion along with an increase in *iso*-butane selectivity. This was ascribed to coke formation inside the zeolite pores, which plays a crucial role in limiting the side reactions and enhancing the isomerisation efficiency. Furthermore, it was found that the regenerated Pt-modified zeolites possess higher isomerisation efficiency than the fresh catalysts owing to the modification of the pore size and structure by coke deposits (Villegas et al., 2006).

The role of coke deposits on the catalytic performance of SAPO-34 was also highlighted in the conversion of methanol to olefins (MTO). It has been demonstrated the carbonaceous deposits form rapidly (4 wt.%) in the first few minutes of reaction, however, these deposits play a significant role in reducing the rate of coking. In addition, the selectivity to olefins, in particular, ethylene and propylene was maximised at a coke content of about 5.7 wt.% (Qi et al., 2007).

2.5.2 Carbonaceous deposits as an active species

In catalytic hydrocarbon transformations, various carbonaceous intermediates can be formed over the surface of the catalyst, these hydrocarbon species are produced from the dissociation of reactant molecules. Previous research proposed that the carbonaceous overlayer with or without oxygen can have a positive role on catalyst performance and can be considered as the active layer in several hydrocarbon reactions such as Mobil methanol to gasoline process and Fischer-Tropsch synthesis (Menon, 1990).

The role of coke as an active species had been and continue to be the subject of interest of several studies for instance; a study performed by Chen *et al.* on the role of coke deposits originated from different hydrocarbon precursors in MTO over SAPO-34. It has been proposed that carbonaceous species originated from oxygenates promoted olefin yield and are considered as the active surface in the reaction, whereas carbonaceous species originated from olefins have only a deactivating effect through pore blockage (Chen *et al.*, 1997b).

Another study conducted by Lee *et al.*, suggested that carbonaceous residues formed over FCC catalyst *via* isopropanol pre-coking at 773 K, were catalytically active in the alkylation of *p*-xylene at 473 K, and it has been observed that no reaction occurred over the fresh catalyst at this temperature (Lee *et al.*, 2004).

McGregor *et al.* investigated the role of coke as catalytically active species in the dehydrogenation of light alkanes where it has been demonstrated that highly ordered carbonaceous deposits encapsulated the surface of VO_x/Al₂O₃ at high reaction temperature, and act as the active layer in the dehydrogenation of butane in the absence of gas-phase oxygen. This was revealed from the significant increase in the yield of C₄ compounds, the high conversion of butane, and the high selectivity to 1-butene (McGregor *et al.*, 2010).

Ethanol conversion into higher hydrocarbons is another relevant transformation in which carbonaceous deposits may play a positive role. Pinard *et al.* concluded that carbonaceous deposits formed over H-ZSM-5 zeolite in ethanol transformation at

623 K and 30 bar are composed mainly of alkylbenzenes and alkyl-naphthalenes, and that radical species present in this aromatic pool are the active species in catalysing ethanol transformation into hydrocarbons over H-ZSM-5 (Pinard et al., 2013).

Guisnet, has reported another type of catalytically active coke involved in the isomerisation-cracking of *n*-alkanes. It has been proposed that the carbonaceous deposits trapped inside the pores of the fresh zeolite during the first minutes of reaction participate in catalysing the isomerisation reaction selectively at the catalyst pore mouth. This has been suggested to interpret the high selectivity to *iso*-butene observed in the skeletal isomerisation of *n*-butene over aged H-FER. It has been proposed that coke molecules located near the pore mouth and interacting with protonic sites are most likely the active sites for the selective *n*-butene isomerisation as illustrated in Figure 2.11. A similar conclusion has been reported for the hydroisomerisation of long chain *n*-alkanes over Pt/H-TON. It has been assumed that the hydroisomerisation of *n*-decane over TON zeolite is catalysed by tertiary carbenium ions formed at the pore mouth as a result of the adsorption of methyl alkenes trapped in the zeolite pores during the first minutes of reaction, as shown in Figure 2.12 (Guisnet, 2002a).

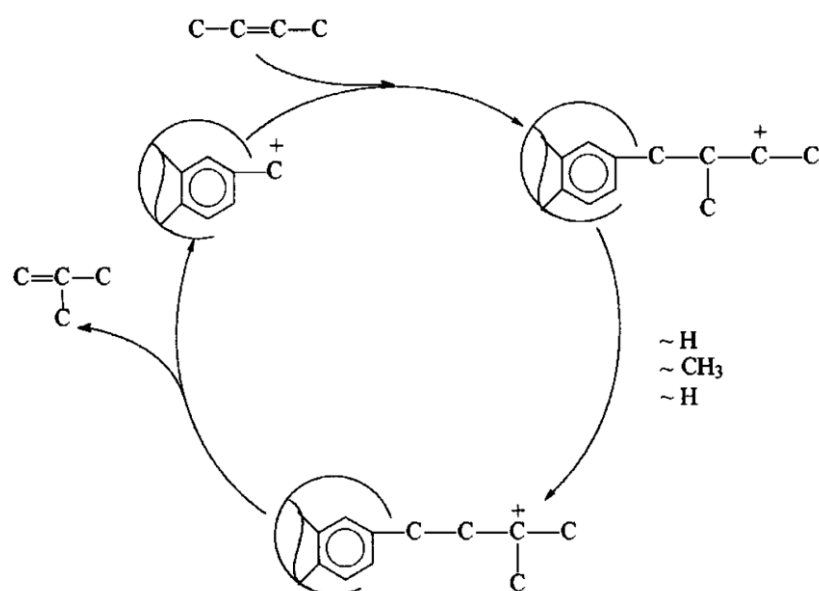


Figure 2.11 The proposed mechanism of *n*-butene isomerisation into *iso*-butene over coked H-FER (Andy et al., 1998).

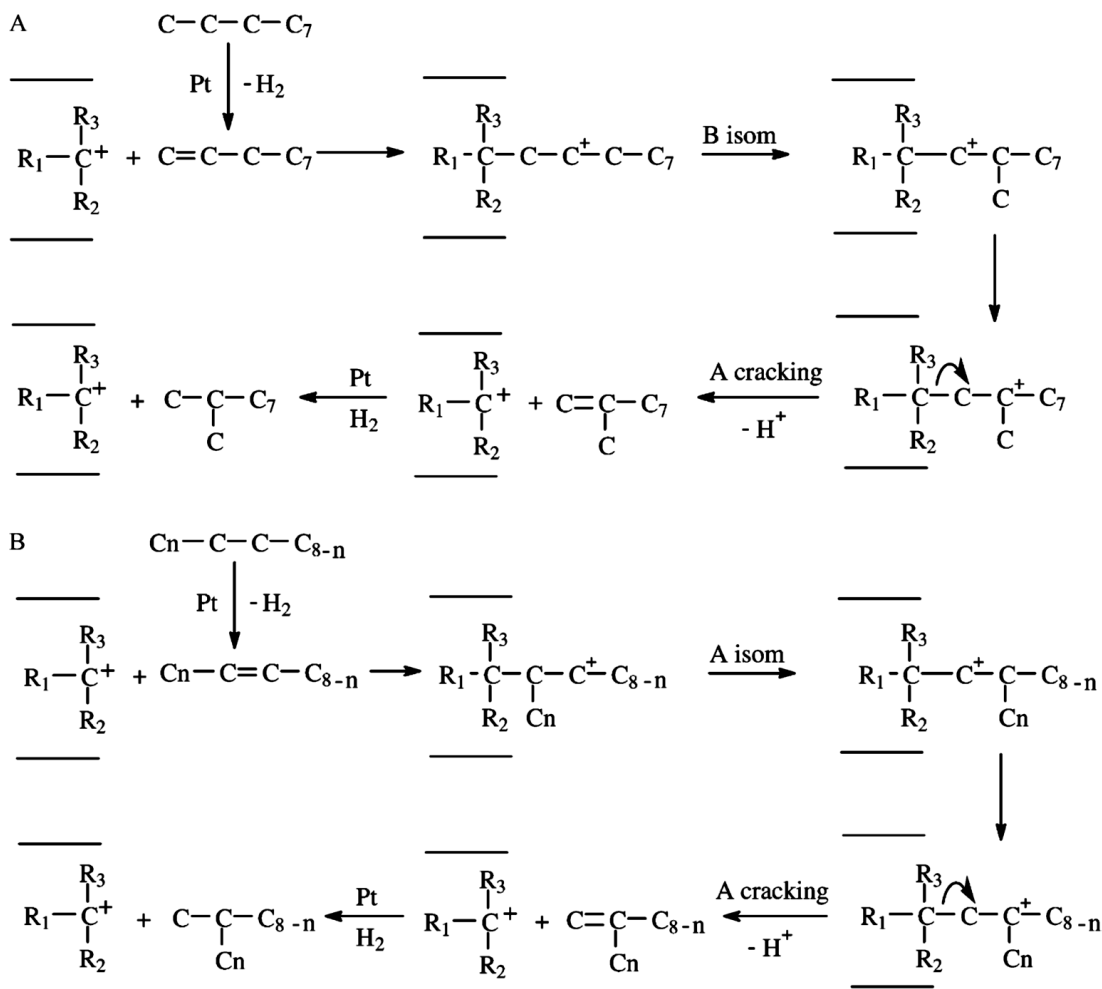


Figure 2.12 The proposed mechanism of *n*-decane hydroisomerisation over tertiary carbenium ions located at TON pore mouth (Guisnet, 2002a).

The presented examples confirm that coke deposition can play a positive role in improving product selectivity in hydrocarbon transformations. In this research, the role of carbonaceous deposits formed during the isomerisation-cracking of *n*-pentane and *n*-hexadecane over Pt/H-Beta will be investigated in Chapter 5 and 6, respectively. Whilst, Chapter 7 will demonstrate that tailored carbon deposition through catalyst pre-coking can be utilised to enhance the catalytic performance in *n*-hexadecane conversion. Further details from the literature specific to each chapter can be found in the introduction of each relevant chapter.

Chapter 3

Experimental work

3 Chapter 3: Experimental work

3.1 Introduction

This chapter explains the materials and methods used in preparing the catalysts employed in the present work in heterogeneous reactions. It also describes the equipment set-ups and procedures utilised to perform the catalytic activity measurements for both *n*-pentane conversion (Chapter 5) and *n*-hexadecane conversion (Chapter 6 and 7). A general explanation regarding the principles of gas chromatography alongside methods developed for component detection is presented in Section 3.5. Finally, Section 3.6 in this chapter gives details about the calculation of the catalytic performance indicators (conversion and selectivity) and experimental error quantification.

3.2 Materials

The specification and the application of gases used in this work are listed in Table 3.1. All of the employed gases were supplied by BOC industrial gases. The zeolites and the chemical reagents utilised in this research with their specifications are identified in Table 3.2.

Table 3.1 Specifications of gases employed.

Gas	Application
Air (Zero grade)	Catalyst calcination, TGA reactive gas
Argon (Zero grade)	TPR carrier gas
Helium (>99.996%)	GC carrier gas, TPO carrier gas, purging gas
Hydrogen (99.995 %)	Hydroisomerisation reaction carrier gas
5 % Hydrogen /Argon	TPR reactive gas
Nitrogen (Oxygen free)	GC make-up gas, TGA carrier gas
5 % Oxygen / Helium	TPO reactive gas

Table 3.2 Names and specifications of chemicals and zeolites used in this work.

Material	Supplier	Specifications
Alkane standard solution	Sigma-Aldrich	C8-C20, ~ 40 mg/L each, in hexane
Ammonium nitrate	Acros Organics	99+ %, for analysis
2,6-Di-tert-butylpyridine	Acros Organics	97 %
Ethanol	Sigma-Aldrich	Absolute \geq 99.8 %
Hydrochloric acid	Sigma-Aldrich	ACS reagent, 37 %
<i>n</i> -Heptane	Fischer-Scientific	HPLC grade, 99 %
<i>n</i> -Hexane	Sigma-Aldrich	\geq 99 %
<i>n</i> -Hexadecane	VWR	\geq 99 %
<i>n</i> -Pentane	VWR	99.8 %
Sodium hydroxide	Sigma-Aldrich	97 %
Tetraammineplatinum (II) chloride hydrate	Sigma-Aldrich	98 %
Tetraethylorthosilicate	Sigma-Aldrich	\geq 99 %
Toluene	Sigma-Aldrich	99.5 %
2,2,4-Trimethylpentane	Acros Organics	99+ %
Zeolite ZSM-5	ACS material	Extrudate, 38:1 SiO ₂ /Al ₂ O ₃ mole ratio
Zeolite H-Beta	Alfa Aesar	Powder, 360:1 SiO ₂ /Al ₂ O ₃ mole ratio

3.3 Catalyst preparation

For the purpose of this research, the high silica zeolite H-Beta has been exposed to different surface modifications:

- Zeolite desilication by base leaching using diluted NaOH to reduce silicon content in the zeolite framework.
- Selective poisoning of Brønsted acid sites located at the external surface of zeolite H-Beta by pre-adsorption of 2, 6-di-tert-butylpyridine (DTBP).
- Metal loading for the synthesis of the bifunctional catalyst.

- Bifunctional catalyst modification by covering the hydroxyl groups located at the external surface and the pore mouth region using chemical liquid deposition of tetraethoxysilane (known as silylation).

3.3.1 Zeolite modification by desilication

The purpose of this post-synthesis treatment is to generate mesoporosity in the zeolite micropore system through the selective removal of silicon atoms from the zeolite framework. This treatment is also known as base leaching or alkaline treatment, and it is widely used to improve the resistance of zeolites to deactivation and enhance catalyst performance in hydrocarbon transformation processes. This is achieved through the improvement of the diffusion rate of reactant and/or product molecules through zeolite channels (Groen et al., 2008, Bleken et al., 2013, Van Donk et al., 2003). A schematic drawing of the desilication treatment is shown in Figure 3.1.

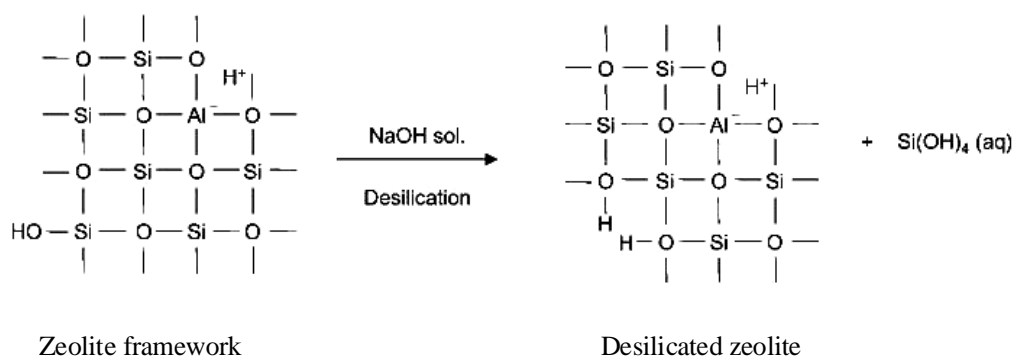


Figure 3.1 Schematic representation of zeolite post-synthesis modification by the desilication treatment to create mesoporosity in zeolite micro-structure (adapted from (Groen et al., 2005)).

In this work, the desilication procedure was adapted from previous work in the literature (Groen et al., 2008, Al-zaidi, 2011, Bleken et al., 2013). The high silica zeolite H-Beta (Alfa Aesar, SiO_2/Al_2O_3 of 360:1 mole ratio, surface area $620 \text{ m}^2 \text{ g}^{-1}$) was desilicated using 0.025 M aqueous NaOH solution as a desilication agent. This molarity was selected after several attempts of treating zeolite H-Beta with higher concentration of NaOH such as 0.1 M, which resulted in a total dissolution of the zeolite.

To perform the desilication treatment, each 1 g of zeolite H-Beta was suspended in 25 mL of 0.025 M NaOH solution. This was followed by heating to 80 °C under reflux with continuous stirring for 1 h. Afterwards, the mixture was cooled down rapidly using an ice bath to quench the desilication reaction. The suspended zeolite was separated from the solution using a centrifuge (Heraeus Multifuge 3SR plus refrigerated centrifuge, Thermo Scientific) operated at 6000 rpm at 20 °C for 5 min. Subsequently, the treated zeolite was thoroughly washed with distilled water followed by centrifuge separation. This was repeated several times until the pH of the solution dropped to 7 as measured by pH indicator paper. The treated zeolite was then dried at 110 °C in an oven overnight to remove any moisture from the solid.

The generated zeolite after the base leaching was in the cationic Na-form, therefore, the zeolite was first ion exchanged with 0.5 M of NH₄NO₃ aqueous solution to produce the H-form using 10 mL of the solution for each 1 g of the zeolite in two consecutive treatments at 80 °C under reflux with a continuous mixing for 2 h.

The H-form of the desilicated zeolite was then obtained through calcination of the treated zeolite in a static air furnace at 550 °C for 4 h. Finally, the desilicated H-Beta zeolite was further modified by metal loading to prepare the bifunctional catalyst, as described in Section 3.3.3.

3.3.2 Pre-adsorption of 2,6-di-tert-butylpyridine (DTBP)

Brønsted acid sites located at the external surface of zeolite crystals are thought to be responsible for catalysing the undesired reactions that ultimately lead to coke formation. One of the approaches that have been applied for the deactivation of such sites is the pre-adsorption of base molecules that selectively poisoning these sites (Yaluris et al., 1996).

In this work, 2,6-di-tert-butylpyridine (DTBP) was used as a poisoning agent to deactivate these sites through liquid phase adsorption. DTBP is considered a moderate base with a kinetic diameter of 0.79 nm (Jentoft, 2014, Wang et al., 2011). This molecule is larger than the pore openings of zeolite Beta, which has large channels with a cross section of 0.66×0.67 nm and medium channels with a cross section of

0.56×0.56 nm (Baerlocher et al., 2007). Consequently, DTBP cannot penetrate through the zeolite pores, and is mainly adsorbed by Brønsted acid sites located at the external surface of the zeolite crystal and the accessible acid sites located in the pore mouth region (Wang et al., 2011). The surface reaction of DTBP with zeolite Brønsted acid sites is shown in Figure 3.2.

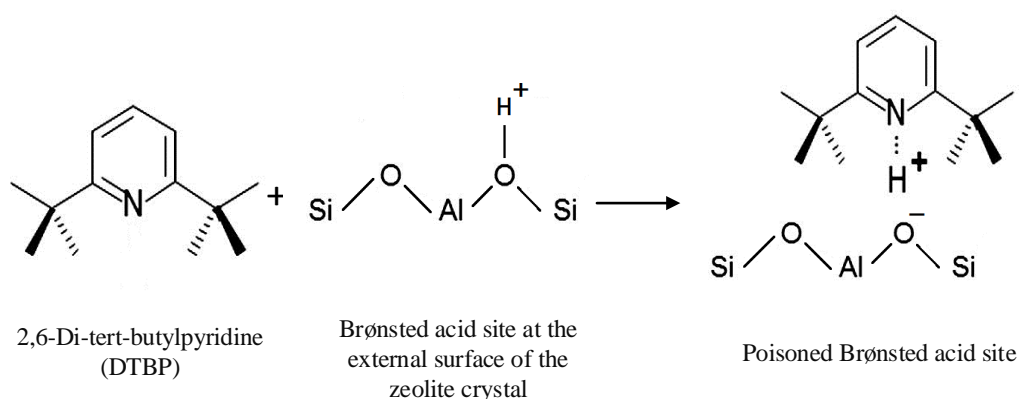


Figure 3.2 Poisoning of zeolite Brønsted acid sites located at the external surface by the pre-adsorption of DTBP (adapted from (Gounder et al., 2012)).

The poisoning of zeolite H-Beta was carried out by adding ~3 vol.% of DTBP to the zeolite-solvent mixture. *n*-Pentane was used as a solvent. Each 1 g of zeolite was added to 60 mL of *n*-pentane, followed by the addition of 2 mL of DTBP. The mixture was stirred constantly for 24 h at 4 °C. Afterwards, pentane was allowed to evaporate from the catalyst at ambient temperature followed by further drying at 250 °C in an oven overnight.

3.3.3 Zeolite modification by metal loading

The original and modified zeolite H-Beta employed in the present work were subjected to further modification by metal loading to synthesise the bifunctional catalysts. This catalyst consists of 0.45 wt.% Pt supported on zeolite H-Beta and was used in both *n*-pentane conversion (Chapter 5) and *n*-hexadecane conversion (Chapters 6 and 7).

Pt was used to provide the catalyst with the metallic sites required for catalysing hydrogenation-dehydrogenation reactions, and zeolite H-Beta was utilised as an acidic support for carbon-carbon bond rearrangement. The percentage of Pt loading was selected following a study of previous work. It has been established that a noble metal

such as Pt or Pd at a loading of between 0.4-0.6 wt. % can create a balance between metallic and acidic sites to enhance hydroisomerisation over hydrocracking (Gary and Handwerk, 2001, Deldari, 2005). The preparation of this catalyst has previously described in the literature (Tsai et al., 2011, López et al., 2010, Park and Ihm, 2000). In this work, 0.5 wt.% of Pt was introduced to zeolite H-Beta *via* wet impregnation with excess water. The modification steps is shown in Figure 3.3.

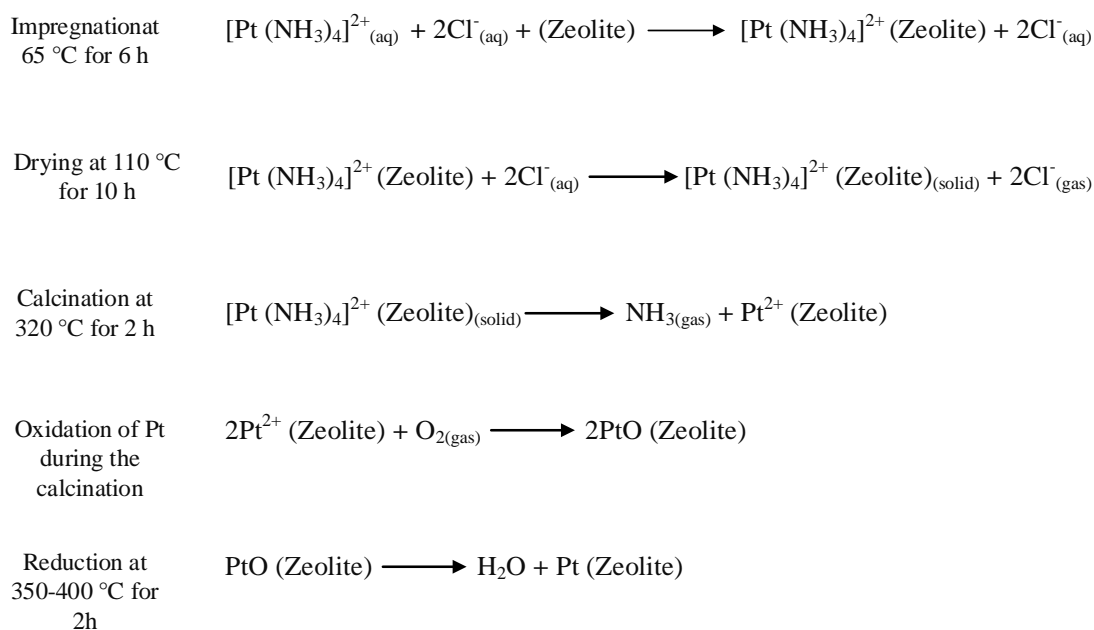


Figure 3.3 The preparation steps of Pt/H-Beta (adapted from (Abudawood, 2010, Yao and Yao, 2016)).

First, the zeolite was suspended in an aqueous solution of tetra-ammine platinum (II) chloride ($\text{Pt}(\text{NH}_3)_4\text{Cl}_2 \cdot x\text{H}_2\text{O}$) (98 wt.%, Sigma-Aldrich) in a ratio of 1:20 by weight. This contained the amount of salts required to achieve 0.5 wt.% metal loading, assuming a complete uptake of Pt by the catalyst. Then, the solution was kept under reflux at 65 °C for 6 h with constant stirring to ensure a homogeneous distribution of Pt on the support. After impregnation, the catalyst was dried at 110 °C in an oven for 10 h. It was then calcined in a tubular flowing air furnace (Elite Thermal System Limited) using a controlled heating programme, from ambient temperature to 320 °C at a ramp rate of 10 °C min⁻¹, and then maintained at the final temperature for 2 h. The

prepared catalyst was reduced prior to the reaction using pure H₂ at a temperature range 350-400 °C for 2 h.

3.3.4 Silylation modification

In this modification, the hydroxyl groups present at the external surface and close to the pore opening (pore mouth region) of the bifunctional catalyst were covered with an inert layer of silica (SiO₂) through the chemical deposition of a bulky organosilicon compounds, such as tetraethoxysilane (TEOS). It was found that this modification resulted in the narrowing of the pore-opening size and the deactivation of the external surface (Hibino et al., 1991, Chudasama et al., 2005, Bauer et al., 2007).

The silylation agent used for this purpose was tetraethoxysilane (TEOS), as the large kinetic diameter of this molecule (0.89 nm) prevents its penetration inside the pores of zeolite Beta (Chudasama et al., 2005). The surface reaction of TEOS with zeolite hydroxyl groups is shown in Figure 3.4.

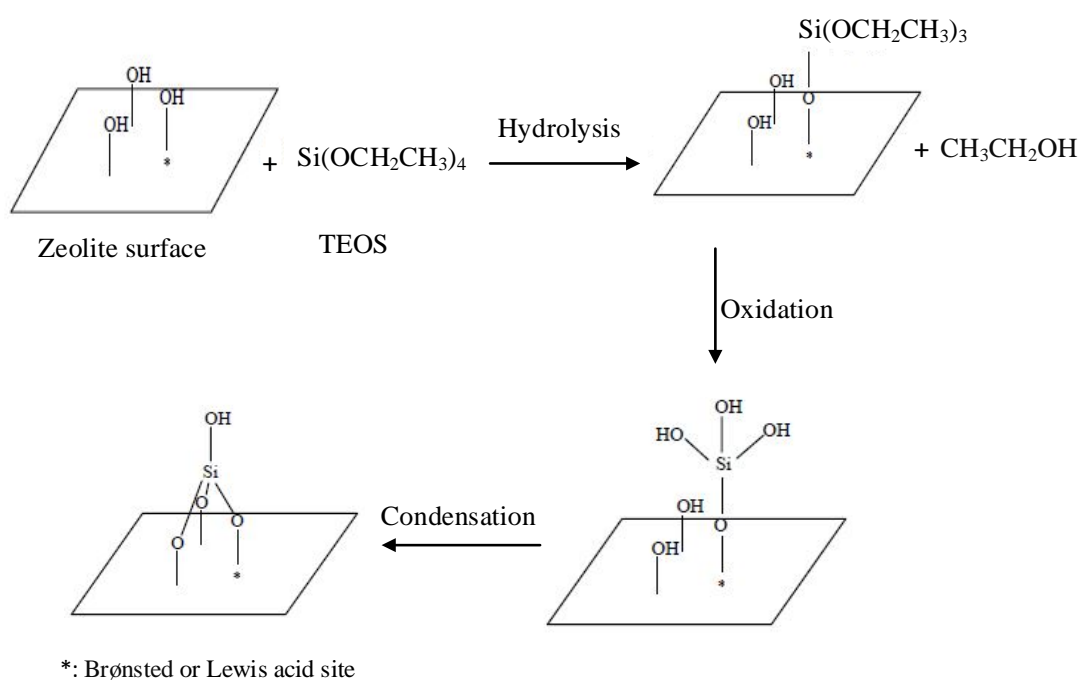


Figure 3.4 Schematic representation of the silylation reaction between TEOS and the surface hydroxyl groups of zeolite (Zheng et al., 2002).

The silylation was performed following previous work in the literature (Zheng et al., 2002). Each 1 g of the prepared Pt/H-Beta catalyst was suspended in 25 mL of *n*-hexane and the mixture was heated with continuous stirring under reflux. Then, 0.15 mL of TEOS was added to the mixture and the reaction was carried out for 1 h under reflux and continuous stirring. Afterwards, the reaction was stopped by immersing the flask in an ice bath; *n*-hexane was then removed using a vacuum evaporator at 50 °C. The collected catalyst was dried at 120 °C in an oven to remove ethanol, which is a side product of the silylation reaction, and then calcined at 500 °C in a furnace for 4 h to remove the unreacted TEOS and other physisorbed materials (Weber et al., 2000). The silylation reaction was performed in 2 cycles, including the calcination step, to ensure the coverage of the external and pore mouth acid sites with silica.

3.4 Experimental set-ups and procedures

3.4.1 Catalytic isomerisation-cracking of *n*-pentane

3.4.1.1 Reactor set-up

The catalytic isomerisation-cracking reaction of *n*-pentane (Chapter 5) was carried out in the gas phase under atmospheric pressure using a continuous flow-fixed bed reactor (Cone Closure Reactor Assembly Model # 401C-1209, Parker-Autoclave Engineers). A labelled schematic drawing of the reactor unit is shown in Figure 3.5. The reaction unit consists of a tubular reactor constructed from 316 stainless steel, with an internal diameter of 7.9 mm and total length of 279.4 mm, placed inside a single heating zone furnace. The reactor temperature was controlled and monitored using a UHC-240 Series Temperature Controller (Parker-Autoclave Engineers) connected to a movable K-type thermocouple that approaches the catalyst bed to measure the process temperature. In addition, another K-type thermocouple was attached to the internal wall of the furnace to control the heater over-temperature. The reactor was isolated using an insulation jacket to minimise temperature gradients.

The flow rate of the inlet gas was controlled using an electronic mass flow controller (Aalborg Gas Flow Controller GFC) and was calibrated for both H₂ and He flow rates. For switching between these two gases, a three-way ball valve was installed upstream

of the inlet of the mass flow controller. The reactor inlet and outlet lines were all heated to 80-100 °C with temperature controlled rope heaters and insulated to avoid condensation of reactants or products. The temperature of these heaters was controlled using a temperature controller made in-house with K-type thermocouples.

n-Pentane was fed to the reactor as a vapour by the gas flow saturation method, using H₂ as a carrier gas. For this purpose, a three-legged glass saturator fitted with a bypass was utilised. The partial vapour pressure of *n*-pentane in the H₂-pentane mixture was held at 0.243 bar calculated *via* Antoine equation at 0 °C, by immersing the saturator in a temperature-controlled bath containing an ethylene glycol and water mixture in ratio of 1:3 by volume.

The composition of the outlet gases was determined simultaneously by on-line gas chromatography (Shimadzu QP2010SE) fitted with an auto-sampling loop. A schematic drawing of the system employed in the *n*-pentane isomerisation-cracking reaction is shown in Figure 3.6.

3.4.1.2 Catalyst pelletisation

Before packing the catalyst in the reactor to perform the catalytic testing, it is necessary to granulate it to a suitable particle size in order to avoid channelling through the catalyst bed. For fixed bed reactors in gas-solid operations, the ratio of the tube diameter (d_t) to catalyst particle diameter (d_p) plays a significant role in reducing pressure drop (ΔP) across the catalyst bed. ΔP is very sensitive to the bed voids, therefore, it is essential to keep this ratio more than 10 according to the rules suggested for laboratory scale heterogeneous catalyst testing (Pérez-Ramírez et al., 2000, Afandizadeh and Foumeny, 2001). In addition, the ratio of the catalyst bed length (L_b) to particle diameter (d_p) has to be more than 50 to justify neglecting the effect of axial dispersion (Pérez-Ramírez et al., 2000, Sie, 1996).

In the present work, a particle size of 250-425 μm was chosen to achieve a ratio of 23 for $d_t/d_{p(Avg)}$ and a ratio of 60 for $L_b/d_{p(Avg)}$. The catalyst was first shaped to pellets of 13 mm in diameter. Each pellet was formulated by pressing approximately 0.2 g of the powder into a die (Specac) to approximately 5 tons using a pneumatic press

(Specac). Afterwards, the pellets were crushed carefully using a mortar and sieved to a particle size of 250-425 μm using a sieve shaker (AS-200, Retsch).

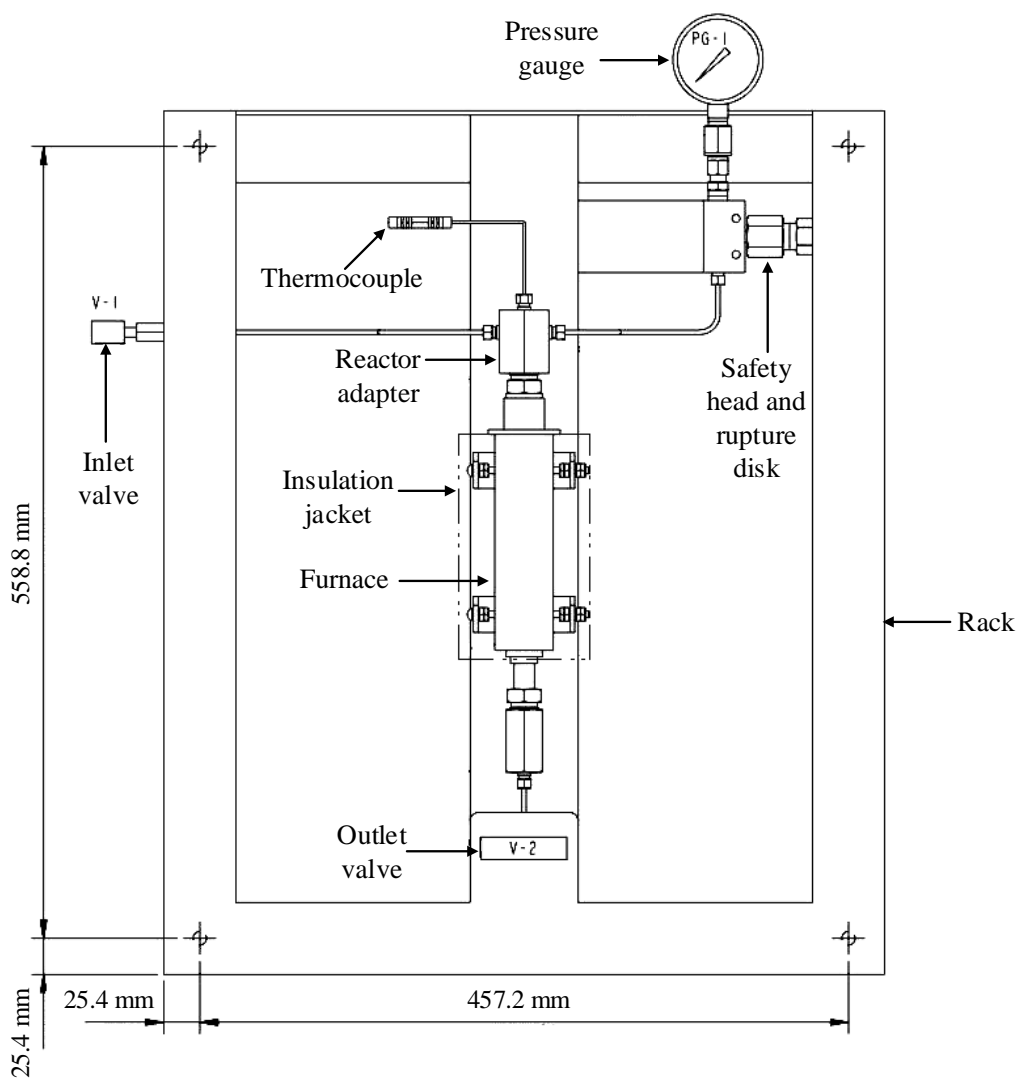


Figure 3.5 Schematic diagram of the reactor unit employed in the catalytic conversion of *n*-pentane.

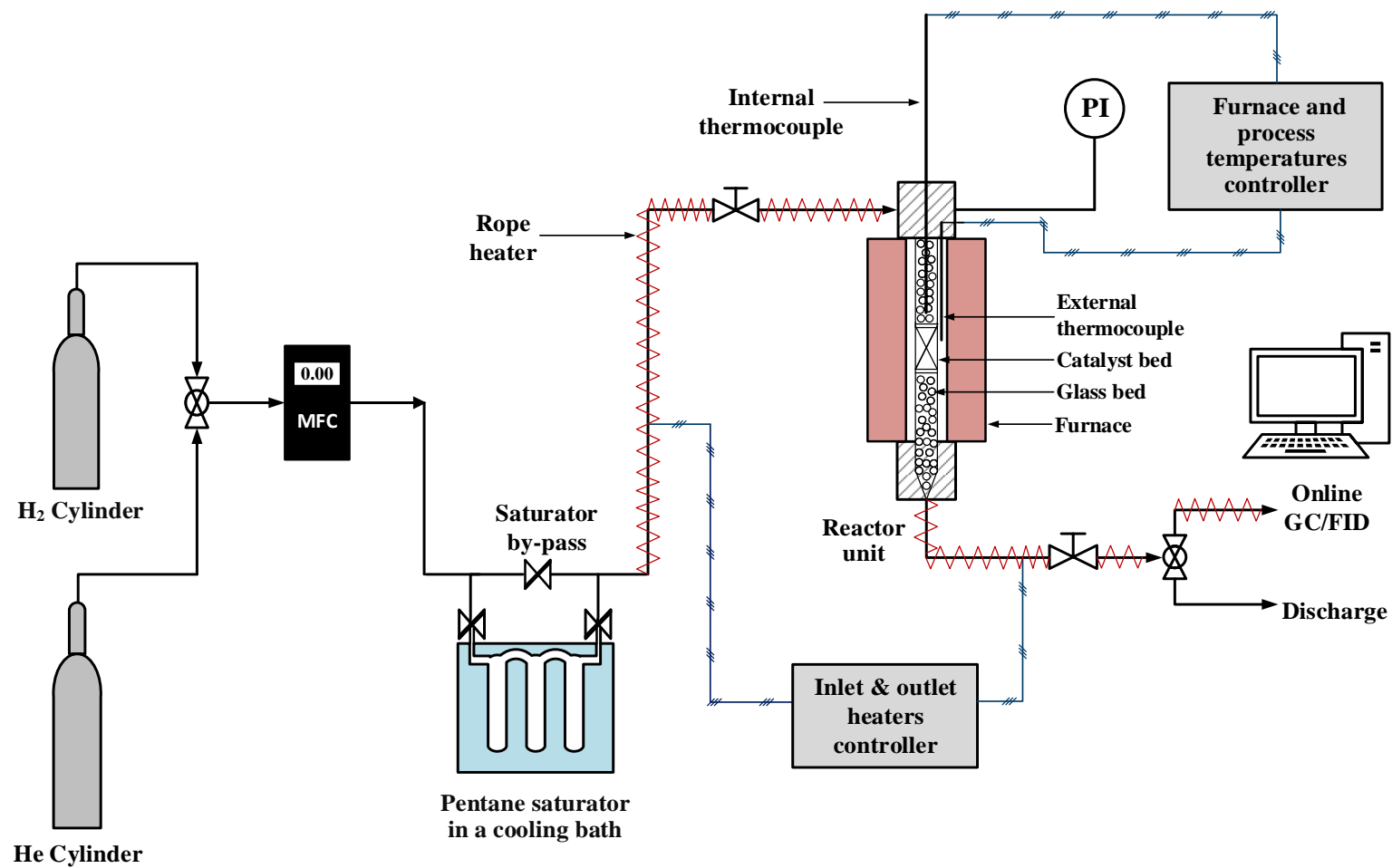


Figure 3.6 Schematic diagram of the system employed in the catalytic conversion of *n*-pentane.

3.4.1.3 Experimental procedure

Approximately 0.5 g catalyst of particle size 250-425 μm (bed length of 20 mm) was loaded into the tubular reactor described in Section 3.4.1.1. Spherical glass particles of 3 mm diameter (Sigma-Aldrich) were used to fill the dead volume of the reactor with the catalyst bed in between. In addition, two thin layers of inert quartz wool (Fischer Scientific) were used to separate the catalyst bed from the glass beds. The purpose of the glass beds is to hold the catalyst bed to the heating zone of the reactor as shown in Figure 3.6. The upper bed was used to avoid the back mixing of the catalyst with the carrier gas and to approximate plug flow conditions.

After catalyst packing, the metallic phase of the catalyst was reduced *in situ* with pure H_2 with a flow rate of 30 ml min^{-1} at 400 $^\circ\text{C}$ for 2 h. The aim of catalyst reduction process is to transform the Pt ions to elemental form. The reduction process was carried out by heating the reactor gradually to 400 $^\circ\text{C}$ whilst maintaining the flow of H_2 passing through the saturator bypass at 30 ml min^{-1} .

After reduction, the reactor was cooled down to the desired reaction temperature and the H_2 flow rate was adjusted to the required value. Once the system stabilised at the desired conditions, the flow of H_2 gas was redirected to pass through the liquid *n*-pentane in the saturator. The inlet and outlet gas lines were heated to 80-100 $^\circ\text{C}$ to prevent condensation of the reactants or products.

The GC time-on-stream measurements were recorded every 30 min using an online GC (Shimadzu QP2010SE) equipped with a flame ionisation detector (FID) to detect the composition of the reaction products. The initial concentration of *n*-pentane was determined prior to each experiment by running a blank reaction without catalyst, thus allowing determination of the feed composition. For this aim, six measurements of *n*-pentane peak areas in the GC were recorded and averaged.

At the end of the reaction, the saturator inlet and outlet were closed and the carrier gas was switched to He and bypassed through the saturator. The catalyst was purged at reaction temperature with He at a flow rate of 40 ml min^{-1} for 1 h in order to strip any retained reactant or product from the catalyst. Afterwards, the reactor was allowed to

cool down to room temperature and the catalyst was collected for *ex situ* characterisation.

3.4.2 Catalytic conversion of *n*-hexadecane

3.4.2.1 Reactor set-up

The catalytic conversion of *n*-hexadecane under high pressure (Chapter 6 and 7) was carried out in a batch reactor. The system employed is schematically presented in Figure 3.7. The reaction unit consisted of a stirred tank reactor (Parker-Autoclave Engineers) having a capacity of 100 ml and an internal diameter of 46 mm.

The vessel was heated using a heating jacket. The jacket temperature was regulated and monitored together with the process temperature using a Solo Temperature Controller model 4824 (Autoclave Engineers), which also controlled the speed of the mixer. A cooling system was used to cool down the mixer engine and to prevent overheating.

The pressure inside the reactor was measured using a pressure gauge with a range from 1 bar to 350 bar, however, for a more accurate measurement a pressure transducer model PX319-3KG5V was used. This measured the pressure at the reactor head, where the signal generated by the transducer was recorded using an electronic voltmeter (ISO-TECH IDM 103). The measured voltage was then converted to pressure by considering that each 2.524 V corresponds to approximately 103.5 bar, as specified by the transducer manufacturer. The system was protected by a rupture disc that can hold a pressure up to 300 bar.

More details about the interior elements of the reactor are shown in Figure 3.8 (a) and (b). The reactor vessel was attached to the body of the reactor unit by an O-ring to prevent any potential gas leakage as shown in Figure 3.8 (a).

The shaft of the mixer shown in Figure 3.8 (b) has a diameter of 12.5 mm attached to an impeller with a circular hole. The purpose of this hole is to improve the gas circulation around the impeller. The internal thermocouple was introduced to the reactor through the thermocouple cover. The reactor is also fitted with a liquid

sampling tube; however, in the present work the liquid samples were collected after opening the reactor.

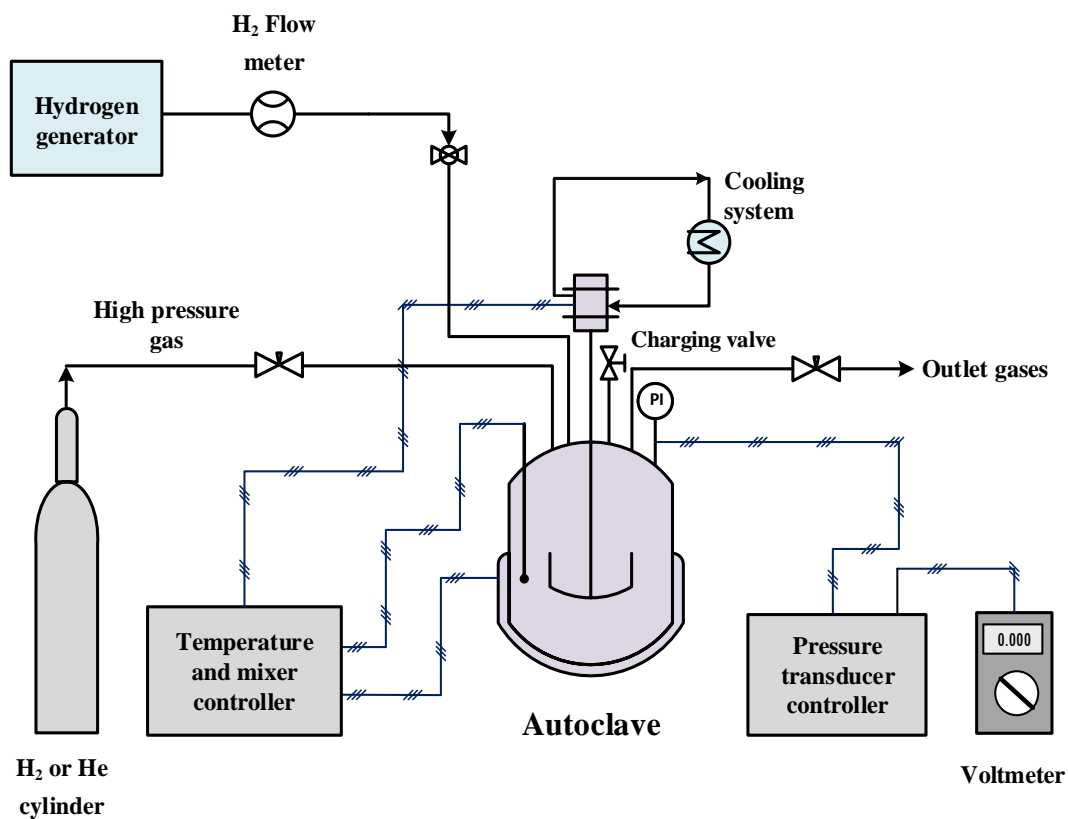


Figure 3.7 Schematic drawing for the reaction system employed in *n*-hexadecane reaction.

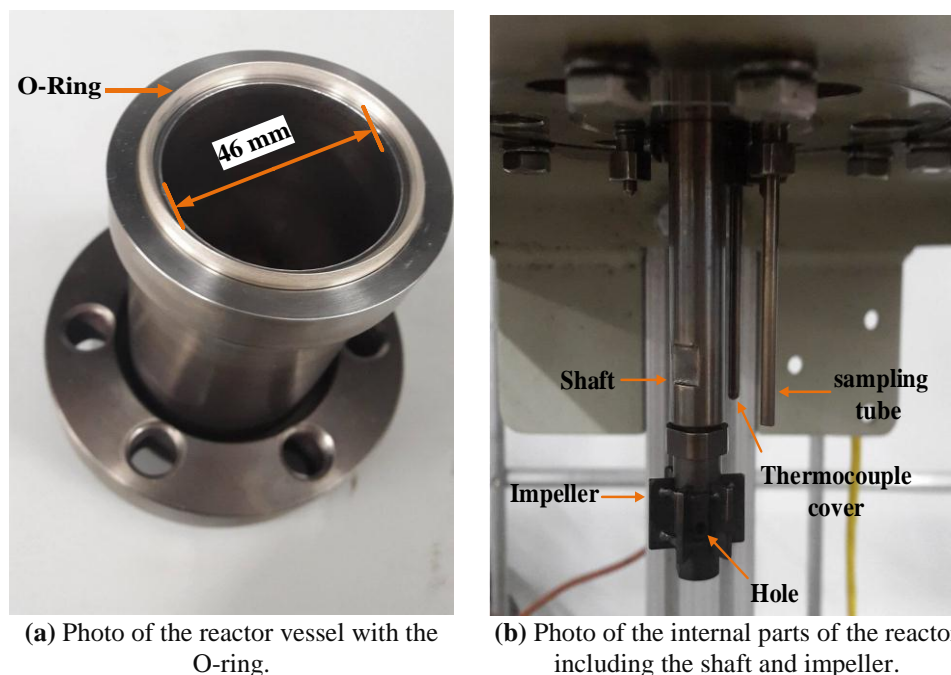


Figure 3.8 Configuration of the internal parts of the batch reactor employed in *n*-hexadecane conversion.

3.4.2.2 Experimental procedure

In the present study, the catalytic conversion of *n*-hexadecane was carried out over zeolites (H-Beta and commercial ZSM-5) in an inert atmosphere, and over the 0.5 wt.% Pt/H-Beta catalyst (prepared as described in Section 3.3.3) in the presence of hydrogen. In both cases, approximately 0.5 g of the catalyst in powder form was loaded into the reactor (described in Section 3.4.2.1). In the case of Pt/H-Beta, the platinum phase of the catalyst was then reduced prior to reaction at atmospheric pressure in a flow rate of 80 ml min^{-1} of H_2 supplied by a hydrogen generator (Parker Balston hydrogen generator). The flow rate was controlled by utilising a H_2 flow controller with a scale of $0\text{-}100 \text{ ml min}^{-1}$.

Afterwards, the reactor temperature was increased to $350 \text{ }^\circ\text{C}$ whilst keeping the H_2 flow constant. Once this temperature was reached, the mixer was switched on at a speed of 600 rpm and these conditions were held for 2 h. After performing the catalyst reduction step, the mixer and the heater were stopped and the heating jacket was removed. The reactor was then cooled down to room temperature using an ice bath.

Once cool, 15 ml of *n*-hexadecane (98 wt.%, VWR) was fed carefully to the reactor through the charging valve. After releasing the gases resulting from catalyst reduction by twice purging the reactor with H₂, the reactor was pressurised to the desired pressure. Thereafter, the reactor was gradually heated to the reaction temperature. The mixer was switched on at 600 rpm when the temperature reached the desired reaction temperature, and the reaction was kept at these conditions for the designated time-on-stream. In the case of using the Pt-free zeolite as a catalyst to perform the reaction in He atmosphere, the same mentioned process was carried out but omitting the reduction step.

After reaction, the reactor was cooled down to room temperature using an ice bath which also stopped the reaction. A sample of the headspace gases was collected using an inert foil gas sampling bag (Supelco), with a capacity of 1 L. Afterwards, the reactor was completely depressurised and opened. The liquid product was then collected and analysed off-line using a GC (Thermo Scientific, TRACE 1310) equipped with a FID detector. The gas sample was also analysed using a GC (Shimadzu QP2010SE) equipped with a FID detector.

3.4.2.3 Spent catalyst separation and cleaning

Any products or reactants retained on the spent catalyst could lead to misinterpretation of the carbonaceous deposits that are laid down on the catalyst surface after reaction. Therefore, these products have to be stripped and removed from the spent catalyst before characterisation. For this purpose, the spent catalyst was collected after reaction by washing the walls of the reactor vessel with *n*-pentane (technical grade, VWR), as this a short alkane solvent which is recommended for the removal of long chained paraffin (Bauer et al., 2014). Afterwards, the liquid–solid mixture was separated using a centrifuge (Heraeus Multifuge 3SR plus refrigerated centrifuge, Thermo Scientific) operated at 5500 rpm at 20 °C for 15 min. The separated catalyst was then washed again with *n*-pentane and filtered by vacuum filtration, followed by drying at 120-130 °C in an oven overnight to remove any remaining volatile materials.

3.5 Analysis by gas chromatography (GC)

Gas chromatography (GC) is a physical separation method used to separate compounds in a mixture according to their different affinities in a particular GC column. In the GC, the sample is distributed between two interacting phases: a stationary phase and a mobile phase. The mobile phase is usually an inert carrier gas such as He or N₂, whilst the stationary phase is usually a high molecular weight material. This is either deposited on the surface of fine particles contained in a packed column, or on the walls of a hollow and long capillary column (Annino and Villalobos, 1992).

A typical gas chromatograph has three main parts: the injection port, the fractionation column, and the detector. Usually, the sample is presented to the injection port using a microliter syringe, and introduced with a stream of a carrier gas to the fractionation column at a temperature high enough to evaporate all of the sample components. The detector is attached directly to the end of the column to identify the chemical composition of each component in the sample. An efficient heating system for the GC parts and the transfer lines is very important to achieve good separation, therefore, GC analysis is suitable only for materials which vaporise without decomposition. The chromatogram consists of qualitative and quantitative data for the analysed sample. The component identity is characterised according to the retention time of each component in the column, and component concentration is calculated and calibrated from the peak area (Karasek and Clement, 2012, Sparkman et al., 2011).

The sample components pass through the column at different velocities depending on their solubility in the stationary phase; the least soluble component is eluted first, whilst the most soluble one remains for a longer time in the column. The sample molecules spend part of the time in the mobile phase and the other part in the stationary phase. The total time required by a component to pass through the column is called the retention time (t_R), whilst the time required by a component to pass through just the mobile phase is termed the hold-up time (t_M). Therefore, the real interaction time between the component and the stationary phase is defined as shown in Equation 3.1 and is called the adjusted retention time (t_R') (Annino and Villalobos, 1992).

$$t_{R'} = t_R - t_M \quad (3.1)$$

Several types of detectors are used with the GC, such as a flame ionization detector (FID), mass spectrometer (MS), thermal conductivity detector (TCD), flame photometric detector (FPD) and electron-capture detector (ECD) (Sparkman et al., 2011).

Generally, GC detectors are classified as selective or universal detectors. A selective detector responds to a range of compounds with common physical or chemical properties, whilst a universal detector responds to any component eluted from the GC column. For instance, the FID is a selective detector, since it responds selectively to hydrocarbons and it can detect very low levels of these compounds. However, this response is decreased with the presence of heteroatoms such as oxygen, sulphur, and halogens. In contrast to the FID, the TCD is considered as a universal or non-selective detector, as it can respond to any component in the carrier gas stream that has a thermal conductivity different from that of the carrier gas itself (Grob and Barry, 2004).

In the present work, two types of detection systems were employed with the GC:

- i. FID: this is a mass-sensitive detector, and works based on the ionization mechanism in which the components eluted from the GC column are burned and ionised by the detector H₂-air flame, and form electrically charged species. These species are then collected at an electrode, producing an electrical current proportional to the amount of carbon burned off in the flame. This current is then collected and amplified to form the signal. The response factor of the FID for a specific component is the peak area divided by the mass of the component injected (MacNair and Miller, 1998, Grob and Barry, 2004).
- ii. MS: this is a detection system used to determine both the concentration and the identity of the eluting compound. It consists of three fundamental parts: the ion source, the mass analyser, and the ion detector. The process involves introducing the analyte molecules to an ion source in order to convert the molecules to their ionised form, which has both mass and charge, by using an appropriate ionization method. Afterwards, the generated ions are accelerated in the mass analyser and separated according to their mass to charge ratio (m/z)

using an electric and/or magnetic field. The last stage is the ion detection, where the ions are passed through a detector and produce an electrical current, which is then amplified and detected. The signal is then sent to the data processing system where different m/z values are stored together with their relative abundance (Gross, 2006, Downard, 2007).

3.5.1 GC analysis of the reaction products of *n*-pentane conversion

The GC analysis for the reaction products of *n*-pentane conversion was performed by introducing the sample of the produced gas to the GC (Shimadzu QP2010SE) using an on-line method. The GC was equipped with a FID detector and fitted with a CP-Al₂O₃/KCl (Agilent) PLOT column (50 m L×0.32 mm ID×5.0 μm active phase thickness), having a maximum working temperature of 200 °C. This column has a polar surface to separate ppm levels of C1-C5 hydrocarbons.

The GC was programmed to analyse gas samples every 30 minutes during the reaction by utilising a gas sampling loop. The injection port was operated in a split mode, thus, the sample was split-up into a number of parts equal to the selected split ratio. Consequently, only one part enters the column with the carrier gas. The carrier and make-up gas used was He, whilst H₂ and air at flow rates of 40 ml min⁻¹ and 400 ml min⁻¹ respectively were used to generate the H₂-air flame. The detector was heated to 200 °C to prevent condensation of water or any high boiling point components. The GC method used for the analysis is described in Table 3.3.

In addition, reaction products of *n*-pentane conversion were identified by employing a GC coupled with MS (Shimadzu QP2010SE) using the same column and method described for the GC/FID. The MS was operated using GCMSolutions software version 4.44. This included the NIST MS Search version 2.0 library with mass spectra of several compounds, thereby allowing the identification of reaction products.

Table 3.3 GC/FID method conditions used in the analysis of *n*-pentane reaction products.

Conditions	Setting
Gas sampling temperature (°C)	80
Injection temperature (°C)	150
Split ratio	150
Carrier linear velocity (cm sec ⁻¹)	40
Initial column temperature (°C)	60
Isothermal time 1 (min)	5
Ramp rate (°C min ⁻¹)	10
Final column temperature (°C)	165
Isothermal time 2 (min)	5

3.5.2 GC analysis of the reaction products of *n*-hexadecane conversion

The samples of the headspace gases of *n*-hexadecane conversion were analysed using the GC (Shimadzu QP2010SE) equipped with a FID detector. The column used was a Rt-Q-BOND (Restek) capillary column (30 m L×0.32 mm ID×0.1 µm active phase thickness), having a maximum working temperature of 300 °C. The injection port was operated in a split mode. The carrier and make-up gas used was He, and the gases used for the FID flame are the same as that described in Section 3.5.1. The analysis was carried out by injecting 2 mL of the collected gas using a 5 mL gas syringe (SGE) using the GC method described in Table 3.4.

Table 3.4 Conditions of the GC/FID method employed in the analysis of headspace gases following *n*-hexadecane conversion.

Conditions	Setting
Injection temperature (°C)	240
Split ratio	50
Carrier linear velocity (cm sec ⁻¹)	30
Initial column temperature (°C)	60
Isothermal time 1 (min)	5
Ramp rate (°C min ⁻¹)	10
Final column temperature (°C)	220
Isothermal time 2 (min)	2

Liquid products collected after *n*-hexadecane conversion were analysed off-line by GC (Thermo Scientific, TRACE 1310), equipped with FID detector and connected to a DB-5HT (Agilent) capillary column (30 m L×0.32 mm ID×0.1 µm active phase

thickness), with a maximum working temperature of 400 °C. The GC was operated by Chromeleon 7.2 SR4 software. In this GC, the carrier gas was He, and N₂ was used as the make-up gas. A flow rate of 35 ml min⁻¹ of H₂ and 350 ml min⁻¹ of air were used to generate the detector flame. The GC method employed for the analysis of liquid products is described in Table 3.5.

Table 3.5 Conditions of the GC/FID method employed in the analysis of liquid products following *n*-hexadecane conversion.

Conditions	Setting
Injection temperature (°C)	200
Split ratio	150
Carrier flow rate (ml min ⁻¹)	1.370
Initial column temperature (°C)	40
Isothermal time 1 (min)	2
Ramp rate 1 (°C min ⁻¹)	10
Second temperature (°C)	100
Isothermal time 2 (min)	2
Ramp rate 2 (°C min ⁻¹)	10
Third temperature (°C)	150
Isothermal time 3 (min)	3
Ramp rate 3 (°C min ⁻¹)	10
Final column temperature (°C)	250
Isothermal time 4 (min)	5
Detector temperature (°C)	250

In liquid phase analysis, the sample was introduced to the injection port of the GC by injecting 1 µL *via* manual injection using a 10 µL syringe (Thermo Scientific). The liquid product of each reaction was analysed twice in the GC. The first analysis was performed after diluting the sample with toluene (99.5 %, Sigma Aldrich) as a nonpolar solvent in a dilution ratio of 1:50. This was to get clear and symmetric peaks for the unreacted *n*-hexadecane and clear resolved peaks for the produced *iso*-hexadecane. This allowed the concentration of both components to be determined. The second analysis was performed using undiluted sample to detect all the peaks of liquid products lighter than hexadecane. Each sample was injected three times and the peak areas were averaged.

The retention time of each *n*-alkane in the liquid reaction products was identified by injecting 1 μ L of an analytical standard solution. This solution comprised *n*-alkanes with carbon numbers ranging from C8 to C20, each in a concentration of 40 mg L⁻¹ (Sigma-Aldrich), dissolved in hexane. Besides establishing the retention time of each individual *n*-alkane, this analytical standard allows the calculation of the molar response factor (*RF*) for these compounds, which is required for the calculation of the number of moles for each product as shown in Equation 3.2.

$$n_i = \frac{A_i}{RF_i} \quad (3.2)$$

where n_i is the number of moles of *i* component, A_i is the peak area of *i* component expressed in terms of amperes-seconds (A.s), and RF_i is the chromatographic molar response factor for component *i*.

The retention times of *n*-alkanes lighter than octane (*n*-pentane, *n*-hexane, *n*-heptane) were determined by GC analysis of a prepared solution consisting of 10 % of each component dissolved in *n*-hexadecane.

3.6 Calculations

3.6.1 Calculation of products composition

3.6.1.1 Composition of gaseous compounds

The composition of gases produced from the *n*-pentane isomerisation-cracking reaction was determined by employing the effective carbon number approach (ECN). This approach assumes that the relative response of the FID for a given hydrocarbon molecule is equivalent to the number of carbon atoms presented in that molecule as mentioned in Section 3.5, (MacNair and Miller, 1998). Consequently, the absolute response factor of each component in the hydrocarbon gas mixture can be estimated by applying Equation 3.3 and assuming a response factor of 1 for a reference material (Grob and Barry, 2004) .

$$RF_i = F_i \cdot RF_S \quad (3.3)$$

Where RF_i and F_i are the absolute and the relative response factors of component i respectively, and RF_s is the response factor of a reference material.

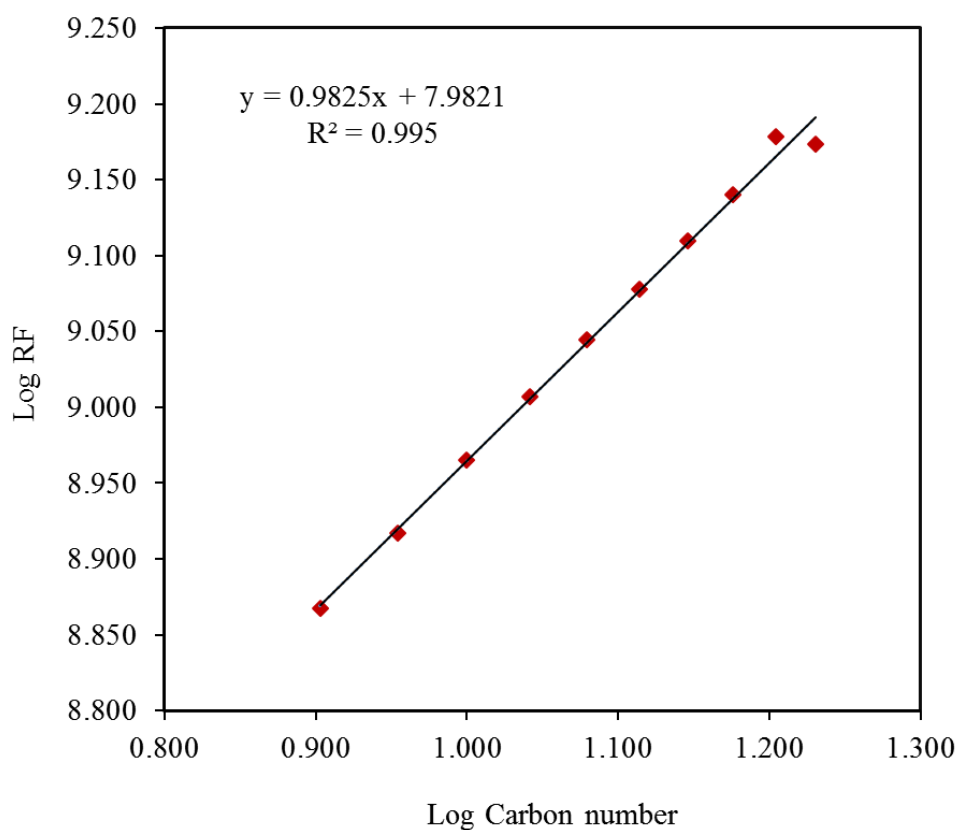
3.6.1.2 Composition of liquid products

In the reaction of n -hexadecane in the liquid phase, the molar composition of liquid products was determined by applying Equation 3.2 and the chromatographic response factor for each alkane was estimated experimentally by injecting 1 μL of the analytical standard solution, consisting of 40 mg L^{-1} of each component, into the GC as described in Section 3.5.2. Consequently, the molar response factor for each n -alkanes could be calculated from the resulting peak area, the weight concentration of the component and the molecular weight. The response of non-linear alkane was assumed to be the same as the response of a linear alkane with the same carbon number. To acquire an accurate calibration, the analytical standard solution was injected three times and the average value of the peak area was used in the calculations. Besides, the RF for other liquid compounds that were not presented in the calibration standard mixture (*i.e.* C5, C6, and C7) was estimated from the logarithmic relationship resulting from plotting the number of carbon atoms (C_n) in each compound in the standard mixture against their corresponding RF value as summarised in Table 3.6 and Figure 3.9.

The molar concentration of n -hexadecane after reaction was determined by applying the equation of the n -hexadecane calibration line. This calibration line was obtained by injecting 1 μL of prepared calibration solutions of n -hexadecane at different concentrations, diluted in toluene. Afterwards, the GC peak areas of these calibration solutions were plotted against their corresponding concentrations to obtain the calibration line shown in Figure 3.10. The moles of n -hexadecane in the product can be determined by using the volume of liquid products collected after reaction and the molecular weight.

Table 3.6 Experimentally determined chromatographic RF for C5-C18 *n*-alkanes.

Compound	Carbon number	Retention time (min)	RF (unit area mol ⁻¹)
<i>n</i> -Pentane	5	0.957	4.665E+08
<i>n</i> -Hexane	6	1.050	5.580E+08
<i>n</i> -Heptane	7	1.285	6.492E+08
<i>n</i> -Octane	8	1.879	7.368E+08
<i>n</i> -Nonane	9	3.119	8.257E+08
<i>n</i> -Decane	10	4.682	9.231E+08
<i>n</i> -Undecane	11	6.255	1.016E+09
<i>n</i> -Dodecane	12	7.735	1.107E+09
<i>n</i> -Tridecane	13	9.365	1.196E+09
<i>n</i> -Tetradecane	14	11.455	1.287E+09
<i>n</i> -Pentadecane	15	13.119	1.381E+09
<i>n</i> -Hexadecane	16	14.510	1.509E+09
<i>n</i> -Heptadecane	17	15.833	1.491E+09
<i>n</i> -Octadecane	18	17.620	1.524E+09

**Figure 3.9** The logarithmic relation between the carbon number and the RF for C8-C17 *n*-alkanes.

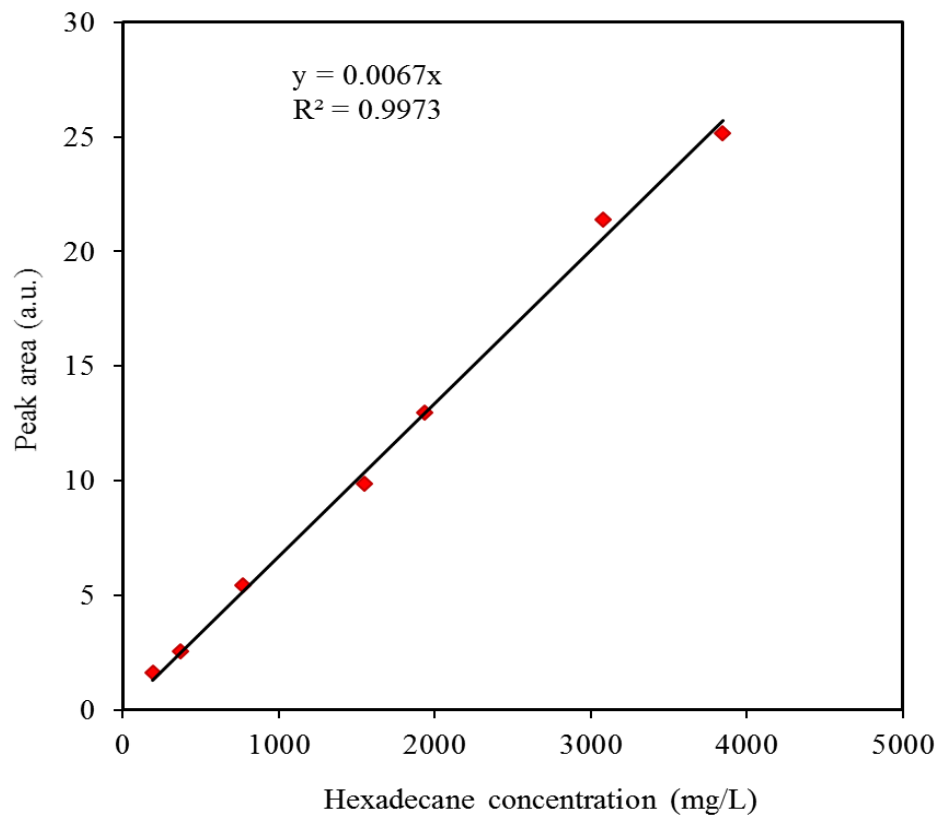


Figure 3.10 *n*-Hexadecane calibration line determined by GC analysis.

3.6.2 Calculation of reactant conversion

The molar conversion of the reactant (*n*-pentane or *n*-hexadecane) is defined in Equation 3.4:

$$X = \frac{(n_{ao} - n_a)}{n_{ao}} * 100 \quad (3.4)$$

where *X* is the percentage molar conversion of reactant *a*, *n_{ao}* is the initial moles of reactant *a* fed to the reactor, and *n_a* is the moles of reactant *a* after reaction.

3.6.3 Calculation of product selectivity

The selectivity to the desired product can be defined as the ratio between the rate of formation of the desired product, and the rate of conversion of the reactant (Figueiredo et al., 2008). In this work, the selectivity to any reaction product was determined using a carbon mole balance between reactant inlet and product outlet. Coke was considered as one of reaction products. Therefore, the selectivity to any product was calculated as the moles of carbon in product divided by moles of carbon of reactant consumed as shown in Equation 3.5:

$$S_i = \frac{n_i \cdot C_i}{(n_{ao} - n_a) \cdot C_a} * 100 \quad (3.5)$$

where S_i is the selectivity to product i , n_i is the moles of product i , C_i is the carbon number of product i , n_{ao} is the initial moles of reactant a , n_a is the moles of reactant a after reaction, and C_a is the carbon number of reactant a .

The moles of carbon in coke were determined by difference as shown in Equation 3.6:

$$n \cdot C_{coke} = n_{ao} \cdot C_{ao} - n_a \cdot C_a - \sum_{i=1}^x n_i \cdot C_i \quad (3.6)$$

3.6.4 The reproducibility error calculation

The experimental error was calculated by the replication of a model experiment three times at different periods. The total molar conversion of the reactant and the molar selectivity to the target products was calculated for each repeated reaction as described in Sections 3.6.2 and 3.6.3, then the reproducibility error was calculated by applying Equation 3.7:

$$E (\%) = \frac{\sigma}{\mu} * 100 \quad (3.7)$$

$$\sigma = \sqrt{\frac{1}{N} \sum_{i=1}^N (x_i - \mu)^2} \quad (3.8)$$

$$\mu = \frac{1}{N} \sum_{i=1}^N x_i \quad (3.9)$$

where E is the error percentage, σ is the standard deviation of the measurements calculated according to Equation 3.8, μ is the mean of the three measurements determined by applying Equation 3.9, N is the number of experiments ($N = 3$), and x_i is the value of the measurement (conversion or selectivity) in the i experiment.

Chapter 4

*Characterisation
techniques*

4 Chapter 4: Characterisation techniques

4.1 Introduction

A wide range of thermal and spectroscopic techniques were used in the current research. Some of these techniques were utilised to investigate the properties of the fresh catalyst after modification while others were used to explore the nature and type of the coke species laid down on the catalyst after reaction. This chapter gives a brief description of the theoretical background behind each technique as well as a description of the methods developed to perform each analysis. The aim is to ensure a comprehensive understanding of the results presented in the subsequent chapters. Fresh catalysts were assessed by inductively coupled plasma (ICP), X-ray diffraction (XRD), N₂ adsorption isotherms, and temperature programmed reduction (TPR). Coke was investigated by elemental analysis, thermogravimetric analysis (TGA), temperature programmed oxidation (TPO), and Raman spectroscopy, with N₂ adsorption isotherms used for determining the BET surface area.

4.2 Inductively Coupled Plasma (ICP)

Inductively Coupled Plasma (ICP) is an analytical technique used to determine the elemental composition of an analyte. This technique has the ability to accurately identify and quantify most of the elements in the periodic table including elements that are present in a very low concentrations in an analyte sample (Taylor, 2001).

The ICP instrument is composed of three basic components: the sample introduction system, the plasma generator, and the spectrometer. However, some types of samples need to be modified prior to introduction into the ICP. These primary modifications can be digestion, dissolution, fusion, grinding, etc. Ultimately, the sample which must be in a liquid form, is converted to a fine aerosol in the sample introduction system using a high flow rate of Ar gas (Taylor, 2001, Thomas, 2004).

In the plasma source, the plasma (electron cloud) is formed by passing Ar through a quartz torch placed in a load coil supplied with a radio frequency power. The purpose of the plasma is to transform the sample into ions. The temperature of Ar plasma is between 6000 and 10000 K, therefore, once the aerosol is introduced to the ICP torch

it is rapidly gasified, atomised, and then ionised. Predominantly, most of the elements in the periodic table generate single and positively charged ions under the high temperature conditions of the Ar plasma (Nelms, 2005).

Different detection techniques were used with the ICP to detect sample ions. The inductively coupled plasma mass spectrometry (ICP-MS) is the most sensitive technique that has the ability to detect elements present in parts per trillion in an analyte sample, while inductively coupled plasma optical emission spectrometry (ICP-OES) is usually used to detect elements in higher concentrations (Thomas, 2004).

In this work, the ICP technique was used to measure the amount of Pt dispersed on zeolite H-Beta prepared as described in Section 3.3.3. In addition, it was used to determine the Si/Al weight ratio of zeolite H-Beta before and after the desilication treatment described in Section 3.3.1. The analysis was carried out at the Department of Chemistry, University of Sheffield, using a Spectro-Ciros-Vision ICP-Emission instrument following digestion of the sample in aqua-regia/HF.

4.3 X-ray diffraction (XRD)

X-ray diffraction (XRD) is a technique used to give information about the crystalline bulk of the materials (Che and Védrine, 2012a). The XRD data are considered as a “fingerprint” in the identification of materials, in which each type of a crystalline solid has a unique XRD pattern. In zeolites, XRD is commonly used to monitor the structure of the zeolite during the synthesis process or to study the effect of post synthesis modifications on zeolite structure (Robson, 2001).

The XRD equipment is composed of an X-ray source, a sample holder, and a detector. X-rays are high-energy electromagnetic radiation with a wavelength approximately between 10^{-3} to 5 nm, which is shorter than ultraviolet (UV) radiation and longer than the γ -rays. XRD is typically conducted at a wavelength between 0.05-0.25 nm (Suryanarayana and Norton, 2013).

When an X-ray beam interacts with a crystalline solid, it excites the electrons of the atoms and is then scattered by the electron clouds in different directions at a wavelength similar to that of the incident ray. The interference pattern occurs when the wavelength of the incident X-ray is at the same order of magnitude as the separation distance between the atoms in the lattice (the interatomic distance) (Dann, 2000).

The XRD interference can be constructive, destructive, or partially destructive. Constructive interference is produced when the conditions of the XRD fundamental equation of Bragg (Equation 4.1) are fulfilled (Che and Védrine, 2012a):

$$n\lambda = 2d \sin \theta \quad (4.1)$$

where n is the order of diffraction, λ is the wavelength of X-ray source, d is the interatomic distance and θ is the angle of incident or Bragg's angle. A schematic representation of the constructive interference is shown in Figure 4.1.

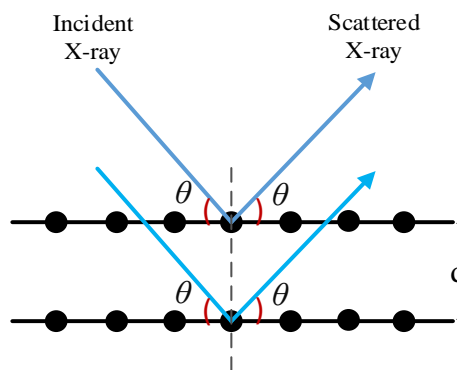


Figure 4.1 Schematic drawing of the scattering of X-ray from a parallel planes in a constructive interference (adapted from (Che and Védrine, 2012a)).

In contrast to the constructive interference where the waves are moving in phase with each other to give sharp peaks in the XRD spectrum, destructive interference occurs when the waves are out of phase, therefore, no peaks can be observed in the resulting spectrum.

In the present work, the XRD analysis was carried out to observe the structure of zeolite H-Beta after the desilication treatment. The XRD data were recorded with a STOE STADI P diffractometer using Cu K α radiation operated at 40 kV and 35 mA, scanning speed of 10° min⁻¹, and a radiation wavelength of 0.154 nm. The total run time was approximately 28 min.

4.4 Specific surface area using N₂ adsorption isotherm

Surface area and pore size distribution are considered as important measurements in the characterisation of solid catalysts as the available surface area of the catalyst is related to the catalytic activity. This is of particular importance for highly porous catalysts such as zeolites that are categorised as efficient catalytic materials in hydrocarbon transformations (Ertl et al., 2008).

The adsorption isotherm measurement is generally based on the phenomenon of physical adsorption-desorption of an inert gas such as N₂ and Ar at the condensation temperature of the adsorbed gas based on the fact that adsorption is favoured at low temperature (Che and Védrine, 2012a).

Physisorption results from a weak interaction (van der Waals forces) between the solid surface and the gas molecules in a reversible process, thus all the adsorbed gas can be released from the solid at the same temperature. The first model proposed for gas adsorption isotherms was in 1918 by Langmuir, which was based on the assumption of monolayer coverage of the adsorbed gas. Afterwards, in 1938, Brunauer, Emmett and Teller modified Langmuir's approach by using the hypothesis of multilayer gas adsorption, known as the BET model (Fan and Zhu, 2005). In this model it was assumed that the gas molecules adsorbed on the monolayer are working as adsorption sites to adsorb the next layer of gas molecules which allows for the adsorption of a number of layers (Che and Védrine, 2012a).

The BET theory is widely applied in the measurement of the specific surface area and pore size distribution of solids and porous materials using the adsorption data and by applying Equations 4.2 and 4.3:

$$\frac{P}{V_a (P^\circ - P)} = \frac{1}{V_m C} + \frac{(C-1) P}{V_m C P^\circ} \quad (4.2)$$

where P and P° is the equilibrium and the saturation pressure of the adsorbed gas at the temperature of adsorption, V_a is the measured volume of adsorbed gas at the equilibrium pressure and the temperature of adsorption, V_m is the volume of the adsorbed gas in the monolayer at standard temperature and pressure (STP), and C is the BET constant, which is related to the energy of adsorption in the first adsorbed layer.

A straight line relationship can be obtained by plotting $[P/V_a (P^\circ - P)]$ versus the relative pressure $[P/P^\circ]$ at an approximate relative pressure range between 0.05 to 0.3 (Fan and Zhu, 2005). From the values of the slope $(\frac{C-1}{V_m \cdot C})$ and the intercept $(\frac{1}{V_m \cdot C})$, the values of V_m and C can be mathematically determined as the following:

$$V_m = \frac{1}{\text{Slope} + \text{Intercept}} \quad C = \left(\frac{\text{Slope}}{\text{Intercept}} \right) + 1$$

The specific surface area (S_v) can then be calculated from Equation 4.3 :

$$S_v = \frac{V_m n_a S_m}{V_{gm} m} \quad (4.3)$$

where, n_a is Avogadro's number (6.02×10^{23}), S_m is the area per molecule of the adsorbed gas, V_{gm} is the molar volume of the adsorbed gas, and m is the mass of the sample.

The isotherm curve can be obtained by plotting the amount of the gas adsorbed per gram of the solid as a function of the relative pressure (P/P°) as recommended by IUPAC. However, most commercial equipment represents the plot as the volume of gas adsorbed versus the relative pressure. The IUPAC classified the isothermal adsorption into six different types shown in Figure 4.2, but only four types can be found in catalysts characterisation, these four types are I, II, IV, VI (Leofanti et al., 1998, Bekkum, 2001b). The characteristic of each adsorption type is presented in Table 4.1.

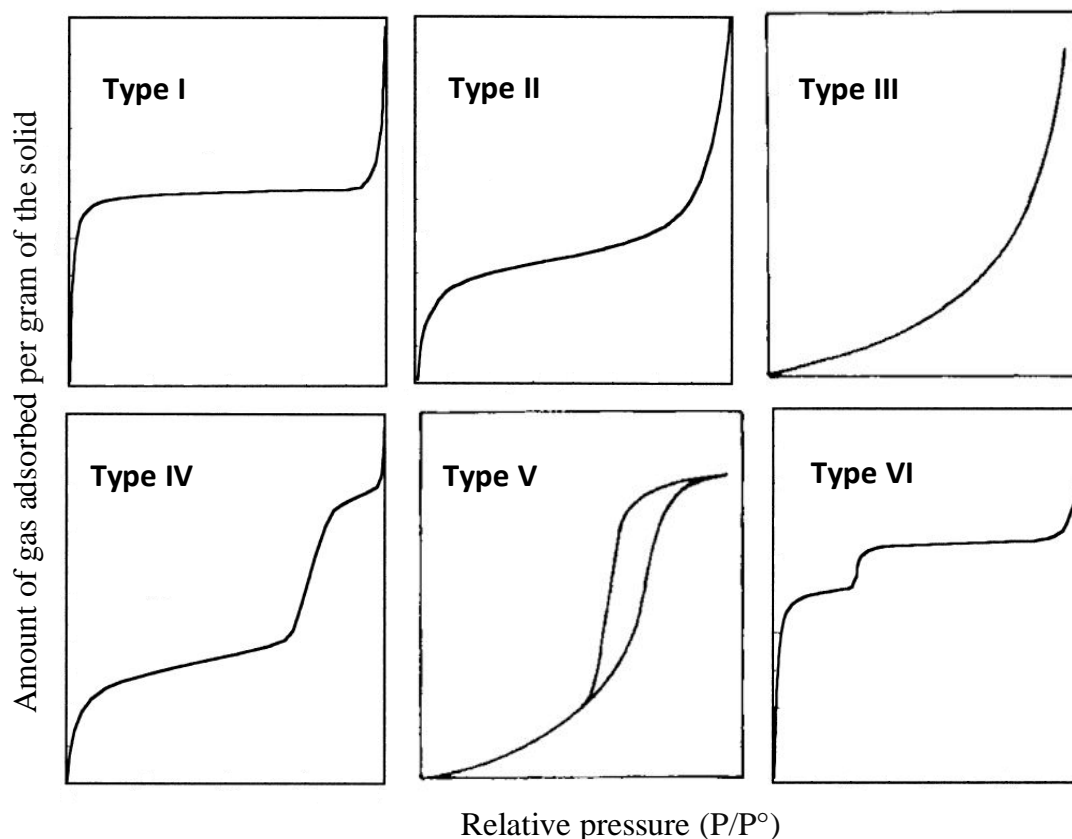


Figure 4.2 Types of adsorption isotherms (adapted from (Leofanti et al., 1998, Bekkum, 2001a)).

Table 4.1 Type and characteristics of adsorption isotherms (adapted from (Bekkum, 2001a)).

Type of isotherm	Characteristics
I	Adsorption in microporous solids such as zeolites
II	Multi-layer adsorption in macroporous solids
III	Weak gas-solid interaction
IV	Multi-layer adsorption in mesoporous solids
V	Weak gas-solid interaction
VI	Adsorption on non-pores solids

An example of an N₂ adsorption isotherm plot is given in Figure 4.3 for a solid porous material (adapted from (Che and Védrine, 2012a)). The figure shows different regions of N₂ adsorption. At point A the relative pressure is zero, and the amount of gas adsorbed can be related to the volume of micropores. Point B corresponds to the

adsorption of a monolayer of gas molecules on the solid surface. The semi-linear region between B and C, is related to the multilayer gas adsorption. Then, a significant increase in the amount of gas adsorbed can be observed at the region between C and D, which is due to the presence of the mesoporosity in the solid. When the pressure of the adsorbed gas is approximate or equal to the saturation pressure ($P=P^\circ$) at the region between D and E, then the pores of the solid are filled with the gas, and point E indicates the end of pore filling. The amount of gas adsorbed at this region can be associated with the total pore volume. Afterwards, the reversible process of desorption starts at point F.

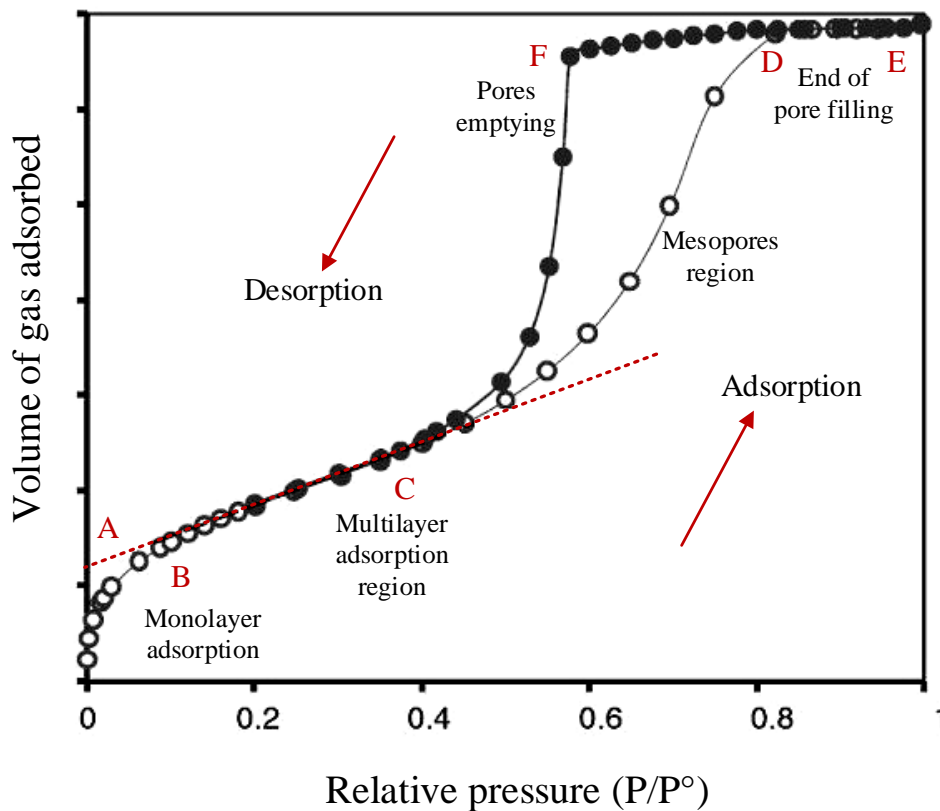


Figure 4.3 Plot of the N_2 adsorption-desorption isotherms of a porous glass at $-196\text{ }^\circ\text{C}$ (adapted from (Che and Védrine, 2012a)).

The BET theory is commonly used for the determination of surface area of zeolites and other microporous solids because of its convenience, and it is considered a standard procedure for comparing different adsorbents. However, some limitations have been reported in the literature regarding the validity of applying this approach in

the calculation of surface areas of porous materials that contain “ultra micropores” (pore diameter $< 7 \text{ \AA}$). These limitations are associated with the enhancement of the adsorption in the small pores at very low P/P° , which may lead to a primary micropore-filling mechanism that invalidates one of the BET assumptions (Sing, 1985, Walton and Snurr, 2007, Llewellyn et al., 2007). On the other hand, a study conducted by Bae *et al.* concluded that the BET method is an effective approach for determining surface areas of materials having ultra-micropores or heterogeneous pores such as metal-organic frameworks (MOFs) and zeolites if the BET analysis is performed using the appropriate pressure range (Bae et al., 2010).

In the present work, N_2 gas sorption measurements were performed using Micromeritics ASAP 2020 Plus (Micromeritics Instrument Corporation, Norcross, USA) with high purity gases. Samples of around 100 mg were heated to $120 \text{ }^\circ\text{C}$ for at least 12 hours under dynamic vacuum before each gas sorption measurement was performed. N_2 isotherms were collected at 77 K ($-196 \text{ }^\circ\text{C}$) over a pressure range of 1-1000 mbar. The linear region of the BET plot was chosen at the relative pressure range 0.05-0.3. The validity of the employed relative pressure range in BET surface area measurement was verified by the analysis of BET surface area of a sample of zeolite H-Beta having a surface area of $620 \text{ m}^2 \text{ g}^{-1}$ as measured by the supplier (Alfa Aesar). The measured BET surface area of zeolite H-Beta sample using the developed N_2 adsorption isotherm method was the same as that measured by the supplier, which confirm the validity of the selected relative pressure range in BET surface area calculations.

4.5 Temperature programmed reduction (TPR)

Temperature programmed reduction (TPR) is a traditional technique used to study the reducibility of catalytic precursors (Subramanian, 1992). The chemical reaction that occurs during the reduction process can be described by the following equation:



In the present work, TPR analysis was carried out to reveal the reduction temperature of the bifunctional catalyst, prepared as described in Section 3.3.3 that contains 0.45 wt.% Pt supported on zeolite H-Beta. TPR experiments were performed using a chemisorption instrument (ChemiSorb 2720, Micromeritics) equipped with a temperature controller (Eurotherm 2416) and fitted with a thermal conductivity detector (TCD). The system was operated using ChemSoft TPx V1.03 software. The TPR experiment was conducted using a catalyst sample of approximately 40 mg. The sample was loaded in a quartz U-tube reactor placed inside the instrument furnace and purged with pure Ar at a flow rate of 25 mL min⁻¹ at ambient temperature to release the air from the system. After 30 min, the gas was changed to the reactive gas, which contained 5% H₂ in Ar, whilst maintaining a constant flow rate. The temperature was then increased in a rate of 10 °C min⁻¹ from ambient temperature to 700 °C. The TPR profile is a plot of the TCD response *versus* temperature. The peak position in the TPR profile represents the reduction temperature of platinum while the peak area reflects the amount of H₂ consumed in the reaction.

4.6 Elemental Analysis

The determination of H/C ratio is the first step in coke characterisation, as the H/C ratio of coke indicates different kinds of coke species. Generally, two types of coke species are identified in the literature based on the value of H/C ratio (Bauer and Karge, 2006):

- i. Hydrogen-rich carbonaceous deposits or amorphous coke with H/C weight ratio > 1. These are usually formed at reaction temperatures lower than 250 °C.
- ii. Hydrogen-deficient coke or hard coke with H/C ratio < 0.8. These are typically formed at reaction temperatures higher than 270 °C.

The elemental analyser is composed from an autosampler that can run a sequence of samples, a combustion chamber (furnace), a GC column, and a TCD to detect the elements eluted from the GC column. The instrument is usually used to measure the percentage of the C, N, H, and S in solid or liquid samples. The carrier gas used is usually He, whilst pure O₂ used as the combustion gas.

In this work, The H/C ratio was determined for the spent catalysts using a Flash 2000 organic elemental analyser (Thermo Scientific) fitted with a MAS 200R carousel autosampler for solids. A sample of 2-3 mg was introduced to the instrument using tin capsules (CE instruments). Afterwards, the sample was burned off in the presence of pure O₂ in the instrument furnace seated at 900 °C. The combustion products were analysed using a GC column, and then detected by the TCD. The carrier gas employed was He at a flow rate of 130 mL min⁻¹. The instrument was calibrated using a calibration standard that has a known percentage of C, N, H, and S. The data were collected as elemental weight percentage using Eager Xperience software version 1.1.

4.7 Thermogravimetric analysis (TGA)

Thermogravimetric analysis (TGA) is a very useful and informative technique for the study of solid-gas systems. It is used to measure the change in weight of a material as a function of temperature and/or time in a controlled atmosphere (Imelik and Vedrine, 1994). This weighing technique has a wide range of applications in heterogeneous catalysts such as in the study of oxidation, decomposition, catalyst preparation and regeneration (Auroux, 2013).

TGA is commonly employed in coke investigation to determine the quantity of coke accumulated on the catalyst after reaction. In addition, the differential curve (DTG) allows the detection of any thermal transformation of the material being studied. The DTG peak is associated with the mass variation rate of the sample with temperature. It can reveal the thermal decomposition of any substance or precursor adsorbed on the catalyst (Imelik and Vedrine, 1994). The atmosphere within the TG instrument plays an important role in the analysis, therefore, the composition of the gas employed, for example inert or reactive, depends on the nature of the analysis to be performed.

In the present study, TGA/DTG was utilised to measure the coke content of the catalyst after reaction. It was also used to investigate the decomposition temperature of materials adsorbed on the catalyst after modification, such as the determination of the appropriate calcination temperature required for decomposing the platinum precursor in bifunctional catalyst synthesis. The analysis was performed using TGA 4000 Thermobalance (Perkin Elmer) in which the sample weight loss as a function of

temperature was recorded continuously. The instrument was operated using Pyris V10.1.0.0412 software for on-line data acquisition and processing.

For the measurement of the quantity of coke, a sample of approximately 15 mg of the spent catalyst was loaded in a ceramic pan (7 mm diameter and 5 mm length) and placed on a sensitive microbalance. The sample was first thermally pre-treated with N₂ in a flow rate of 20 ml min⁻¹ from 40-200 °C at a heating rate of 10 °C min⁻¹, then the temperature was held at 200 °C for 1 h whilst maintaining a constant flow of N₂. The weight loss at this stage is attributed to the removal of the adsorbed water and the unbounded volatile materials, and not considered as coke. Afterwards, the N₂ gas was switched to air to start the oxidation of carbonaceous materials. The sample was heated to 850 °C, using the same heating rate and gas flow rates. The weight percent of the total coke removed from the sample was determined by the mass difference of the sample at the period after switching to air to 850 °C, when the hard coke was completely burnt off. This calculation is shown in Equation 4.4:

$$Coke \% = \frac{W_{200} - W_{850}}{W_{850}} * 100 \quad (4.4)$$

where W_{200} is the weight of the sample at 200 °C which is considered as the initial weight, and W_{850} is the final weight of the sample at 850 °C. All samples were repeated three times, each on a different day and the standard deviation from the mean value was calculated.

For investigating the decomposition of the materials adsorbed on the catalyst, a sample of approximately 15 mg was loaded in the instrument pan. The temperature was increased linearly at a rate of 10 °C min⁻¹ from 40 to 100 °C to remove moisture, using a flow rate of 20 mL min⁻¹ of N₂. The gas was then switched to air in case of probing the calcination temperature of Pt/H-Beta catalyst, or maintaining the N₂ gas in case of investigating the decomposition temperature of DTBP, and TEOS adsorbed on H-Beta and Pt/H-Beta catalysts respectively. In both cases, the temperature increased at a rate of 10 °C min⁻¹ from 100 to 850 °C. After data collection, the DTG curves for the parent and modified catalyst were compared to determine the thermal decomposition temperature of the adsorbed material.

4.8 Temperature-programmed oxidation (TPO)

Temperature-programmed oxidation (TPO) is one of the most extensively used techniques in coke characterisation. Coke has been characterised by this technique in several catalyst systems such as zeolites, reforming catalysts and Ni catalysts (Querini and Fung, 1997). This technique is widely applied in coke characterisation owing to its simplicity and utility in providing information concerning coke location, composition (such as hydrogen to carbon ratio), determining the quantity of carbon species deposited on the catalyst, estimating the mechanism and kinetics of the coke oxidation reaction, and characterising coke morphology (Chen et al., 2013, Spivey and Roberts, 2004). Such coke properties can affect the peak shape of the TPO profile and can be inferred from the area under the peak and the peak positions (Li and Brown, 1999).

The oxidation of coke usually begins at a temperature of about 250 °C, starting with the removal of hydrogen from the hydrogen-rich coke that consequently forms water and oxygenated intermediates. These intermediates then decompose into CO and CO₂ gases (Bauer and Karge, 2006).

TPO is considered as a suitable tool for the discrimination between different types of coke, in which the TPO profile consists of several heat peaks; each peak was ascribed to the presence of a type of carbon species with different oxidation reactivity. Chen *et al.* identified three heat peaks related to three types of carbon species (Chen et al., 2013):

- i. Hydrogen-rich chemisorbed carbon species peak, located at temperatures lower than 300 °C in the TPO profile. This peak infers the presence of carbon species with high reactivity
- ii. The amorphous carbon peak, which appears at around 400 °C
- iii. Graphitic coke or structurally ordered carbon peak, centred at temperatures around and higher than 500 °C

Furthermore, in the review of Bauer and Karge, coke was classified into two main categories: (i) hydrogen-rich carbonaceous residues or low-temperature coke which

are burned at temperatures around 327 °C; and, (ii) highly condensed, polyaromatic residues or high-temperature coke that oxidised at temperatures higher than 430 °C (Bauer and Karge, 2006).

In a typical TPO experiment, the coked catalyst is placed in a sample tube and subjected to a constant flow rate of O₂ diluted in He. The sample temperature is then increased linearly at a desired heating rate from room temperature to a temperature high enough to achieve complete oxidation of all the carbonaceous deposits. Then the evolved gases, which contains a mixture of CO, CO₂, H₂O, and He are detected by using different detection systems such TCD, MS, *etc.* (Querini and Fung, 1997, Spivey and Roberts, 2004).

In the present work, TPO experiments were conducted on the spent catalysts using a chemisorption instrument (ChemiSorb 2720, Micromeritics), which is also used for TPR analysis. First, the sample of the spent catalyst was dried prior to analysis in an oven at a temperature of 125 °C overnight to reduce the amount of the adsorbed moisture. Then approximately 50 mg of the dried sample was placed in the instrument quartz U-tube reactor and purged with He at a flow rate of 25 mL min⁻¹ for 30 min at ambient temperature. Afterwards, the gas was changed to the reactive gas, which consisted of 5 % O₂ in He. The same flow rate of 25 mL min⁻¹ was maintained for 20 min. After system stabilisation, the temperature was increased linearly from ambient temperature to 850 °C at a rate of 10 °C min⁻¹. The final temperature was held for 15 min to ensure the oxidation of all carbonaceous deposits existing on the catalyst sample. The results of a TPO experiment are typically presented as a trace of the TCD response *versus* temperature, which is known as the TPO profile.

4.9 Raman spectroscopy

Raman spectroscopy is one of the most recognised vibrational spectroscopic techniques used for coke assessment in catalysis. Its high sensitivity allows the analysis of catalysts with low coke content (0.3-0.5 wt. %), and the study of the structure and the degree of graphitisation of coke, for example, pregraphitic or highly organised carbon (Spivey and Roberts, 2004).

When a monochromatic beam of light of a specific frequency (energy) is incident on a sample then this light may be reflected, absorbed, or scattered. The Raman phenomenon occurs when some of the incident photons are scattered at frequencies lower than that of the incident light. If the frequency of the scattered photons is the same as the incident photons then the effect is known as Rayleigh scattering. In Raman scattering, the light interacts with the molecule, causing polarization of the electron cloud around the molecule to form a temporary and unstable molecular state called a “virtual state”. Then the photons are rapidly re-emitted at different vibrational levels. Raman scattering is an inelastic process. In some cases, the energy of the photon may be absorbed by the molecule, and therefore the photon is scattered to an energy level lower than that of the incident light, leading to Stokes scattering. In other cases, the photon may gain energy from the molecule and be scattered to a higher energy level, leading to anti-Stokes scattering. These processes are illustrated in Figure 4.4. The majority of photons lose energy, however, a small fraction of these photons may gain energy. Raman scattering is therefore mainly Stokes scattering (McCreery, 2005, Smith and Dent, 2013). Typically, Rayleigh scattering dominates the scattered light while Raman scattering is very weak in which approximately one photon out of 10^8 photons of the incident light could be Raman scattered (Ferraro et al., 2003, Che and Védrine, 2012b).

In vibrational spectroscopy, the energy change of the photon causing nuclear motion (vibration) is a characteristic of the type of a bond in a molecule. Since each molecule has a unique vibrational energy level, Raman spectra can be considered as an optical fingerprint of a specific molecule (Larkin, 2011).

In addition to Raman Stokes and anti-Stokes scattering, resonance Raman and resonance fluorescence effects can also occur. Both effects happen when the light interacts with the molecule and the molecule transitions to an excited electronic state. The effect of resonance Raman can significantly improve the Raman bands, and occurs when the photons are scattered to the vibrational electronic state at the same frequency as the incident light (Smith and Dent, 2013).

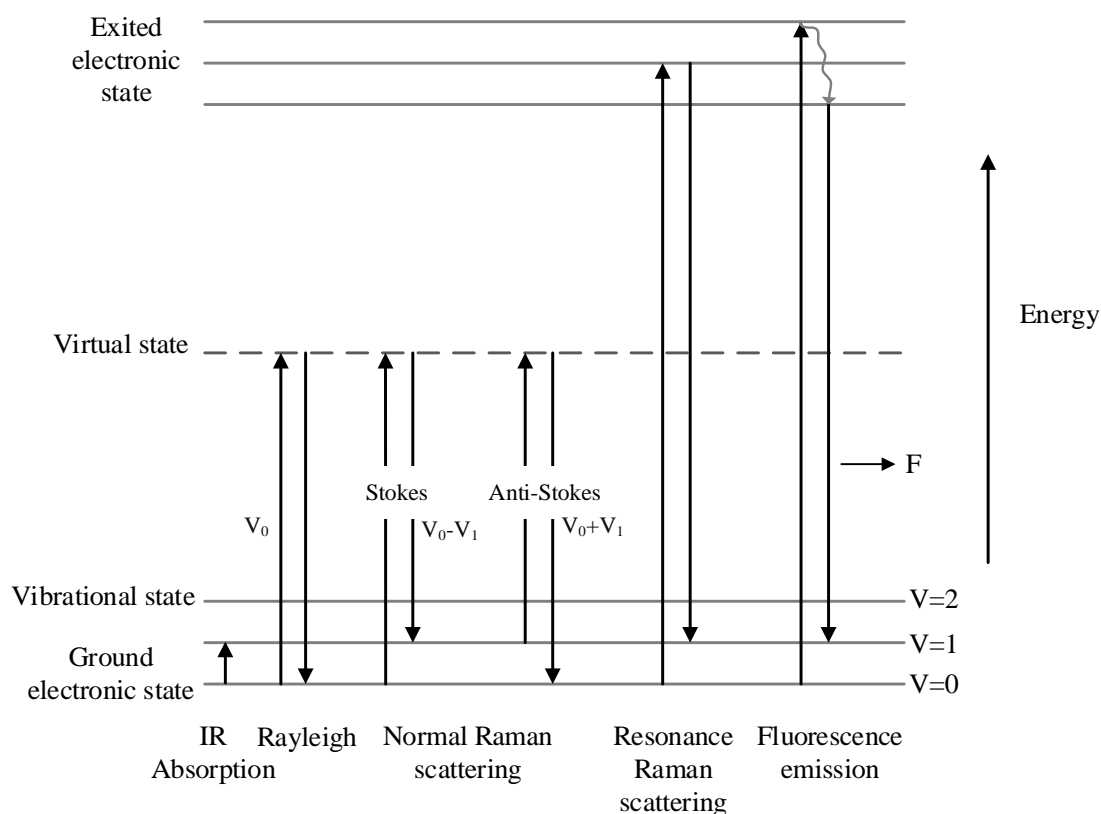


Figure 4.4 Diagram of Rayleigh, Raman scattering, Resonance Raman, and Fluorescence emission (adapted from (Ferraro et al., 2003)).

In contrast to resonance Raman, the competitive effect of fluorescence is a serious problem associated with Raman scattering in which even weak fluorescence can prevent the detectability of a Raman signal (McCreery, 2005). Fluorescence is produced mainly from the emission of photons which cascade down from the excited electronic states to the vibrational state, as shown in Figure 4.4 (Ferraro et al., 2003). It generates a broad and intense band which can be stronger than the intensity of Raman band in several orders of magnitude (Che and Védérine, 2012b).

Usually fluorescence bands appear at excitation wavelengths in the range from 300 to 700 nm as shown in Figure 4.5 (a). Therefore, one of the approaches applied to avoid fluorescence is shifting the excitation source from the visible region at a conventional wavelength of 514.5 nm to infrared (IR) or ultraviolet (UV) regions, as shown in Figure 4.5 (a) (Che and Védérine, 2012b, Jin et al., 2015).

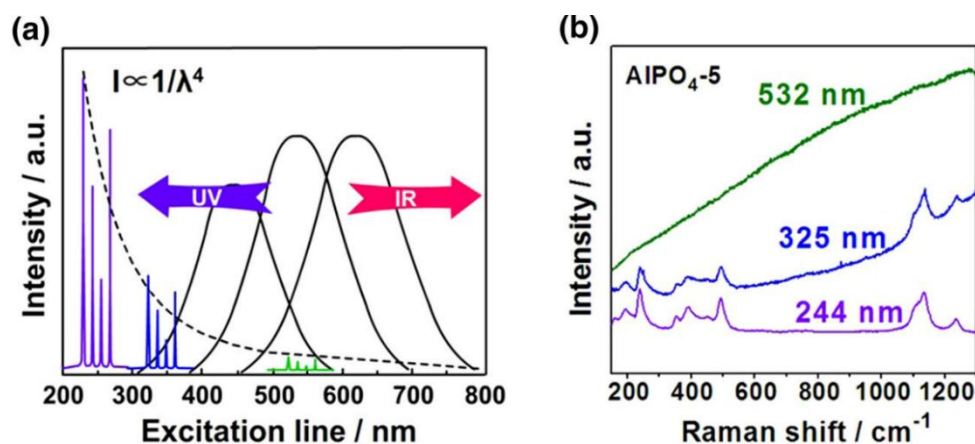


Figure 4.5 (a) UV Raman spectroscopy enhancing Raman scattering intensity; (b) Raman spectra of AlPO_4^{-5} excited at 532, 325, and 244 nm wavelength (Jin et al., 2015).

A large fraction of solid catalysts such as zeolites exhibit strong surface fluorescence. The Raman signal of such materials at the conventional excitation wavelength is completely obscure as shown in Figure 4.5 (b) for the example of the Raman signal of aluminophosphate (AlPO_4^{-5}) molecular sieve at excitation wavelengths lower than 532 nm. This kind of materials are described as weak Raman scatterers, in particular when contaminated with carbonaceous deposits (Bauer and Karge, 2006, Spivey and Roberts, 2004). For the characterisation of carbonaceous deposits accumulated over zeolites, UV Raman with excitation wavelengths lower than 260 nm has been widely applied rather than using the conventional visible laser which is usually dominated by fluorescence (Stair, 2007).

Although UV Raman spectroscopy is considered as a powerful technique in catalysis because it can avoid the fluorescence interference occurring in visible Raman spectroscopy and concurrently enhance the Raman scattering intensity, the decrease in the laser wavelength can reduce the penetration depth of the laser beam into the material (Kreisel et al., 2012). A UV Raman study on silicon device structures shows that the penetration depth goes from 300 nm in the case of a 485 nm laser to only ~ 15 nm for a UV 364 nm laser (Dombrowski et al., 1999).

The Raman spectrum of the carbonaceous materials has been previously studied (Sadezky et al., 2005, Pimenta et al., 2007). Generally, the spectrum of coke shows two main bands: a band centred at ~ 1580 cm^{-1} corresponding to the presence of

graphite in a single crystal, defined as G band, and a band at $\sim 1350\text{ cm}^{-1}$ called the D (D1) band, which is associated with the existence of disordered graphite and other types of carbon. The amorphous (non-graphite-like) carbon is typically composed of polycyclic aromatic compounds, which can be considered as graphene layer precursors. The ratio of the intensity or the peak areas of D1/G has been used to characterise the degree of structural order of carbon (Shamsi et al., 2005). In addition to these two main bands, other bands called D2, D3, and D4 centred at ~ 1620 , $1500\text{-}1550$, 1200 cm^{-1} respectively, are also appear in the Raman spectrum of coke. Each band is corresponds to a type of carbon structure as shown in Table 4.2.

Moreover, UV-Raman spectra of some polyaromatic compounds with more than two aromatic rings have been identified in the literature (Chua and Stair, 2003). Figure 4.6 shows Raman spectra and the molecular structure of these aromatic compounds.

In the present work, catalyst samples collected after reactions were examined using the Raman microscope systems: Renishaw inVia Raman Microscope, and Horiba Jobin Yvon LabRAM HR spectrometer. UV laser at wavelength of 325 nm was employed as the excitation source. The laser power was adjusted at a 5% of the source power, focused for 10 sec using a $15\times$ UV objective lens. The sample was introduced to the spectrometer by placing a thin layer of the sample, in the form of a loose powder, on a glass stripe. The sample stripe was then placed on the sample holder of the microscope at room temperature.

Table 4.2 Raman bands for carbonaceous materials (Sadezky et al., 2005).

Band	Raman shift (cm^{-1})	Assignment
G	~ 1580	Ideal graphitic lattice
D1(D)	~ 1350	Disordered graphitic lattice (graphene layer edges)
D2	~ 1650	Disordered graphitic lattice (surface graphene layers)
D3	~ 1500	Amorphous carbon
D4	~ 1200	Disordered graphitic lattice, polyenes, ionic impurities

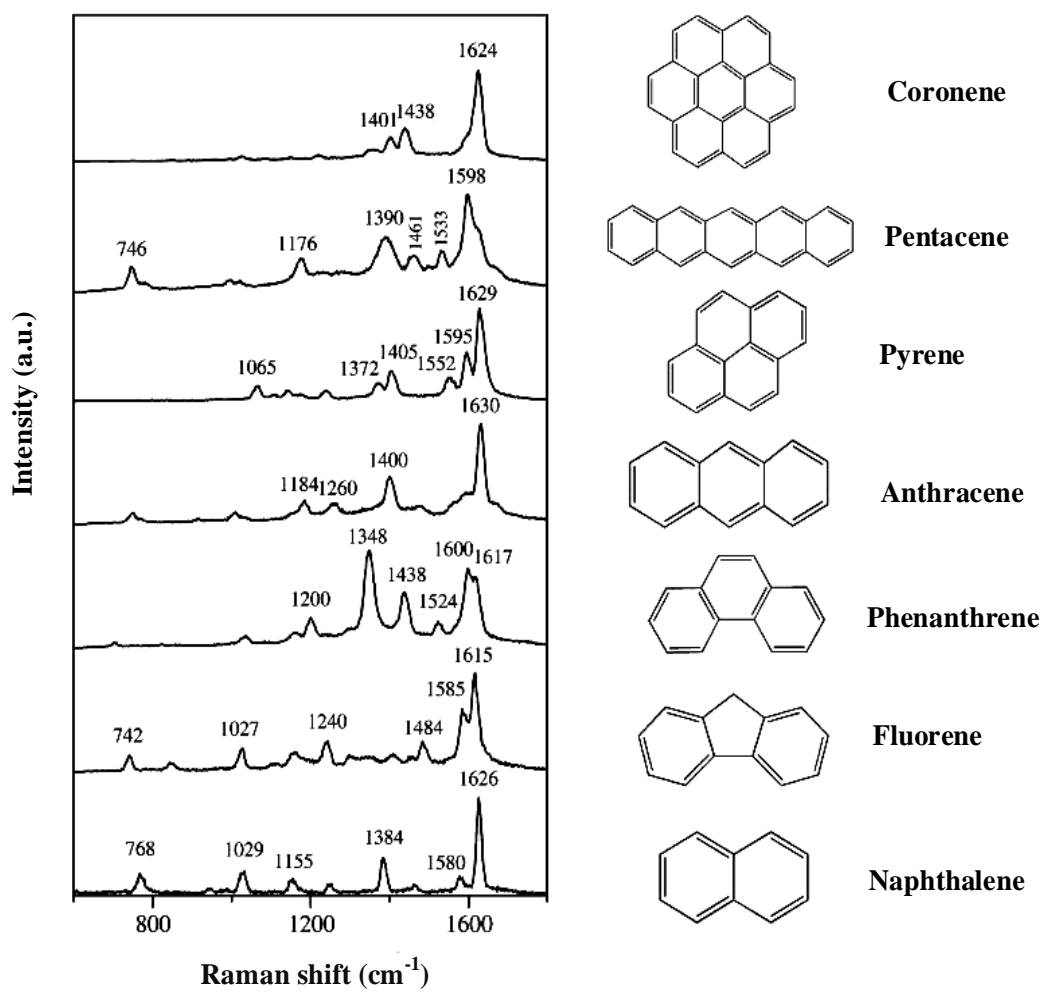


Figure 4.6 UV-Raman spectra of some polyaromatic hydrocarbons (Chua and Stair, 2003).

Chapter 5

*Role and nature of coke
deposits in n-pentane
isomerisation over
Pt/H-Beta*

5 Chapter 5: Role and nature of coke in *n*-pentane isomerisation over Pt/H-Beta

5.1 Introduction

The skeletal isomerisation of *n*-alkanes is a key catalytic process related to the energy field. The catalytic conversion of light linear alkanes such as *n*-pentane and *n*-hexane into their corresponding branched isomers is considered as the basis for the production of gasoline with high octane number and low concentrations of air pollutants such as olefins and aromatics (Ertl et al., 2008, Okuhara, 2004, Wittcoff et al., 2004). The commercial catalysts employed to perform this process are platinum supported on solid acids, such as chlorinated alumina and zeolite (Chica and Corma, 1999, Ertl et al., 2008). The reaction usually takes place in the presence of hydrogen. The function of using platinum in the catalyst and the hydrogen in the feed is to reduce the build-up of carbonaceous deposits, thus prolonging catalyst lifetime (Ono, 2003, Wulfers and Jentoft, 2013).

The reaction mechanism suggested and widely accepted for the skeletal isomerisation of *n*-pentane over the bifunctional catalyst is the monomolecular mechanism as described in Section 2.3.2.

Pt/Mordenite is commercially used as a catalyst for the isomerisation of Light Straight Run (LSR) naphtha. This large pore (12-membered rings) zeolite was favoured over the so-called narrow and medium-pore (8- and 10-membered rings) zeolites due to the easy transport of reactants and products through zeolite microstructure (Ertl et al., 2008, Lenoir et al., 2005).

Beta zeolite has also found wide applications in the isomerisation of hydrocarbons (Chica and Corma, 1999, Van de Runstraat et al., 1997, Föttinger et al., 2003, Kamarudin et al., 2012). This is owing to its unique catalytic properties as a high Si/Al ratio that reflects high thermal stability, the three-dimensional interlinked channels structure, and the large pore size that enable faster diffusion rates of reactants and products (Halgeri and Das, 1999, López et al., 2010, Liu et al., 2009).

Several investigations have been performed to study the isomerisation of *n*-pentane, *n*-hexane, and LSR naphtha consisting mainly of *n*-pentane and *n*-hexane over H-Beta. Lee and Rhee, compared the performance of Pt/H-mordenite and Pt/H-Beta catalysts in the isomerisation of *n*-hexane. It has been found that the selectivity to high octane isomers was higher over Pt/H-Beta than that over the commercial Pt/H-mordenite (Lee and Rhee, 1997). Chica and Corma, reported that LSR naphtha has been successfully isomerised over a nanocrystalline Beta zeolite (Chica and Corma, 1999). Another study demonstrated that Pt-containing dealuminated H-Beta showed the best performance in the isomerisation of *n*-pentane in comparison to Pt-containing ZSM-5 and SAPO-11 (López et al., 2008). Modhera *et.al.*, investigated the isomerisation of *n*-hexane over Pt-containing nanocrystalline Beta; a high conversion of *n*-hexane and high isomerisation selectivity were observed at the studied reaction conditions. In addition, it was found that 0.5 wt.% Pt is the optimum metal loading to provide a balance between acid and metal sites (Modhera et al., 2009). *n*-Pentane isomerisation was further studied over Pt promoted acid zeolites including mordenite, ZSM-5, and Beta with similar acidity. The highest selectivity was observed over Pt/H-Beta; additionally it was found that the structure of zeolite plays the major role in the performance of the catalyst in such reactions rather than acidity (López et al., 2010).

Although the isomerisation reaction of light *n*-alkanes over Pt/zeolites has been widely studied in the literature, very few works have been published on coke deposition and the deactivation of these catalysts in such reactions. Some attention has been paid on studying the deactivation of Pt/mordenite as a commercial catalyst during the isomerisation of *n*-pentane (Lenoi et al., 2004, Lenoir et al., 2005). A more recent study on the conversion of *n*-butane, *n*-pentane, and *n*-hexane conversion over H-mordenite showed that the carbonaceous deposits formed over H-mordenite during these reactions were originated from olefins (Wulfers and Jentoft, 2013).

The literature showed that carbonaceous deposits formed as a side product during acid catalysed reactions, in addition to being implicated in catalyst deactivation, may have a beneficial or active role in enhancing the catalytic performance (Guisnet, 2002a). Therefore, a key focus of the present study is to explore the potential role of the carbonaceous species in the catalytic isomerisation of *n*-pentane, and to understand

the relationship between the chemistry of these carbonaceous materials and the catalytic performance.

This chapter comprises of two parts: the first part includes a reaction study of the catalytic isomerisation of *n*-pentane, as a representative short-chain *n*-alkane, over the synthesised Pt/H-Beta catalyst. The influence of reaction temperature and time-on-stream on the performance of the catalyst has been studied and compared over the temperature range of 200-350 °C, and after 1, 6, and 92 h time-on-stream.

The second part of the chapter composes an investigation into the properties of the carbonaceous deposits that are laid down over the catalyst at different stages of *n*-pentane isomerisation reaction and their influence on the catalytic performance in this reaction. These carbonaceous species were formed over the Pt/H-Beta after reactions at a temperature of 300 °C, weight hourly space velocity (WHSV) of 1.5 h⁻¹ and at 1, 6, and 92 h time-on-stream. A range of thermal and spectroscopic characterisation techniques were employed to investigate the quantity, structure, nature, and location of these deposits.

5.2 Materials and methods

The catalyst employed for the catalytic isomerisation-cracking reaction of *n*-pentane is a 0.45 wt.% Pt supported on a high silica H-Beta zeolite (SiO₂/Al₂O₃ mole ratio of 360:1). The preparation method of this catalyst is described in Section 3.3.3.

The properties of the prepared Pt/H-Beta catalyst were investigated using a range of characterisation techniques including: differential thermogravimetry (DTG); inductively coupled plasma (ICP); temperature programmed reduction (TPR); and N₂-adsorption isotherms. A detailed description of the instruments employed, with the methods developed to perform these analyses, is contained in Chapter 4.

The reaction was performed in the presence of H₂, under atmospheric pressure in a fixed bed, continuous flow reactor using the reactor set-up and the experimental procedure described in Sections 3.4.1.1 and 3.4.1.3, respectively.

On-line gas chromatography measurements were taken every 30 min by utilising an on-line GC/FID and using the GC column and the GC method described in Section 3.5.1. The methods for calculating the catalytic performance indicators (conversion and selectivity) and the reproducibility error are explained in Section 3.6.

Post-reaction, the catalyst samples were characterised *ex situ* by a combination of thermal and spectroscopic techniques to investigate the quantitate, type, and nature of the carbonaceous deposits that are laid down on the catalyst surface after reaction. UV-Raman was used as a spectroscopic technique whilst elemental analysis, thermogravimetric analysis (TGA), and temperature-programmed oxidation (TPO) were used as thermal techniques. The experimental parameters employed for each of these measurements are described in Chapter 4.

5.3 Results and discussion

5.3.1 Catalyst characterisation

After the preparation of the Pt/H-Beta catalyst using the wet impregnation method (Section 3.3.3), the appropriate calcination temperature required for the decomposition of the Pt precursor loaded over zeolite H-Beta was investigated using TGA/DTG. The analysis was carried out for the fresh zeolite H-Beta as shown in Figure 5.1(a) as well as for the impregnated Pt/H-Beta catalyst before calcination, as shown in Figure 5.1(b). The peak associated with the decomposition of the Pt precursor was observed at approximately 310 °C in the DTG curve of the catalyst sample before calcination. The calcination temperature of that catalyst proposed in the literature is 300-350 °C (Park and Ihm, 2000, López et al., 2010, Tsai et al., 2011).

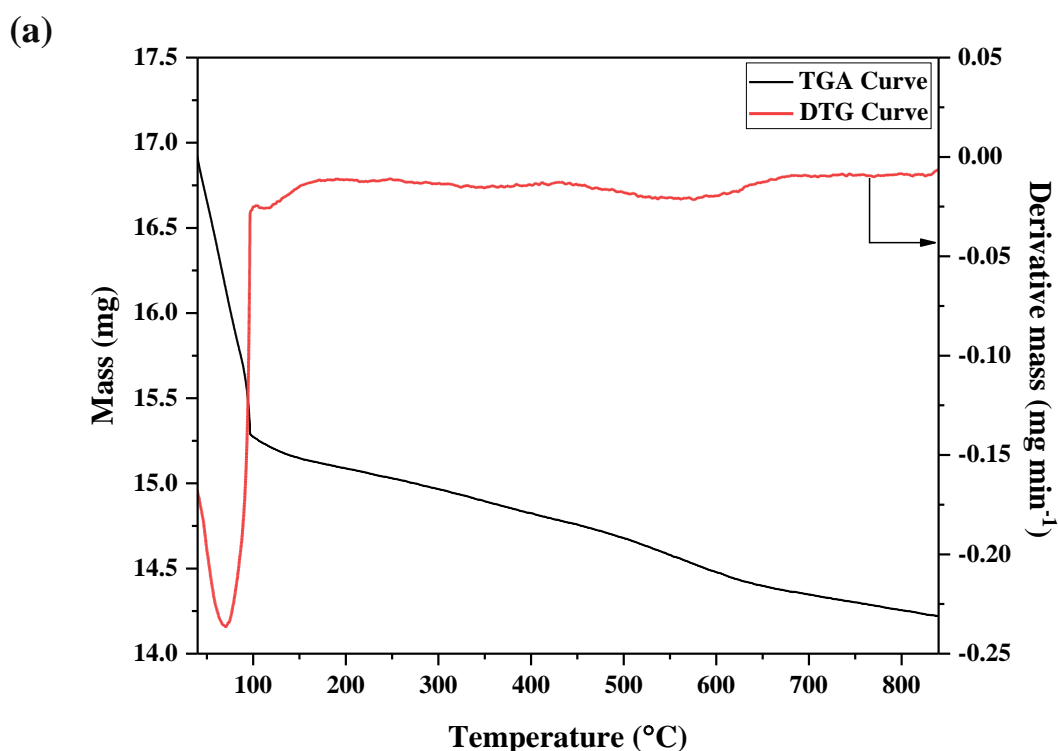
Based on DTG analysis and following the preparation procedure in the literature, the catalyst was calcined at 320 °C using dry air in a flowing air furnace. The decomposition of the Pt precursor was confirmed in the DTG curve of the catalyst sample after calcination as shown in Figure 5.1(c) where the Pt precursor exothermic peak observed in Figure 5.1(b) is not present in Figure 5.1(c).

The Pt content of the calcined catalyst was determined by elemental analysis *via* ICP. The sample of the calcined Pt/H-Beta catalyst was digested in Aqua regia-Hydrofluoric acid solution to dissolve the Pt as well as the Si and Al presented in the zeolite H-Beta. The percentage of Pt loading measured by ICP was 0.45 wt.% (4500 mg Kg⁻¹). This compared to the theoretical loading of 0.5 wt.% based on the mass of Pt used in the synthesis.

The BET surface area of the synthesised 0.45 wt.% Pt/H-Beta was determined by BET analysis as described in Section 4.4. The surface area was found to be 533 m² g⁻¹. This is lower than the surface area of the support without metal loading (620 m² g⁻¹). The decrease in BET surface area after zeolite impregnation can be attributed to the accumulation of Pt particles at the mouth of the pores and/or channels causing pore blockage. It is widely known that metal loading reduces zeolite BET surface area due

to the diffusion of metal particles into zeolites micropores during the impregnation leading to pore blockage (Qian and Yan, 2001, Dewajani et al., 2016).

The reduction temperature of the platinum phase of the prepared catalyst was investigated using TPR analysis. The reduction temperature of 0.45 wt.% Pt/H-Beta was 325 °C. The instrument employed was calibrated by testing the reduction temperature of silver oxide as a standard reference material (reduction temperature 125 ± 15 °C). TPR profiles of the prepared Pt/H-Beta and silver oxide as a reference material are shown in Figure 5.2. It can be observed that H₂ consumption of 0.45 wt.% Pt/H-Beta sample is low compared to silver oxide due to the low Pt loading of the prepared catalyst.



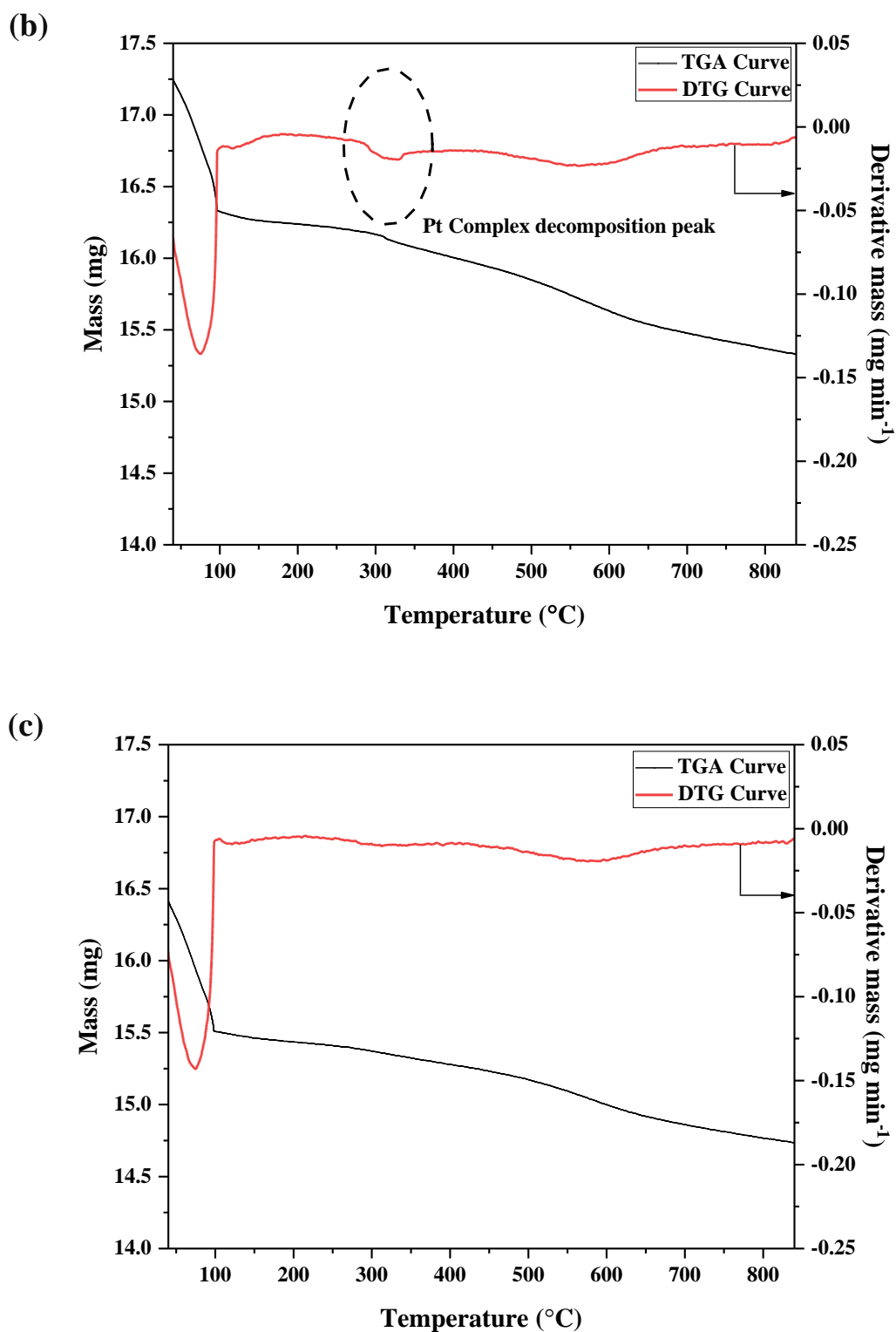


Figure 5.1 TGA/DTG curves for the decomposition of (a) fresh zeolite H-Beta; (b) 0.45 wt.% Pt/H-Beta before calcination; (c) 0.45 wt.% Pt/H-Beta after calcination at 320 °C in air. In all the presented analysis, air was employed as a carrier gas.

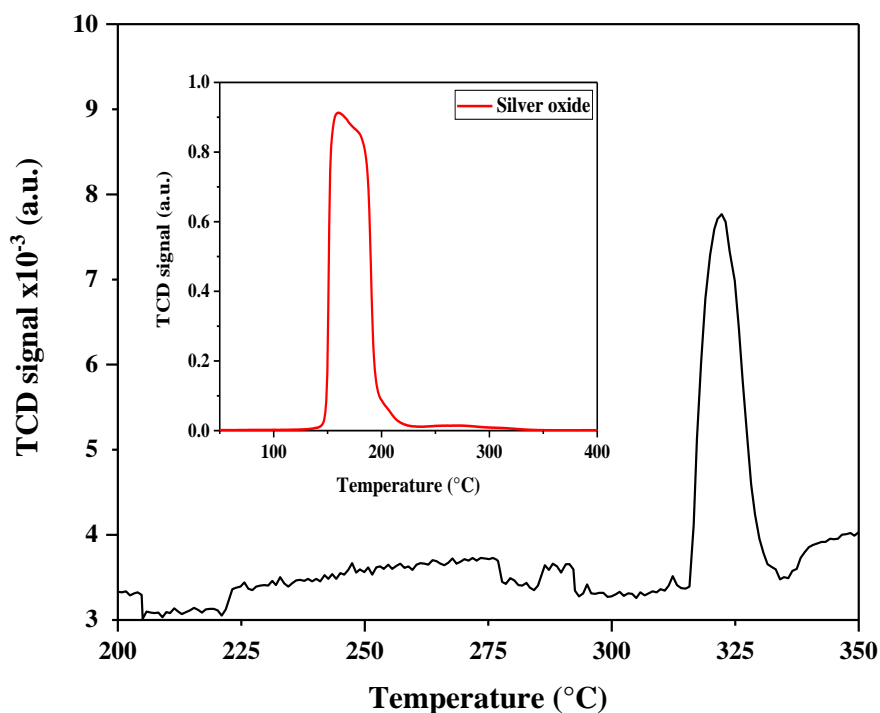


Figure 5.2 TPR profile of 0.45 wt.% Pt loaded on H-Beta catalyst. Inserted TPR profile of a silver oxide, used as a reference material.

5.3.2 Catalytic activity measurements

The catalytic conversion of *n*-pentane was carried out under atmospheric pressure in a continuous flow-fixed bed reactor in the presence of H₂. The main variables that are affecting this reaction are reaction temperature, space velocity, H₂/*n*-pentane molar ratio in the feed, and reaction time-on-stream (TOS). However, it is worth mentioning that the typical operating conditions of the commercial isomerisation process of the light straight run (LSR) naphtha (consisting mainly of pentane and hexane) are: H₂/*n*-pentane molar ratio of 2.75, weight hourly space velocity (WHSV) of approximately 1.5 h⁻¹, and a total pressure of 20 bars (López et al., 2008).

In the present work, the H₂/*n*-pentane molar ratio was kept constant at 3.12 by maintaining the partial pressure of *n*-pentane in the H₂-pentane mixture introduced to the reactor at approximately 0.24 bar calculated *via* the Antoine equation at 0 °C and ambient pressure. In addition, to simulate the industrial conditions, the WHSV was

maintained at 1.53 h^{-1} for the reactions performed at different temperatures and TOS using 0.5 g of the catalyst and a H_2 flow rate of 12.5 ml min^{-1} .

The reproducibility of the experiments was verified by repeating a model reaction (carried out at $300 \text{ }^\circ\text{C}$, WHSV of 1.53 h^{-1} , H_2/n -pentane molar ratio at 3.12, and TOS of 360 min) three times, each on a different day. The reproducibility error was 3.8% relative to the *n*-pentane conversion measurement, and 3.7% for the selectivity to *iso*-pentane which reflects a good reproducibility of the experiment.

Reaction products were identified using the library of the GC/MS software (GCMSsolution, version 4.44). An example of the chromatogram of the *n*-pentane reaction products with the compounds names identified by the MS is shown in Figure 5.3. This reaction was performed at $300 \text{ }^\circ\text{C}$, WHSV of 1.53 h^{-1} , and after 120 minutes TOS.

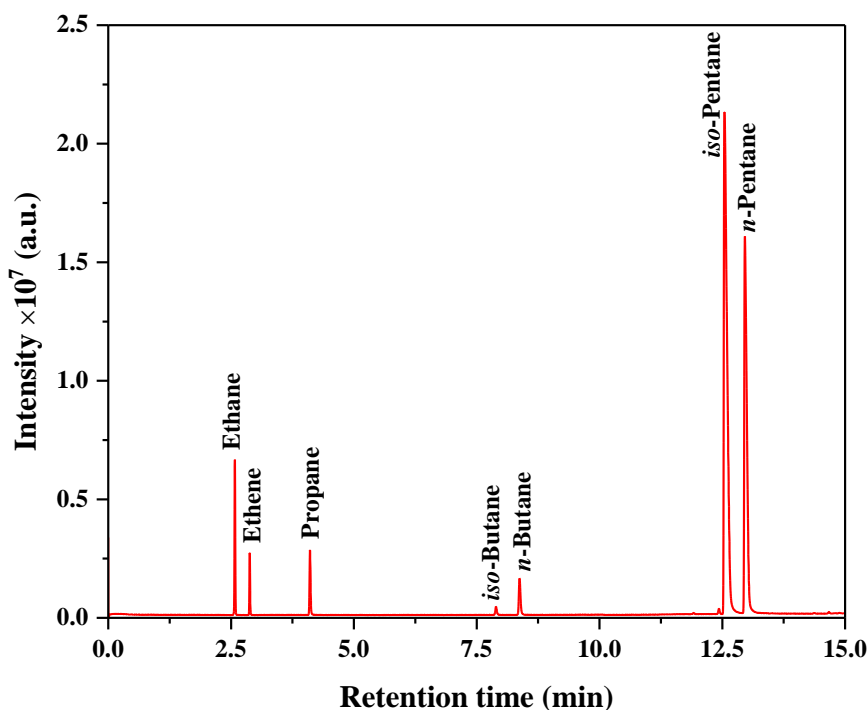


Figure 5.3 GC/MS Chromatogram for reaction products of *n*-pentane conversion over 0.5 g Pt/H-Beta, at $300 \text{ }^\circ\text{C}$, WHSV of 1.5 h^{-1} , H_2 /pentane mole ratio of 3.12, and after 120 min TOS.

From the GC chromatogram shown in Figure 5.3, it can be observed that *iso*-pentane is the main product of the reaction, however, cracking products lighter than pentane including ethane, ethene, propane, *iso*-butane, and *n*-butane are also present. Generally, no significant peaks for compounds heavier than pentane were observed in the GC chromatogram at the studied reaction temperatures. Any other reaction products that not presented in the gas phase were assumed to be as coke. Therefore, reaction products were grouped as: (i) *iso*-pentane; (ii) unreacted *n*-pentane; (iii) cracking products lighter than pentane; and (iv) coke.

5.3.2.1 Influence of reaction temperature

The selection of the optimum reaction temperature for this reaction is largely dependent on the activity of the catalyst employed. However, it has been reported that the equilibrium conversion to isomers in such reactions is enhanced at lower reaction temperatures (Gary and Handwerk, 2001).

The performance of the prepared 0.45 wt.% Pt/H-Beta catalyst was examined over a reaction temperature range of 200-350 °C and at WHSV of 1.53 h⁻¹ for 360 min TOS using 0.5 g of the catalyst. The values of *n*-pentane conversion, and the selectivity to *iso*-pentane and other products were collected every 30 minutes during reaction and averaged over the steady-state regime, which occurred from 60 min onwards as shown in Figure 5.4 for the reaction at 300 °C, WHSV of 1.53 h⁻¹ and 360 min TOS.

Figure 5.5 shows the catalytic behaviour in terms of the total molar conversion of *n*-pentane and the molar selectivity to *iso*-pentane as a function of reaction temperature in the range 200-350 °C.

From Figure 5.5, it can be observed that the conversion of *n*-pentane increases along with the increase of reaction temperature to a maximum of 74% at 350 °C. However, the activity of the catalyst was very low at 200 °C, with only 5% conversion of *n*-pentane. This poor activity at 200 °C is possibly attributed to the high SiO₂/Al₂O₃ molar ratio of the employed zeolite (360:1) which indicates a low acidity of the catalyst (see Section 2.2.3). Therefore, a higher temperature is required to enhance the activity of the employed catalyst.

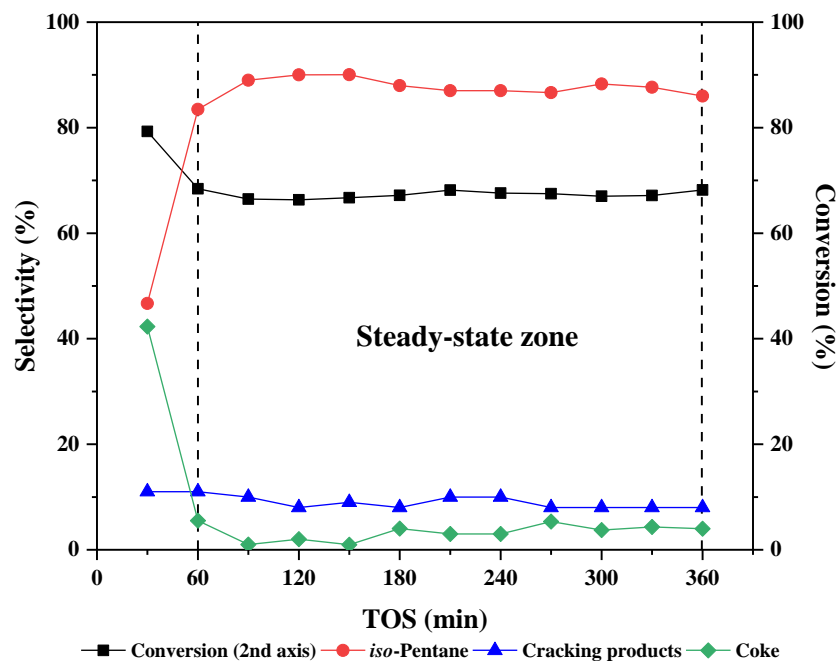


Figure 5.4 Steady state regime of *n*-pentane conversion over 0.5 g Pt/H-Beta catalyst, at 300 °C, WHSV of 1.5 h⁻¹, H₂/pentane mole ratio of 3.12, and 360 min TOS.

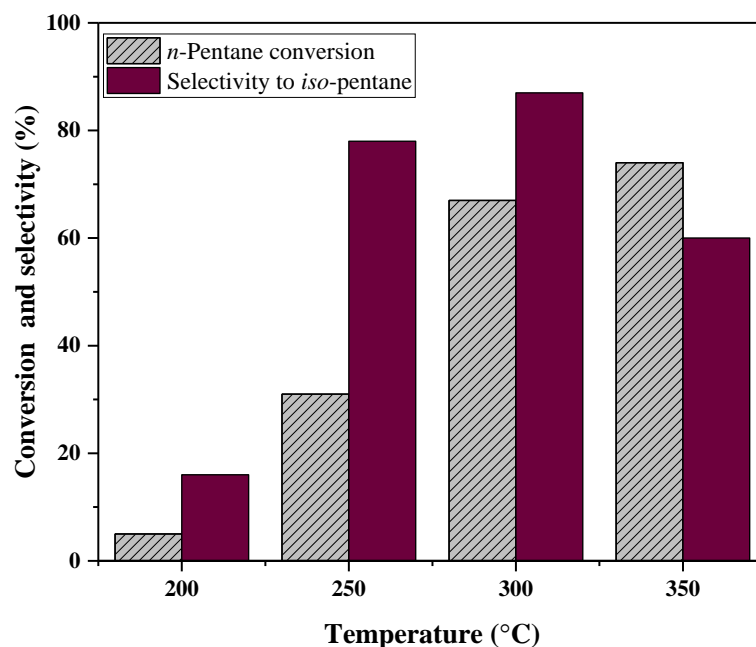


Figure 5.5 Conversion of *n*-pentane and selectivity to *iso*-pentane of the catalytic isomerisation of *n*-pentane over 0.5 g Pt/H-Beta catalyst at WHSV of 1.5 h⁻¹, H₂/pentane mole ratio of 3.12, and at 200, 250, 300, and 350 °C reaction temperatures.

Similarly, the prepared 0.45 wt.% Pt/H-Beta catalyst exhibited a high selectivity towards *iso*-pentane over the whole range of the studied temperatures as shown in Figure 5.5 and Figure 5.6. The highest level of selectivity to *iso*-pentane was 87% at 300 °C. This high selectivity to isomerisation possibly indicates that the prepared catalyst could have an effective balance between the acidic and metallic sites; it has been reported that the catalyst behaviour is directly related to the balance between the metallic and the acidic sites (Guisnet et al., 1987, Deldari, 2005, Batalha et al., 2013c). Nevertheless, at 350 °C the selectivity to *iso*-pentane was reduced and cracking begins to take over. Although the selectivity to *iso*-pentane was the highest among other products at 350 °C, a decline of 30% from the maximum selectivity was observed whilst the selectivity to cracking increased to 40%.

The selectivity to coke and coke precursors at the studied TOS reduced with increasing temperature, as shown in Figure 5.6. This can be attributed to the enhancement of oligomerisation reactions at lower reaction temperatures that lead to coke formation. It has been established that coke formation is more pronounced at lower reaction temperatures due to the occurrence of oligomerisation reaction (Föttinger et al., 2003). Also, Stucky and Dwyer reported that the conversion of C₂-C₁₀ olefins to higher molecular weight products over zeolites is favoured at low temperature (200-260°C) and long contact time (0.5-1 WHSV). At these conditions the reaction proceeds through the acid-catalysed steps of (i) oligomerisation, (ii) isomerisation-cracking, and (iii) copolymerisation (Stucky and Dwyer, 1983). These reactions can lead to coke formation, and therefore fewer acid sites are available for skeletal isomerisation at 250 °C as a result of coke deposition. Additionally, at higher reaction temperatures a potential gasification of coke can take place in the presence of H₂. This might be one of the reasons behind the lower selectivity to coke at 300 and 350 °C than that at 250 °C.

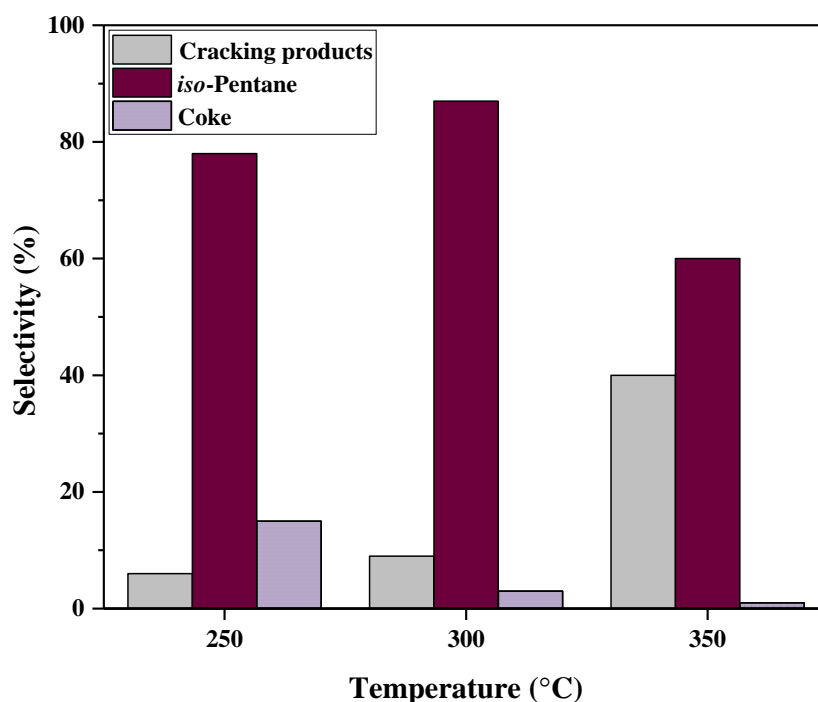


Figure 5.6 Selectivity to different reaction products of the catalytic isomerisation of *n*-pentane over 0.5 g Pt/H-Beta catalyst at WHSV of 1.5 h⁻¹, H₂/pentane mole ratio of 3.12, and at 250, 300, and 350 °C reaction temperatures.

Several authors have reported reasonable activity (>50%) and the high selectivity to isomerisation over Pt/H-Beta in the isomerisation of light *n*-alkanes. This behaviour has been ascribed mainly to the large pore diameter and the three-dimensional interlinked channels of zeolite Beta rather than to its acidity (Ramos et al., 2007, Liu et al., 2008, López et al., 2010). The behaviour of the examined 0.45 wt.% Pt/H-Beta catalyst is consistent with that mentioned in the literature where approximately 70% conversion of *n*-pentane and greater than 85% selectivity to *iso*-pentane were obtained at 300 °C.

Based on the obtained results, a reaction temperature of 300 °C was chosen for further investigation due to the reasonable activity and the high selectivity to *iso*-pentane achieved at this temperature.

5.3.2.2 Influence of TOS

The behaviour of the synthesised 0.45 wt.% Pt/H-Beta catalysts was tested at a temperature of 300 °C, WHSV of 1.53 h⁻¹, H₂/pentane mole ratio of 3.12, and at different TOS. The aim is to examine the activity and the stability of the catalyst at different stages of the reaction.

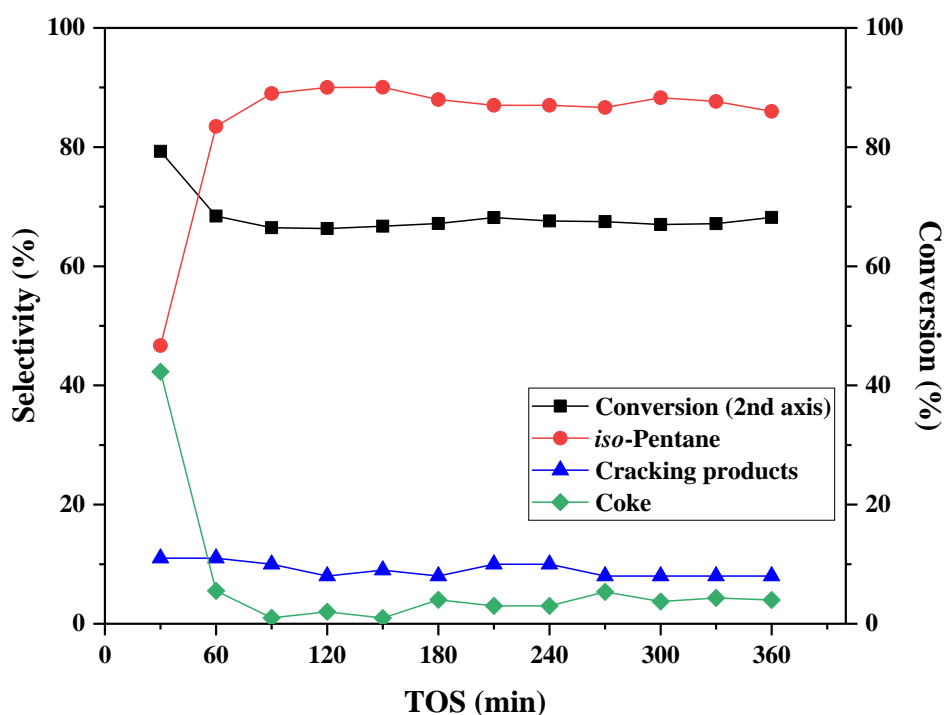


Figure 5.7 *n*-Pentane conversion and the selectivity to reaction products as a function of TOS for *n*-pentane conversion over 0.5 g Pt/H-Beta at 300 °C, WHSV of 1.5 h⁻¹, and H₂/pentane mole ratio of 3.12. The same data are presented in Figure 5.4.

Figure 5.7 shows the performance of the catalyst in terms of *n*-pentane conversion and selectivity to different products *versus* TOS. It can be seen that the highest conversion of 80% was achieved after 30 min of the reaction and then decreased to approximately 68% after 60 min, and remained almost constant to the end of the studied TOS. In the same time interval, the selectivity to isomerisation was 46% after 30 min reaction, then increased to about 85% after 60 min, and maintained around that level until the end of the 360 min reaction.

Furthermore, it can be observed that the catalyst exhibits a significant tendency to form carbonaceous deposits during this induction period, in which the selectivity to coke was more than 40%. However, this selectivity rapidly decreased to less than 5% after 60 min of reaction along with a corresponding increase in the selectivity to skeletal isomerisation.

The selectivity to cracking products lighter than pentane was approximately 10% after 30 min of reaction and was maintained around this level over all the studied TOS. After 60 min TOS, the conversion, and the selectivity to all the products reached a steady-state which might be due to the build-up of the carbonaceous deposits at the early stage of the reaction. Thus, 60 min TOS is considered the induction period of the reaction required for catalyst stabilisation, and the start point of the steady-state stage.

Similar catalytic behaviour over the 0.45 wt.% Pt/H-Beta was also observed at all the studied reaction temperatures (250, 300, 350 °C) but with different levels of conversion and selectivity as discussed in Section 5.3.2.1.

The performance of the synthesised 0.45 wt.% Pt/H-Beta catalyst was further examined at longer TOS. A reaction was performed for almost 4 days (92 h) at the same mentioned conditions of temperature, WHSV, and H₂/pentane mole ratio. The molar conversion of *n*-pentane and the selectivity to *iso*-pentane were measured every 1 h until 5 h and then every 6 h as shown in Figure 5.8.

From Figure 5.8 it can be seen that there is a slight increase in the total conversion of *n*-pentane from an initial level of 68% after 1 h to 72% at the latter stages of the studied TOS. In addition, the selectivity to *iso*-pentane decreased from the highest level of 86% after 6 h to 73% after 78 h. However, the general trend demonstrates a considerable stability of the catalyst during the studied TOS, and no significant deactivation has been observed. The slight fluctuation in the obtained results could be attributed to a variation in the GC measurement.

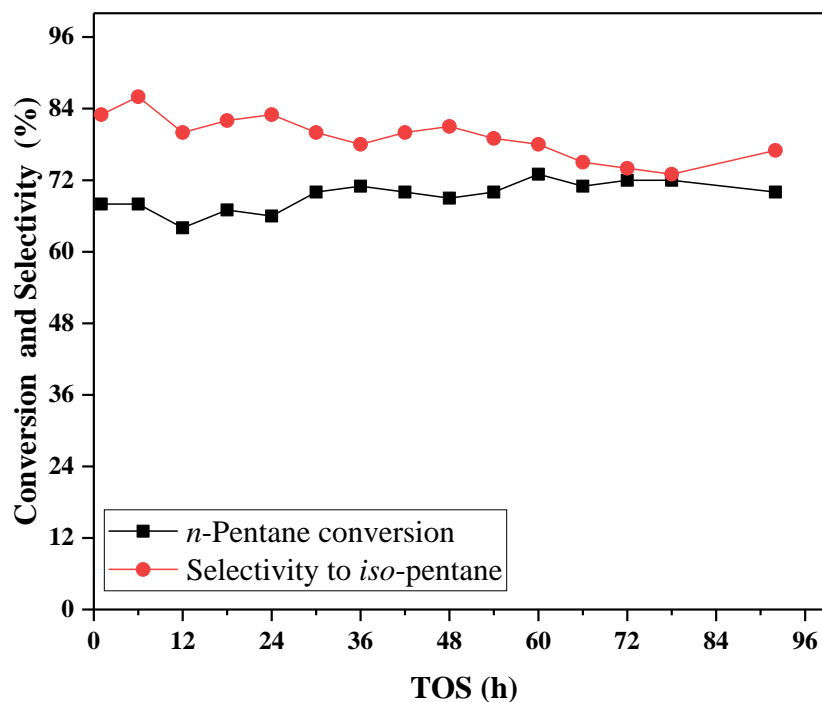


Figure 5.8 *n*-Pentane conversion and selectivity to *iso*-pentane as a function of TOS over 0.5 g Pt/H-Beta at 300 °C, WHSV of 1.5 h⁻¹, and H₂/pentane mole ratio of 3.12.

The relative stability of the catalyst after a short TOS is possibly due to the formation of carbonaceous deposits. These deposits were assumed to be formed as a result of side reactions such as oligomerisation, dimerisation, and hydrogen transfer *via* the bimolecular mechanisms on the high energy acid sites located inside zeolite channels. Such reactions are responsible for coke formation. Additionally, the 3-dimensional interconnected channels structure of zeolite Beta can provide enough space for the formation of such large molecules.

The carbonaceous deposits formed at the early stage of the reaction are believed to be responsible for the enhancement of the isomerisation reaction and control coking and other side reactions through:

- i. The improvement in catalyst shape selectivity, which may prevent the formation of dimers and oligomers as a result of restricted transition-state selectivity.

- ii. The deactivation of the strong acid sites responsible for catalysing the undesired reactions.
- iii. The potential presence of catalytically active carbonaceous species that promote the isomerisation reaction most likely at catalyst pore mouth. Guisnet proposed that the carbonaceous compounds formed inside the zeolite pores and located close to the pore mouth can interact with zeolite protonic sites and form active sites that are most likely responsible for the skeletal isomerisation reaction of *n*-alkanes (Guisnet, 2002a).

5.3.3 Coke characterisation

Post-reaction, the catalyst samples have been analysed using TGA, elemental analysis, TPO, and UV-Raman in order to investigate the quantity, the structure, the location, and the chemical composition of the carbonaceous materials accumulated over the synthesised 0.45 wt.% Pt/H-Beta catalyst at different TOS. The aim is to investigate how the properties of these carbonaceous deposits changed with TOS, and to develop an understanding about the relationship between the chemistry of the coke deposits formed and the activity data discussed in the previous sections.

Coke deposits have been studied after reaction at 300 °C, WHSV of 1.53 h⁻¹, H₂/pentane mole ratio of 3.12, and at different TOS including: (i) the initial stage (after 1 h), (ii) the steady-state operation stage (after 6 h), and (iii) after long TOS (aged catalyst after 4 days of operation).

5.3.3.1 Thermogravimetric analysis (TGA)

The quantity of coke accumulated over the 0.45 wt.% Pt/H-Beta catalyst at different stages of *n*-pentane conversion is shown in Table 5.1. The coke has been classified as a “soft coke” which is removed by the TGA at a temperature from 200 to 400 °C, and a “hard coke” which is removed at temperatures higher than 400 °C (Siddiqui et al., 2000, Kozhevnikov et al., 2001, Ahmed et al., 2011). The sample weight loss at temperatures lower than 200 °C is attributed to the desorption of physisorbed water and weakly bound volatile materials (Wang and Manos, 2007).

From the TGA data presented in Table 5.1, it can be seen that coke was rapidly formed over the catalyst during the early stage of *n*-pentane conversion. Afterwards, no significant change in coke quantity was observed at the subsequent stages. These data confirm the results obtained from the study of the selectivity and conversion as a function of TOS presented in Section 5.3.2.2. The low tendency to coke formation and the high stability of the catalyst after the first hour of reaction give rise to the significant role of coke formed at the early stage of the reaction in redirecting the reaction to a more selective pathway.

Table 5.1 Coke content percent of the spent 0.45 wt.% Pt/H-Beta catalysts in *n*-pentane conversion at 300 °C, WHSV of 1.53h⁻¹, H₂/pentane mole ratio of 3.12, and at different TOS. The measurement was repeated three times for each sample and the standard deviation from the mean value was calculated.

TOS	Soft coke (wt.%) (200-400 °C)	Hard coke (wt.%) (400-850 °C)	Total coke (wt.%) (200-850 °C)
1 h	1.0 ± 0.00	3.3 ± 0.08	4.3 ± 0.08
6 h	1.2 ± 0.15	3.2 ± 0.21	4.4 ± 0.07
4 days	1.2 ± 0.10	3.3 ± 0.07	4.5 ± 0.03

The composition of the soft coke and the hard coke has previously been studied for several catalytic reactions over zeolites and zeolite-supported metal catalysts. Generally, these studies concluded that the soft coke is composed mostly of alkylated mono- and di-aromatics and smaller amounts of polyaromatics, whilst the hard coke is mainly poly-condensed aromatic compounds (Magnoux et al., 1989, Chen and Manos, 2004, Sahoo et al., 2004). The data in Table 5.1 show that the largest part of the coke formed over the catalyst in this work is hard coke, as it represents more than 80% of the total coke formed. However, no attempt has been made in this work to identify the specific composition of the hard and the soft coke formed during the reaction.

5.3.3.2 Elemental analysis

The percentage of C and H present on the spent Pt/H-Beta catalyst at different stages of *n*-pentane conversion was determined by elemental analysis and is given in Table 5.2.

Table 5.2 Elemental analysis data showing the wt.% of C and H and the H/C mass ratio after different stages of *n*-pentane conversion over 0.5 g Pt/H-Beta at 300 °C, WHSV of 1.53h⁻¹, and H₂/pentane mole ratio of 3.12.

TOS	%C (wt.%)	%H (wt.%)	H/C ratio
1 h	0.4 ± 0.01	0.5 ± 0.07	1.1 ± 0.01
6 h	0.5 ± 0.05	0.5 ± 0.04	1.0 ± 0.19
4 days	0.5 ± 0.04	0.5 ± 0.00	0.9 ± 0.09

From the overall H/C mass ratio of the formed carbonaceous deposits, and according to the criteria previously defined in Section 4.6, the structure of coke formed during each reaction period can be described as at the transition between amorphous and graphitic coke. In agreement with the TGA results, a slight decrease in the H/C ratio can be observed with increased coke loading, indicating an increase in coke aromaticity. Nevertheless, the structure and the chemical identity of the carbonaceous deposits are still ambiguous. Therefore, the quantitative techniques of TGA and elemental analysis have been complemented with other thermal and spectroscopic techniques to identify the molecular structure and the composition of the carbonaceous deposits.

5.3.3.3 Temperature-programmed oxidation (TPO)

The TPO profile of the spent catalyst samples after *n*-pentane conversion at different TOS is shown in Figure 5.9. It can be observed that the obtained profiles consisted of several overlapping peaks that are assigned to different types of carbonaceous materials. However, these peaks are not well resolved and deconvolution is needed to resolve and identify the types of these carbonaceous deposits.

The TPO profiles were deconvoluted to four Gaussian peaks using OriginLab software, version 9.40. The initial position of the peaks and the line shapes were chosen in agreement with those reported in the literature for TPO analysis of coke

formed on acidic support and supported metal catalysts (Larsson et al., 1996, Bayraktar and Kugler, 2002, Chen et al., 2013).

The deconvoluted TPO profiles for the spent catalyst samples after 1 h, 6 h, and 4 days of reaction are shown in Figure 5.10 (a), (b), and (c), respectively. The resolved peaks after each stage of the reaction are labelled as A, B, C, and D in which peak A is centred at the lowest temperature followed by the subsequent peaks at higher temperatures. These peaks are attributed to the presence of coke with different structure, oxidation reactivity, and location.

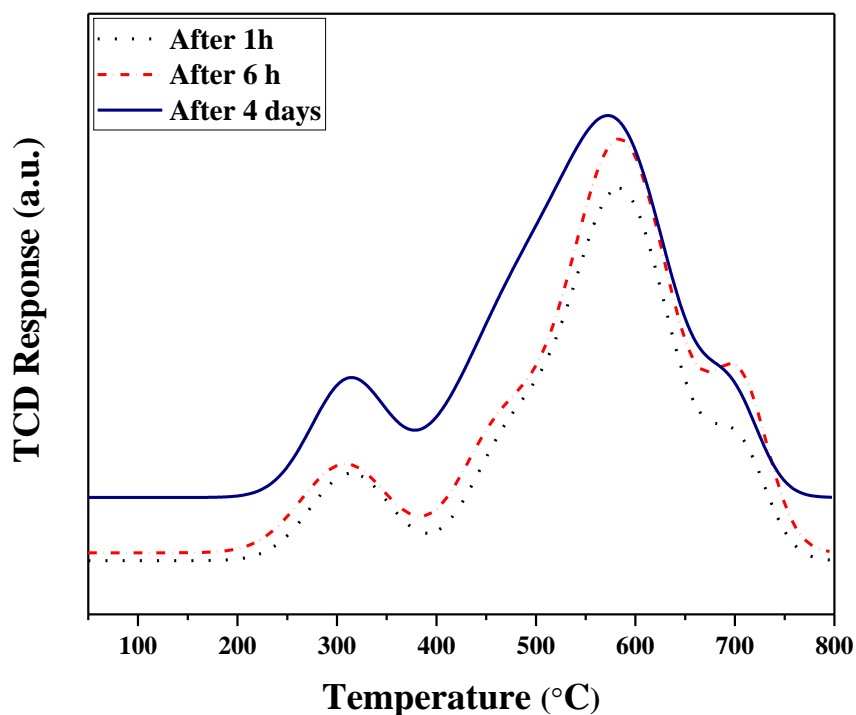
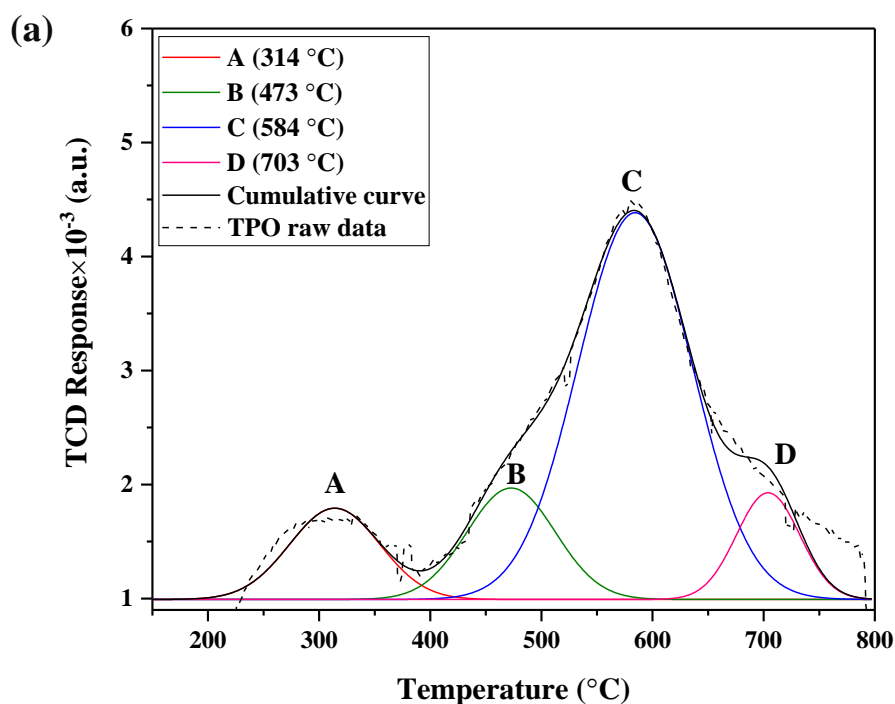


Figure 5.9 TPO fitted profile of the spent catalyst samples after *n*-pentane conversion over 0.5 g of 0.45 wt.% Pt/H-Beta at 300 °C, WHSV of 1.5 h⁻¹, H₂/pentane mole ratio of 3.12, and at 1, 6, 92 h TOS.

As discussed in Section 4.8, observation of a peak centred around 300 °C can be ascribed to the presence of hydrogen-rich carbonaceous species with high reactivity to oxygen, whilst a peak centred around 400 °C corresponds to amorphous carbon, and

a peak at oxidation temperature around and higher than 500 °C is attributed to graphitic-like carbon with lower reactivity (Chen et al., 2013).

The results obtained in this study are consistent with the types of coke described above. The peaks A, B, C presented in Figure 5.10 (a), (b), and (c) centred at temperatures around 300, 460, and 580 °C are most likely belong to hydrogen-rich species, amorphous carbon, and graphitic-like carbon, respectively. The last peak D centred around 700 °C is likely due to the presence of well-crystallised graphitic carbon. In order to probe the expected oxidation temperature of graphitic carbon, a sample of pure graphite (Sigma Aldrich) was analysed with the TPO. This showed a peak at around 740 °C, supporting the assumption of the nature of the coke described by peak D.



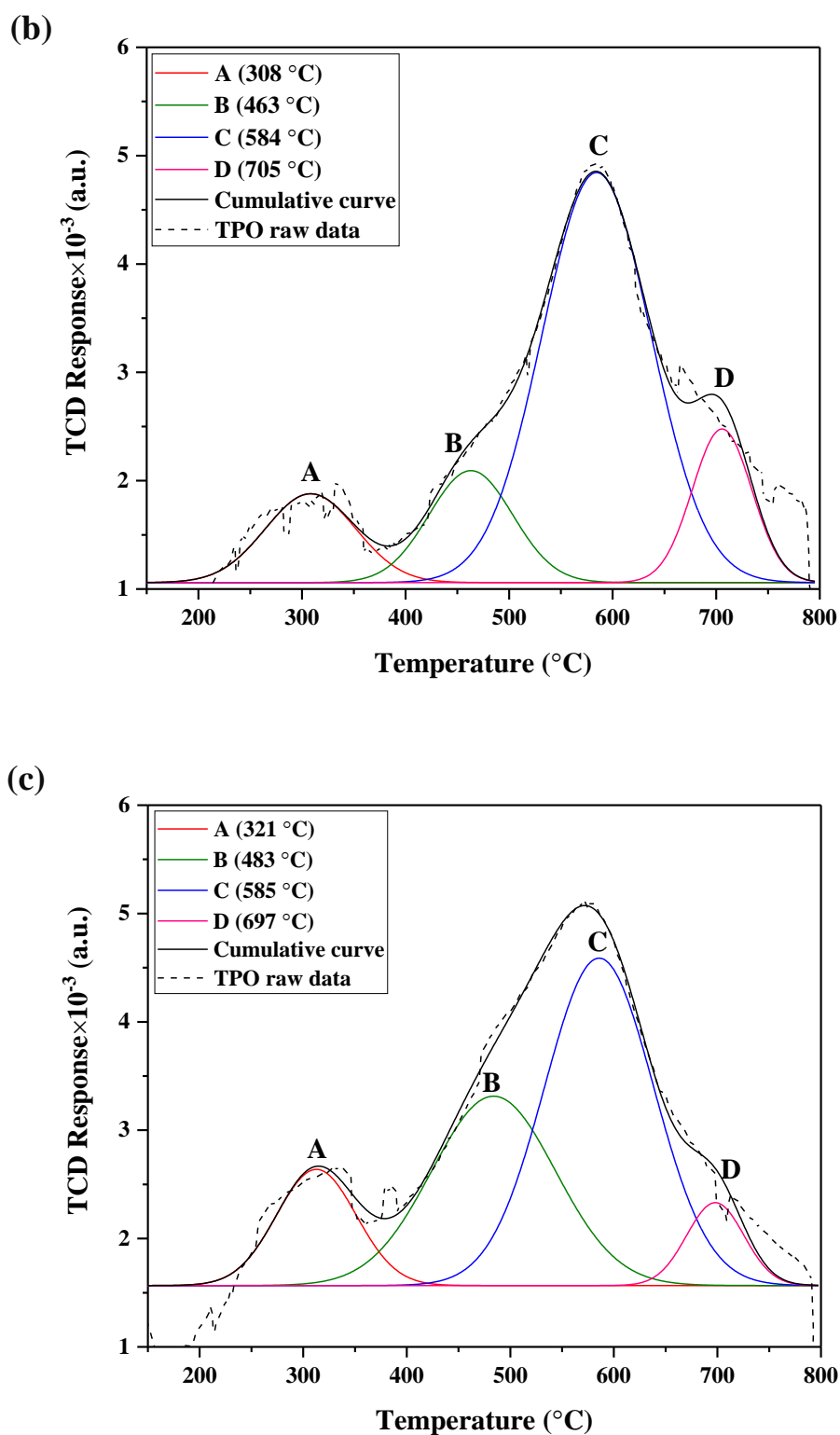


Figure 5.10 TPO profiles after baseline subtraction and peak deconvolution using Gaussian function for the spent catalyst samples of *n*-pentane conversion over 0.5 g Pt/H-Beta at 300 $^{\circ}\text{C}$, WHSV of 1.5 h^{-1} , H_2 /pentane mole ratio of 3.12, and after (a) 1 h; (b) 6 h; and (c) 4 days TOS. The temperature shown in brackets corresponds to centre of the oxidation peak.

Table 5.3 The peak area of different types of coke resulted from the deconvolution of the TPO profile shown in Figure 5.10.

TOS	Peak area (a.u.)				Sum of peak areas	Cumulative curve area
	A	B	C	D		
1 h	0.081	0.097	0.437	0.066	0.681	0.681
6 h	0.089	0.104	0.498	0.102	0.794	0.789
4 days	0.103	0.261	0.409	0.052	0.825	0.818

The TPO profile also allows for discrimination between the coke located on or near the metal and the coke laid down on the support. The carbonaceous species formed on the spent 0.45 wt.% Pt/H-Beta are varied in their reactivity to oxygen, and their bonding strength to the catalyst surface. The literature shows that, with respect to this technique, the coke oxidised at a temperature around 450 °C is positioned close to the metal sites and is assisted by the metal in combustion, whereas the coke oxidised at temperatures higher than 500 °C is located on the support and oxidised without the influence of the metal (Larsson et al., 1996, Martín et al., 2004, Shamsi et al., 2005).

Peak A around 314 °C can therefore be considered as a highly reactive coke that is weakly bound to the catalyst surface, and therefore it easily desorbed and oxidised before other types of coke during the TPO analysis. This is followed by coke presented in peak B which is likely formed near the metal-support interface, such that it can be oxidised and removed earlier than the coke in the subsequent peaks. Peak C is the dominant peak in the TPO profile; it exhibits the highest area among other peaks as shown in Table 5.3. This coke is graphitic-like or pre-graphitic carbon that is strongly bound to the acid sites. On the zeolite, the last peak D has the lowest oxidation reactivity, and it can be ascribed to well organised graphitic carbon that is strongly bound to the acid sites.

The area of each individual peak in addition to total area of the cumulative curve is presented in Table 5.3. It has been reported that the peak area is proportional to the amount of coke on the catalyst (Bayraktar and Kugler, 2002). From peak areas, it can be concluded that the majority of the coke was formed on the acidic support at the early stage of the reaction, whereas at the steady-state operation after 6 h TOS, only a minor change in the peak areas were observed. For the aged sample after 4 days

operation, the area of peak A is slightly increased by 0.01, whilst a significant increase in the area of peak B was observed, which reflects an increase in the amount of the amorphous carbon that may be located in the vicinity of Pt sites.

Table 5.4 The expected structure, location, and bounding strength of the carbon species presented in the deconvoluted peaks A, B, C, and D of TPO profile of *n*-pentane isomerisation over 0.45 wt.% Pt/H-Beta.

Carbon peak	Carbon structure	Bounding site	Bounding strength
A	Soft	Near the metal sites	Weak
B	Amorphous	Metal-support interface	Moderate
C	Hard	Acid sites	Strong
D	Crystalline hard	Acid sites	Strong

From the above observations, it can be hypothesised that the coke formed during *n*-pentane conversion is a mixture of various types of carbonaceous materials with different structures, oxidation reactivity, and are located on both the metallic and the acidic sites as summarised in Table 5.4. However, coke is formed more extensively on the acid sites of the zeolite. Peaks A and B represent hydrogen-rich (soft) and amorphous carbon, respectively. These are likely located near the metal sites where more easily oxidised in the TPO experiment. The carbonaceous species represented by peaks C and D are graphitic-like (hard) and well crystallised graphitic carbon, respectively. These are produced from the acid catalysed reactions and strongly bound to the acid sites. Generally, the same types and quantities of these carbonaceous species are observed over the catalyst surface with increased TOS, however, an increase in the area of peak B was observed over the aged sample after 4 days of reaction as shown in Table 5.3.

5.3.3.4 UV-Raman spectroscopy

UV-Raman is employed in the present study to investigate the structural organisation of the carbonaceous deposits as well as their chemical identity. Only fluorescence was detected in the analysis of the spent catalyst samples using conventional laser Raman at an excitation wavelength of 514.5 nm. This fluorescence interference was avoided by using the UV laser at a wavelength of 325 nm (see Section 4.9).

Figure 5.11 shows the UV-Raman spectra of the spent catalysts at the three defined stages of the reaction. The most valuable data related to the microstructure of the carbons are usually recorded in the spectral region between 1000 and 1800 cm^{-1} (Jawhari et al., 1995). In that region, two major bands centred at around 1610 cm^{-1} and 1365 cm^{-1} can be observed in the Raman spectra of the spent catalyst samples displayed in Figure 5.11. In addition, the bands at 1578, 1445, and 1225 cm^{-1} are also observed in all stages of the *n*-pentane reaction. These bands are assigned to the presence of a complex mixture of chemical species.

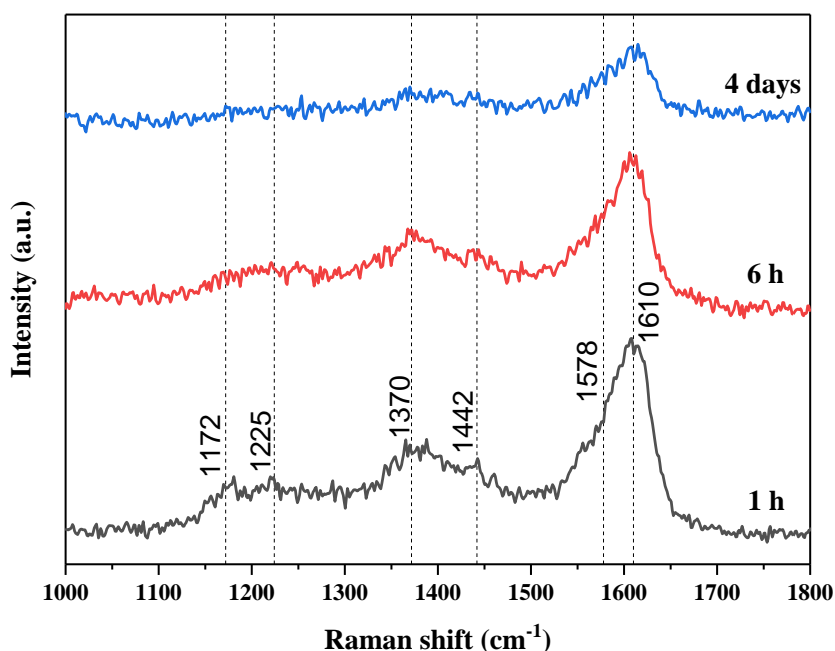


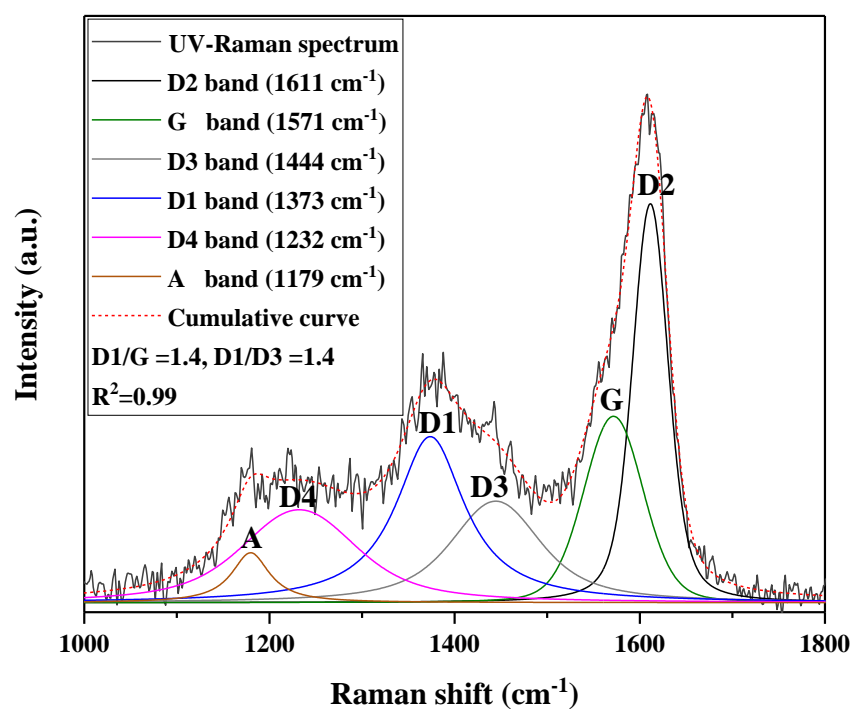
Figure 5.11 UV-Raman spectra of the spent catalyst samples of *n*-pentane conversion over 0.5 g Pt/H-Beta at 300 °C, WHSV of 1.5 h⁻¹, H₂/pentane mole ratio of 3.12, and after different stages of reaction.

The Raman spectrum is usually deconvoluted into several peaks using a combination of the Gaussian and the Lorentzian line shapes for curve fitting (Sadezky et al., 2005, Sattler et al., 2013). The Voigt function has also been used for Raman spectra decomposition; this involves both the Gaussian and the Lorentzian line shapes (Kouketsu et al., 2014).

Accordingly, and in order to obtain detailed information from such spectra, the UV-Raman spectrum of each catalyst sample shown in Figure 5.11 was deconvoluted into five to six bands using the OriginLab software (version 9.40) leaving all the spectral parameters free to progress. The Voigt function was utilised for curve fitting, and the initial values of the bands position were chosen based on a previous investigation on the Raman bands of different types of carbon (Sadezky et al., 2005, Pimenta et al., 2007) as described in Section 4.9.

The deconvoluted spectra of the spent catalyst samples after 1 h, 6 h, and 4 days of *n*-pentane conversion are shown in Figure 5.12 (a), (b), and (c) respectively.

(a)



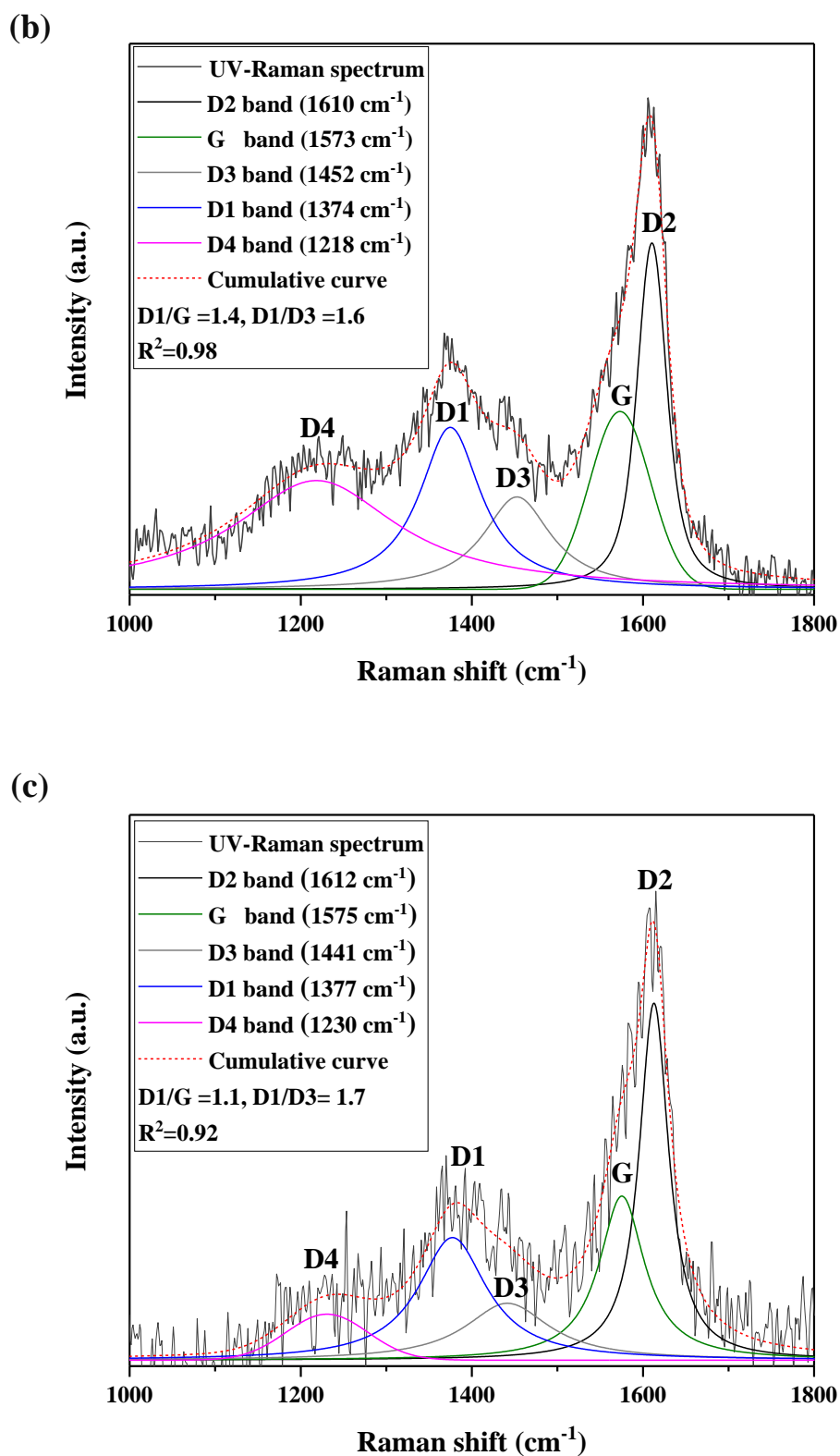


Figure 5.12 UV-Raman spectra of spent Pt/H-Beta of *n*-pentane conversion over at 300 °C, WHSV of 1.5 h^{-1} , H_2 /pentane mole ratio of 3.12, and after (a) 1 h; (b) 6 h; and (c); 4 days TOS.

The broad band at around 1610 cm⁻¹ is deconvoluted into two bands: the G band at around 1575 cm⁻¹ and the D2 band at 1610 cm⁻¹ as suggested in the previous Raman investigations on carbon (Lahfid et al., 2010, Kouketsu et al., 2014). The other bands corresponded to: D1 at 1365 cm⁻¹, D3 at 1440 cm⁻¹, D4 at 1225 cm⁻¹, in addition to a band at 1172 cm⁻¹ labelled as band ‘A’, which is observed only in the spectrum of the spent catalyst sample at the early stage of the reaction and vanished in the later stages.

Generally, the G band is assigned to the presence of poly-condensed aromatics in a well-organised graphitic structure, whereas the D1 band is associated with a disordered graphite structure (pregraphitic particles) which is usually found in sp² carbons (Kuba and Knözinger, 2002, Sadezky et al., 2005). The D2 band is ascribed to the existence of polyolefinic and/or polyaromatics species in a disordered graphitic lattice, and the D3 band is assigned to the amorphous carbon from organic components such as aliphatic and alkyl-aromatic compounds (Bauer and Karge, 2006, Sadezky et al., 2005). The D4 band is associated with sp³-sp² bonds or C–C and C=C stretching vibration of polyene-like structure (Gomez Sanz et al., 2016). The A band near 1180 cm⁻¹ is detected in the Raman spectrum of the spent catalyst after 1 h of reaction and it is assigned to the C–H bending in aromatic compounds (Wu and Stair, 2006). The typical wave number and the assignment of the Raman bands are summarised in Table 5.5.

Table 5.5 Typical wave number and assignment of Raman bands derived from the literature.

Band	Typical wave number (cm ⁻¹)	Assignment
G	~ 1580	Poly-condensed aromatics in ideal graphitic lattice
D1(D)	~ 1350	sp ² carbon stretching vibration in disordered graphitic lattice (graphene layer edges)
D2	~ 1650	Polyolefinic and/or polyaromatics species in a disordered graphitic lattice (surface graphene layers)
D3	~ 1500	Amorphous carbon from organic components such as aliphatic and alkyl-aromatic compounds
D4	~ 1200	sp ³ -sp ² stretching vibration in disordered graphitic lattice (polyene-like structure)
A	-	C–H bending in aromatic compounds

The ratio of the peak area of the D1 and G bands has been widely used to characterise the degree of the structural order of carbon, where the decrease in the D1/G ratio indicates an increase in the degree of graphitisation (Nakamura et al., 1990, Jawhari et al., 1995, Pimenta et al., 2007). However, it has been reported that this parameter is not reliable when the value of D1/G is higher than 1.1. In such cases, D1/D3 ratio is used as an indicator of the structural development of carbon deposits with lower graphiticity than graphite (Gomez Sanz et al., 2016).

The values of D1/G and D1/D3 ratios were calculated as the ratios between the peak areas obtained from the deconvolution of the Raman spectra of the spent catalyst samples after 1 h, 6 h, and 4 days of *n*-pentane conversion as shown in Figure 5.12 (a), (b), and (c). The D1/G ratio of all the studied TOS was ≥ 1.1 ; therefore, D1/D3 ratio has been employed as a measurement of graphitisation degree.

From Figure 5.12 (a) and (b), it can be seen that there is no significant change in the band positions as well as in the D1/G ratio (1.4). The only difference is the disappearance of A band in the spectrum of the sample after 6 h of reaction which may be due to the transformation of the compounds to the carbon presented in the D4 band. The value of the D1/D3 ratio increased from 1.4 to 1.6 after 1 h and 6 h of reaction, respectively, indicating the change of the coke structure from aliphatic and alkyl-aromatic compounds to polyaromatics in graphene layer edges. For the aged catalyst sample after 4 days of operation (Figure 5.12 (c)), the D1/G ratio decreased to 1.1 and the value of D1/D3 increased to 1.7 which reveal an increase in the structural organisation of the carbonaceous deposits.

In addition to the structural order, the UV-Raman bands can reveal the topology of the carbonaceous deposits. It has been reported that the polyaromatic compounds typically display pronounced bands at the spectral regions around 1300-1450 cm^{-1} and around 1600-1650 cm^{-1} . Two-dimensional aromatic compounds in a sheet-like topology, such as pyrene and coronene, exhibit a higher band intensity in the region at 1600-1650 cm^{-1} than at 1300-1450 cm^{-1} . In contrast, the aromatic compounds in a chain-like topology such as phenanthrene, anthracene, and pentacene are present when the band intensity of these two spectral regions is nearly equal (Chua and Stair, 2003).

According to this study and the observed intensity of the UV-Raman bands shown in Figure 5.12 (a), (b), and (c), it can be assumed that the coke formed over Pt/H-Beta during *n*-pentane conversion is composed of aromatic compounds in a sheet-like topology.

5.4 Conclusions

n-Pentane isomerisation has been performed over 0.45 wt.% Pt/H-Beta catalyst. The best performance of the catalyst under steady-state operation was observed at a reaction temperature of 300 °C, whilst the reaction WHSV and the H₂/*n*-pentane molar ratio were kept constant at values close to these used in the commercial process. At these conditions, *n*-pentane conversion was 65%, and the selectivity to *iso*-pentane was 87%.

The catalyst exhibits a high stability with increasing the TOS, in which after 60 min of reaction, the conversion and the selectivity to different reaction products was almost constant. This was ascribed to the build-up of the carbonaceous deposits during the early stage of the reaction. Therefore, it is believed that these carbonaceous deposits may play a crucial role in reducing the side reactions that lead to coke formation and redirecting the reaction to a more selective pathway.

The retained carbonaceous species have been investigated at different stages of *n*-pentane conversion using a combination of thermal and spectroscopic techniques to study the development in the properties of coke with increased TOS. TGA measurements show that no significant change in the quantity of coke was observed after the induction period (1 h), and the majority of the coke deposited was so-called hard coke, which is likely composed from poly-condensed aromatic compounds. In addition, a slight decrease in the H/C ratio was observed with increasing TOS, indicating an increase in coke aromaticity.

TPO results reveal the presence of a mixture of carbonaceous materials with different structure, oxidation reactivity, and location. The hydrogen-rich and the amorphous carbon deposits are likely located nearby the metal sites, whilst the graphitic-like and the highly crystallite carbon deposits are more likely strongly bound to the acid sites.

In agreement with TPO, UV-Raman spectra indicate the presence of highly organised graphitic carbon, disordered (graphitic-like) carbon, and amorphous carbon. The D1/G intensity ratio of the spent catalyst samples after 1 and 6 h TOS was fairly constant at 1.4, however, the D1/D3 ratio increased from 1.4 after 1 h to 1.6 after 6 h. In addition, a decrease in D1/G intensity ratio to 1.1 and an increase in D1/D3 intensity ratio to 1.7 were observed in the aged catalyst sample, indicating an increase in the degree of graphitisation. However, D1/D3 ratio was considered to be more realistic indicator than D1/G to provide information about the degree of coke order. The carbonaceous deposits were likely composed from aromatic compounds in a sheet-like topology such as pyrene and coronene.

Chapter 6

n-Hexadecane

isomerisation-cracking

over Pt/H-Beta

6 Chapter 6: *n*-Hexadecane isomerisation-cracking over Pt/H-Beta

6.1 Introduction

The isomerisation-cracking of long-chain *n*-alkanes is considered a key process in modern refining industry due to the increased demand for liquid fuel and petrochemical products (Calemma et al., 2000, Zhang et al., 2016). This process can be considered as a sustainable process where low-value hydrocarbons such as heavy petroleum fractions, renewable hydrocarbons produced from plastics recycling, and Fischer-Tropsch waxes and heavy paraffins are upgraded into value-added products such as fuels (gasoline, jet fuel and other middle distillates) and lubricants with superior properties (Calemma et al., 2010, Busto et al., 2011, Batalha et al., 2015, Zhang et al., 2016, Regali et al., 2013).

Bifunctional catalysts are typically employed in this process; these consist of metallic sites (Pt or Pd) for hydrogenation-dehydrogenation function, and an acidic support for the isomerisation-cracking function. Zeolites such as Y, Beta, and ZSM-5, have been widely used as an acidic support for this catalyst due to their significant acidity and shape selectivity (Deldari, 2005, Ertl et al., 2008, Soualah et al., 2008).

Isomerisation and cracking of *n*-alkanes are usually considered to occur simultaneously over bifunctional catalysts *via* the classical monomolecular mechanism (described in Section 2.3.2). However, the reactivity of *n*-alkanes increases with increasing chain length; consequently long chained alkane cracking is very rapid resulting in a decrease in isomerisation selectivity (Calemma et al., 2000, Guisnet, 2002a, Soualah et al., 2008).

In order to enhance isomerisation over cracking, a bifunctional catalyst with a high hydrogenation activity and low degree of acidity is required, with a general understanding that the acidity requirement is inversely proportional to chain length (Deldari, 2005, Busto et al., 2011, Bauer et al., 2014).

Over time, such bifunctional catalysts typically experience deactivation in such reactions as a result of coke formation. The fast build-up of coke deposits is attributed

to the presence of olefinic reaction intermediates which act as precursors for the formation of carbonaceous deposits (Regali et al., 2013).

Recently, the catalytic isomerisation-cracking of long-chain *n*-alkanes has been widely investigated in the literature e.g. *n*-hexadecane isomerisation-cracking over Pt/zeolites (Park and Ihm, 2000, Christensen et al., 2004, Soualah et al., 2008, Batalha et al., 2013a, Batalha et al., 2013b, Bauer et al., 2014, Batalha et al., 2015, Zhang et al., 2016), and over Pt/amorphous SiO₂-Al₂O₃ (Calemma et al., 2000), also over Pt/sulphated zirconia catalysts (Busto et al., 2011). However, only a few investigations have been focused on coke deposition and the deactivation of these catalysts in the isomerisation-cracking of long-chain alkanes (Nam et al., 2010, Regali et al., 2013, Bauer et al., 2014). The characterisation of these carbonaceous deposits is key to understanding the mechanism behind coke formation and thereby to the possibility of designing a catalyst which is more selective to the desired products and generates lower amounts of coke thus exhibiting greater resistance to deactivation, ultimately increasing catalyst life time.

The objectives of this work are: (i) studying the isomerisation-cracking of *n*-hexadecane as an exemplar of long chained *n*-alkane over zeolite and Pt/zeolite at different reaction conditions (temperature and pressure), and selecting the best conditions to perform a TOS study; (ii) investigating the reasons behind coke formation over the catalyst employed through studying the influence of catalyst surface modification by external surface pre-poisoning and desilication treatments to elucidate whether the formation of coke deposits is attributed to the existence of strong and non-selective acid sites on the external surface of the catalyst crystal or to the presence of diffusional limitations inside catalyst channels and pores, respectively; and (iii) studying the properties of coke deposits formed over the catalysts employed during *n*-hexadecane conversion *via* the *ex situ* characterisation of the spent catalysts.

Based on the above objectives, this chapter is composed of three parts: the first part comprises a reaction study of *n*-hexadecane conversion over ZSM-5 and H-Beta zeolites without metal loading, at reaction temperatures of 200, 250, and 300 °C, under 30 bar of He as an inert gas, for 120 min TOS is presented in Section 6.3.2.1. A study

on the effect of H₂ pressure on the performance of the synthesised Pt/H-Beta catalyst at H₂ pressure range of 20-50 bar and at 300 °C for 2 h is presented in Section 6.3.2.2. Then, the influence of TOS has been studied at 300 °C, 50 bar H₂ and over 30, 60, 120, and 240 min, and presented in Section 6.3.2.3.

The second part of the chapter, shown in Section 6.3.3, consists an investigation on the reasons behind the rapid formation of carbonaceous deposits over Pt/H-Beta at 300 °C, 50 bar H₂, and 30 min reaction time through the selective poisoning of external Brønsted acid sites, and the desilication treatment of the employed zeolite.

Finally, the third part of this chapter, presented in Section 6.3.4, investigates the characteristics of the carbonaceous deposits formed over the spent Pt/H-Beta before and after modification using a range of characterisation techniques including TGA, elemental analysis, TPO, and UV-Raman spectroscopy.

6.2 Materials and methods

The catalysts employed in the catalytic isomerisation-cracking reaction of *n*-hexadecane are Pt/H-Beta, Pt/pre-poisoned H-Beta, and Pt/desilicated H-Beta. The preparation methods of these catalysts are described in Section 3.3.

The physicochemical properties of the prepared catalysts were investigated using a range of characterisation techniques including: inductively coupled plasma (ICP); X-ray diffraction (XRD); thermogravimetric analysis (TGA) / differential thermogravimetry (DTG); and N₂ adsorption isotherms. A detailed description of the instruments employed, with the methods developed to perform these analyses, is contained in Chapter 4.

The catalytic conversion of *n*-hexadecane was conducted in a high pressure batch reactor using the reactor set-up and the experimental procedure described in Section 3.4.2.

The gas chromatography measurements for the head space gases and the liquid products were conducted off-line using the GC column and the GC methods described in Section 3.5.2.

The methods used for calculating the catalytic performance indicators (conversion and selectivity) and the reproducibility error are explained in Section 3.6.

Post-reaction, the catalyst samples were characterised *ex situ* by a combination of thermal and spectroscopic techniques to investigate the quantity, structure, location, and the chemical composition of the carbonaceous deposits that are laid down over the catalyst surface after reaction. Thermogravimetric analysis (TGA), elemental analysis, and temperature-programmed oxidation (TPO), and UV-Raman were employed for this purpose. The experimental parameters used to perform each analysis are described in Chapter 4.

6.3 Results and discussion

6.3.1 Catalyst characterisation

6.3.1.1 Characterisation of Pt/H-Beta

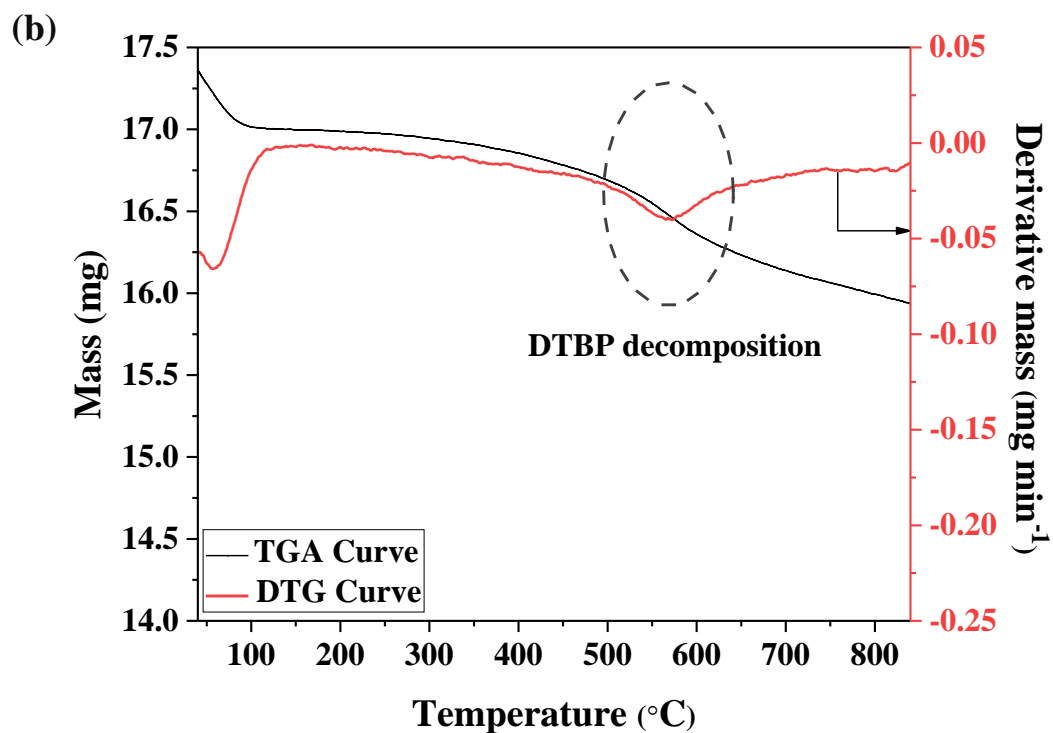
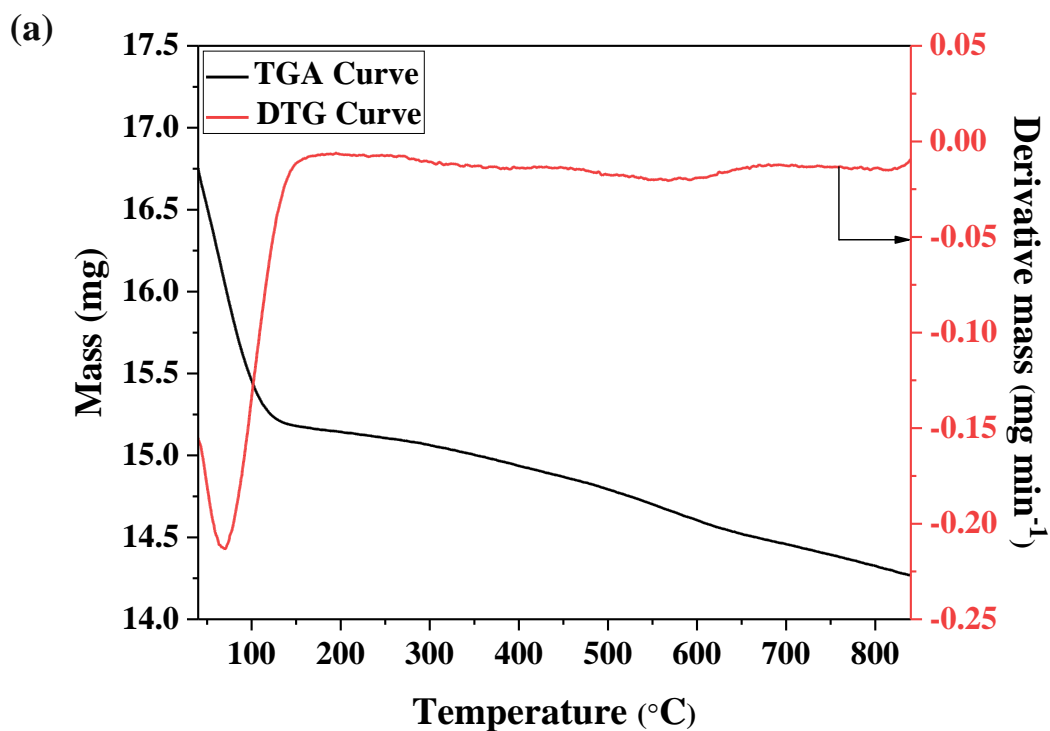
The physicochemical properties the synthesised 0.45 wt.% Pt/H-Beta catalyst including TGA/DTG, ICP, N₂ adsorption isotherm for BET surface area measurement, and TPR are described in Section 5.3.1.

6.3.1.2 Characterisation of Pt/pre-poisoned H-Beta

The Pt/pre-poisoned H-Beta was characterised using DTG. The temperature required for the decomposition of DTBP on the surface of H-Beta zeolite was investigated using the DTG curve as shown in Figure 6.1(a) and (b) for fresh and pre-poisoned H-Beta respectively. The exothermic peak associated with DTBP decomposition was observed at around 570 °C (Figure 6.1(b)). The peak at a temperature lower than 100 °C is related to the desorption of adsorbed water.

The presence of DTBP material after Pt loading using the wet impregnation method, and after the final calcination of the impregnated Pt/pre-poisoned H-Beta at 320 °C, was confirmed using DTG as shown in Figure 6.1 (c), and (d) using air as a carrier gas. There are three evident exothermic peaks in the DTG curve shown in Figure 6.1 (c); the peak at around 70 °C corresponds to the desorption of water; the second peak

at around 300 °C is related to the decomposition of Pt precursor; and the third peak at 570 °C is corresponded to the decomposition of DTBP.



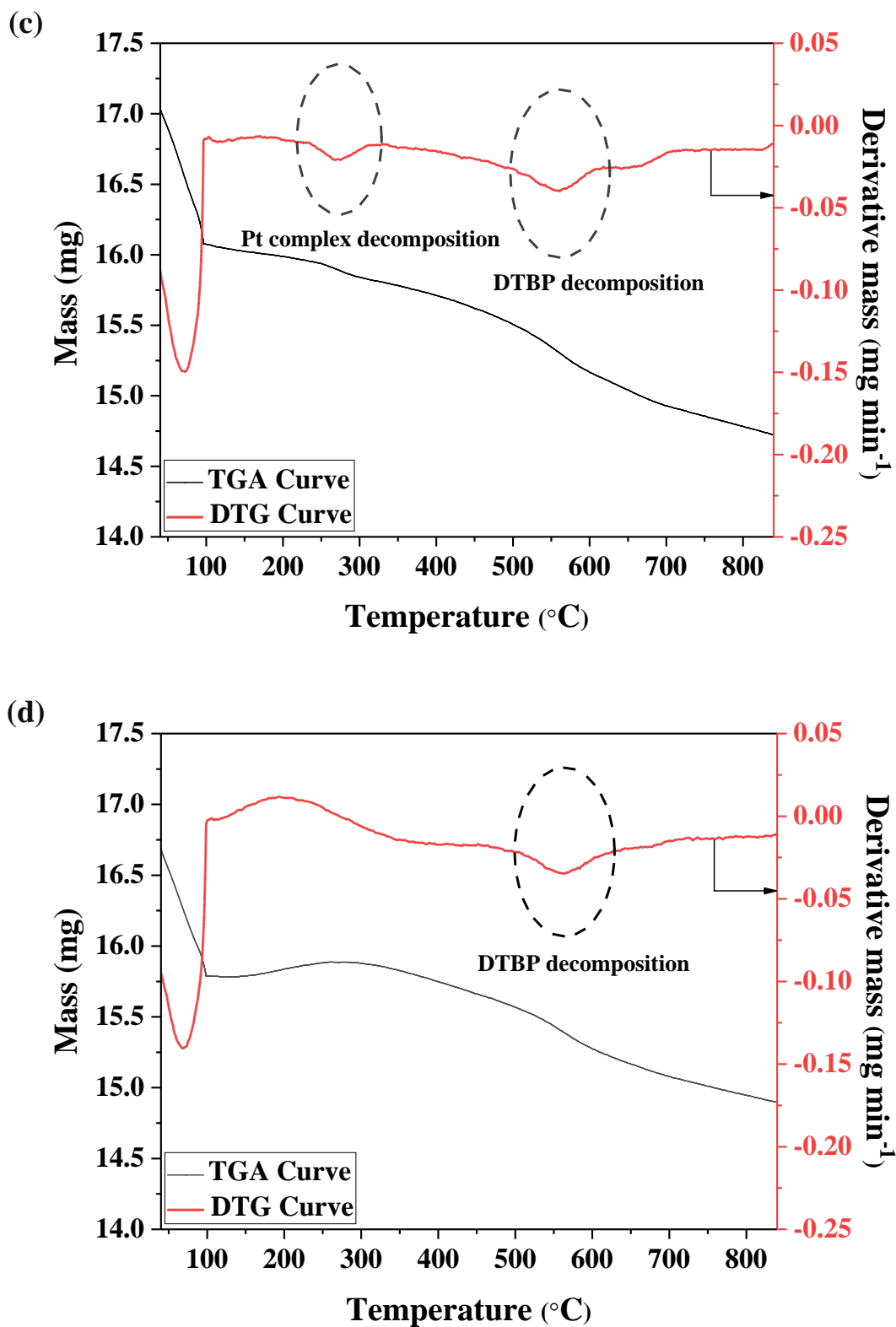


Figure 6.1 TGA/DTG curves for the decomposition of (a) fresh H-Beta zeolite; (b) pre-poisoned H-Beta; (c) Pt/pre-poisoned H-Beta before calcination; (d) Pt/pre-poisoned H-Beta after calcination in air at 320 °C.

6.3.1.3 Characterisation of Pt/desilicated H-Beta

The H-Beta zeolite after desilication treatment and before Pt loading was characterised using ICP, XRD, and N₂ adsorption isotherm.

Si and Al content of fresh and desilicated H-Beta samples were measured by ICP. The Si/Al molar ratio of the fresh H-Beta was 126, while after desilication treatment it decreased to 116. The relatively small difference in Si/Al ratio between the fresh and the desilicated H-Beta is due to the low concentration of NaOH solution used in this treatment (see Section 3.3.1).

The XRD pattern of the fresh and the desilicated H-Beta is shown in Figure 6.2. It can be observed that although the intensity of most of the characteristic reflections of the desilicated H-Beta has decreased in comparison to the fresh zeolite, the structural fingerprint of H-Beta is maintained and the position of individual diffraction lines of XRD patterns remain unchanged.

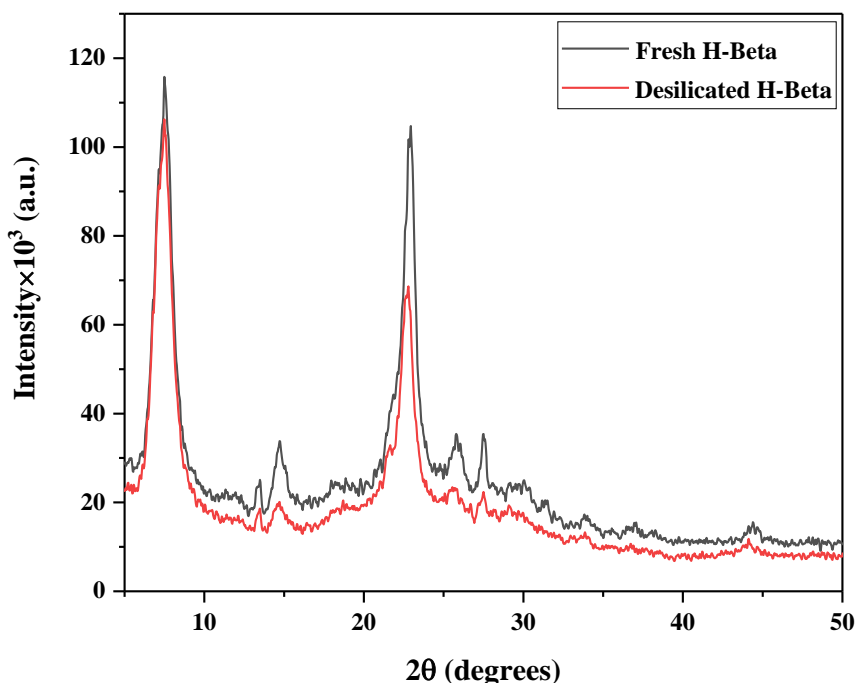


Figure 6.2 XRD patterns of the fresh and the desilicated H-Beta samples.

N₂ adsorption isotherm hysteresis loop of the fresh and desilicated H-Beta zeolite are shown in Figure 6.3. Both the fresh and the desilicated H-Beta exhibits IUPAC type I isotherms (described in Section 4.4), which indicates the preservation of zeolite microporous structure.

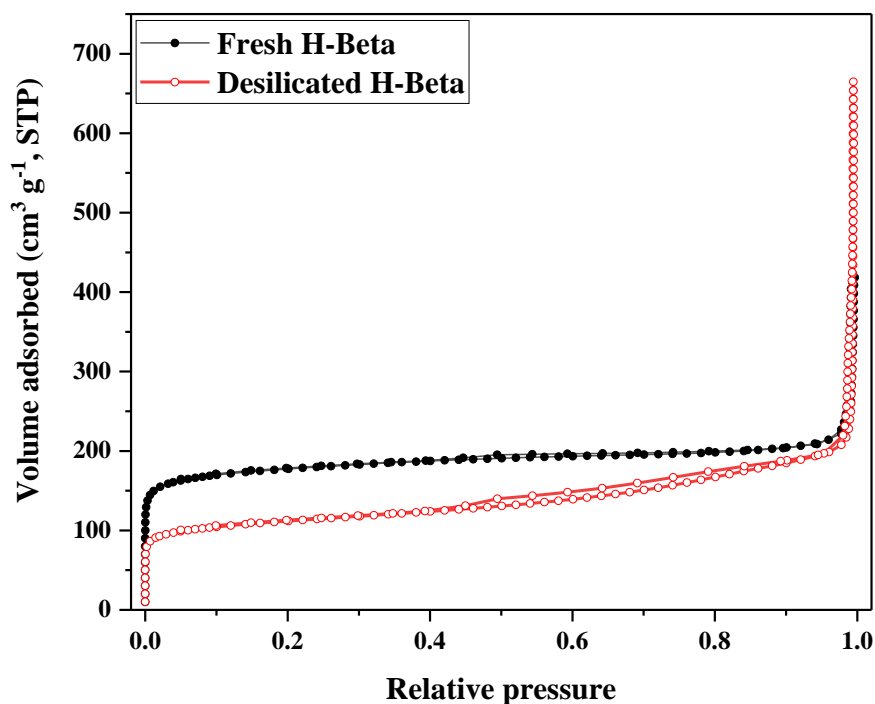


Figure 6.3 N₂ adsorption-desorption isotherms of fresh and desilicated H-Beta zeolite.

The surface area data of the fresh and desilicated H-Beta are listed in Table 6.1. The specific surface area was determined from the adsorption isotherm by BET method. The mesopore volume was calculated by the difference between the total pore volume and the micropore volume. The BET surface area of the desilicated zeolite was lower than that of the fresh zeolite, decreasing from 620 m² g⁻¹ for the fresh zeolite to 377 m² g⁻¹ after the desilication. These results are contrary to expectations; where it is widely known that the desilication treatment is expected to lead to an increase in BET surface area (Van Donk et al., 2003, Groen et al., 2008). Such behaviour can be explained by the blocking of part of microporous by the deposition extra-framework materials. Nevertheless, the data in Table 6.1 show that the mesopore volume was

increased from 0.11 to 0.2 cm³ g⁻¹ and the micropore volume was decreased from 0.20 to 0.10 cm³ g⁻¹ for the fresh and desilicated H-Beta respectively. In addition, the average pore size of the modified sample is centred around 3.2 nm. These results confirmed the formation of mesoporosity in H-Beta microstructure.

Table 6.1 Surface area data of fresh and desilicated H-Beta zeolite.

Catalyst	BET surface area (m ² g ⁻¹)	Volume (cm ³ g ⁻¹)			Average pore diameter(nm)
		Total	Micro-	Meso-	
Fresh H-Beta	620	0.326	0.209	0.117	2.107
Desilicated H-Beta	378	0.302	0.106	0.196	3.204

6.3.2 Catalytic activity measurements

The catalytic conversion of *n*-hexadecane was carried out over zeolites (ZSM-5 and H-Beta) without Pt loading, in an inert atmosphere as well as over the synthesised 0.45 wt.% Pt/H-Beta catalyst in the presence of H₂. Reaction conditions including: reaction temperature, pressure, and TOS have been investigated.

Reaction products were identified as described in Section 3.5.2. Liquid-phase products are grouped into: cracking products lighter than hexadecane, *iso*-hexadecane, unreacted *n*-hexadecane, and coke. No gas-phase products were observed in the headspace gases of *n*-hexadecane conversion analysed by GC/FID.

A representative example of GC chromatogram of liquid products produced from *n*-hexadecane conversion over 0.45 wt.% Pt/H-Beta is shown in Figure 6.4.

The reproducibility of the reaction was determined by performing a model reaction conducted at 300 °C, 50 bar H₂, and 30 min TOS, three times and the reproducibility error was 1.8% relative to the *n*-hexadecane conversion, 3.9% for the selectivity to *iso*-hexadecane, 5% for the selectivity to cracking products, and 10% for the selectivity to coke.

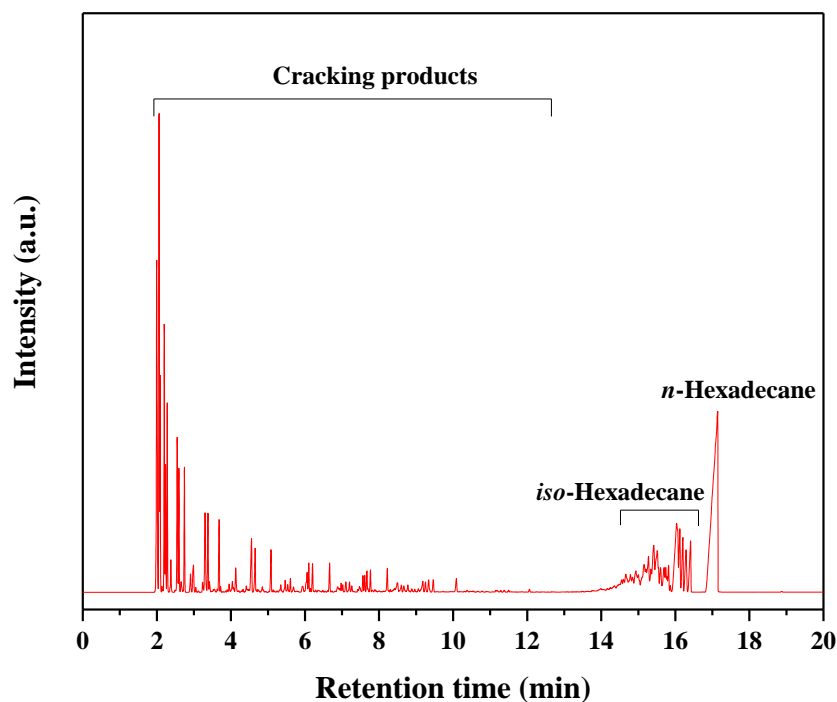


Figure 6.4 GC/FID Chromatogram for reaction products of *n*-hexadecane conversion over 0.5 g of 0.45 wt.% Pt/H-Beta at 300 °C, 50 bar H₂, and after 30 min TOS.

6.3.2.1 Influence of reaction temperature and zeolite structure

The influence of reaction temperature on the overall conversion of *n*-hexadecane has been investigated over two types of zeolites with different structure and pore size, without Pt loading. The reaction was carried out in an inert atmosphere under He. The zeolites employed are commercial ZSM-5 (10 member ring medium pore size) and H-Beta (12 member ring large pore size) which are widely known to be active catalysts for the isomerisation-cracking of *n*-alkanes (Weitkamp et al., 2001, Jiménez et al., 2003, Zhang and Smirniotis, 1999, Bauer et al., 2014). Both zeolites were in protonic form.

The reaction was studied at 200, 250, and 300 °C, whilst reaction pressure and TOS were maintained constant at 30 bar He (at ambient temperature) and 120 min,

respectively. This range of reaction temperature has been selected based on previous investigations on *n*-hexadecane isomerisation-cracking over zeolites (Christensen et al., 2004, Kustova et al., 2004) and over Pt containing zeolites (Busto et al., 2011, Batalha et al., 2013a, Batalha et al., 2015).

The results corresponding to the influence of reaction temperature on the conversion of *n*-hexadecane over these two zeolites are shown in Figure 6.5(a). These results generally indicate that increasing reaction temperature resulting an increase in zeolites activity, consequently, increase *n*-hexadecane conversion. The greatest activity was observed over H-Beta zeolite, in which the conversion is maximised to 89% at 300 °C. This performance is attributed to the large pores and the three-dimensional channels structure of this zeolite that enables the accommodation of the long-chains of *n*-hexadecane and allow for their conversion to branched hexadecane and cracking products. In contrast, lower conversion is observed over the commercial ZSM-5. Although the SiO₂/Al₂O₃ mole ratio of the employed H-ZSM-5 (38:1) is lower than that of H-Beta (360:1), which consequently reflects higher acid site density, the highest conversion achieved over H-ZSM-5 was only 20% at 300 °C. A possible reason for this poor performance of H-ZSM 5 is the diffusional limitations related to its narrower channels that restrict the formation of the cabenium ions as a reaction intermediate inside zeolite pores.

In addition to the conversion, the degree of hexadecane isomerisation was also investigated over both zeolites as shown in Figure 6.5 (b). No attempt has been made to determine the selectivity to each product at this stage of the study. From the results presented in Figure 6.5 (b), it can be seen that hexadecane isomerisation degree is also enhanced with increasing reaction temperature. However, the highest degree was only 9% over zeolite H-Beta at 300 °C. Although the isomerisation degree is low, indicating that the major conversion of the reacted *n*-hexadecane was to produce cracking products and coke, this siliceous zeolite exhibits the ability to produce isomers even in the absences of the metallic sites required to produce olefinic intermediates that are easily reacted over the acid sites and form the branched hexadecane.

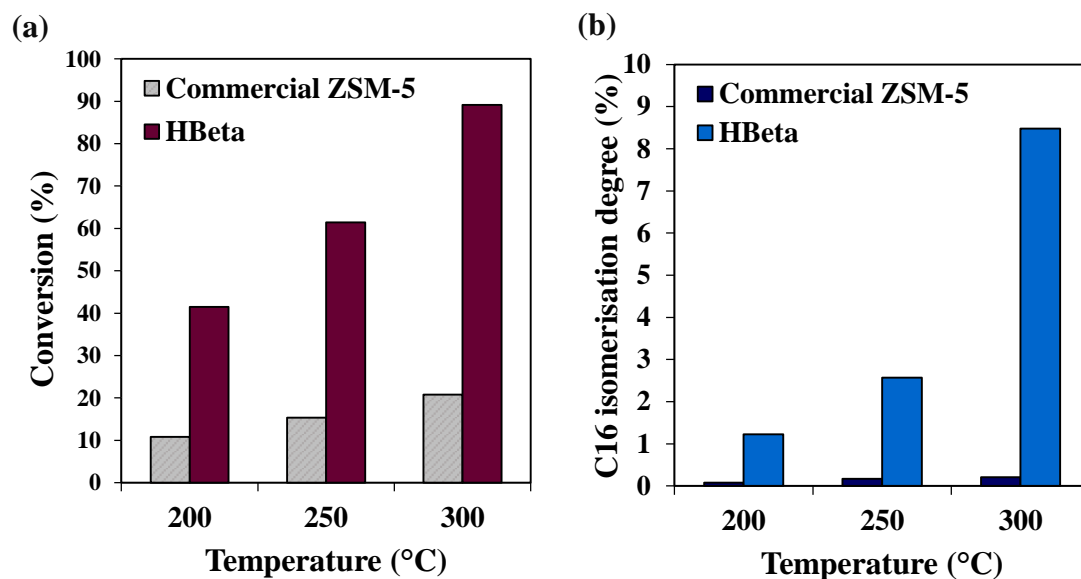


Figure 6.5 Influence of reaction temperature on (a) overall *n*-hexadecane conversion; and (b) hexadecane isomerisation degree, over 0.5g of the commercial ZSM-5 and H-Beta zeolites at 200, 250, 300 °C reaction temperatures, 30 bar He, and 120 min TOS. Isomerisation degree was determined as $iso\text{-}C16 / (iso\text{-}C16 + n\text{-}C16 \text{ unreacted})$ (Christensen et al., 2004).

On the other hand, the isomerisation degree over H-ZSM-5 was less than 0.5% at 300 °C. This behaviour is again ascribed to the steric constraints inside the zeolite channels that hinder the formation of reaction intermediates (transition state shape selectivity). Similar results were observed by Christensen *et al.* for *n*-hexadecane conversion over conventional H-ZSM-5 at 280 °C and under 20 bar He. It has been found that the maximum conversion was 17%, and the isomerisation degree was only 1.4%, also it was observed that the cracking reaction was favoured over the skeletal isomerisation (Christensen et al., 2004).

According to the obtained results, a reaction temperature of 300 °C was selected to study the influence of reaction pressure on *n*-hexadecane conversion. In addition, H-Beta zeolite was chosen as an acidic support for the bifunctional catalyst due to the high conversion level of *n*-hexadecane over that zeolite at 300 °C, and the enhancement of the isomerisation reaction even in the absence of the hydrogenation/dehydrogenation sites.

6.3.2.2 Influence of H₂ pressure

The influence of H₂ pressure on the performance of the employed 0.45 wt.% Pt/H-Beta catalyst was studied at a pressure range of 20-50 bar (at ambient temperature) at reaction temperature of 300 °C for 120 min TOS. The typical pressure of the industrial isomerisation process for long-chained paraffins is between 20 to 80 bar depending on catalyst activity (Bauer et al., 2014). Therefore, a pressure range of 20-50 bar (equivalent to 35-80 bar at 300 °C) was selected to examine the performance of the employed catalyst at a reaction temperature of 300 °C.

The overall conversion of *n*-hexadecane and the selectivity to reaction products as a function of H₂ pressure are shown in Figure 6.6. Generally, it can be seen that the conversion of *n*-hexadecane was maximised to 99% at 20 bar, afterwards no significant change from that level was observed with increasing H₂ pressure. In addition, the cracking reaction was favoured over all the studied pressure range.

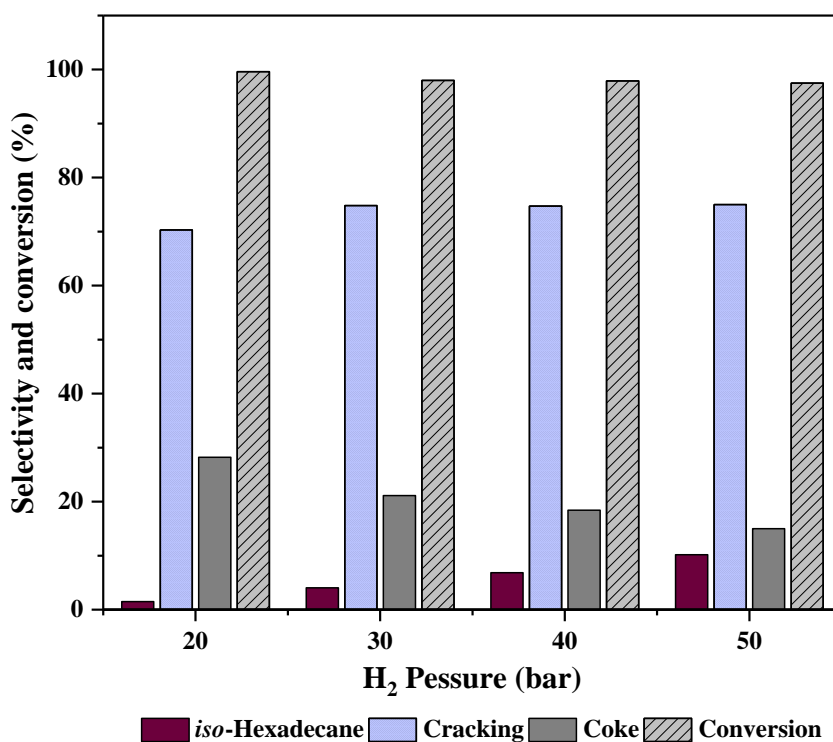


Figure 6.6 *n*-Hexadecane conversion and selectivity to reaction products as a function of H₂ pressure over 0.5 g of 0.45 wt.% Pt/H-Beta at 300 °C and 120 min TOS.

The selectivity to hexadecane isomers was enhanced with increasing H₂ pressure; it increased from 5% at 20 bar to 10% at 50 bar. However, this is considered as a low isomerisation activity in comparison to the selectivity to cracking products that show a selectivity level of 70-75% during reactions at 20-50 bar. From a kinetic point of view, increasing H₂ partial pressure favours the hydrogenation and hydrocracking reactions (Busto et al., 2011). However, it is well established in the reaction mechanism that isomerisation occurs first and cracking afterwards (Deldari, 2005). Therefore, the high selectivity to cracking in the present study can be attributed to the occurrence of a consecutive cracking reaction of the initially formed hexadecane isomers. Also, increasing the contact time of the produced mono-branched hexadecane with the acid sites can lead to further branching to produce multi-branched products. These multi-branched hexadecane isomers can easily crack to smaller molecules and hydrogenate to form cracking products, consequently lowering the isomerisation selectivity.

At the same time, increasing H₂ pressure remarkably reduces the selectivity to coke. It decreased from 28% at 20 bar to 15% at 50 bar. This can be explained by the fast hydrogenation of the olefinic intermediates in the presence of high H₂ pressure. These intermediates can act as coke precursors, and therefore, the presence of H₂ contributes to hydrogenating these intermediates to cracking products and prevents further transformation to coke deposits. Another possibility is that increasing the molecular H₂ pressure may increase the concentration of Brønsted acid sites on the support. It has been proposed that molecular hydrogen reduces surface Lewis sites and creates new Brønsted acid sites on the acidic support (Shishido and Hattori, 1996). Therefore, the new sites may contribute in catalysing the isomerisation reaction and the cracking of coke precursors to smaller molecules.

It is worth mentioning here that the employed catalyst shows a very high selectivity to skeletal isomerisation of *n*-pentane at 300 °C (see Section 5.3.2). The low selectivity to hexadecane isomerisation in the present reaction, is therefore due to the increase in reactivity of *n*-alkanes with increasing chain length. It has been reported that the selectivity to isomerisation decreased with increasing paraffin chain length due to the occurrence of fast cracking reaction (Calemma et al., 2000, Busto et al., 2011).

Nevertheless, all reaction products (except coke) were in liquid phase and no significant presence of compounds in the gas phase was observed.

In summary, increasing H₂ pressure has a negligible influence on hexadecane conversion over the employed catalyst. Simultaneously, this slightly increased the selectivity to hexadecane isomerisation, and effectively reduces coking.

6.3.2.3 Influence of TOS

The influence of extending reaction time on *n*-hexadecane conversion over 0.45 wt.% Pt/H-Beta catalyst was studied at 300 °C and under 50 bar H₂. The results of conversion and selectivity to reaction products are shown in Figure 6.7. From these results, it can be observed that extending reaction time affects positively on the overall conversion of *n*-hexadecane. A conversion of 86% was performed after 30 min TOS, afterwards, slightly increasing to reach approximately a full conversion of 97% after 120 min TOS.

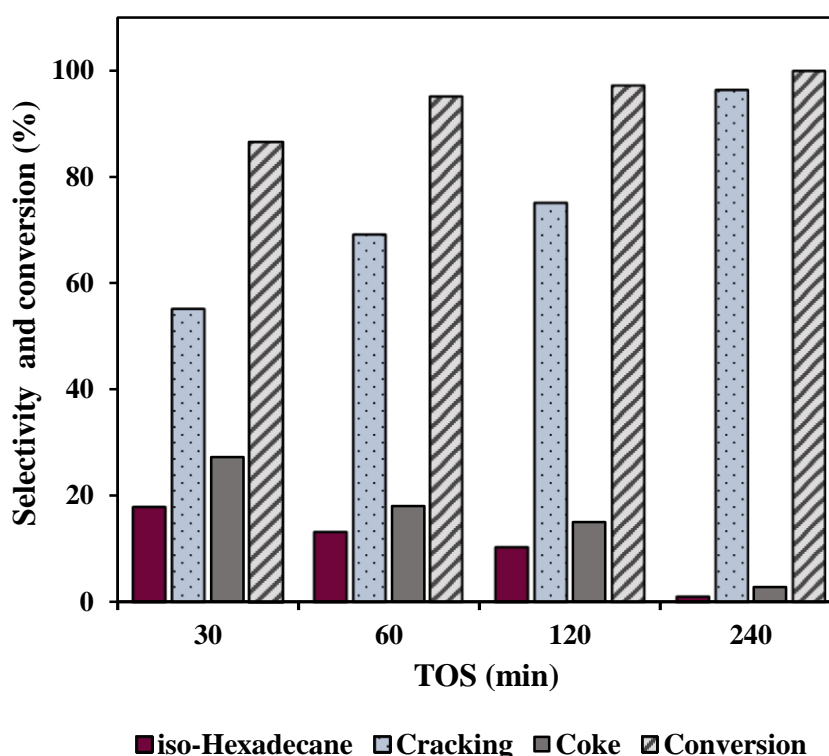


Figure 6.7 *n*-Hexadecane conversion and selectivity to reaction products as a function of TOS over 0.5 g of 0.45 wt.% Pt/H-Beta at 300 °C and 50 bar H₂.

The maximum selectivity to *iso*-hexadecane was 18% after 30 min TOS accompanied by 55% selectivity to cracking products. Carbonaceous species were formed rapidly on the catalyst at this duration, where 27% of the reacted hexadecane was transformed to coke. The high selectivity to cracking and the rapid formation of coke deposits can be attributed to the long residence time of the mono- and multi-branched olefinic intermediates of hexadecane inside zeolite pores. This lead to either the cracking of these intermediates to smaller molecules or the formation of relatively bulky molecules produced from oligomerisation reaction. These oligomers are then retained inside zeolite channels and further transformed to form coke deposits.

Increasing TOS resulted in a decrease in hexadecane isomers and coke products along with an increase in cracking products. This behaviour indicates that the produced *iso*-hexadecane in the liquid phase, and coke precursors retained inside the catalyst pores were subjected to consecutive cracking reactions with lengthening the contact time with the acid sites leading to the production of cracking molecules. H₂ consumption increased with increasing TOS as shown in Figure 6.8, indicating the effective hydrogenation function of the employed catalyst.

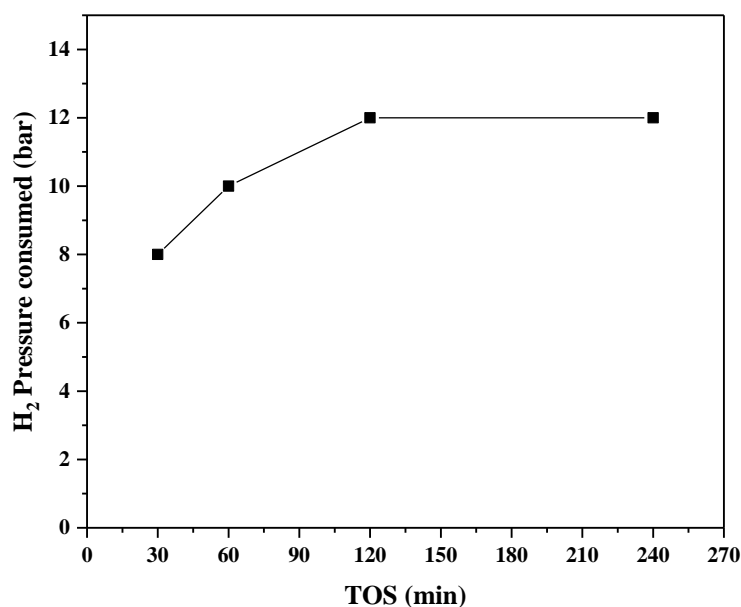


Figure 6.8 Pressure of H₂ consumed *versus* TOS in *n*-hexadecane conversion over 0.5 g of 0.45 wt.% Pt/H-Beta at 300 °C and 50 bar H₂.

The selectivity to each reaction product in the liquid phase after 30 and 240 min TOS is compared as shown in Figure 6.9. Although the cracking reaction was being favoured over the isomerisation of hexadecane, the selectivity to *iso*-hexadecane at 30 min TOS was the highest among other products in liquid-phase. Increasing TOS, *i.e.* increasing the contact time with the acid sites, resulted in successive cracking of the long-chained products (C15 and C16) in addition to the cracking of coke precursors to light hydrocarbons mainly C5 to C9 alkanes.

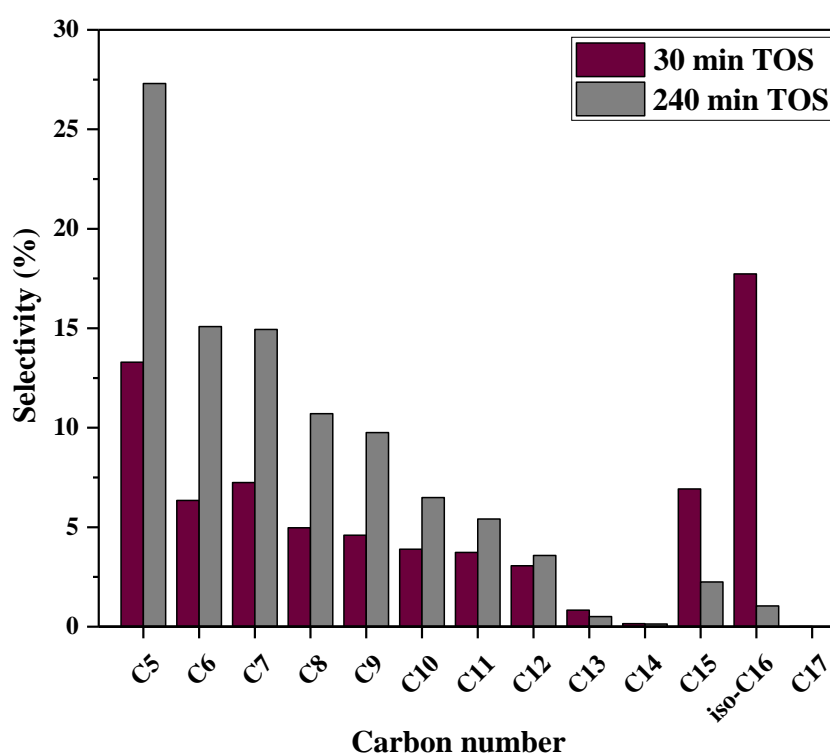


Figure 6.9 The selectivity to different reaction products in liquid-phase produced from *n*-hexadecane conversion over 0.5 g of 0.45 wt.% Pt/H-Beta at 300 °C, 50 bar H₂, and after 30 and 240 min TOS.

Generally, this study demonstrates that carbonaceous species have been formed rapidly on the catalyst surface at the employed reaction conditions. However, the presence of molecular H₂ in reaction media diminished the extent of carbon build-up with increasing TOS. The activity of the catalyst slightly increased with TOS, with the cracking reaction being favoured over the isomerisation of *n*-hexadecane.

6.3.3 Influence of catalyst surface modification

The aim of this study is to verify whether the enhancement of the cracking activity over the isomerisation of *n*-hexadecane, and the rapid formation of coke deposits on the employed catalyst were attributed to: (i) the existence of strong and non-selective acid sites on the external surface of the catalyst crystal (ii) diffusional limitations that cause the retention of reaction intermediates inside catalyst channels where they cracked to smaller molecules, or transformed to carbon deposits. Both hypotheses have been examined in this section in *n*-hexadecane conversion at 300 °C, 50 bar H₂, and 30 min TOS.

6.3.3.1 *n*-Hexadecane conversion over Pt/pre-poisoned H-Beta

The isomerisation-cracking reaction of *n*-hexadecane was carried out over the fresh Pt/H-Beta and the catalyst poisoned with DTBP using the same reaction conditions of 300 °C, 50 bar H₂, and 30 min TOS. The aim is to evaluate the influence of poisoning the external sites of the zeolite crystallites on the performance of the catalyst. It has been proven in previous studies that DTBP can selectively deactivate Brønsted acid sites located at the external surface of the zeolite crystal without affecting the acidic sites inside the pore system (Marczewski et al., 2003, Góra-Marek et al., 2014, Maseloane, 2011).

The TG/DTG analysis of the poisoned catalyst showed that DTBP material started desorbing from catalyst surface upon heating to a temperature higher than 500 °C, as illustrated in Figure 6.1. Therefore, DTBP is expected to be chemically bound to the external protonic sites at the employed reaction temperature.

The effect of the deactivation of the external acidity on the performance of the unmodified and modified catalysts is shown in Figure 6.10. It can be seen that the pre-poisoning treatment resulted in a decrease in catalyst activity, where the total conversion of *n*-hexadecane was reduced by 13% in comparison to the conversion over the fresh catalyst (86%) at the same reaction conditions. This demonstrates that pre-poisoning treatment with DTBP was effective in poisoning Brønsted acid sites at the external surface of catalyst crystal.

On the other hand, no significant change in the selectivity to *iso*-hexadecane or selectivity to coke was observed at that conversion, confirming that the reactions responsible for the formation of these products occurred at the acidic sites located inside catalyst channels. The selectivity to cracking was slightly increased by 7% relative to the fresh catalyst (55%). This minor increase in selectivity to cracking could be due to the presence of Lewis acid sites or un-poisoned Brønsted acid sites on catalyst surface.

In summary, the external acid sites of the catalyst are not the main reason behind the high selectivity to cracking and the high tendency to coke formation at the studied reaction conditions.

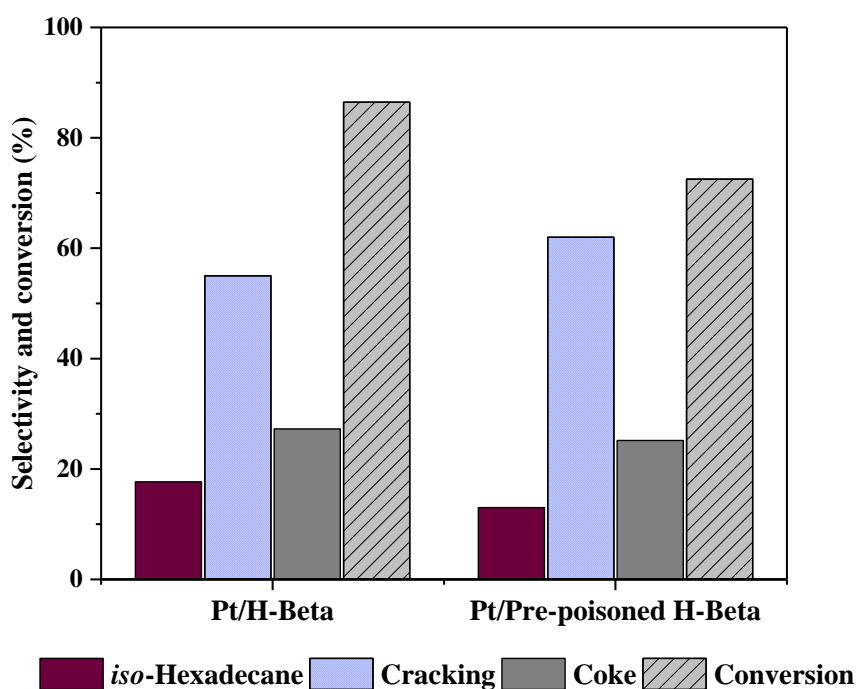


Figure 6.10 Selectivity to reaction products, and the total conversion of *n*-hexadecane over 0.5 g of the fresh and the pre-poisoned Pt/H-Beta with DTBP at 300 °C, 50 bar H₂, and 30 min TOS.

6.3.3.2 *n*-Hexadecane conversion over Pt/desilicated H-Beta

The performance of the fresh, pre-poisoned, and desilicated Pt/H-Beta in *n*-hexadecane conversion is presented and compared in Figure 6.11. The displayed data show that the desilication treatment has a significant impact in improving the

selectivity to isomerisation of hexadecane. It increased from 18% over the fresh catalyst to 28% over the desilicated catalyst. In addition, the selectivity to coke was remarkably reduced to 10% which is lower by 63% than that of the fresh catalyst. This indicates the modifications in zeolite pore size by the desilication treatment reduces the residence time of reaction intermediates inside zeolite channels and shortens diffusion path lengths. This in turn ultimately allows the desorption of the hexadecane isomers and the cracking products before exposure to further transformations that lead to coke formation and pore blockage. It has previously been established that the shape and the size of the product molecules were controlled by the shape and the size of zeolite channel and the ability of the products to diffuse out of the catalyst pores (Chen and Bridger, 1996, Gil et al., 2010).

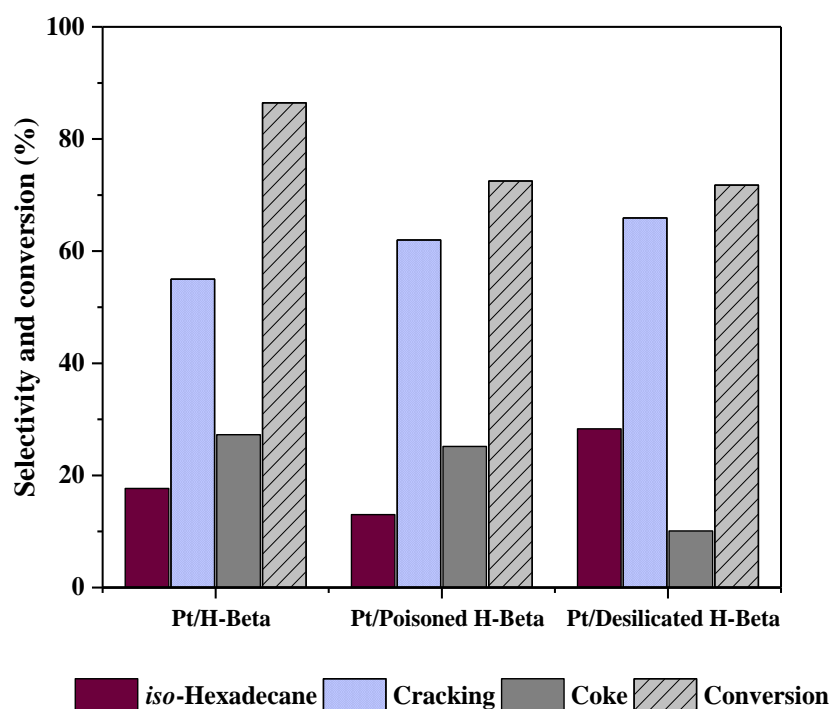


Figure 6.11 Selectivity to reaction products, and the total conversion of *n*-hexadecane over 0.5 g of the fresh, pre-poisoned, and desilicated Pt/H-Beta at 300 °C, 50 bar H₂, and 30 min TOS.

Beside the improvement in the selectivity to hexadecane isomerisation and the reduction in the selectivity to coke over Pt/ desilicated H-Beta, a lower conversion was observed in comparison to the fresh catalyst. It shows a conversion level of 73%, *i.e.* 13% lower than the conversion obtained over the unmodified catalyst. The decrease

in catalyst activity is attributed to the reduction in catalyst surface area after the desilication treatment as shown in Table 6.1, this may lead to a decrease in catalyst acidity. It is well established that the desilication treatment produces mesoporosity in zeolite microporous system which consequently improves transport, but has a negative effect on the acidic properties of the treated zeolite, and ultimately the catalyst shows lower activity in acid catalysed reactions (Groen et al., 2008). Based on the obtained data, it can be observed that although the desilication treatment reduced the surface area of zeolite H-Beta by ~ 40%, the decrease in *n*-hexadecane conversion was only 13%. This is due to the high Si/Al molar ratio of the zeolite employed which was slightly affected by the desilication treatment (see Section 6.3.1.3). The slight decrease in the Si/Al molar ratio after the desilication reflects a minor change in the acid property of the treated zeolite and eventually a slight change in *n*-hexadecane conversion was observed. Accordingly, the desilication treatment can be considered as an effective approach to enhance the selectivity to isomerisation and reduce coking over the employed catalyst.

6.3.3.3 Comparison of the performance of catalysts

From the data presented in Figure 6.11, it can be observed that at the studied reaction conditions, the pre-poisoned and the desilicated Pt/H-Beta catalysts show the same conversion level and almost similar selectivity to cracking products, however, the desilication treatment improved the isomerisation activity and effectively reduced coking. This demonstrates that the steric limitations inside the zeolite pores have the major influence to control not only the conversion but also the formation of carbon deposits more than catalyst acidity. However, the general trend of *n*-hexadecane conversion over the fresh and modified catalysts shows that the cracking reaction was favoured over the isomerisation of *n*-hexadecane.

One of the suggested approaches to control cracking and enhance isomerisation activity of bifunctional catalysts in the conversion of the long-chain *n*-alkanes, is to strengthen the hydrogenation/dehydrogenation function of the catalyst. The number of the metallic sites should be high enough to quickly hydrogenate the isomerised carbenium ions before further transformation to smaller or bulkier molecules (Batalha

et al., 2015). Bauer and co-workers observed a high yield of *iso*-hexadecane without extensive cracking at a conversion of 80% of *n*-hexadecane by using a bifunctional catalyst consisting of 0.8 wt.% of a combination of Pt and Pd metals supported on Beta zeolite having a Si/Al mole ratio of 25 (Bauer et al., 2014). Also, Batalha *et.al.* reported that the selectivity of *n*-hexadecane isomerisation was determined by two main parameters: the balance between the metal and acid functions and their degree of intimacy (Batalha et al., 2013b). Another investigation shows that loading H-Beta (26 Si/Al ratio) with 1 wt.% Pt gives an optimum balance to allow the bifunctional process of hexadecane conversion to be limited by the acid steps (Batalha et al., 2015).

In the present work, the selected H-Beta zeolite has a high Si/Al ratio (125 mole ratio) which reflects a low number of protonic sites. A 0.5 wt.% of Pt loading has been widely employed in the synthesis of the bifunctional catalyst for the isomerisation of long-chain alkanes (Park and Ihm, 2000, Busto et al., 2011), however, at the studied conditions using a batch system, a higher Pt loading may be required to overcome the high reactivity to cracking. Therefore, increasing the Pt loading to 0.8-1.0 wt.% may suppress cracking, reduce coking, and augment isomerisation. Nevertheless, the synthesised catalyst can be considered as an effective catalyst to produce light alkanes in liquid phase without significant conversion to gaseous products.

6.3.4 Coke characterisation

The influences of TOS and catalyst surface modification on the characteristics of the carbonaceous deposits laid over the Pt/H-Beta catalyst have been investigated using TGA, elemental analysis, TPO, and UV-Raman spectroscopy.

6.3.4.1 Thermogravimetric analysis (TGA)

The quantity of coke accumulated over the 0.45 wt.% Pt/H-Beta catalysts with increasing TOS is summarised in Table 6.2. From these data, it can be observed that the highest quantity of coke (7.2 %) was observed after 30 min TOS, then decreased with extending TOS to reach 4.7% after 240 min. Following the criteria described in Section 5.3.3.1, carbonaceous deposits are classified into “soft coke” which is removed by TGA at a temperature range of 200-400 °C, and “hard coke” which is

removed at temperatures higher than 400 °C. The major part of the carbonaceous deposits formed at any reaction period was hard coke which is composed of poly-condensed aromatic compounds, as suggested in previous studies (Magnoux et al., 1989, Chen and Manos, 2004, Sahoo et al., 2004).

These results are in agreement with the selectivity study as a function of TOS discussed in Section 6.3.2.3, where the selectivity to coke decreased with increasing reaction time. This suggest that increasing the contact time of reaction products with the acidic sites in the presence of H₂ leads to the transformation of a fraction of the poly-condensed aromatics contained in the hard coke to compounds with lesser degree of aromaticity in the soft coke. These alkylated mono- and di-aromatics compounds that may be present in the soft coke can be cracked to smaller molecules producing cracking products in liquid-phase.

Table 6.2 Coke content percent of the spent 0.45 wt.% Pt/H-Beta catalysts in *n*-hexadecane conversion at 300 °C, 50 bar H₂, and at increasing TOS. Analysis was repeated three times for each sample and the standard deviation from the mean value was calculated.

TOS (min)	Soft coke (wt.%) (200-400 °C)	Hard coke (wt.%) (400-850 °C)	Total coke (wt.%) (200-850 °C)
30	1.4 ± 0.15	5.8 ± 0.17	7.2 ± 0.12
60	1.5 ± 0.10	5.0 ± 0.10	6.5 ± 0.10
120	1.2 ± 0.32	4.6 ± 0.20	5.8 ± 0.30
240	1.4 ± 0.10	3.4 ± 0.10	4.7 ± 0.10

The quantity of coke deposits over the catalysts modified by the pre-poisoning and desilication treatments in comparison to the unmodified catalyst are shown in Table 6.3. The results show that both treatments have influenced the amount of coke formed, and both types of coke (soft and hard) were decreased as compared to the unmodified catalyst. The reduction in the external acidity of the catalyst slightly decreased the total coke percent to 6.4% relative to the unmodified catalyst (7.2%) indicating that carbonaceous deposits were mainly formed inside the catalyst pores (internal coke). This was also observed on coke amount formed over Pt/desilicated H-Beta catalyst, where the coke percentage reduced to 5.4%. The presence of the mesoporosity in the zeolite lattice shortens the resident time of the olefinic intermediates inside the pores and, consequently, prevents further transformation to coke deposits inside catalyst pores.

Table 6.3 Coke percent formed over the fresh and modified Pt/H-Beta catalysts in *n*-hexadecane conversion at 300 °C, 50 bar H₂, and 30 min TOS. All samples were repeated three times and the standard deviation from the mean value was calculated.

Catalyst	Soft coke (wt.%) (200-400 °C)	Hard coke (wt.%) (400-850 °C)	Total coke (wt.%) (200-850 °C)
Pt/H-Beta	1.4 ± 0.15	5.8 ± 0.17	7.2 ± 0.12
Pt/Pre-poisoned H-Beta	1.3 ± 0.20	5.1 ± 0.07	6.4 ± 0.15
Pt/Desilicated H-Beta	0.9 ± 0.18	4.5 ± 0.18	5.4 ± 0.20

6.3.4.2 Elemental analysis

The percentage of C and H, and the H/C mass ratio of the carbonaceous deposits over the spent Pt/H-Beta at increasing TOS of *n*-hexadecane conversion were determined by elemental analysis and are given in Table 6.4.

Table 6.4 Elemental analysis data showing the wt.% of C and H, and the H/C mass ratio of coke deposits after *n*-hexadecane conversion over 0.5 g of 0.45 wt.% Pt/H-Beta at 300 °C, 50 bar H₂, and at increasing TOS.

TOS (min)	%C (wt.%)	%H (wt.%)	H/C ratio
30	2.9 ± 0.01	0.9 ± 0.14	0.3 ± 0.05
60	2.5 ± 0.02	0.9 ± 0.00	0.4 ± 0.00
120	2.0 ± 0.06	1.0 ± 0.10	0.5 ± 0.07
240	1.6 ± 0.05	1.1 ± 0.05	0.7 ± 0.04

The H/C presented in Table 6.4 shows that the carbon deposits formed at any stage of *n*-hexadecane conversion are “hard” or hydrogen-deficient coke, as described in Section 4.6. The %C decreased gradually with increasing TOS along with an increase in the H%. This reflects the transformation of the structure of coke deposits to softer coke or compounds with less aromaticity.

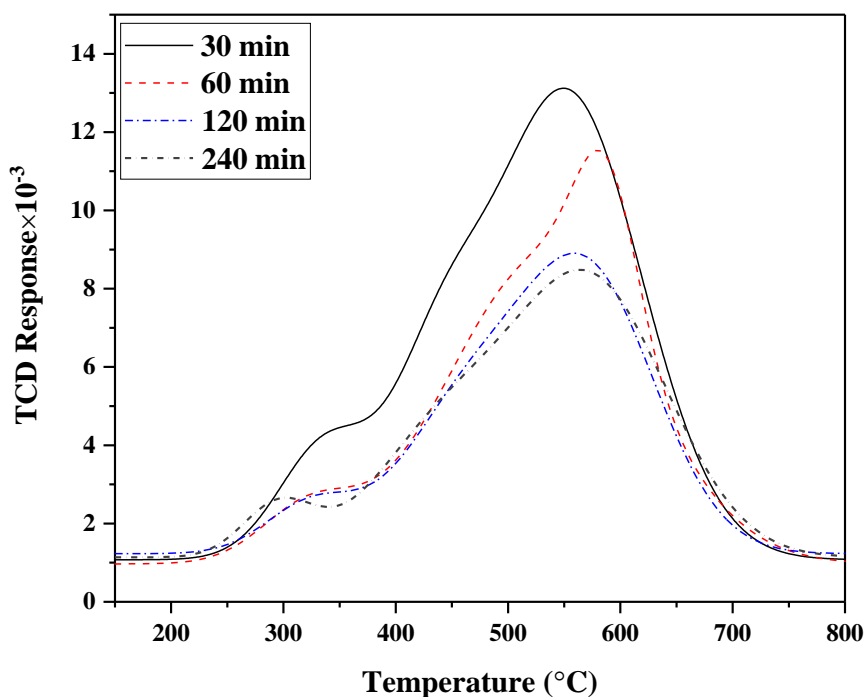
The %C, %H, and H/C mass ratio of coke formed over modified catalysts are shown in Table 6.5. Similar to the TGA observation, no significant decrease in the H/C ratio was observed in the spent catalyst after reducing the external acidity in comparison to the unmodified catalyst, whilst the H/C ratio of the spent desilicated catalyst was decreased indicating the formation of harder coke.

Table 6.5 Elemental analysis data of the coke formed over the unmodified and modified Pt/H-Beta catalysts during *n*-hexadecane conversion at 300 °C, 50 bar H₂, and 30 min TOS.

Catalyst	%C (wt.%)	%H (wt.%)	H/C ratio
Pt/H-Beta	2.9 ± 0.01	0.9 ± 0.14	0.3 ± 0.05
Pt/Pre-poisoned H-Beta	2.9 ± 0.27	0.9 ± 0.01	0.3 ± 0.12
Pt/Desilicated H-Beta	2.5 ± 0.26	0.7 ± 0.04	0.2 ± 0.04

6.3.4.3 Temperature-programmed oxidation (TPO)

The modification in the structure of the carbonaceous deposits accumulated over Pt/H-Beta with increasing TOS was further investigated using TPO analysis as shown in Figure 6.12.

**Figure 6.12** TPO fitted profile of the spent catalyst samples after *n*-hexadecane conversion over 0.5 g of 0.45 wt.% Pt/H-Beta at 300 °C, 50 bar H₂, and at 30, 60, 120, and 240 min TOS.

The TPO profile of the spent catalyst samples after 30 and 240 min TOS was deconvoluted into four Gaussian peaks using the OriginLab software as shown in Figure 6.13 (a) and (b), respectively.

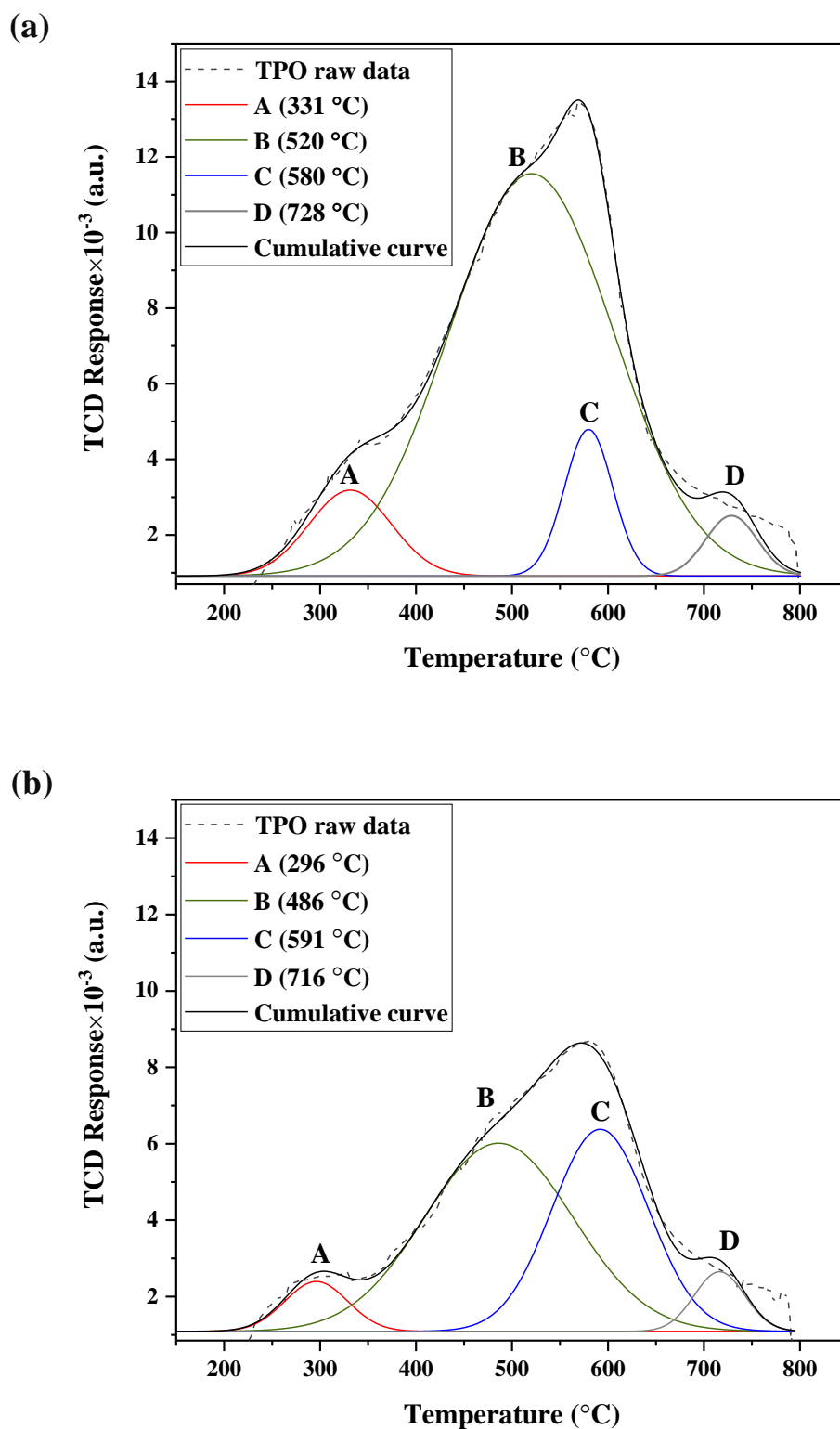


Figure 6.13 TPO profiles after baseline subtraction and peak deconvolution using Gaussian function of the spent catalyst samples of *n*-hexadecane conversion over 0.5 g of 0.45 wt.% Pt/H-Beta at 300 °C, 50 bar H₂, and after (a) 30 min; (b) 240 min TOS. The temperature shown in brackets corresponds to centre of the oxidation peak.

The oxidation peak at the lowest temperature is labelled as A, and the following peaks at increasing analysis temperature are labelled as B, C, and D.

Bayraktar and Kugler observed three peaks in the TPO profile of the spent catalyst of fluid catalytic cracking of hexadecane. The first peak observed at around 330 °C has been assigned to the desorption of homogenous hydrocarbons from coke. The second peak at around 440 °C has been ascribed to a type of coke named “contaminant coke” and it is believed to be produced by metal reactions. The third peak centred at around 550 °C has been assigned to the coke produced by acid catalysed reactions (Bayraktar and Kugler, 2002). In addition, Li and Brown identified two types of coke in the TPO profile of coke deposited by 1-octene on fresh cracking catalysts. These types are: saturated coke that oxidised at temperatures lower than 550 °C, and unsaturated or highly aromatic coke that oxidised at higher temperatures (Li and Brown, 1999).

Consistent with the criteria described in Section 4.8 and the previous observations of TPO analysis of spent cracking catalysts, peak A in Figure 6.13 (a) can be assigned to a reactive saturated coke that is weakly bound to the catalyst surface. Peak B centred at 520 °C, can be ascribed to graphitic-like carbon with lower reactivity. Peak C at 580 °C can be described as extended graphitic-like carbon that is strongly bound to the acidic sites. The last peak D is assigned to well-structured graphite and it also strongly bound to the acidic sites.

Extending reaction time in the presence of H₂ resulted in a modification of carbon deposits structure and chemical composition as shown in Figure 6.13 (b). The centre of peak B was shifted to a lower oxidation temperature of 486 °C and peak C was slightly shifted to a higher temperature of 591 °C indicating a change in the structure and the oxidation reactivity of coke.

The area of each individual peak in addition to the cumulative curve area is presented in Table 6.6. From these data it can be observed that the area of peak B, which is corresponds to pre-graphitic carbon, is decreased after 240 min TOS along with an increase in the area of peak C. This can be interpreted as the transformation of the graphitic-like coke formed after 30 min of reaction to amorphous or saturated carbon after 240 min TOS. In the meantime, the strong acid sites were probably enhanced in

the presence of molecular H₂ leading to the transformation of a fraction of coke in B to higher degree of graphitisation presented in peak C. Similarly, the hydrogen-rich coke in peak A has been decreased after 240 min TOS, demonstrating its conversion to lighter compounds.

Table 6.6 Peak areas of the resolved peaks of TPO profiles shown in Figure 6.13

TOS (min)	Peak area (a.u.)				Sum of peak areas	Cumulative curve area
	A	B	C	D		
30	0.243	2.289	0.244	0.107	2.883	2.852
240	0.106	0.953	0.666	0.102	1.827	1.822

The TPO profiles of the carbonaceous deposits formed over the spent catalysts modified by pre-poisoning and desilication treatments are shown in Figure 6.14 (a) and (b), respectively. Similar oxidation peaks can be observed in TPO profile of the spent Pt/pre-poisoned H-Beta as compared to the TPO profile of the unmodified catalyst shown in Figure 6.14 (a) and Figure 6.13 (a), respectively. This indicates that the reduction in the external acidity of the catalyst has a minor influence on the modification of carbon structure formed during the reaction, whereas the desilication treatment resulted in the disappearance of peak D which correspond to well-structured graphite as shown in Figure 6.14 (b). This can be interpreted by the improvement in transport as a result of the presence of mesoporosity that prevents the formation of such extended structure of carbon deposits which is most likely bound to the acid sites located inside catalysts pores.

The area of the deconvoluted peaks of TPO profile of spent Pt/pre-poisoned H-Beta and Pt/desilicated H-Beta are summarised in Table 6.7.

Table 6.7 Peak areas of the resolved peaks of TPO profiles shown in Figure 6.14

Catalyst	Peak area (a.u.)				Sum of peak areas	Cumulative curve area
	A	B	C	D		
Pt/poisoned H-Beta	0.134	0.970	0.439	0.025	1.569	1.569
Pt/desilicated H-Beta	0.113	1.214	0.661	0.000	1.988	1.987

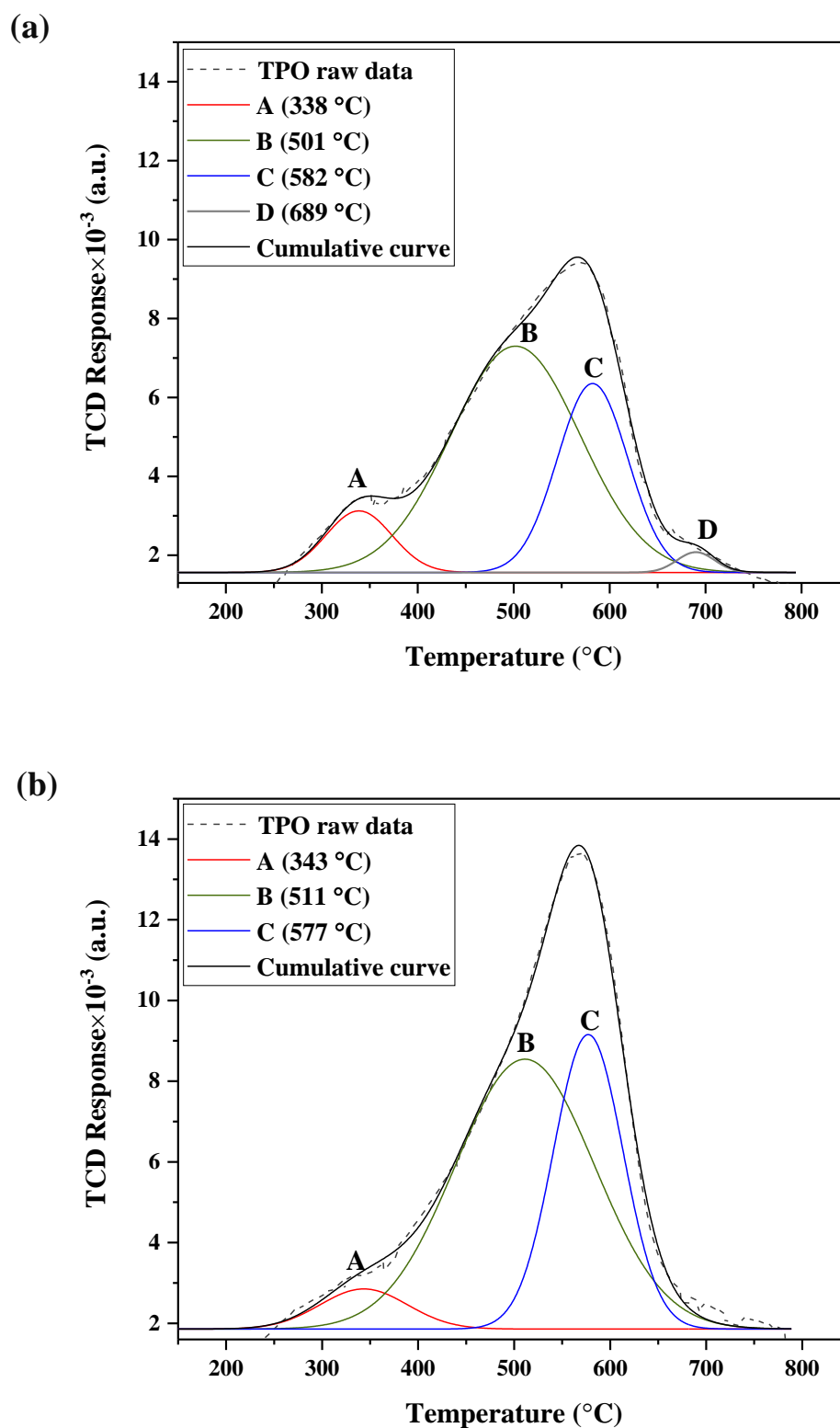


Figure 6.14 TPO profiles of spent catalysts of *n*-hexadecane conversion over 0.5 g of (a) 0.45 wt.% Pt/pre-poisoned H-Beta; (b) 0.45 wt.% Pt/desilicated H-Beta, at 300 $^{\circ}\text{C}$, 50 bar H_2 , and 30 min TOS. Fitting was performed using Gaussian function after baseline subtraction.

The peak areas show that the major part of coke was in peak B which corresponds to graphitic-like carbon. However, the area is decreased and the oxidation temperature has been shifted to a lower temperature relative to the unmodified catalyst. This indicates that the major part of coke was in a transition from amorphous to graphitic-like carbon.

6.3.4.4 UV-Raman spectroscopy

UV-Raman was employed to distinguish the chemical nature of the coke deposited on Pt/H-Beta during *n*-hexadecane isomerisation-cracking reaction. The influence of TOS and catalyst surface modification on the nature of coke has been revealed from the Raman spectra. The spectra were deconvoluted into five bands corresponding to G, D1, D2, D3, and D4 using the Voigt function for curve fitting as discussed in Section 5.3.3.4. The fitting was performed by setting the initial positions of these bands according to the values reported in the literature at the spectral region between 1000 to 1800 cm⁻¹ (Beysac et al., 2003, Sadezky et al., 2005, Pimenta et al., 2007). The typical wave number, the structural order, and the chemical composition of each band were described in Table 5.5, Section 5.3.3.4.

The deconvoluted spectra of the spent catalyst samples after 30 and 240 min TOS are shown in Figure 6.15 (a) and (b), respectively. In both spectra, the D1/G intensity ratio is higher than 1.1, therefore, D1/D3 ratio was used to measure the development in the structural order of the coke as it represents the ratio of graphitic-like carbon with edge defect to amorphous carbon. This ratio was 3.2 after 30 min of reaction indicating the fast formation of carbon deposits in pre-graphitic structure. It has been reported that the bands in the range between 1380 and 1340 cm⁻¹ (represents D1 band in this work) are assigned to C–H deformation and/or to a defect in pre-graphitic or graphitic particles (Kuba and Knözinger, 2002). After 4 h TOS, the D1/G ratio increased to 1.8 and the D1/D3 ratio decreased to 2.0. This indicates the change of coke structure to a lower graphitisation degree due to the transformation of a fraction of coke compounds from sp² carbon in pre-graphitic structure to combination of aliphatic and alkyl-aromatic compounds.

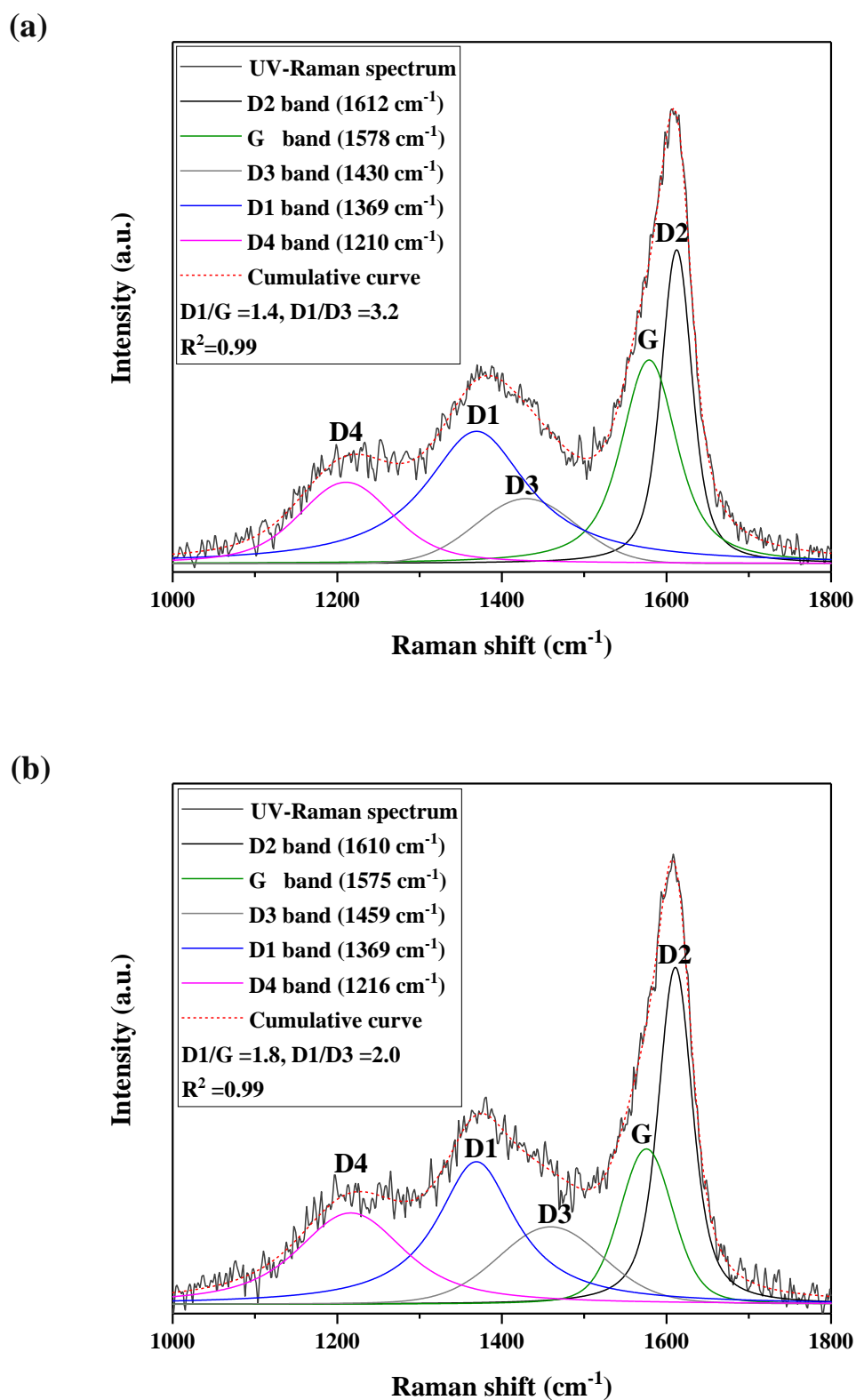


Figure 6.15 UV-Raman spectra of spent 0.45 wt.% Pt/H-Beta of *n*-hexadecane conversion at 300 °C, 50 bar H₂, and after (a) 30 min; (b) 240 min. Deconvolution performed after baseline subtraction and curve fitting using Voigt function.

In addition, bands at 1610 cm^{-1} are more pronounced than those between $1300\text{-}1450\text{ cm}^{-1}$, thus the carbonaceous deposits may be in a sheet-like topology, such as pyrene and coronene, as discussed in Section 5.3.3.4.

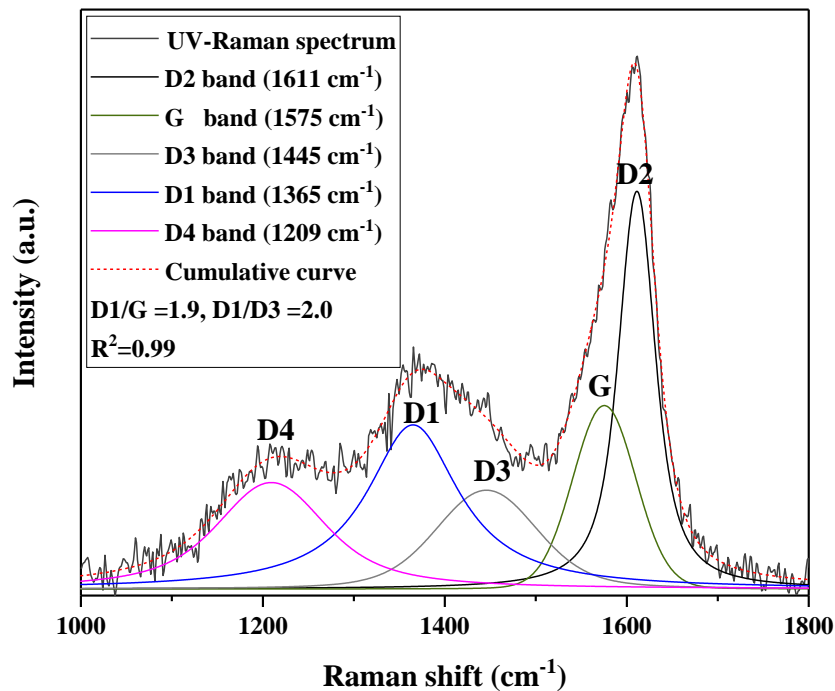
The influence of catalyst surface modification by external acid site poisoning and desilication treatment on the structure of coke is shown in Figure 6.16 (a) and (b). From Figure 6.16 it can be observed that the same bands are present in comparison to the spectrum of the spent Pt/H-Beta without modification shown in Figure 6.15 (a). This indicates the presence of the same coke species. However, both D1/G and D1/D3 ratios have been changed as summarised in Table 6.8. Both modifications influenced the structure and the composition of the carbonaceous deposits. Generally, the increase in D1/G and the decrease in D1/D3 ratios give an indication that the carbon deposits have been transformed to lower graphitisation degree.

Table 6.8 D1/G and D1/D3 area ratios of the carbonaceous deposits accumulated over the fresh and the modified Pt/H-Beta catalysts of *n*-hexadecane conversion at $300\text{ }^{\circ}\text{C}$, 50 bar H_2 , and 30 min TOS.

Ratio	Pt/H-Beta	Pt/poisoned H-Beta	Pt/desilicated H-Beta
D1/G	1.4	1.9	2.5
D1/D3	3.2	2.0	2.2

The pre-poisoning treatment resulted in a lower number of acid sites, thus decreasing the graphitisation degree of the carbon deposits. In contrast, the desilication treatment shortens the contact time of reactant and products with the acidic sites, and therefore, reduces further transformation of the carbonaceous deposits.

(a)



(b)

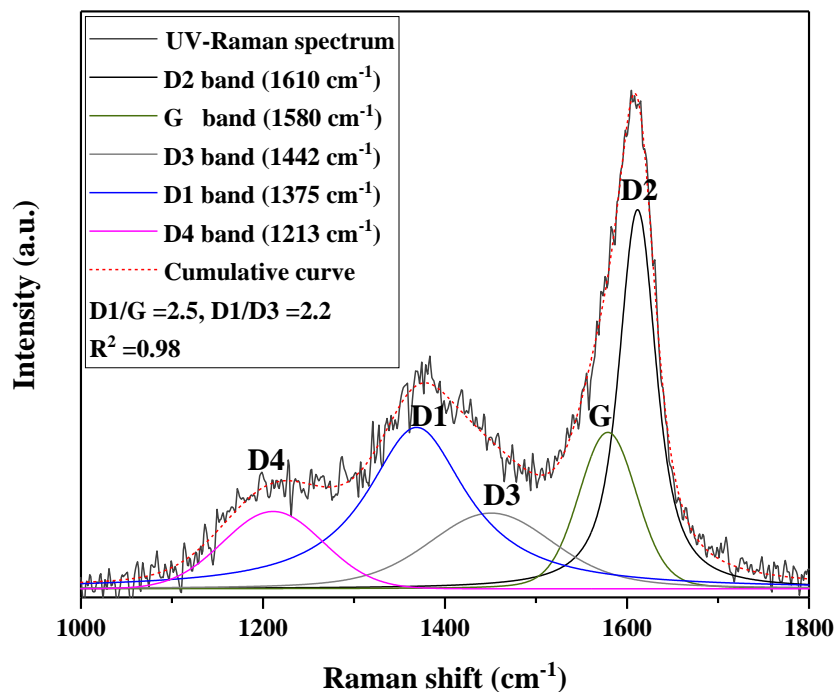


Figure 6.16 UV-Raman spectra of spent catalyst of *n*-hexadecane conversion over (a) 0.45 wt.% Pt/pre-poisoned H-Beta; (b) 0.45 wt.% Pt/desilicated H-Beta, at 300 °C, 50 bar H₂, and 30 min TOS. Deconvolution was performed after baseline subtraction and curve fitting using Voigt function.

6.4 Conclusions

Isomerisation-cracking reaction of *n*-hexadecane as a representative long-chained *n*-alkane has been studied over H-Beta and ZSM-5 zeolites as well as over Pt/zeolite. H-Beta was chosen as an acidic support for the bifunctional catalyst due to the high conversion of *n*-hexadecane obtained over that zeolite and the enhancement of the isomerisation reaction even in the absence of the metallic sites responsible for the production of olefinic intermediates that easily reacted on the acid sites.

The study of the influence of reaction temperature over H-Beta zeolite showed that a temperature of 300 °C is the optimal reaction temperature to achieve high conversion of *n*-hexadecane and to augment the isomerisation activity. In addition, increasing H₂ pressure in the reaction over Pt/H-Beta resulted in an increase in the selectivity to *iso*-hexadecane, and effectively reduces coke build-up. Therefore, 50 bar H₂ was found to be the appropriate pressure to perform the reaction.

Carbonaceous deposits were formed rapidly on the bifunctional catalyst during the first 30 min of *n*-hexadecane conversion at 300 °C and under 50 bar H₂, where 27% of the reacted *n*-hexadecane was transformed to coke deposits. Extending the reaction time in the presence of molecular H₂ resulted in a successive cracking of the long-chain products in liquid-phase as well as the cracking of coke precursors to lighter products, in particular, C5 to C9 alkanes.

The reasons behind the extensive cracking of hexadecane and the high tendency to coke formation were investigated. Reducing zeolite acidity by the selective poisoning of external Brønsted sites using DTBP resulted in a decrease in the overall conversion. Nevertheless, no significant change in the selectivity to reaction products was observed. This indicated that the reactions responsible for cracking and coke formation occur inside zeolite channels. In contrast, the presence of mesoporosity in zeolite microstructure significantly improved hexadecane isomerisation and reduces coking. This indicates that mesoporosity produced by the desilication treatment enhanced the rate of diffusion and prevents the blocking of reaction intermediates and/or products inside catalyst channels where they cracked to smaller molecules or transformed to bulkier molecules and form coke deposits. Thus, the isomerisation of

n-hexadecane and the coke formation reactions are determined by the pore size and structure of the employed zeolite.

The quantity and the structure of the accumulated carbonaceous deposits over the parent and the modified Pt/H-Beta have been investigated. TGA measurements showed that prolonging reaction time in the presence of hydrogen reduced the quantity of coke. The majority of coke deposits were hard coke, which are likely composed from poly-condensed aromatic compounds. The desilication treatment effectively reduced coke deposition in comparison to the unmodified catalyst at the same reaction conditions.

Consistent with TGA results, elemental analysis demonstrated that the nature of carbon deposits formed at any stage of *n*-hexadecane conversion over Pt/H-Beta are hard or hydrogen-deficient coke due to the low H/C mass ratio (less than 0.8). The same type of coke was observed over the modified catalyst samples.

TPO measurements showed the presence of four types of carbon species which differed in structure and oxidation reactivity. These deposits are mostly graphitic-like carbons that are strongly bound to the acid sites. With the prolongation of hexadecane reaction time, a fraction of the graphitic-like coke was transformed to amorphous-type coke due to the presence of molecular hydrogen that contributed in the hydrogenation of coke deposits to softer carbon. TPO measurements conducted over modified Pt/H-Beta catalysts at same reaction conditions showed that the nature of coke deposits did not change substantially since the values of oxidation temperatures are almost similar. However, the presence of the mesoporosity in zeolite microstructure produced by the desilication treatment resulted in the disappearance of the oxidation peak corresponds to well-structured graphite in the deconvoluted TPO profile.

In agreement with TPO results, UV-Raman spectra indicated the presence of highly organised graphite, amorphous, and disordered or graphitic-like carbon. D1/D3 ratio was used to provide information regarding the graphitisation degree of coke deposits. This ratio was decreased as the TOS increased over Pt/H-Beta due to the transformation of a part of the coke compounds from sp^2 carbon in a pre-graphitic structure to a combination of aliphatic and alkyl-aromatic compounds in amorphous

carbon. Similarly, reducing catalyst surface acidity or shortening the contact time with the acid sites *via* desilication treatment resulted in a decrease in D1/D3 ratio indicating a lower degree of graphitisation when compared to the unmodified Pt/H-Beta.

Chapter 7

*Tailored carbon deposition
of Pt/H-Beta for
n-hexadecane conversion*

7 Chapter 7: Tailored carbon deposition of Pt/H-Beta for n-hexadecane conversion

7.1 Introduction

It is widely known that hydrocarbon transformations over zeolite and zeolite-supported metal catalysts are accompanied by the deposition of carbonaceous residues on the solid catalyst. These carbonaceous deposits reduce the catalytic activity with time, and eventually lead to a complete deactivation of the catalyst by poisoning of active sites and/or blocking access to them (Uguina et al., 1993, Bartholomew, 2001). However, recent studies demonstrated that coke does not always have a detrimental effect on the catalytic performance of zeolites, and certain coke species can be used to improve the selectivity to the desired products (Guisnet, 2002a).

Several studies have been performed to develop methods for surface modification of zeolites and zeolite based catalysts to boost the selectivity of products. Such methods include the poisoning of Brønsted acid sites located at the external surface of zeolite crystal by the adsorption of base molecules (Yaluris et al., 1996, Maseloane, 2011), pre-coking treatments (Gorra et al., 1992, Uguina et al., 1993, Al-Khattaf, 2007), deactivation of non-selective acid sites in zeolites by chemical vapour/liquid deposition of organosilicon compounds (Hibino et al., 1991, Zheng et al., 2002), and impregnation with metals such as cerium (Kim et al., 1995).

The pre-coking or tailored carbon deposition approach over zeolites was a subject of interest for many investigations relating to catalytic hydrocarbon transformations. For instance, Uguina *et al.* studied toluene disproportionation over pre-coked ZSM-5 using mesitylene, toluene and isobutene as coke precursors. The study revealed that the amount, nature, and location of the carbonaceous material deposited during the disproportionation reaction strongly depend on the hydrocarbon used as coke precursor and that these have different effects on the catalytic performance of ZSM-5 (Uguina et al., 1993). Bauer *et al.* studied the effects of pre-coking on the improvement of the selectivity to *p*-xylene during xylene isomerisation over Pt/H-ZSM-5. It was found that pre-coking using methanol as a pre-coking agent facilitated the selective deactivation of external acid sites leading to a significant

reduction in xylene loss (Bauer et al., 2004). Another study was performed by Al-Khattaf on *m*-xylene transformation which showed that the deactivation of the external active sites of ZSM-5 using 1,3,5-tri-isopropyl-benzene (TIPB) as a pre-coking agent improved *p*-xylene selectivity (Al-Khattaf, 2007). In addition, it was found that the pre-coked catalyst reduced the activation energy required for *p*-xylene formation as compared to the fresh catalyst. Elsewhere, it has been shown that pre-coking using methanol as a coke precursor improved the selectivity for xylene isomerisation over H-ZSM-5 (Bauer et al., 2007). McGregor and co-workers studied the role of carbon deposits in hydrogenation of C5 hydrocarbons including pentenes, pentenenitriles, and 1-pentyne over Al₂O₃ supported Ni and Pd catalysts. Therein it was established that hydrocarbonaceous overlayer derived from different isomers of the same compound could have different effects on the subsequent hydrogenation reaction. Hence, hydrocarbonaceous deposits can enhance C5 hydrogenation through either poisoning of acid sites, pore blocking or deposition of active coke (McGregor and Gladden, 2008). A recent study on the enhancement of catalytic ethylbenzene dehydrogenation over pre-coked CrOx/Al₂O₃ demonstrated that tailored coke deposition suppressed undesired reactions such as cracking to benzene and coking (Gomez Sanz et al., 2016). In addition, the pre-coking approach using reactant and product molecules as coke precursors allows for the identification of the precursor molecules involved in the formation of carbonaceous deposits in that reaction.

Considering the present work, the catalytic isomerisation-cracking of heavy *n*-alkanes is a commercially interesting reaction which produces a mixture of short and long hydrocarbon chains. These hydrocarbons, in particular the light fractions, are used for the production of fuels and feedstocks to petrochemical industries, whilst the heavy hydrocarbons are used for the manufacture of high quality lubricants.

The present work focuses its attention on the surface modification of Pt/H-Beta by pre-coking and silylation treatments in order to determine the effect of these modifications on the selectivity to the desired light products and reduce the rate of coking. Therefore, the objectives of this study are: (i) to develop controlled pre-coking procedures to produce a carbonaceous overlayer on the parent Pt/H-Beta using *n*-pentane and toluene as paraffinic and aromatic coke precursors; (ii) to study the

characteristics of these carbonaceous species including quantity, structure, location and nature *via* characterisation of the pre-coked catalysts using thermogravimetric analysis (TGA); N₂ adsorption isotherm for BET surface area measurement; temperature-programmed oxidation (TPO); and Raman spectroscopy; (iii) to examine the performance of the pre-coked and silylated Pt/H-Beta in the isomerisation-cracking of *n*-hexadecane as a model reaction.

7.2 Materials and methods

7.2.1 Catalyst preparation

The catalysts employed in this study are: 0.45 wt.% Pt/H-Beta modified by silylation treatment, 0.45 wt.% Pt/H-Beta pre-coked with *n*-pentane as paraffinic precursor, and 0.45 wt.% Pt/H-Beta pre-coked with toluene as aromatic precursor.

7.2.1.1 Silylation treatment

Pt/H-Beta catalyst was prepared by incipient wetness impregnation using the preparation method described in Section 3.3.3. The catalyst was then subjected to further modification by covering the hydroxyl groups located at the external surface and pore mouth region with an inert layer of silica using tetraethoxysilane (TEOS) as a silylation agent. The silylation method is described in Section 3.3.4.

7.2.1.2 Pre-coking of Pt/H-Beta with n-pentane

Pre-coking of 0.45 wt.% Pt/H-Beta catalyst with *n*-pentane, as a paraffinic coke precursor, was performed using a fixed-bed reactor connected to an on-line GC equipped with a FID detector, and fitted with a CP-Al₂O₃/KCl PLOT column (Agilent). The description of the reactor and the GC method employed are shown in Sections 3.4.1.1 and 3.5.1, respectively. *n*-Pentane was introduced to the catalyst by employing the gas flow saturation method, using H₂ as a carrier gas.

Pt/H-Beta was pre-coked at a temperature of 300 °C, WHSV of 1.5 h⁻¹, and at 360 min TOS. These conditions were selected based on the study of *n*-pentane conversion over Pt/H-Beta presented in Chapter 5. At these conditions, Pt/H-Beta showed a high

conversion of *n*-pentane (65%) and the greatest selectivity to *iso*-pentane (86%). In addition, the quantity of coke deposits formed during this reaction was 4.4%; it has been hypothesised that these deposits play a role as active species in catalysing the reaction at the catalyst pore mouth.

The method employed for *n*-pentane pre-coking is the same as the experimental procedure utilised to perform *n*-pentane conversion presented in Chapter 5. Briefly, 0.5 g of Pt/H-Beta in a particle size of 250-425 μm was initially loaded into the reactor and reduced using 30 ml min^{-1} of H_2 at 400 $^\circ\text{C}$ for 2 h. The pre-coking reaction was subsequently started after cooling the reactor to 300 $^\circ\text{C}$. The H_2 was allowed to pass through a saturator containing *n*-pentane, the flow rate was adjusted to 12.5 ml min^{-1} in order to obtain a WHSV of 1.5 h^{-1} . The reaction was then conducted for 360 min TOS.

After reaction, the pre-coked catalyst was purged *in situ* using He at a flow rate of 40 ml min^{-1} for 1 h at the reaction temperature in order to strip any retained reactant or product from the catalyst. The spent Pt/H-Beta of *n*-pentane conversion was carefully crashed into powder using a mortar and then employed as a pre-coked catalyst for *n*-hexadecane conversion.

7.2.1.3 Pre-coking of Pt/H-Beta with toluene

Pre-coking of Pt/H-Beta with toluene, as an exemplar aromatic coke precursor, was performed after modifying the catalyst surface with silylation treatment. The silylation treatment was employed in order to temporarily cover the hydroxyl groups located at the external surface and pore mouth regions with inert silica. Afterwards, the catalyst was allowed to adsorb toluene (*vide infra*), followed by pre-coking in a static and inert atmosphere at 650 $^\circ\text{C}$. This temperature was selected based on the studies described in Section 7.3.1.1. The aim of this treatment is to allow for the accumulation of carbonaceous deposits originating from toluene inside the pores of the catalyst and to maintain the acid sites located at the external surface and the pore mouth region free of coke.

Two methods were employed for toluene adsorption:

- i. Toluene liquid adsorption: in this method, 0.5 g of the silylated Pt/H-Beta was suspended in 10 ml of liquid toluene using a 50 ml round bottom flask. The mixture was then gradually heated to 50 °C under reflux with constant stirring for 6 h to ensure homogeneous impregnation of the catalyst with toluene. This adsorption temperature was selected to avoid any potential surface reaction of toluene with the surrounding atmosphere over this acid catalyst. The adsorption was quenched by immersing the flask in an ice bath. The catalyst was separated by filtration at ambient temperature and pressure. After separation, the catalyst was left over night at room temperature to allow for the evaporation of the non-adsorbed toluene. The volume of toluene after filtration was 5 ml indicating the adsorption of approximately 5 ml by the catalyst. GC analysis was conducted for the remaining toluene after filtration. The GC was equipped with a FID detector and fitted with a DB-5HT (Agilent) capillary column. Analysis showed that only toluene was present indicating that no reaction was carried out during toluene adsorption.
- ii. Toluene vapour adsorption: in this method, 0.5 g of the silylated Pt/H-Beta was loaded into the fixed bed reactor described in Section 3.4.1.1. The catalyst bed was sandwiched between two thin layers of inert quartz wool, and glass bead were used to fill the dead volume of the reactor and to hold the catalyst bed to the heating zone of the furnace. The catalyst was first pre-treated with 40 ml min⁻¹ of He at 100 °C for 60 min to allow for the desorption of any adsorbed moisture. Afterwards, the reactor was cooled to 50 °C. Toluene vapour was introduced to the catalyst using the gas flow saturation method, employing He as a carrier gas. He at a flow rate of 40 ml min⁻¹ was passed through a saturator filled with toluene at 50 °C. The adsorption process continued for 12 h in order to allow for the saturation of catalyst pores with toluene.

After toluene adsorption using both methods, the catalyst samples were loaded in borosilicate ampoules having dimensions of 22 mm internal diameter, 4 mm thickness, and 135 mm total length. After catalyst packing, the ampoules were placed in a liquid

N₂ bath and evacuated. The purpose of using the liquid N₂ bath was to avoid the desorption of the adsorbed toluene under vacuum. The ampoules were then sealed as shown in Figure 7.1(a).

Pyrolysis of the coke precursors was carried out by placing the sealed ampoules in a furnace at 650 °C for 2 h. This pre-coking temperature was selected to allow for the decomposition of TEOS that covered the hydroxyl groups located at the external and pore mouth region of catalyst crystal (see Section 7.3.1.1). The ampoules were swollen after catalyst pre-coking indicating the expansion of gases released from the adsorbate as shown in Figure 7.1 (b). After the pre-coking treatment, the ampoules were opened and the pre-coked catalysts were collected and characterised to investigate the quantity, structure, and chemical composition of the carbonaceous deposits.

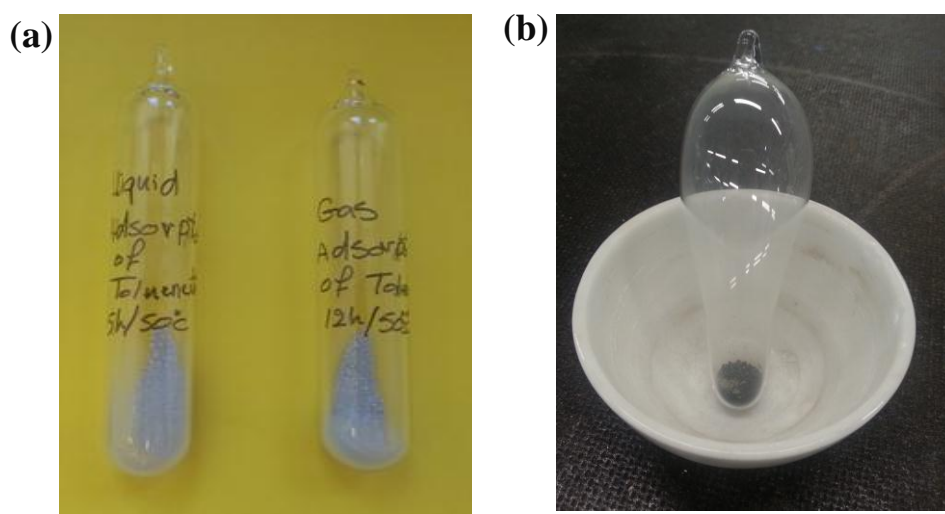


Figure 7.1 Ampoules used in the preparation of pre-coked Pt/H-Beta with toluene **(a)** before pre-coking; **(b)** after pre-coking at 650 °C.

7.2.2 Coke characterisation

The properties and the structure of coke deposits after the pre-coking of Pt/H-Beta with different coke precursors were investigated using thermogravimetric analysis

(TGA); temperature-programmed oxidation (TPO); and Raman spectroscopy. In addition, N₂ adsorption isotherm was utilised for BET surface area measurement. The methods and the experimental parameters employed for these techniques are described in Chapter 4.

7.2.3 Catalytic activity measurements and GC analysis

Catalytic conversion of *n*-hexadecane over fresh Pt/H-Beta and pre-coked Pt/H-Beta with different coke precursors was conducted using the reactor set-up and the experimental procedure described in Section 3.4.2.1 and 3.4.2.2, respectively.

Gas chromatography measurements for the headspace gases and the liquid products were conducted off-line using the GC columns and methods described in Section 3.5.2. The methods for calculating the catalytic performance indicators (conversion and selectivity) and the reproducibility error are explained in detail in Section 3.6.

7.3 Results and discussion

7.3.1 Characterisation of the pre-treated catalysts

7.3.1.1 Characterisation of Pt/H-Beta after silylation

The deposition of TEOS on Pt/H-Beta after two cycles of silylation treatment was confirmed by DTG using N₂ as a carrier gas. This analysis allows for the determination of the temperature required for TEOS decomposition.

DTG curves of the fresh Pt/H-Beta and after silica loading are shown in Figure 7.2 (a) and (b), respectively. In both figures, the peak at a temperature lower than 100 °C is related to the desorption of adsorbed water. The exothermic peak observed around 650 °C in Figure 7.1 (b) corresponds to the desorption of TEOS.

This observation, is the bases of the choice of 650 °C as the furnace temperature in order to form coke deposits on the catalyst surface after toluene adsorption. This temperature ensures the decomposition of the TEOS that covered the external surface and the pore mouth region.

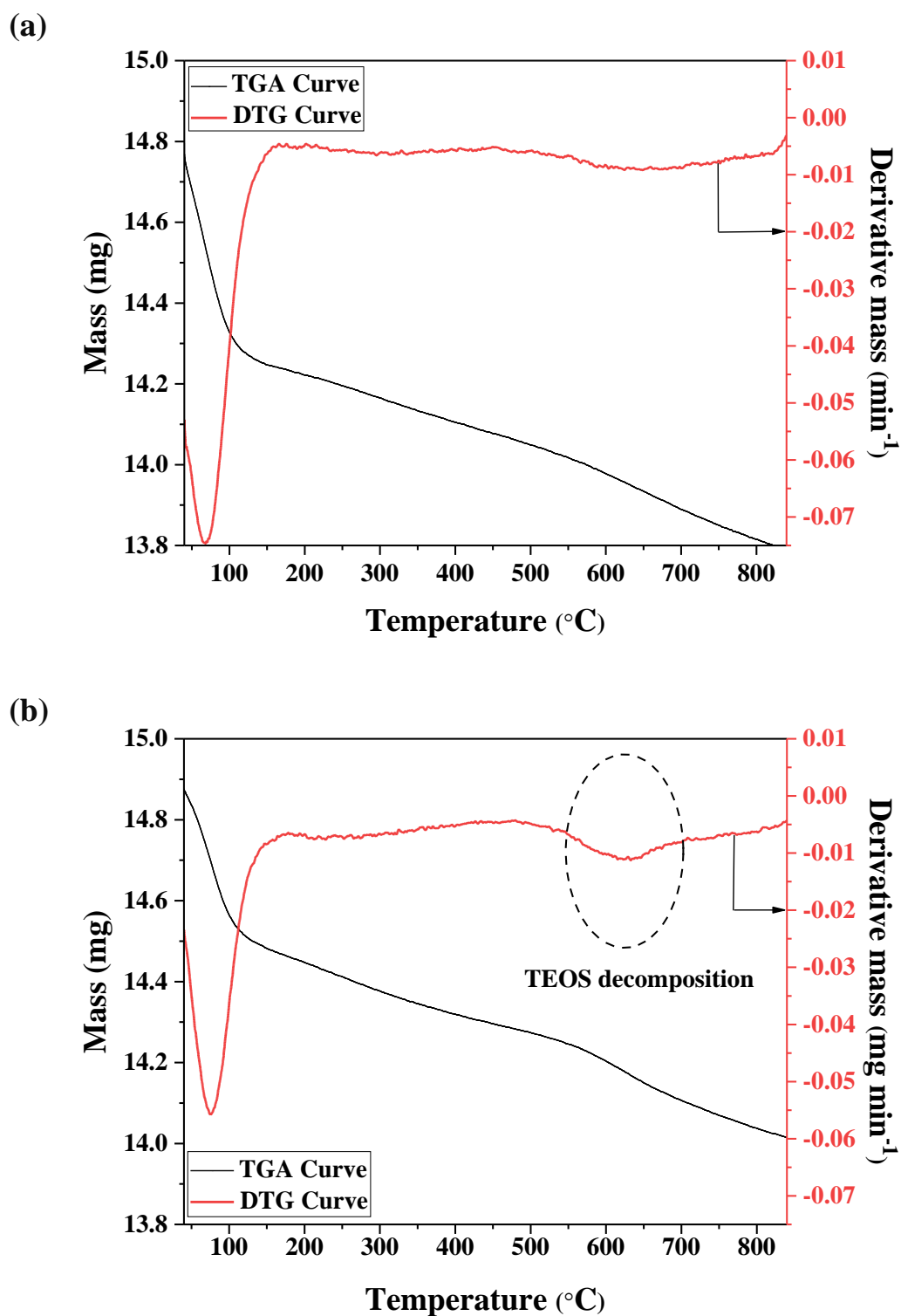


Figure 7.2 TG/DTG analysis for the decomposition of (a) fresh Pt/ H-Beta; (b) TEOS loaded on Pt/H-Beta, using N₂ a carrier gas.

The BET surface area of the silylated Pt/H-Beta was $420 \text{ m}^2 \text{ g}^{-1}$, determined by BET analysis as described in Section 4.4. This is lower than the BET surface area of the fresh Pt/H-Beta before modification ($533 \text{ m}^2 \text{ g}^{-1}$). The decrease in BET surface area after silylation treatment is ascribed to the blockage of a fraction of catalyst pores as a result of silylation treatment.

7.3.1.2 Characterisation of pre-coked Pt/H-Beta

The catalysts after pre-coking treatments with *n*-pentane and toluene precursors were characterised using TGA; N_2 adsorption isotherm for BET surface area measurement; TPO; and UV-Raman spectroscopy.

7.3.1.2.1 Thermogravimetric analysis (TGA)

The quantity of carbonaceous species accumulated over Pt/H-Beta after the pre-coking treatments using *n*-pentane and toluene is summarised in Table 7.1.

Table 7.1 Coke content in wt.% formed over Pt/H-Beta after pre-coking with *n*-pentane and toluene. The analysis was repeated three times for each sample and the standard deviation from the mean value was determined.

Pt/H-Beta pre-coked with:	Soft coke (wt.%) (200-400 °C)	Hard coke (wt.%) (400-850 °C)	Total coke (wt.%) (200-850 °C)
<i>n</i> -Pentane /6 h	1.2 ± 0.06	3.2 ± 0.15	4.4 ± 0.19
Toluene (liquid adsorption /6 h)	1.0 ± 0.00	3.0 ± 0.15	4.1 ± 0.10
Toluene (vapour adsorption /12 h)	1.0 ± 0.03	9.7 ± 0.14	10.7 ± 0.12

From the data presented in Table 7.1, it can be observed that the total quantity of coke laid down over *n*-pentane pre-coked Pt/H-Beta is 4.4% which is close to the quantity of coke accumulated over toluene pre-coked Pt/H-Beta after 6 h of toluene liquid adsorption (4.1%). In contrast, more coke accumulated over the toluene pre-coked Pt/H-Beta after 12 h of toluene vapour adsorption (10.7%). Both toluene pre-coked catalysts have been heated at the same temperature (650 °C), however, the higher initial adsorption time (at 50 °C) resulted in a higher coke content.

The largest fraction of the coke formed over the three samples of pre-coked catalysts was hard coke, which indicates the presence of poly-condensed aromatic compounds, whilst the percentage of the soft coke is lower; this is composed mainly of alkylated mono- and di aromatics and smaller amounts of polyaromatics.

7.3.1.2.2 Surface area measurements

The BET surface area of the fresh and the pre-coked Pt/H-Beta is shown in Table 7.2.

Table 7.2 BET Surface area of Pt/H-Beta before and after pre-coking treatments with *n*-pentane and toluene.

Catalyst	BET Surface area (m ² g ⁻¹)
Fresh Pt/H-Beta	533
Pentane pre-coked Pt/H-Beta /6 h	453
Toluene pre-coked Pt/H-Beta (liquid adsorption /6 h)	340

Data presented in Table 7.2 show that the pre-coking treatment resulted in a decrease in the BET surface area. This is ascribed to the blockage of catalyst micropores with carbonaceous deposits. Although TGA results showed that the quantity of coke laid down over pentane and toluene pre-coked catalysts after 6 h was almost the same, the pentane pre-coked catalyst shows higher BET surface area than toluene pre-coked catalyst. This can be explained as carbonaceous deposits formed over *n*-pentane pre-coked catalyst are assumed to be located at the external surface as well as inside catalyst pores as concluded in Chapter 5, whereas, coke formed over toluene pre-coked Pt/H-Beta was mainly accumulated inside catalyst pores leading to an extensive reduction in BET surface area in comparison to the fresh catalyst. These results confirm that the methodology employed in toluene pre-coking was successful in directing the location of coke formation as desired.

7.3.1.2.3 Temperature-programmed oxidation (TPO)

Pre-coked catalysts were analysed by temperature-programmed oxidation (TPO). The TPO profile of *n*-pentane pre-coked Pt/H-Beta at 300 °C and 360 min TOS is shown in Figure 5.10 (b), Section 5.3.3.3. In addition, it has been demonstrated that carbonaceous deposits accumulated over Pt/H-Beta at the defined pre-coking

conditions are a combination of hydrogen-rich, amorphous, graphitic-like, and highly crystalline carbon species. However, the deconvolution result of the TPO profile showed that the largest fraction of these deposits was graphitic-like carbon. This type of carbon was oxidised at around 585 °C and it is most likely bound to acid sites located inside the pores.

TPO profiles of toluene pre-coked Pt/H-Beta catalysts are shown in Figure 7.3. The profiles show that both toluene pre-coked catalysts present a pronounced peak at oxidation temperature higher than 500 °C. This suggests the formation of homogeneous carbon deposits in graphitic-like structures with high aromatic content. The oxidation peak of toluene pre-coked Pt/H-Beta using liquid adsorption /6 h is centred at 600 °C, and that for toluene vapour adsorption /12 h is centred at around 650 °C. The higher oxidation temperature is an indication of higher graphitisation degree. These deposits have low oxidation reactivity, and are most likely bound to acid sites located inside catalyst pores.

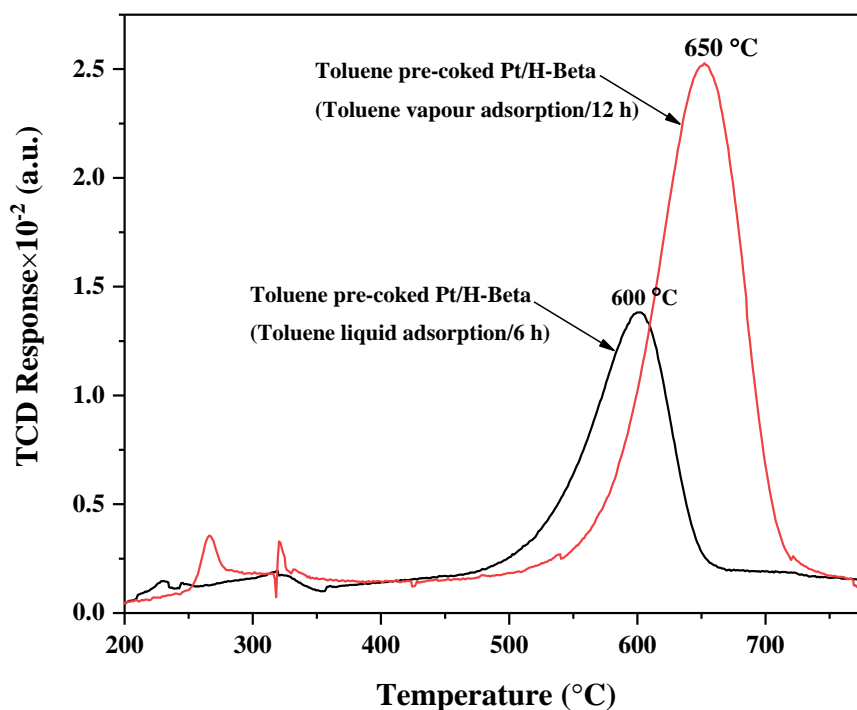


Figure 7.3 TPO profile of pre-coked Pt/H-Beta at 650 °C using toluene as a coke precursor.

The peak area of the pre-coked Pt/H-Beta using vapour adsorption /12 h is clearly larger than that for pre-coked Pt/H-Beta using liquid adsorption /6 h, thus a greater amount of carbon was deposited over the catalyst as shown in Table 7.3. This result matches the TGA measurement where the quantity of coke resulted from toluene pre coking /12 h was 10.7%, which is much greater than that produced from toluene pre coking /6 h that shows a total coke quantity of 4.1%.

Table 7.3 Integrated peak areas of the pronounced peaks of TPO profiles shown in Figure 7.3.

Catalyst	Integrated peak area (a.u.)	Temperature (°C)
Toluene pre-coked Pt/H-Beta (liquid adsorption /6 h)	0.94	600
Toluene pre-coked Pt/H-Beta (vapour adsorption /12 h)	1.93	650

Additionally, the pre-coked Pt/H-Beta by toluene vapour presented small peaks at oxidation temperature lower than 350 °C. This indicates the presence of hydrogen-rich compounds with high reactivity and weakly bound to the catalyst surface.

7.3.1.2.4 UV-Raman spectroscopy

The chemical identity and the graphitisation degree of the carbonaceous species formed over the pre-coked catalysts were investigated using UV-Raman spectroscopy. The spectrum of *n*-pentane pre-coked Pt/H-Beta is shown in Figure 5.12 (b), Section 5.3.3.4. The spectra of toluene pre-coked catalysts using liquid adsorption / 6 h and vapour adsorption /12 h methods, are shown in Figure 7.4 (a) and (b), respectively. Deconvolution of G, D1, D2, D3, and D4 bands was performed by considering Voigt functions in all cases. Both D1/G and D1/D3 ratios were determined as a measurement of the graphitisation degree or structural organisation of the carbonaceous deposits. Fitting was performed by setting the initial positions of these bands according to the values reported in the literature for carbonaceous materials (Sadezky et al., 2005, Pimenta et al., 2007). The typical wavenumber, the structural order, and the chemical composition of carbonaceous materials presented in each band were described in Table 5.5, Section 5.3.3.4. The D1/G and D1/D3 integrated intensity ratios and the band positions for the pre-coked catalysts are summarised in Table 7.4.

Table 7.4 Position of the Raman bands, D1/G and D1/D3 ratios of the Raman spectra of pre-coked Pt/H-Beta. The results involve a degree of uncertainty due to the noisy Raman signal.

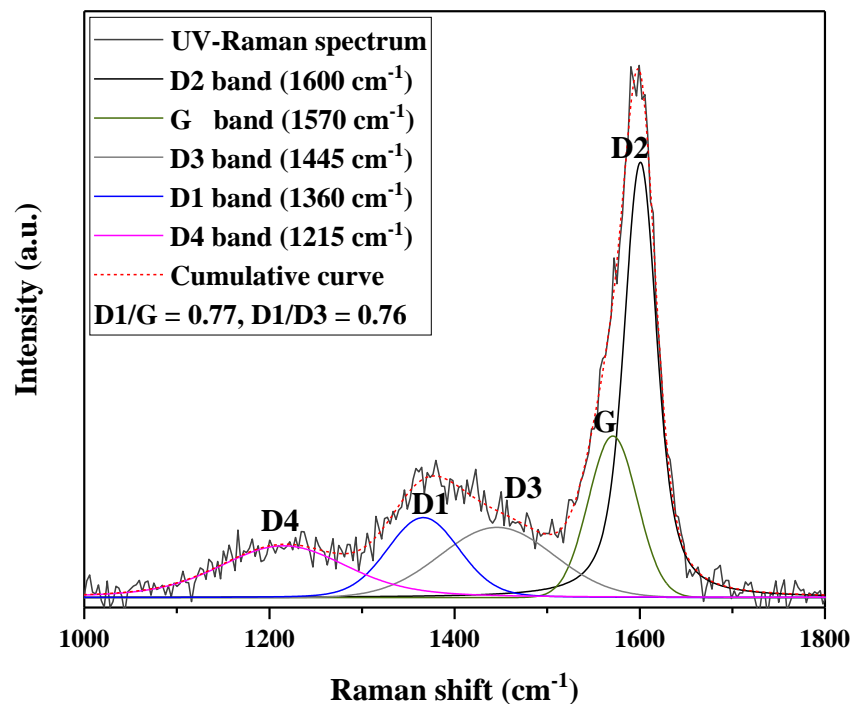
Pt/H-Beta pre-coked with:	Band position (cm ⁻¹)					D1/G ratio	D1/D3 ratio
	D2	G	D3	D1	D4		
<i>n</i> -Pentane	1610	1573	1452	1374	1218	1.4	1.6
Toluene (liquid adsorption /6 h)	1600	1570	1445	1360	1215	0.77	0.76
Toluene (vapour adsorption /12 h)	1612	1573	1428	1365	1250	0.56	0.87

As described in Section 7.2, *n*-pentane pre-coked Pt/H-Beta is the spent catalyst of *n*-pentane isomerisation over fresh Pt/H-Beta. The coking temperature of that pre-coked catalyst was 300 °C, whereas, the temperature employed for toluene pre-coked Pt/H-Beta (both liquid and vapour adsorption methods) was 650 °C. This is reflected in the graphitisation degree of the pre-coked catalysts. Hence, D1/G ratio of *n*-pentane coke is higher than that of toluene coke due to the lower pre-coking temperature.

The D1/G ratio of toluene coke originating from toluene liquid adsorption /6 h was 0.77, which is higher than that originated from toluene vapour adsorption /12 h that showed a D1/G ratio of 0.56. This suggests an increase in structural organisation of coke deposits in the later case. This result matches the TPO results where toluene pre-coked catalyst by vapour adsorption /12 h showed a higher oxidation temperature than the toluene pre-coked catalyst by liquid adsorption /6 h, which reflects a higher graphitisation degree, and the TGA results which showed a greater fraction of hard coke.

Furthermore, in order to compare the structural order of the carbonaceous deposits originated from *n*-pentane pre-coking to those originating from toluene pre-coking, the D1/D3 ratio was determined. It has been reported that D1/G is not reliable when the value of the parameter is higher than 1.1, and that the D1/D3 ratio can instead be used as an indicator of the structural development of carbon deposits (Gomez Sanz et al., 2016). The *n*-pentane pre-coked catalyst showed a higher D1/D3 ratio (1.6) than that of the toluene-liquid and vapour pre-coked catalysts (0.76 and 0.87 respectively). This indicates that a change of coke structure from amorphous to more disordered coke (polyaromatics in graphene layer edges) occurred between the two samples.

(a)



(b)

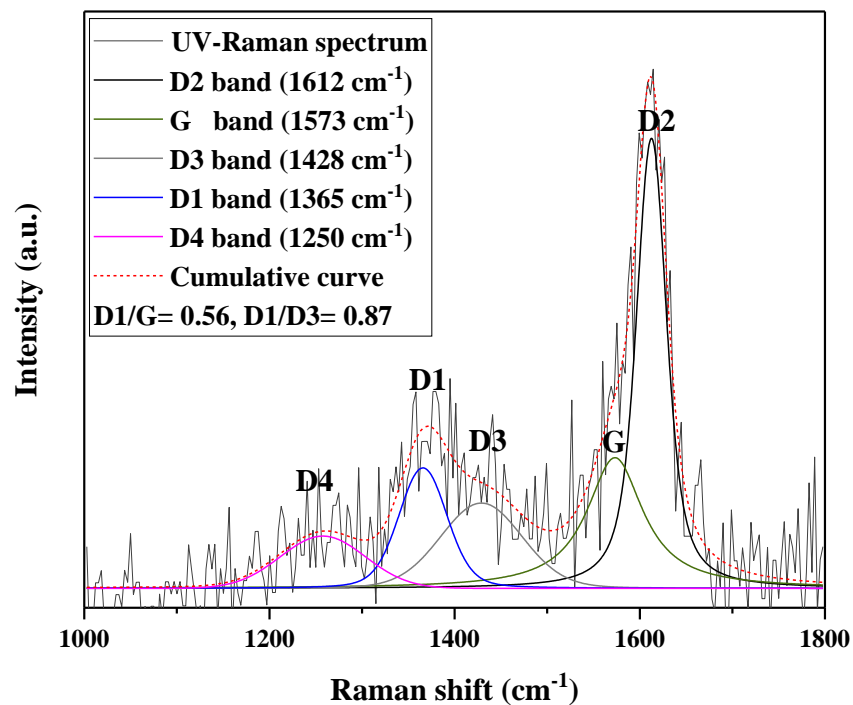


Figure 7.4 UV-Raman spectra of the pre-coked 0.45 wt.% Pt/H-Beta with (a) toluene liquid adsorption /6 h; (b) toluene vapour adsorption /12 h. Deconvolution was performed after baseline subtraction and curve fitting using Voigt function.

For all of the pre-coked catalysts, the D2 band is shifted to a value lower than the typical value at 1650 cm^{-1} which is indicative of a higher condensation degree of the carbonaceous deposits. In addition, this band is more intense for the toluene pre-coked catalysts. This feature is associated with the ring stretches of polyaromatic species (Chua and Stair, 2003). As discussed in Section 5.3.3.4, the presence of a strong band in the spectral region between 1600 to 1650 cm^{-1} is an indication of the presence of polyaromatic compounds in a sheet-like topology such as pyrene and coronene. Therefore, it is assumed that most of carbonaceous deposits presented in *n*-pentane and toluene pre coked catalysts are polyaromatic compounds and most likely in a two dimensional, sheet-like topology.

7.3.2 *n*-Hexadecane isomerisation-cracking over pre-treated catalysts

This section presents a study on the influence of catalyst surface modification by pre-coking and silylation treatments on the activity and the selectivity of the synthesised Pt/H-Beta in the isomerisation-cracking of *n*-hexadecane as a model long chain *n*-alkane. More specifically, the objective is to explore the potential role of the hydrocarbon species derived from *n*-pentane and toluene as coke precursors on the performance of the catalyst. The study can provide an understanding into the relationship between the chemistry of these hydrocarbon species and the catalytic performance in this reaction.

7.3.2.1 *Catalytic activity measurements*

n-Hexadecane isomerisation-cracking was performed over the fresh and pre-treated Pt/H-Beta catalysts. Reactions were conducted at $300\text{ }^{\circ}\text{C}$, 50 bar H_2 , and at 30 min TOS . The values of conversion and selectivity after 30 min over the fresh and pre-treated catalysts are shown in Figure 7.5. Generally, the highest value of *n*-hexadecane conversion was achieved over the fresh Pt/H-Beta (86%), whilst the lowest conversion of 48% was observed over the toluene pre-coked Pt/H-Beta (liquid adsorption / 6 h).

As discussed in Chapter 6, the reaction profile of *n*-hexadecane conversion over fresh Pt/H-Beta at the defined reaction conditions showed that cracking reaction was

favoured over the isomerisation of *n*-hexadecane. The selectivity to cracking products lighter than hexadecane was 55%, whereas, the selectivity to *iso*-hexadecane was only 18%. Coke was formed rapidly over the catalyst; the selectivity to coke after 30 min of reaction was 27%. This was ascribed to diffusional limitations, whereby reaction intermediates and/or products are blocked inside catalyst channels where they cracked to smaller molecules which then diffused out from the pores, or alternatively they remained trapped inside the pores and transformed to bulkier hydrocarbon molecules to form retained carbonaceous species.

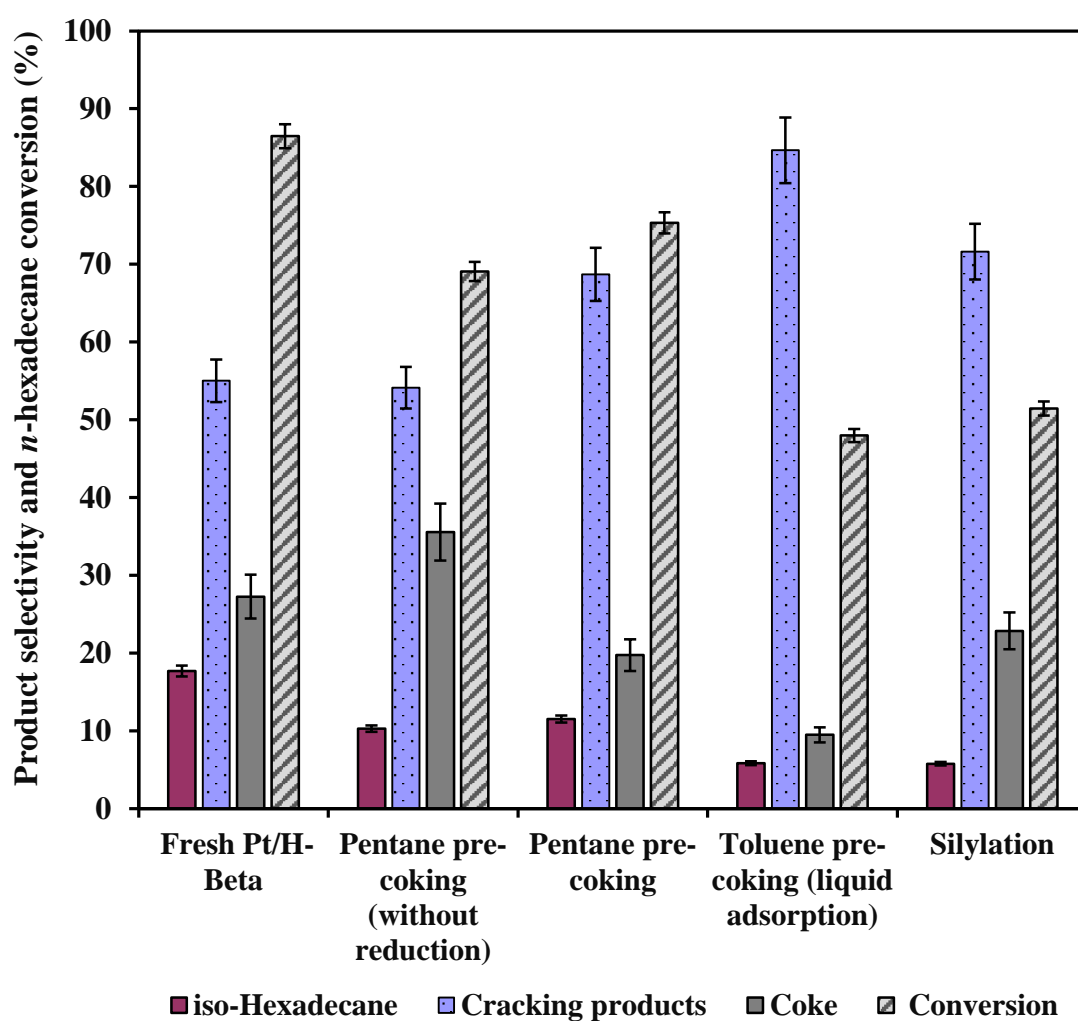


Figure 7.5 Selectivity and conversion profile of *n*-hexadecane conversion over 0.5 g of fresh and pre-treated Pt/H-Beta at 300 °C, 50 bar H₂, and 30 min TOS.

The performance of the pre-treated catalysts is explained as follows:

- i. *n*-Pentane pre-coked Pt/H-Beta without H₂ treatment: this catalyst was collected after *n*-pentane isomerisation-cracking reaction at 300 °C, WHSV of 1.5 h⁻¹, and after 360 min TOS. As discussed in Chapter 5, the carbonaceous species formed over Pt/H-Beta after *n*-pentane conversion were found to be a mixture of hydrocarbon species of different nature, structure, location, and oxidation reactivity. However, it has been concluded that the majority of these species were composed of polyaromatic compounds in graphitic-like structure and strongly bound to the acid sites. These hydrocarbon species are believed to play a significant role during *n*-pentane conversion through: (i) modification of the catalyst pore structure, thus improving catalyst shape selectivity; and (ii) the deactivation of the high-energy acid sites, hence reducing cracking of *n*-pentane and coke formation. Additionally, those coke deposits may potentially form catalytically beneficial hydrocarbon species whereby the isomerisation of *n*-pentane is catalysed at catalyst pore mouth with the contribution of these hydrocarbon species. The performance of this catalyst in *n*-hexadecane conversion was studied both with and without prior hydrogen treatment which would be required for the reduction of the Pt sites of the bifunctional catalyst. The unreduced *n*-pentane pre-coked catalyst showed a conversion level of 69%, which is lower than that obtained over the fresh catalyst (86%). Data in Table 7.2 showed that the surface area of the catalyst decreased after the *n*-pentane pre-coking treatment, however, the decrease in the catalytic activity of the pre-coked catalyst is not a simple function of surface area. Instead, it can be ascribed to the selective deactivation of a fraction of the active sites. Considering the reaction products, the selectivity to *iso*-hexadecane decreased to 10% as compared to 18% over the fresh catalyst. The selectivity to cracking products maintained at the same level of 54%. Coke selectivity increased to 36%, which is higher than that of the fresh catalyst by 10%. This suggests that the Pt sites of the pre-coked catalyst have been partially oxidised after the exposure to the atmosphere and /or covered with carbonaceous deposits, thus a reduction in the number of hydrogenation-

dehydrogenation sites took place, leading to a lower catalytic activity and the formation of larger quantity of coke deposits.

- ii. *n*-Pentane pre-coked Pt/H-Beta after reduction: the same pre-coked catalyst as in (i) was subjected to H₂ treatment prior to *n*-hexadecane conversion. The catalyst was reduced under 80 ml min⁻¹ of H₂, 350 °C, and for 2 h. The activation of Pt sites by H₂ treatment affected the conversion level of *n*-hexadecane resulting in a conversion of 75%. This is lower than that obtained over the fresh catalyst only by 11%. This suggests either, (i) that the coke has deposited non-selectively over the catalyst favouring neither active sites nor inert regions; or (ii) the potential presence of active hydrocarbon species that participate in the reaction and compensate the loss in the catalytic activity of the pre-coked catalyst as a result of pore blockage and/or acid sites deactivation by coke deposits. After pre-coking, the selectivity to *iso*-hexadecane decreased to 12% in comparison to that observed over the fresh catalyst (18%). In contrast, the cracking selectivity to produce the desired light liquid products was enhanced over the pre-coked catalyst reaching 69%. In addition, the selectivity to coke was decreased to 20%. These differences confirm that pre-coking does not deactivate all sites uniformly and instead exerts a differing influence over different reactions. By comparing the performance of the *n*-pentane pre-coked Pt/H-Beta to the fresh Pt/H-Beta, it can be concluded that the pre-coking treatment using *n*-pentane resulted in an enhancement of the selectivity to cracking and a reduction in the selectivity to coke. It is widely known that cracking requires the strongest acidity among other hydrocarbon conversion reactions (Kulprathipanja, 2010). Therefore, it is believed that the hydrocarbon species derived from *n*-pentane pre-coking are possibly participated in enhancing the cracking selectivity either by increasing the relative strength of the present acid sites (e.g. by deactivating lower energy sites) or by the contribution of these hydrocarbon species in the creation of new and strong active sites. The previous work of Guisnet (Guisnet, 2002a), hypothesised that active sites may be generated by the interaction of the carbonaceous species with the protonic sites located at the pore mouth region

and form reactive species that catalysing hydrocarbon reactions more likely at the catalyst pore mouth (described in Section 2.5.2). While not conclusively confirming this hypothesis, the present data are consistent with such mechanism.

- iii. Toluene pre-coked Pt/H-Beta (liquid adsorption / 6 h): the aim of this pre-coking treatment was to deposit carbonaceous species originating from toluene as an aromatic precursor inside the catalyst pores, whilst keeping the acid sites located at the external surface and the pore mouth region free from coke species. The success of this was evidenced by surface area measurements (see Section 7.3.1.2.2). The hydrocarbon species derived from toluene are likely homogeneous poly-condensed aromatic compounds in graphitic-like structure, as concluded in Section 7.3.1.2. The data in Figure 7.5 show that *n*-hexadecane conversion was the lowest level of any of the systems studied, at 48%. This lower activity is due to the blockage of catalyst pores by coke deposits as well as the deactivation of the acid sites located inside catalyst pores as a result of the pre-coking treatment. The selectivity to *iso*-hexadecane was reduced to 6%, which is one-third the selectivity to *iso*-hexadecane over the fresh Pt/H-Beta (18%). On the other hand, the cracking activity to produce the desired liquid hydrocarbons was remarkably enhanced over the toluene pre-coked catalyst where the selectivity to cracking products lighter than hexadecane reached 85%. Additionally, the selectivity to coke was reduced to 10%. This is significantly lower than selectivity to coke observed over the fresh catalyst (27%). This co-incidence between the increase in cracking activity and the decrease in coke selectivity was also observed over the pentane pre-coked catalyst. The obtained results therefore suggest the presence of strong acid sites on the catalyst surface that rapidly cracked the hexadecane chain to lighter liquid products; the hydrocarbon species derived from toluene may play a role in the presence of these sites. Moreover, the low selectivity to coke emphasized the occurrence of *n*-hexadecane conversion outside catalyst pores, *i.e.* on the external surface of the zeolite, where no diffusional limitations of reaction intermediates and/or products were present. In contrast,

coke preferentially forms inside pores of the fresh catalyst in the form of bulky hydrocarbon molecular species.

- iv. Toluene pre-coked Pt/H-Beta (vapour adsorption /12 h): *n*-hexadecane conversion over toluene pre-coked Pt/H-Beta / 12 h was 0%. This indicates a complete deactivation of the catalyst as a result of coke deposition. The quantity of carbon deposits over Pt/H-Beta was more than 10% (see Section 7.3.1.2.1). This suggests that catalyst pores have been completely filled with coke and carbon deposits have been overflowed into the outer surface causing both pore blockage and the deactivation of acid and metal sites.

- v. Pt/H-Beta after silylation: this treatment is considered as external modification of the catalyst crystal, whereby the hydroxyl groups present at the external surface and the pore mouth region were deactivated by the deposition of inert silica *via* degradation of TEOS. Figure 7.5 shows that *n*-hexadecane conversion was decreased to 50% as compared to the fresh catalyst (86%). The selectivity to *iso*-hexadecane was only 6%, whereas the selectivity to cracking was 72%. In contrast to (ii) and (iii) this increased selectivity was obtained without pre-coking however the measured selectivity to coke in this case was 23%, which is close to that observed over the fresh catalyst (27%). This behaviour highlights the importance of the acid sites located at the pore mouth region in hexadecane conversion and in the enhancement of isomerisation activity. It is widely known that the silylation treatment leads to narrowing the pore openings in addition to the deactivation of the external hydroxyl groups (Hibino et al., 1991, Chudasama et al., 2005, Bauer et al., 2007). Therefore, the high selectivity to coke is correlated with the retention of reaction intermediates and/or products inside catalyst pores and channels hence transformed to bulky molecules or cracked to produce light products in liquid phase.

A summary of the influence of the various catalyst pre-treatments is shown in Table 7.5.

Table 7.5 The influence of catalyst modification by pre-coking and silylation on the performance of Pt/H-Beta during *n*-hexadecane conversion at 300 °C, 50 bar H₂, and 30 min TOS. Treatment (iv) by toluene (vapour adsorption /12 h) is not shown as it resulted in total deactivation of the catalyst for the studied reaction.

Pre-treatment type	Sites coked			Conversion %		Selectivity %		Coke %
	Pore	External	Pore mouth	X	X normalised	S _{iso}	S _{cracking}	
(i) Pentane (no H ₂)	✓	✓	✓	↓	↓	↓	-	↓
(ii) Pentane (with H ₂)	✓	✓	✓	↓	-	↓	↑	↓↓
(iii) Toluene (liquid /6 h)	✓	✗	✗	↓	↓	↓	↑↑	↓↓
(v) Silylation	✗	✓	✓	↓	↓↓	↓	↑	↓

The results in Table 7.5 show that with all pre-treatments a reduction in coke formation was observed, it is likely that Pt sites play a key role in coke formation (comparing (i) and (ii)), while reactions inside catalyst pores also play a crucial role (e.g. (ii) and (v)) likely due to the reaction of bulky species within the pores.

While selectivity towards isomerisation reduced regardless of pre-treatment, selectivity towards cracking product, increasing desirable short-chained species, can be enhanced. This is most evident when the internal surface area is selectively pre-coked suggesting that cracking occurs preferentially at external active sites and/or the pore mouth.

7.3.2.2 Study on the selectivity to reaction products

The selectivity to each individual compound in the liquid phase resulting from *n*-hexadecane conversion over fresh Pt/H-Beta, *n*-pentane pre-coked Pt/H-Beta (after reduction), toluene pre-coked Pt/H-Beta (liquid adsorption / 6 h), and silylated Pt/H-Beta is shown in Figure 7.6. As discussed in Section 6.3.2.3, the cracking reaction was favoured over the isomerisation of hexadecane in the reaction over fresh Pt/H-Beta. However, the selectivity to *iso*-hexadecane was 18 %, which is the highest selectivity in comparison to other liquid products. This followed by pentane, hexane, heptane with selectivity levels of 13%, 6.5%, and 7.5%, respectively. These light hydrocarbons are considered the main components of LSR naphtha required for gasoline production (Gary and Handwerk, 2001) and the manufacture of olefins in petrochemical industries (Corma et al., 2005, Mol, 2004). Other compounds from

octane to dodecane show selectivity levels between 5% to 3%. Moreover, the selectivity to tridecane and tetradecane was less than 1%, while the selectivity pentadecane was 7%.

The general trend in the selectivity to liquid products over the pre-treated catalysts in comparison to the fresh catalyst was lower selectivity levels to long chain products such as *iso*-hexadecane and pentadecane, and higher selectivity levels to lighter products starting from pentane to tetradecane. A significant increase in the selectivity to pentane, hexane, and heptane was observed over the pre-treated catalysts, whilst products from octane to tetradecane show selectivity levels slightly higher than that observed over the fresh catalyst.

The total selectivity to cracking products over the fresh and pre-treated catalysts and the sum of the selectivity to pentane, hexane, and heptane are summarised in Table 7.6. The data in that table demonstrated that the selectivity to pentane, hexane, and heptane represent more than 50% of the selectivity to cracking products obtained over the fresh and pre-treated catalysts. The highest selectivity to these light products was observed over toluene pre-coked catalyst.

Table 7.6 Total selectivity to cracking products and the selectivity to pentane, hexane, and heptane obtained in *n*-hexadecane conversion over 0.5 g of fresh and pre-treated Pt/H-Beta, at 300 °C, 50 bar H₂, and 30 min TOS.

Catalyst	Total selectivity to cracking products (%)	Selectivity to pentane, hexane, and heptane (%)
Fresh Pt/H-Beta	55	26.8
Pentane pre-coked Pt/H Beta	69	35.5
Toluene pre-coked Pt/H-Beta (liquid adsorption / 6 h)	85	53.0
Silylated Pt/H-Beta	72	45.0

The data presented in Figure 7.6, show that pentane pre-coked catalyst has a greater fraction of heavy products such as *iso*-hexadecane and pentadecane than other pre-treated catalyst. The selectivity to *iso*-hexadecane and pentadecane over that per-coked catalyst was 11.5% and 6.5%, respectively. This trend was also observed

over the fresh catalyst in which the selectivity to these compounds was 18% and 7%, respectively. One explanation for these results could be that more uniform coking resulted from *n*-pentane pre-coking than other pre-treatments, and thus the conversion of *n*-hexadecane was performed on both the internal and the external sites of the catalyst.

Contrarily, the selectivity to the long-chain compounds was largely reduced over toluene pre-coked catalyst alongside a remarkable increase in the selectivity to light hydrocarbons such as pentane, hexane, and heptane. The selectivity to *iso*-hexadecane and pentadecane was only 5.8% and 2.7%, respectively, whereas the sum of the selectivity to pentane, hexane, and heptane was 53%. In addition, the selectivity to larger cracking products from octane to tetradecane was 23.5%. This again suggests the presence of strong acid sites on the catalyst surface. The acid sites located at the external surface and the pore mouth region of this catalyst were assumed to be free of carbonaceous species, therefore, they are considered to be responsible for the fast cracking of the long-chain hydrocarbons to smaller molecules in the liquid phase. It is well established in the literature that the cracking reaction happened on the strongest acid sites of the catalyst (Kulprathipanja, 2010). However, the hydrocarbon species derived from toluene and located inside catalyst pores may contribute in the enhancement of the strength of these sites and/or the formation of new and strong acid sites.

The inactivation of external catalytic sites *via* silylation treatment resulted in lower selectivity to long-chain compounds; the selectivity to *iso*-hexadecane and pentadecane over this catalyst was 6.2% and 3.4%, respectively. In contrast, the sum of the selectivity to pentane, hexane, and heptane was increased to 45%, comparing to 26.8% observed over the fresh catalyst. The selectivity to other cracking products was 17.4%, which is greatly higher than that over the fresh catalyst (3.2%). The reaction over this catalyst is assumed to take place inside catalyst pores, therefore, the enhancement of the cracking activity over this catalyst can be attributed to the presence of strong acid sites inside catalyst pores in addition to the decrease in the diffusivity of the produced long-chain compounds from catalyst pores as a result of narrowing pore openings by silylation treatment. Increasing the residence time of the long-chain

products inside catalyst pores may result in the cracking of these compounds to smaller molecules which are able to diffuse through the modified pores of the catalyst.

Several parameters can be considered as indicators of catalytic performance such as maximum selectivity to the desired products, maximum decrease in selectivity to coke, *etc.* Therefore, the performance of the employed catalysts cannot be discussed independently without correlation to the selectivity to coke.

The controlled pre-coking treatments using both toluene and *n*-pentane as the pre-coking agents resulted in a decrease in selectivity to coke as well as a remarkable enhancement of cracking activity. The toluene pre-coked catalyst showed the lowest selectivity to coke (10%) and the highest selectivity to products lighter than hexadecane (85%). Likewise, selectivity to coke over *n*-pentane pre-coked catalyst was reduced to 20% in comparison to that observed over the fresh catalyst (27%); this is combined with an increase in the selectivity to cracking products (69%). This behaviour demonstrated that the pre-coking treatment is an appropriate method for:

- i. Reducing the rate of coke formation that may prolong catalyst lifetime .
- ii. Redirecting the reaction pathway to produce larger fraction of the desired light hydrocarbons that are highly in demand for the production of commercial fuels and feedstocks to petrochemical industries.

Although the silylation treatment of Pt/H-Beta resulted in a high selectivity to the desired light products, in particular, pentane, hexane, and heptane as demonstrated in Table 7.6, the selectivity to coke was the highest in comparison to other pre-treated catalyst at 23%. The relative high selectivity to coke over the silylated catalyst is more likely due to diffusional limitations as a result of the narrowing of catalyst pores by the deposition of silica at the external surface and pore mouth region. This may limit the diffusion of the relatively large hydrocarbon molecules to the external catalyst surface and ultimately may allow for their transformation to coke deposits inside catalyst pores.

Based on the present selectivity study, it can be concluded that the best pre-treatment to reduce coking and enhance the production of light hydrocarbons in *n*-hexadecane

conversion is the toluene pre-coking (liquid adsorption /6 h) treatment, this is followed by *n*-pentane pre-coking treatment, whereas, silylation is considered the worst pre-treatment due to the high selectivity to coke observed over the silylated catalyst. The study also emphasised on the potential role of the hydrocarbon species originating from toluene and *n* pentane as potentially beneficial species in catalysing *n* hexadecane conversion.

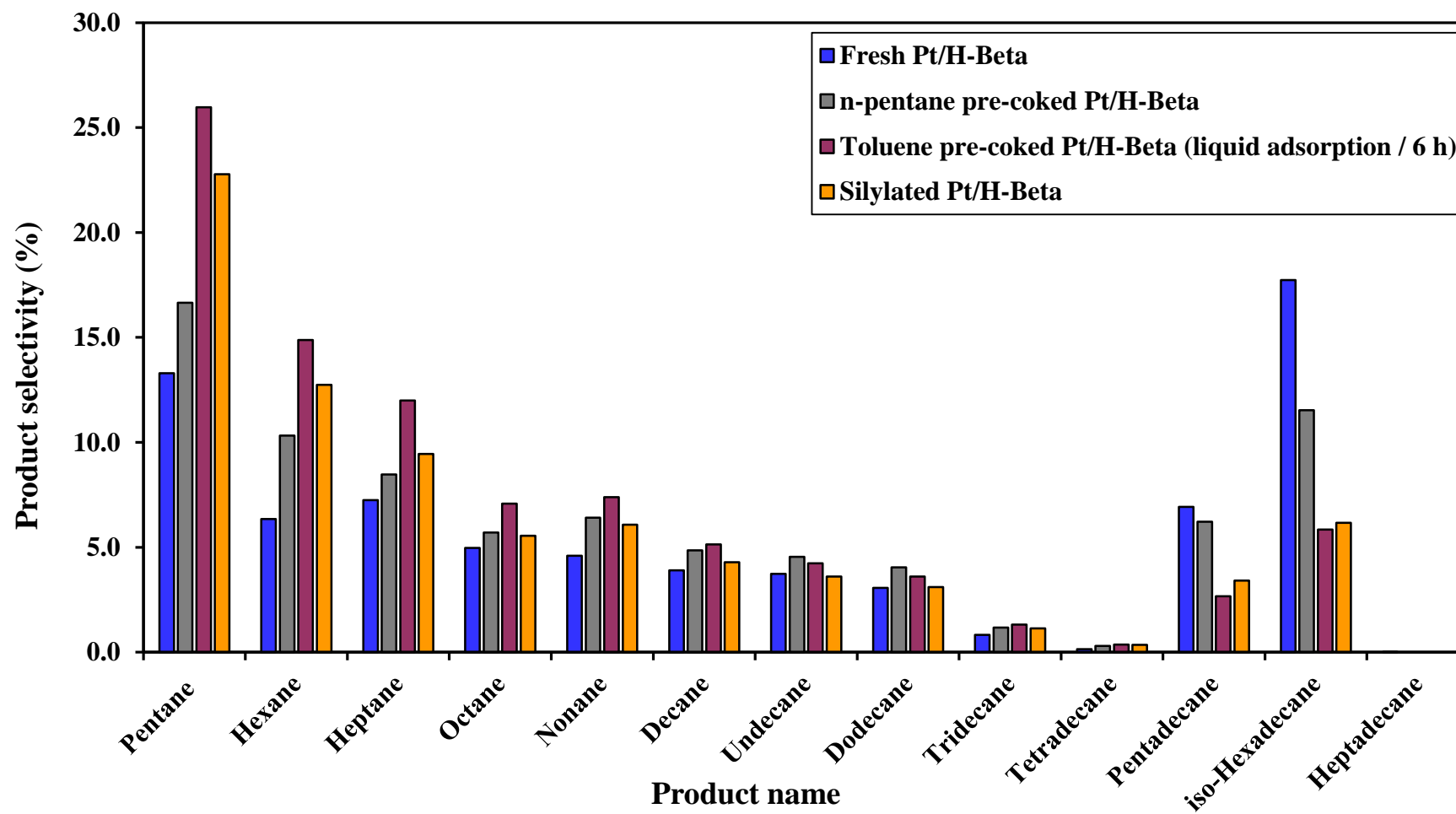


Figure 7.6 Selectivity to different liquid products of *n*-hexadecane conversion at 300 °C, 50 bar H₂, and 30 min TOS over 0.5 g of fresh and pre-treated Pt/H-Beta.

7.3.3 Characterisation of pre-coked catalysts after reaction

The quantity and the chemical composition of the carbonaceous deposits laid down over the pre-treated catalysts after *n*-hexadecane conversion were characterised using TGA and UV-Raman spectroscopy.

7.3.3.1 Thermogravimetric analysis (TGA)

The quantity of carbonaceous species accumulated over the fresh Pt/H-Beta, *n*-pentane pre-coked Pt/H-Beta (after reduction), toluene pre-coked Pt/H-Beta (liquid adsorption / 6 h), and silylated Pt/H-Beta is presented in Table 7.7. The data show the percentage of coke formed over Pt/H-Beta after the controlled pre-coking treatments, as well as the total coke formed over the fresh and pre-coked catalysts after *n*-hexadecane conversion.

Table 7.7 Coke content percent formed over the fresh and the pre-coked Pt/H-Beta before and after *n*-hexadecane conversion at 300 °C, 50 bar H₂, and 30 min TOS. The net coke was calculated as the percentage of total coke minus the percentage of the initial coke. All samples were repeated three times and the standard deviation from the mean value was calculated.

Catalyst	Initial coke (wt.%) (200-850 °C)	Total coke after reaction (wt.%) (200-850 °C)	Net coke formed (wt.%) (200-850 °C)
Fresh Pt/H-Beta	-	7.2 ± 0.12	7.2
<i>n</i> -Pentane pre-coking /6 h	4.4 ± 0.19	6.2 ± 0.20	1.8
Toluene pre-coking (liquid adsorption /6 h)	4.1 ± 0.10	5.0 ± 0.21	0.9
Silylation	-	5.3 ± 0.23	5.3

In agreement with the selectivity study discussed in Section 7.3.2.2 over the employed catalysts, the pre-coking treatments significantly reduced coking not only during the conversion of *n*-hexadecane but also in total, including the pre-coking derived deposits. The highest quantity of coke was formed over the fresh Pt/H-Beta and was more than 7%. This was followed by silylated Pt/H-Beta that showed coke deposits around 5%. A remarkable reduction in the quantity of coke was observed over *n*-pentane pre-coked Pt/H-Beta where the net coke formed after reaction was less than

2%, this represents a 75% reduction in the quantity of coke accumulated as compared to fresh Pt/H-Beta.

The largest reduction in coke quantity was observed over toluene pre-coked Pt/H-Beta (liquid adsorption /6 h). The net coke formed over the toluene pre-coked catalyst after *n*-hexadecane conversion was less than 1%, which is lower than that observed over the fresh Pt/H-Beta by 87%. This performance confirms the positive role of pre-coking treatments in reducing coke deposition.

7.3.3.2 UV-Raman spectroscopy

The chemical identity of the hydrocarbon species formed over the spent pre-treated catalysts after *n*-hexadecane conversion was investigated using UV-Raman spectroscopy. Figure 7.7 shows the spectra of the spent catalyst samples recorded at the spectral region between 1000 and 1800 cm^{-1} . This region provides the most valuable data related to the microstructure of the carbons (Jawhari et al., 1995).

The spectra shown in Figure 7.7 (a), (b), and (c) are clearly from a complex mixture of hydrocarbon species, however, the spectrum of all the spent pre-treated catalysts show a strong band at 1610 cm^{-1} (D2 band), this band is associated to the ring stretches of polyaromatic species (Chua and Stair, 2003, Spivey and Roberts, 2004).

The spectrum of the spent *n*-pentane pre-coked Pt/H-Beta presented in Figure 7.7 (a), shows another band at around 1585 cm^{-1} overlapped with the band observed at 1610 cm^{-1} . Deconvolution of this spectrum was not possible due to the low signal-to-noise resolution of the Raman signal. Nevertheless, the band at 1585 cm^{-1} (G band) is assigned to the presence of poly-condensed aromatic species in well-organised graphitic structure of carbon (Sadezky et al., 2005). Moreover, a weak band at around 1444 cm^{-1} was observed; the vibrational feature of this band is assigned to C–H deformation mode of paraffinic species (Bauer and Karge, 2006).

The spectrum of the spent toluene pre-coked Pt/H-Beta (liquid adsorption /6 h) is shown in Figure 7.7 (b). In addition to the bands observed at 1610, 1580, and 1438 cm^{-1} , bands at around 1373 and 1224 cm^{-1} were detected. These bands are

assigned to the ring stretches of polyaromatic species and the C–C stretches of aromatic species, respectively (Bauer and Karge, 2006) . The spectrum of this catalyst sample was deconvoluted into five bands: G, D1, D2, D3, and D4 using Voigt functions in all cases. The D1/G intensity ratio was 0.71, which is slightly lower than the D1/G intensity ratio measured for the Raman spectrum of the toluene pre-coked catalyst before reaction that shows a value of 0.77 (see Section 7.3.1.2.4). The decrease in the D1/G ration is an indication of an increase in the graphitisation degree of the carbonaceous species. Thus, the structural order of the carbonaceous species of that catalyst was slightly affected by the reaction.

Similar bands were observed in the Raman spectrum of the spent silylated Pt/H-Beta. These bands were positioned at around 1612, 1581, 1432, and 1370 cm^{-1} . The band at around 1220 cm^{-1} was not detected either due to the low signal-to-noise of this sample or the absence of the hydrocarbon species that fits this band.

From the spectra of the spent pre-treated catalyst samples, it can be observed that the carbonaceous species produced from *n*-hexadecane conversion over the pre-treated catalysts are similar in nature to that observed over the spent Pt/H-Beta at the same reaction conditions (see Section 6.3.4.4). In addition, the pattern of the peak intensities of the spectra of the polyaromatic compounds (shown in Figure 4.6, Section 4.9) suggest that these species are more likely in a 2-dimensional, sheet-like topology such as pyrene and coronene .

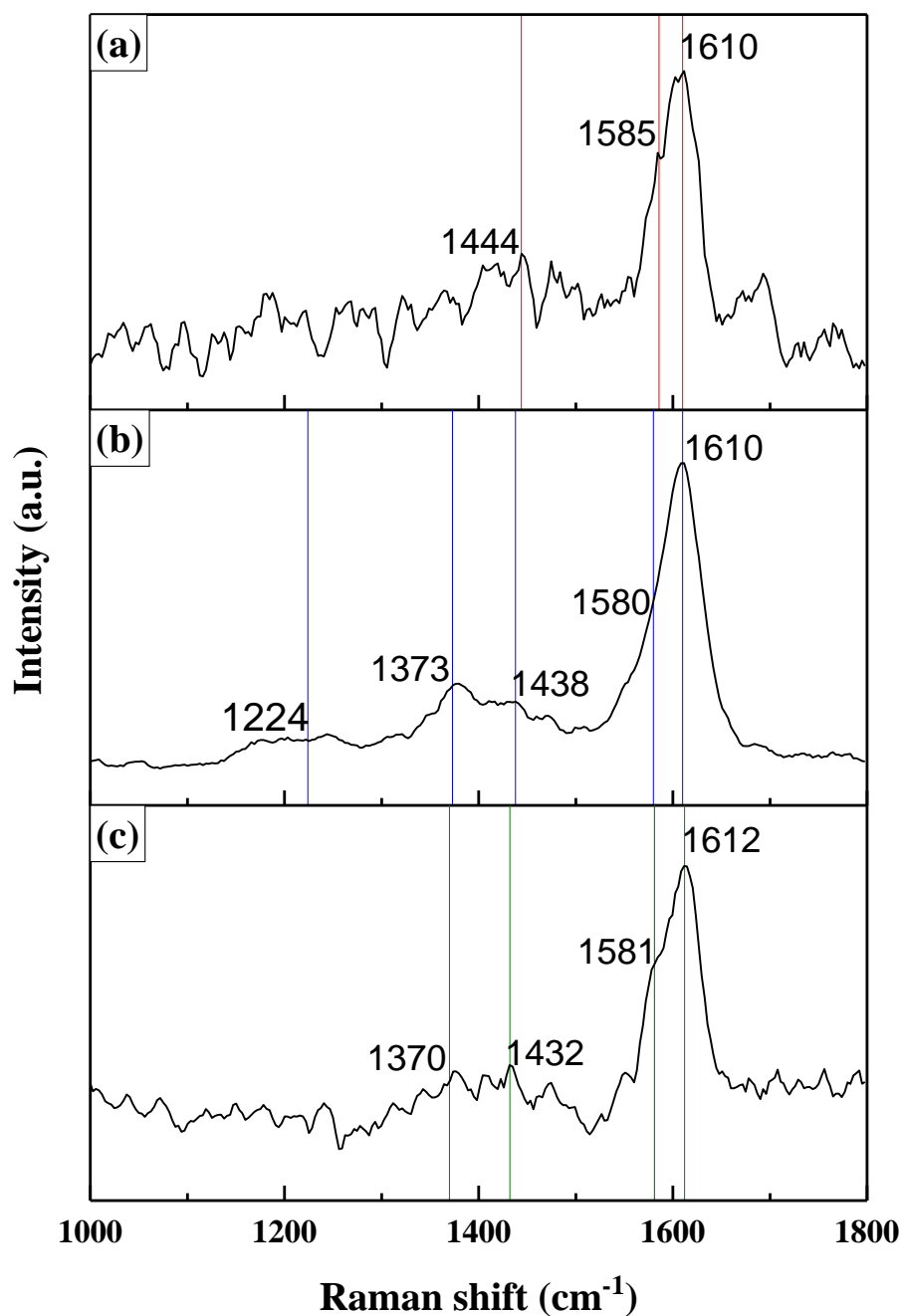


Figure 7.7 UV-Raman spectra of spent pre-treated Pt/H-Beta of *n*-hexadecane conversion at 300 °C, 50 bar H₂, and after 30 min TOS. (a) Spent *n*-pentane pre-coked Pt/H-Beta, (b) Spent toluene pre-coked Pt/H-Beta (liquid adsorption /6 h), (c) Silylated Pt/H-Beta.

7.4 Conclusions

In the present study, the effect of pre-coking and silylation treatments on the performance of Pt/H-Beta in the isomerisation-cracking of *n*-hexadecane has been investigated. *n*-Pentane and toluene have been used as pre-coking agents, while TEOS was used as a silylation agent. Carbonaceous species originated from *n*-pentane pre-coking and toluene pre-coking (liquid adsorption /6 h) were formed over the parent Pt/H-Beta in very similar quantities as measured by TGA. However, *n*-pentane pre-coking treatment resulted in a more uniform coking than toluene pre-coking. Thus, carbonaceous species originating from *n*-pentane were distributed on both the external surface and inside the pores of Pt/H-Beta, while carbonaceous species derived from toluene were directed to be formed inside catalyst pores. The TPO data showed that carbonaceous materials originating from *n*-pentane were formed from a mixture of hydrocarbon species of different nature, structure, and oxidation reactivity. Whereas, carbonaceous species derived from toluene as pre-coking agent were likely homogeneous poly-condensed aromatic compounds in a graphitic-like structure. Catalyst surface modification by silylation treatment was aimed to passivate the strong acid sites located at the external surface and the pore mouth region of the catalyst.

Both the pre-coking and silylation treatments decreased the overall conversion of *n*-hexadecane in comparison to the parent catalyst. The selectivity to cracking products in the liquid phase has been enhanced over the pre-treated catalysts; in particular, the selectivity to the desired light hydrocarbons from pentane to heptane. This was combined with a decrease in the selectivity to hexadecane isomers and other long-chain hydrocarbons. The selectivity to cracking products over the pre-treated catalysts was in the order:

Toluene pre-coking (liquid adsorption / 6 h) > Silylation > *n*-Pentane pre-coking

n-Hexadecane conversion over the toluene pre-coked catalyst (liquid adsorption / 6 h) was assumed to be performed on the acid sites located at the external surface and the pore mouth region, however, the hydrocarbon species originating from toluene were believed to have a beneficial role in enhancing the strength of these sites or contributing as active species in the formation of new and strong active sites that

rapidly cracked the long-chain hydrocarbons and maximised the fraction of the desired light liquid products. Similarly, the hydrocarbon species derived from *n*-pentane in pentane pre-coking were likely play a beneficial and/or active role in the augmentation of the selectivity to light hydrocarbons. The enhancement in the cracking activity over the silylated catalyst was ascribed to the presence of strong active sites inside catalyst pores; in addition, narrowing pore openings as a result of this modification may increase the residence time of the produced long-chained alkanes inside the pores, which consequently leads to the consecutive cracking of these long hydrocarbons to smaller molecules.

In addition to maximising the fraction of the desired light hydrocarbons over the pre-treated catalysts, the rate of coke formation was remarkably reduced in comparison to the fast coking rate observed over the fresh catalyst. The selectivity to coke over the pre-treated catalysts was in the order: toluene pre-coking (liquid adsorption / 6 h) < *n*-pentane pre-coking < silylation. The study of selectivity to coke was in agreement with the TGA measurement, in which the lowest quantity of carbonaceous species was observed over toluene pre-coked catalyst, whereas higher quantity of coke was observed over the silylated catalyst.

According to the values of conversion and selectivity for the fresh and pre-treated catalyst, the best pre-treatment is the pre-coking treatment using toluene as coke precursor. This pre-coked catalyst gives 85% selectivity to cracking products, with only 10% selectivity to coke. While the deactivation of the external sites using the silylation treatment yields a 75% selectivity to cracking products, however, the selectivity to coke was 23%, which is considered at a high level as compared to the other pre-treated catalysts.

Chapter 8

*Conclusions and future
work*

8 Chapter 8: Conclusions and future work

8.1 Conclusions

The principle aim of this thesis is to understand the role of coke deposits in the isomerisation-cracking of *n*-alkanes, and to develop a pre-coking approach to design catalysts suitable for the conversion of long-chained *n*-alkanes with enhanced selectivity to the desired products and a reduced coking rate. Based on the results obtained in the reaction studies and the characterisation of the carbonaceous species, the following conclusions were drawn:

i. The role and nature of coke in n-pentane isomerisation over Pt/H-Beta

n-Pentane isomerisation over 0.45 wt.% Pt/H-Beta was carried out in a continuous flow-fixed bed reactor. The catalyst showed a high conversion of *n*-pentane and the greatest selectivity to *iso*-pentane at a reaction temperature of 300 °C, while space velocity and H₂/*n*-pentane molar ratio in the feed were kept close to that used in the commercial process. At steady state operation, the conversion of *n*-pentane was 65% and the selectivity to *iso*-pentane was at the greatest level of 86%. Product distribution revealed that carbonaceous deposits were formed rapidly at the first 30 min TOS, with the rate of build-up sharply reduced after the induction period (1h).

Pt/H-Beta showed a high stability in *n*-pentane isomerisation after the induction period. This catalytic stability coincided with the build-up of carbonaceous species during the early stage of reaction. Thus, it is believed that these carbonaceous species have a crucial role in reducing the side reactions that lead to coke formation, and redirecting the reaction to a more selective pathway.

Characterisation of the spent catalysts at different reaction stages revealed that there is no significant change in coke quantity, nature, and structure with increasing TOS. It also showed that these coke deposits are composed of a mixture of hydrocarbon materials of different nature, structure, location, and oxidation reactivity. However, the majority of these deposits were composed of polyaromatic compounds in a graphitic-like structure and strongly bound to the acid sites. These hydrocarbon materials are believed to play a beneficial role during *n*-pentane isomerisation through

improving catalyst shape selectivity; also through the deactivation of high-energy acid sites thereby reducing coking and other side reactions. Additionally, these coke deposits may potentially contribute as a partner in the reaction itself as catalytically beneficial hydrocarbon species whereby the isomerisation of *n*-pentane is catalysed at catalyst pore mouth.

ii. The role and nature of coke in *n*-hexadecane isomerisation-cracking over Pt/H-Beta

***n*-Hexadecane isomerisation-cracking over fresh Pt/H-Beta**

The isomerisation-cracking of *n*-hexadecane was carried out in a batch reactor to study the deactivation behaviour of Pt/H-Beta during the reaction. Reaction studies at different temperatures and hydrogen pressures showed that the optimal conditions among those studied to enhance hexadecane isomerisation and reduce coking were at 300 °C and 50 bar H₂. Nevertheless, at these condition carbonaceous deposits were formed rapidly on the catalyst surface after 30 min TOS, with one third of the reacted *n*-hexadecane transformed to carbonaceous deposits. Product distribution revealed that hexadecane cracking was favoured over the isomerisation, however, the selectivity to *iso*-hexadecane was the greatest in comparison to selectivity to other products in the liquid phase.

The reasons behind the high tendency to coke formation during the reaction were investigated through the selective poisoning of external Brønsted sites and the generation of the mesoporosity in zeolite microstructure. The reaction study over the modified catalysts showed that reducing zeolite acidity by the deactivation of external Brønsted sites does not influence product distribution, whereas the presence of mesoporosity improved hexadecane isomerisation and remarkably reduces coking. Therefore, the fast rate of coke formation at the studied reaction conditions was ascribed to diffusional limitations, whereby reaction intermediates and/or products are blocked inside catalyst channels where they cracked to smaller molecules and diffused out of the pores as cracking products, or alternatively they remained trapped inside the pores and transformed to bulkier hydrocarbon molecules to form carbonaceous deposits.

Characterisation of the parent and modified catalysts after *n*-hexadecane conversion at the reference conditions showed that the majority of carbonaceous deposits formed in all cases are likely composed of poly-condensed aromatics in a graphitic-like structure as revealed by TPO and UV-Raman measurements. However, both modifications reduced the graphitisation degree of coke deposits as observed from the decrease in D1/D3 ratio of the deconvoluted Raman spectra.

***n*-Hexadecane isomerisation-cracking over pre-treated Pt/H-Beta**

n-Hexadecane conversion was conducted over pre-coked Pt/H-Beta using *n*-pentane and toluene as coke precursors. In addition, catalyst pre-treatment with TEOS (silylation treatment) was employed in order to deactivate the active sites located at the external surface and the pore mouth region. This work aimed to find an effective strategy to improve the catalytic performance and reduce the rate of coke formation in *n*-hexadecane conversion as compared to the reaction over the fresh catalyst.

Characterisation of the pre-coked catalysts showed that carbonaceous materials derived from *n*-pentane were composed of a mixture of hydrocarbon species of different nature, structure, and oxidation reactivity. Additionally, *n*-pentane pre-coking treatment resulted in a more uniform coking in which carbonaceous deposits were distributed on both the external surface and inside the pores of Pt/H-Beta. In contrast, carbonaceous species derived from toluene accumulated inside catalyst pores, and are most likely composed of homogeneous poly-condensed aromatic compounds in a graphitic-like structure as revealed by TGA, TPO, and Raman spectroscopy.

Product distribution showed that both the pre-coking and the silylation treatments resulted in an enhancement of the selectivity to cracking, however, the selectivity to the desired light hydrocarbons (pentane, hexane, and heptane) represented more than 50% of the cracking products. These hydrocarbons are highly in demand in petrochemical industries for the production of fuels and the manufacture of olefins and other chemicals.

The enhancement of the cracking activity over the pre-treated catalysts was in the order:

Toluene pre-coking (liquid adsorption / 6 h) > silylation > *n*-pentane pre-coking.

Furthermore, the pre-coking treatments effectively reduced the rate of coke formation as compared to the fast coking rate observed over the fresh catalyst, whereas, silylation pre-treatment resulted in the retention of reaction intermediates and/or products inside the pores as a result of narrowing the size of zeolite pore by the deposited silica. This consequently led to increase the residence time of these hydrocarbon species inside catalyst pores and their transformation to coke deposits. The selectivity to coke over the pre-treated catalysts was in the order:

Toluene pre-coking (liquid adsorption / 6 h) < *n*-pentane pre-coking < silylation.

The study of *n*-hexadecane conversion over the pre-coked catalyst demonstrated that the controlled pre-coking approach can be utilised to enhance the production of short-chained hydrocarbons from the heavy feedstocks. In addition, it is considered as a good strategy to reduce the rate of coke formation, and may prolong catalyst lifetime.

8.2 Future work

The following suggestions can be made to continue the work presented here in the future:

1. The study on *n*-hexadecane conversion over 0.45 wt.% Pt/H-Beta presented in Chapter 6 was conducted in a high-pressure batch reactor (see Chapter 3). The best reaction conditions were suggested to be a reaction temperature of 300 °C, 50 bar H₂, and the minimum TOS studied was 30 min. Therefore, performing the reaction in a continuous flow fixed-bed reactor in trickle-bed mode will enable studying the effect of minimising the contact time between the reactants and the catalyst bed on the catalytic performance. This will also allow for the identification of different reaction stages such as the induction period, the study-state operation, and the deactivation stage.

2. In the present work, the properties of the synthesised 0.45 wt.% Pt/H-Beta was investigated using a range of characterisation techniques including: TG/DTG; ICP; TPR; and N₂ adoption isotherms for surface area measurements as shown in Chapter 5, however, it would be useful to estimate metal surface area, dispersion and average particle diameter of Pt particles. This can be performed using the method of volumetric chemisorption of hydrogen and it will allow for probing the location of Pt particles on H-Beta.
3. A range of thermal and spectroscopic characterisation techniques has been employed in the present work to investigate the properties of the carbonaceous deposits; however, further characterisation would provide more information to elucidate the mechanism of coke formation. For instance, acidity measurement using temperature-programmed desorption of ammonia (NH₃-TPD) will provide information regarding the modification in acid sites strength as a result of coke formation. Furthermore, Nuclear Magnetic Resonance (NMR) has a particular importance in studying the mechanisms of coke formation and the identification of different functional groups presented on catalyst surface. This is because of the recent development of sophisticated solid-state experimental methods, such as cross polarization (CP) and magic-angle spinning (MAS) which greatly enhance resolution and sensitivity of the NMR signals. These developments have made ¹³C CP-MAS NMR as well as ¹²⁹Xe NMR spectroscopy particularly important in characterising the nature and the location of carbonaceous deposits formed on zeolites (Pradhan et al., 1997).
4. In this research, the properties of the coked catalysts have been investigated using *ex-situ* characterisation techniques. The current trend in catalysis is to move towards using on-line (*in-situ*) characterisation, which would allow for monitoring the development in the chemical nature, structure character, and quantity of carbonaceous deposits during the reaction. In addition, on-line catalytic activity measurements would facilitate the establishment of the relationship between reaction profiles and coke structure. For example, the Tapered Element Oscillating Microbalance (TEOM) technique coupled to a

gas chromatography would allow for real-time monitoring of the reaction at the studied conditions with TOS in addition to providing insight into the mechanism and the kinetics of coke formation and catalyst deactivation (Sánchez-Galofré et al., 2007). Moreover, studying the reaction *in-situ* in a Diffuse Reflectance Fourier Transform Infrared spectroscopy cell (DRIFTS) connected to gas chromatography would provide both the catalytic activity measurements and information on the surface chemistry with TOS (Zhu et al., 2009, Korhonen et al., 2007).

5. In Chapter 7, the reaction study of *n*-hexadecane conversion over toluene pre-coked Pt/H-Beta has demonstrated that this approach is valuable to enhance the production of light hydrocarbons and reduce coking rate. The toluene pre-coking treatment was targeted to directing the location of the formed carbonaceous species to the internal surface of the catalyst. An interesting investigation would be to explore the role of carbonaceous species derived from toluene and distributed more uniformly on the surface of Pt/H-Beta (uniform coking) in *n*-hexadecane conversion. For instance, employing Pt/H-Beta after toluene disproportionation reaction at 475 °C (Uguina et al., 1993). This will give an insight into the influence of the location of carbonaceous species derived from toluene as aromatic precursor in the isomerisation-cracking of *n*-alkanes.
6. For the clarification of the reaction mechanism, ¹³C-labelled hydrocarbons could be employed as pre-coking precursors, for example ¹³C-labeled toluene or ¹³C-labeled *n*-pentane (Filimonova et al., 2001). This may allow for investigating whether any of the coke ends up in the reaction products.
7. The pre-coking treatment could be developed as a new technique for the design of catalysts with enhanced catalytic activity. Therefore, it would be very useful to broaden the set of characterisation methods of pre-coked catalysts by including advanced microscopic techniques such as transmission electron

microscopy (TEM) which may provide further information on location and morphology of the carbonaceous residues.

References

- Abudawood, R. H. 2010. *Hydroisomerization of Alkanes Over Metal-Loaded Zeolite Catalysts*. Ph.D.Thesis, University of Manchester, UK.
- Adeeva, V., Liu, H.-Y., Xu, B.-Q. & Sachtler, W. H. 1998. Alkane isomerization over sulfated zirconia and other solid acids. *Topics in Catalysis*, 6, 61-76.
- Afandizadeh, S. & Foumeny, E. A. 2001. Design of packed bed reactors: guides to catalyst shape, size, and loading selection. *Applied Thermal Engineering*, 21, 669-682.
- Ahmed, R., Sinnathamb, C. M. & Subbarao, D. 2011. Kinetics of De-coking of spent reforming catalyst. *Journal of Applied Sciences*, 11, 1225-1230.
- Akhmedov, V. M. & Al-Khowaiter, S. H. 2007. Recent Advances and Future Aspects in the Selective Isomerization of High n-Alkanes. *Catalysis Reviews*, 49, 33-139.
- Al-Khattaf, S. 2007. Enhancing p-xylene selectivity during m-xylene transformation using mildly pre-coked ZSM-5 catalyst. *Chemical Engineering and Processing: Process Intensification*, 46, 964-974.
- Al-zaidi, B. Y. S. 2011. *The Effect Of Modification Techniques On The Performance Of Zeolite-Y Catalysts In Hydrocarbon Cracking Reactions*. Ph.D.Thesis, University of Manchester, UK.
- Alvarez, F., Ribeiro, F. R., Perot, G., Thomazeau, C. & Guisnet, M. 1996. Hydroisomerization and Hydrocracking of Alkanes. *Journal of Catalysis*, 162, 179-189.

- Andy, P., Gnep, N. S., Guisnet, M., Benazzi, E. & Travers, C. 1998. Skeletal Isomerization of n-Butenes: II. Composition, Mode of Formation, and Influence of Coke Deposits on the Reaction Mechanism. *Journal of Catalysis*, 173, 322-332.
- Annino, R. & Villalobos, R. 1992. *Process gas chromatography : fundamentals and applications : on-line analysis for process monitoring and control*, Instrument Society of America, Research Triangle Park, NC.
- Arribas, M. A., Márquez, F., Martí & Martínez, A. 2000. Activity, Selectivity, and Sulfur Resistance of Pt/WO_x-ZrO₂ and Pt/Beta Catalysts for the Simultaneous Hydroisomerization of n-Heptane and Hydrogenation of Benzene. *Journal of Catalysis*, 190, 309-319.
- Auroux, A. 2013. *Calorimetry and Thermal Methods in Catalysis*, Springer, Berlin, Heidelberg.
- Bae, Y.-S., Yazaydin, A. Ö. & Snurr, R. Q. 2010. Evaluation of the BET Method for Determining Surface Areas of MOFs and Zeolites that Contain Ultra-Micropores. *Langmuir*, 26, 5475-5483.
- Baerlocher, C., McCusker, L. B. & Olson, D. H. 2007. *Atlas Of Zeolite Framework Types*, Elsevier, Amsterdam.
- Bartholomew, C. H. 2001. Mechanisms of catalyst deactivation. *Applied Catalysis A: General*, 212, 17-60.
- Bartholomew, C. H. F. R. J. 2006. *Fundamentals of industrial catalytic processes*, Wiley, Hoboken, N.J.
- Batalha, N., Astafan, A., Dos Reis, J. C., Pouilloux, Y., Bouchy, C., Guillon, E. & Pinard, L. 2015. Hydroisomerization of n-hexadecane over bifunctional Pt-HBEA catalysts. Influence of Si/Al ratio on activity selectivity. *Reaction Kinetics, Mechanisms and Catalysis*, 114, 661-673.

- Batalha, N., Morisset, S., Pinard, L., Maupin, I., Lemberon, J. L., Lemos, F. & Pouilloux, Y. 2013a. BEA zeolite nanocrystals dispersed over alumina for n-hexadecane hydroisomerization. *Microporous and Mesoporous Materials*, 166, 161-166.
- Batalha, N., Pinard, L., Bouchy, C., Guillon, E. & Guisnet, M. 2013b. n-Hexadecane hydroisomerization over Pt-HBEA catalysts. Quantification and effect of the intimacy between metal and protonic sites. *Journal of Catalysis*, 307, 122-131.
- Batalha, N., Pinard, L., Pouilloux, Y. & Guisnet, M. 2013c. Bifunctional Hydrogenating/Acid Catalysis: Quantification of the Intimacy Criterion. *Catalysis Letters*, 143, 587-591.
- Bauer, F., Chen, W.-H., Ernst, H., Huang, S.-J., Freyer, A. & Liu, S.-B. 2004. Selectivity improvement in xylene isomerization. *Microporous and Mesoporous Materials*, 72, 81-89.
- Bauer, F., Chen, W. H., Bilz, E., Freyer, A., Sauerland, V. & Liu, S. B. 2007. Surface modification of nano-sized HZSM-5 and HFER by pre-coking and silanization. *Journal of Catalysis*, 251, 258-270.
- Bauer, F., Ficht, K., Bertmer, M., Einicke, W.-D., Kuchling, T. & Glaser, R. 2014. Hydroisomerization of long-chain paraffins over nano-sized bimetallic Pt-Pd/H-beta catalysts. *Catalysis Science & Technology*, 4, 4045-4054.
- Bauer, F. & Karge, H. G. 2006. Characterization of coke on zeolites. *Characterization II*. Springer, Berlin, Heidelberg.
- Bayraktar, O. & Kugler, E. L. 2002. Characterization of coke on equilibrium fluid catalytic cracking catalysts by temperature-programmed oxidation. *Applied Catalysis A: General*, 233, 197-213.
- Beale, A. M., Stavitski, E. & Weckhuysen, B. M. 2015. Characterization of catalysts: Surface and in-situ methods. *Encyclopedia of life support systems (EOLSS)*.

- Bekku, H. v. 2001a. Introduction to zeolite science and practice. Amsterdam; New York: Elsevier.
- Bekku, H. v. 2001b. *Introduction to zeolite science and practice*, Elsevier, Amsterdam.
- Beysac, O., Goffé, B., Petit, J.-P., Froigneux, E., Moreau, M. & Rouzaud, J.-N. 2003. On the characterization of disordered and heterogeneous carbonaceous materials by Raman spectroscopy. *Spectrochimica Acta Part A: Molecular and Biomolecular Spectroscopy*, 59, 2267-2276.
- Bleken, F. L., Barbera, K., Bonino, F., Olsbye, U., Lillerud, K. P., Bordiga, S., Beato, P., Janssens, T. V. & Svelle, S. 2013. Catalyst deactivation by coke formation in microporous and desilicated zeolite H-ZSM-5 during the conversion of methanol to hydrocarbons. *Journal of catalysis*, 307, 62-73.
- Blomsma, E., Martens, J. A. & Jacobs, P. A. 1995. Reaction Mechanisms of Isomerization and Cracking of Heptane on Pd/H-Beta Zeolite. *Journal of Catalysis*, 155, 141-147.
- Bond, G. C. 1974. *Heterogeneous catalysis : principles and applications*, Clarendon Press, Oxford.
- Brillis, A. A. & Manos, G. 2003. Coke Formation during Catalytic Cracking of C8 Aliphatic Hydrocarbons over Ultrastable Y Zeolite. *Industrial & Engineering Chemistry Research*, 42, 2292-2298.
- Busca, G. 2014. *Heterogeneous catalytic materials : solid state chemistry, surface chemistry and catalytic behaviour*, Elsevier, Amsterdam
- Busto, M., Vera, C. R. & Grau, J. M. 2011. Optimal process conditions for the isomerization–cracking of long-chain n-paraffins to high octane isomerizate gasoline over Pt/SO₄—ZrO₂ catalysts. *Fuel Processing Technology*, 92, 1675-1684.

- Butt, J. B. P. E. E. 1988. *Activation, deactivation, and poisoning of catalysts*, Academic Press, San Diego.
- Caeiro, G., Carvalho, R. H., Wang, X., Lemos, M. A. N. D. A., Lemos, F., Guisnet, M. & Ramôa Ribeiro, F. 2006. Activation of C₂–C₄ alkanes over acid and bifunctional zeolite catalysts. *Journal of Molecular Catalysis A: Chemical*, 255, 131-158.
- Calemma, V., Gambaro, C., Parker, W. O., Carbone, R., Giardino, R. & Scorletti, P. 2010. Middle distillates from hydrocracking of FT waxes: Composition, characteristics and emission properties. *Catalysis Today*, 149, 40-46.
- Calemma, V., Peratello, S. & Perego, C. 2000. Hydroisomerization and hydrocracking of long chain n-alkanes on Pt/amorphous SiO₂–Al₂O₃ catalyst. *Applied Catalysis A: General*, 190, 207-218.
- Che, M. & Védrine, J. C. 2012a. *Characterization of solid materials and heterogeneous catalysts from structure to surface reactivity (Vol 2)*, Wiley-VCH, Weinheim, Germany.
- Che, M. & Védrine, J. C. 2012b. *Characterization of solid materials and heterogeneous catalysts: From structure to surface reactivity (Vol 1)*, Wiley-VCH, Weinheim, Germany.
- Chen, C. S. H. & Bridger, R. F. 1996. Shape-Selective Oligomerization of Alkenes to Near-Linear Hydrocarbons by Zeolite Catalysis. *Journal of Catalysis*, 161, 687-693.
- Chen, D., Rebo, H. P., Moljord, K. & Holmen, A. 1997a. Influence of Coke Deposition on Selectivity in Zeolite Catalysis. *Industrial & Engineering Chemistry Research*, 36, 3473-3479.

- Chen, D., Rebo, H. P., Moljord, K. & Holmen, A. 1997b. The role of coke deposition in the conversion of methanol to olefins over SAPO-34. *In: Bartholomew, C. H. & Fuentes, G. A. (eds.) Studies in Surface Science and Catalysis*. Elsevier.
- Chen, K., Xue, Z., Liu, H., Guo, A. & Wang, Z. 2013. A temperature-programmed oxidation method for quantitative characterization of the thermal cokes morphology. *Fuel*, 113, 274-279.
- Chen, N. Y. D. T. F. S. C. M. 1994. *Molecular transport and reaction in zeolites : design and application of shape selective catalysts*, VCH, New York, N.Y.
- Chen, S. & Manos, G. 2004. Study of Coke and Coke Precursors During Catalytic Cracking of n-Hexane and 1-Hexene over Ultrastable Y Zeolite. *Catalysis Letters*, 96, 195-200.
- Chica, A. & Corma, A. 1999. Hydroisomerization of pentane, hexane, and heptane for improving the octane number of gasoline. *Journal of catalysis*, 187, 167-176.
- Christensen, C. H., Schmidt, I. & Christensen, C. H. 2004. Improved performance of mesoporous zeolite single crystals in catalytic cracking and isomerization of n-hexadecane. *Catalysis Communications*, 5, 543-546.
- Chua, Y. T. & Stair, P. C. 2003. An ultraviolet Raman spectroscopic study of coke formation in methanol to hydrocarbons conversion over zeolite H-MFI. *Journal of Catalysis*, 213, 39-46.
- Chudasama, C. D., Sebastian, J. & Jasra, R. V. 2005. Pore-Size Engineering of Zeolite A for the Size/Shape Selective Molecular Separation. *Industrial & Engineering Chemistry Research*, 44, 1780-1786.
- Clark, J. H. R. C. N. 2000. *Clean synthesis using porous inorganic solid catalysts and supported reagents*, Royal Society of Chemistry, Cambridge.

- Corma, A. 2003. State of the art and future challenges of zeolites as catalysts. *Journal of Catalysis*, 216, 298-312.
- Corma, A., Melo, F. V., Sauvanaud, L. & Ortega, F. 2005. Light cracked naphtha processing: Controlling chemistry for maximum propylene production. *Catalysis Today*, 107-108, 699-706.
- Dann, S. E. 2000. *Reactions and characterization of solids*, Royal Society of Chemistry, Cambridge.
- De Jong, K. P., Mesters, C. M. A. M., Peferoen, D. G. R., van Brugge, P. T. M. & Groot, C. 1996. Paraffin alkylation using zeolite catalysts in a slurry reactor: Chemical engineering principles to extend catalyst lifetime. *Chemical Engineering Science*, 51, 2053-2060.
- Degnan Jr, T. F. 2003. The implications of the fundamentals of shape selectivity for the development of catalysts for the petroleum and petrochemical industries. *Journal of Catalysis*, 216, 32-46.
- Deldari, H. 2005. Suitable catalysts for hydroisomerization of long-chain normal paraffins. *Applied Catalysis A: General*, 293, 1-10.
- Dewajani, H., Rochmadi, Purwono, S. & Budiman, A. 2016. Effect of modification ZSM-5 catalyst in upgrading quality of organic liquid product derived from catalytic cracking of Indonesian nyamplung oil (*Calophyllum inophyllum*). *AIP Conference Proceedings*, 1755, 050002.
- Dombrowski, K., De Wolf, I. & Dietrich, B. 1999. Stress measurements using ultraviolet micro-Raman spectroscopy. *Applied physics letters*, 75, 2450-2451.
- Downard, K. 2007. *Mass spectrometry: a foundation course*, Royal Society of Chemistry, Cambridge.

- E.M. Flanigen, J. C. J., Herman van Bekkum 1991. *Introduction to zeolite science and practice*, Elsevier, Amsterdam; New York.
- Eapen, M. J., Reddy, K. S. N. & Shiralkar, V. P. 1994. Hydrothermal crystallization of zeolite beta using tetraethylammonium bromide. *Zeolites*, 14, 295-302.
- Ertl, G., Knözinger, H., Schüth, F. & Weitkamp, J. 2008. *Handbook of heterogeneous catalysis*, Wiley-VCH, Weinheim, Germany.
- Fan, L.-S. & Zhu, C. 2005. *Principles of gas-solid flows*, Cambridge University Press.
- Ferraro, J. R., Nakamoto, K. & Brown, C. W. 2003. *Introductory Raman Spectroscopy*, Elsevier Science, Burlington.
- Figueiredo, J. L., Pereira, M. M. & Faria, J. 2008. *Catalysis from theory to application an integrated course*, Universidade de Coimbra, Coimbra.
- Filimonova, S. V., Nosov, A. V., Scheithauer, M. & Knözinger, H. 2001. n-Pentane Isomerization over Pt/WO_x/ZrO₂ Catalysts: A ¹H and ¹³C NMR Study. *Journal of Catalysis*, 198, 89-96.
- Forzatti, P. & Lietti, L. 1999. Catalyst deactivation. *Catalysis Today*, 52, 165-181.
- Föttinger, K., Kinger, G. & Vinek, H. 2003. 1-Pentene isomerization over FER and BEA. *Applied Catalysis A: General*, 249, 205-212.
- Gary, J. H. & Handwerk, G. E. 2001. *Petroleum refining : technology and economics*, Dekker, New York.
- Gil, B., Mokrzycki, Ł., Sulikowski, B., Olejniczak, Z. & Walas, S. 2010. Desilication of ZSM-5 and ZSM-12 zeolites: Impact on textural, acidic and catalytic properties. *Catalysis Today*, 152, 24-32.

- Gomez Sanz, S., McMillan, L., McGregor, J., Zeitler, J. A., Al-Yassir, N., Al-Khattaf, S. & Gladden, L. F. 2016. The enhancement of the catalytic performance of CrO_x/Al₂O₃ catalysts for ethylbenzene dehydrogenation through tailored coke deposition. *Catalysis Science & Technology*, 6, 1120-1133.
- Góra-Marek, K., Tarach, K. & Choi, M. 2014. 2,6-Di-tert-butylpyridine Sorption Approach to Quantify the External Acidity in Hierarchical Zeolites. *The Journal of Physical Chemistry C*, 118, 12266-12274.
- Gorra, F., Breckenridge, L. L., Guy, W. M. & Sailor, R. A. 1992. Selective toluene disproportionation process proven at Italian refinery. *Oil and Gas Journal; (United States)*, Medium: X; Size: Pages: 60-67.
- Gounder, R., Jones, A. J., Carr, R. T. & Iglesia, E. 2012. Solvation and acid strength effects on catalysis by faujasite zeolites. *Journal of Catalysis*, 286, 214-223.
- Grob, R. L. & Barry, E. F. 2004. *Modern practice of gas chromatography*, John Wiley & Sons, Hoboken, New Jersey.
- Groen, J. C., Abelló, S., Villaescusa, L. A. & Pérez-Ramírez, J. 2008. Mesoporous beta zeolite obtained by desilication. *Microporous and mesoporous materials*, 114, 93-102.
- Groen, J. C., Peffer, L. A. A., Moulijn, J. A. & Pérez-Ramírez, J. 2005. Mechanism of Hierarchical Porosity Development in MFI Zeolites by Desilication: The Role of Aluminium as a Pore-Directing Agent. *Chemistry – A European Journal*, 11, 4983-4994.
- Gross, J. H. 2006. *Mass spectrometry: a textbook*, Springer Science & Business Media, Berlin.
- Guisnet, M. 2002a. “Coke” molecules trapped in the micropores of zeolites as active species in hydrocarbon transformations. *Journal of Molecular Catalysis A: Chemical*, 182–183, 367-382.

- Guisnet, M., Alvarez, F., Giannetto, G. & Perot, G. 1987. Hydroisomerization and hydrocracking of n-heptane on Pth zeolites. Effect of the porosity and of the distribution of metallic and acid sites. *Catalysis Today*, 1, 415-433.
- Guisnet, M., Costa, L. & Ribeiro, F. R. 2009. Prevention of zeolite deactivation by coking. *Journal of Molecular Catalysis A: Chemical*, 305, 69-83.
- Guisnet, M. & Magnoux, P. 1989. Coking and deactivation of zeolites: Influence of the Pore Structure. *Applied Catalysis*, 54, 1-27.
- Guisnet, M. & Magnoux, P. 1992. Deactivation of Zeolites by Coking. Prevention of Deactivation and Regeneration. *In: Derouane, E. G., Lemos, F., Naccache, C. & Ribeiro, F. R. (eds.) Zeolite Microporous Solids: Synthesis, Structure, and Reactivity.* Springer Netherlands, Dordrecht.
- Guisnet, M. & Magnoux, P. 1997. Deactivation by coking of zeolite catalysts. Prevention of deactivation. Optimal conditions for regeneration. *Catalysis Today*, 36, 477-483.
- Guisnet, M. & Magnoux, P. 2001. Organic chemistry of coke formation. *Applied Catalysis A: General*, 212, 83-96.
- Guisnet, M. G. J.-P. 2002b. *Zeolites for cleaner technologies*, Imperial College Press, London.
- Guisnet, M. R. F. R. 2011. *Deactivation and regeneration of zeolite catalysts*, Imperial College Press, London.
- Hagen, J. 2006. *Industrial catalysis : a practical approach*, Wiley-VCH, Weinheim.
- Halgeri, A. B. & Das, J. 1999. Novel catalytic aspects of beta zeolite for alkyl aromatics transformation. *Applied Catalysis A: General*, 181, 347-354.

- Hattori, H. 2010. Solid Acid Catalysts: Roles in Chemical Industries and New Concepts. *Topics in Catalysis*, 53, 432-438.
- Haw, J. F. 2002. Zeolite acid strength and reaction mechanisms in catalysis. *Physical Chemistry Chemical Physics*, 4, 5431-5441.
- Hibino, T., Niwa, M. & Murakami, Y. 1991. Shape-selectivity over hzsm-5 modified by chemical vapor deposition of silicon alkoxide. *Journal of Catalysis*, 128, 551-558.
- Higgins, J. B., LaPierre, R. B., Schlenker, J. L., Rohrman, A. C., Wood, J. D., Kerr, G. T. & Rohrbaugh, W. J. 1988. The framework topology of zeolite beta. *Zeolites*, 8, 446-452.
- Iglesia, E., Soled, S. L. & Kramer, G. M. 1993. Isomerization of Alkanes on Sulfated Zirconia: Promotion by Pt and by Adamantyl Hydride Transfer Species. *Journal of Catalysis*, 144, 238-253.
- Imelik, B. & Vedrine, J. C. 1994. *Catalyst characterization : physical techniques for solid materials*, Plenum, New York.
- Jackson, S. D., Thomson, S. J. & Webb, G. 1981. Carbonaceous deposition associated with the catalytic steam-reforming of hydrocarbons over nickel alumina catalysts. *Journal of Catalysis*, 70, 249-263.
- Jawhari, T., Roid, A. & Casado, J. 1995. Raman spectroscopic characterization of some commercially available carbon black materials. *Carbon*, 33, 1561-1565.
- Jentoft, F. C. 2014. *Advances in catalysis, Volume 57*, Elsevier.
- Jiménez, C., Romero, F. J., Roldán, R., Marinas, J. M. & Gómez, J. P. 2003. Hydroisomerization of a hydrocarbon feed containing n-hexane, n-heptane and cyclohexane on zeolite-supported platinum catalysts. *Applied Catalysis A: General*, 249, 175-185.

- Jin, S. Q., Feng, Z. C., Fan, F. T. & Li, C. 2015. UV Raman Spectroscopic Characterization of Catalysts and Catalytic Active Sites. *Catalysis Letters*, 145, 468-481.
- Kamarudin, N. H. N., Jalil, A. A., Triwahyono, S., Mukti, R. R., Aziz, M. A. A., Setiabudi, H. D., Muhid, M. N. M. & Hamdan, H. 2012. Interaction of Zn²⁺ with extraframework aluminum in HBEA zeolite and its role in enhancing n-pentane isomerization. *Applied Catalysis A: General*, 431-432, 104-112.
- Karasek, F. W. & Clement, R. E. 2012. *Basic Gas Chromatography-Mass Spectrometry : Principles and Techniques*, Elsevier Science, Netherlands.
- Karge, H. G. 1991. Chapter 14 Coke Formation on Zeolites. *In: van Bekkum, H., Flanigen, E. M. & Jansen, J. C. (eds.) Studies in Surface Science and Catalysis*. Elsevier, Netherlands.
- Kim, J. H., Sugi, Y., Matsuzaki, T., Hanaoka, T., Kubota, Y., Tu, X., Matsumoto, M., Nakata, S., Kato, A., Seo, G. & Pak, C. 1995. Cerium impregnated H-mordenite as a catalyst for shape-selective isopropylation of naphthalene. Selective deactivation of acid sites on the external surface. *Applied Catalysis A: General*, 131, 15-32.
- Kimura, T. 2003. Development of Pt/SO₄²⁻/ZrO₂ catalyst for isomerization of light naphtha. *Catalysis Today*, 81, 57-63.
- Korhonen, S. T., Airaksinen, S. M. K., Bañares, M. A. & Krause, A. O. I. 2007. Isobutane dehydrogenation on zirconia-, alumina-, and zirconia/alumina-supported chromia catalysts. *Applied Catalysis A: General*, 333, 30-41.
- Kouketsu, Y., Mizukami, T., Mori, H., Endo, S., Aoya, M., Hara, H., Nakamura, D. & Wallis, S. 2014. A new approach to develop the Raman carbonaceous material geothermometer for low-grade metamorphism using peak width. *Island Arc*, 23, 33-50.

- Kozhevnikov, I. V., Holmes, S. & Siddiqui, M. R. H. 2001. Coking and regeneration of H₃PW₁₂O₄₀/SiO₂ catalysts. *Applied Catalysis A: General*, 214, 47-58.
- Kreisel, J., Weber, M. C., Dix, N., Sánchez, F., Thomas, P. & Fontcuberta, J. 2012. Probing Individual Layers in Functional Oxide Multilayers by Wavelength-Dependent Raman Scattering. *Advanced Functional Materials*, 22, 5044-5049.
- Kuba, S. & Knözinger, H. 2002. Time-resolved in situ Raman spectroscopy of working catalysts: sulfated and tungstated zirconia. *Journal of Raman Spectroscopy*, 33, 325-332.
- Kulprathipanja, S. W. I. 2010. *Zeolites in industrial separation and catalysis*, Wiley-VCH, Weinheim.
- Kustova, M. Y., Hasselriis, P. & Christensen, C. H. 2004. Mesoporous MEL – Type Zeolite Single Crystal Catalysts. *Catalysis Letters*, 96, 205-211.
- Lahfid, A., Beyssac, O., Deville, E., Negro, F., Chopin, C. & Goffé, B. 2010. Evolution of the Raman spectrum of carbonaceous material in low-grade metasediments of the Glarus Alps (Switzerland). *Terra Nova*, 22, 354-360.
- Larkin, P. 2011. *Infrared and Raman spectroscopy: principles and spectral interpretation*, Elsevier, Netherlands.
- Larsson, M., Hultén, M., Blekkan, E. A. & Andersson, B. 1996. The Effect of Reaction Conditions and Time on Stream on the Coke Formed during Propane Dehydrogenation. *Journal of Catalysis*, 164, 44-53.
- Le Page, J.-F. 1987. *Applied heterogeneous catalysis : design-manufacture use of solid catalysts*, France.
- Lee, C. K., Gladden, L. F. & Barrie, P. J. 2004. TEOM studies on the adsorption of p-xylene in coked FCC catalysts: observation of coke promoting chemical reaction. *Applied Catalysis A: General*, 274, 269-274.

- Lee, J.-K. & Rhee, H.-K. 1997. Characteristics of Pt/H-beta and Pt/H-mordenite catalysts for the isomerization of n-hexane. *Catalysis Today*, 38, 235-242.
- Lenoi, C., Rohr, F., Allahverdiev, A., Stöcker, M. & Ruiz, P. 2004. Deactivation of Pt/mordenite (MOR) during the hydroisomerisation of n-pentane. *In: van Steen, E., Claeys, M. & Callanan, L. H. (eds.) Studies in Surface Science and Catalysis*. Elsevier.
- Lenoir, C., Rohr, F., Stöcker, M. & Ruiz, P. 2005. Insight in the mechanism of deactivation of a Pt/mordenite (MOR) catalyst during the isomerization of n-pentane 11In memory of Professor Paul Grange. *Comptes Rendus Chimie*, 8, 465-474.
- Leofanti, G., Padovan, M., Tozzola, G. & Venturelli, B. 1998. Surface area and pore texture of catalysts. *Catalysis Today*, 41, 207-219.
- Li, C. e. & Brown, T. C. 1999. Temperature-Programmed Oxidation of Coke Deposited by 1-Octene on Cracking Catalysts. *Energy & Fuels*, 13, 888-894.
- Liu, P., Wang, J., Wei, R., Ren, X. & Zhang, X. 2008. A Highly Efficient H β Zeolite Supported Pt Catalyst Promoted by Chromium for the Hydroisomerization of n-Heptane. *Catalysis Letters*, 126, 346-352.
- Liu, P., Zhang, X., Yao, Y. & Wang, J. 2009. Pt catalysts supported on β zeolite ion-exchanged with Cr(III) for hydroisomerization of n-heptane. *Applied Catalysis A: General*, 371, 142-147.
- Liu, S.-b., Wu, J.-F., Ma, L.-J., Tsai, T.-C. & Wang, I. 1991. On the thermal stability of zeolite beta. *Journal of Catalysis*, 132, 432-439.
- Llewellyn, P., Rodriguez-Reinoso, F., Rouquerol, J. & Seaton, N. 2007. Is the BET equation applicable to microporous adsorbents? *Studies in surface science and catalysis*, 160, 49.

- López, C., Guillén, Y., García, L., Gómez, L. & Ramírez, Á. 2008. n-Pentane Hydroisomerization on Pt Containing HZSM-5, HBEA and SAPO-11. *Catalysis Letters*, 122, 267-273.
- López, C. M., Sazo, V., Pérez, P. & García, L. V. 2010. n-Pentane hydroisomerization on Pt-promoted acid zeolites. *Applied Catalysis A: General*, 372, 108-113.
- MacNair, H. M. & Miller, J. M. 1998. *Basic gas chromatography*, Wiley, New York.
- Magnoux, P., Guisnet, M., Mignard, S. & Cartraud, P. 1989. Coking, aging, and regeneration of zeolites: VIII. Nature of coke formed on hydrogen offretite during n-heptane cracking: Mode of formation. *Journal of Catalysis*, 117, 495-502.
- Marcilly, C. 2000. Where and how shape selectivity of molecular sieves operates in refining and petrochemistry catalytic processes. *Topics in Catalysis*, 13, 357-366.
- Marczewski, M., Migdal, A. & Marczevska, H. 2003. Acidity of the silica-alumina/BX3 superacids. *Physical Chemistry Chemical Physics*, 5, 423-429.
- Martens, J. A., Parton, R., Uytterhoeven, L., Jacobs, P. A. & Froment, G. F. 1991. Selective conversion of decane into branched isomers: A comparison of platinum/ZSM-22, platinum/ZSM-5 and platinum/USY zeolite catalysts. *Applied Catalysis*, 76, 95-116.
- Martín, N., Viniegra, M., Lima, E. & Espinosa, G. 2004. Coke Characterization on Pt/Al₂O₃- β -Zeolite Reforming Catalysts. *Industrial & Engineering Chemistry Research*, 43, 1206-1210.
- Martínez, A., Prieto, G., Arribas, M. A. & Concepción, P. 2006. Hydroconversion of n-hexadecane over Pt/WO_x-ZrO₂ catalysts prepared by a PVA-template coprecipitation route: The effect of tungsten surface coverage on activity and selectivity. *Applied Catalysis A: General*, 309, 224-236.

- Maseloane, M. A. 2011. *Dimerization of naphtha-range Fischer-Tropsch olefins into diesel-range products over zeolite H-ZSM-5 and amorphous silica-alumina*. M.Sc.Thesis, University of Cape Town, South Africa.
- Matsushashi, H., Shibata, H., Nakamura, H. & Arata, K. 1999. Skeletal isomerization mechanism of alkanes over solid superacid of sulfated zirconia. *Applied Catalysis A: General*, 187, 99-106.
- McCreery, R. L. 2005. *Raman spectroscopy for chemical analysis*, John Wiley & Sons, New York.
- McGregor, J. & Gladden, L. F. 2008. The role of carbon deposits in the hydrogenation of C5 hydrocarbons. *Applied Catalysis A: General*, 345, 51-57.
- McGregor, J., Huang, Z., Parrott, E. P. J., Zeitler, J. A., Nguyen, K. L., Rawson, J. M., Carley, A., Hansen, T. W., Tessonier, J.-P., Su, D. S., Teschner, D., Vass, E. M., Knop-Gericke, A., Schlögl, R. & Gladden, L. F. 2010. Active coke: Carbonaceous materials as catalysts for alkane dehydrogenation. *Journal of Catalysis*, 269, 329-339.
- Menon, P. G. 1990. Coke on catalysts-harmful, harmless, invisible and beneficial types. *Journal of Molecular Catalysis*, 59, 207-220.
- Miyaji, A., Echizen, T., Li, L., Suzuki, T., Yoshinaga, Y. & Okuhara, T. 2002. Selectivity and mechanism for skeletal isomerization of alkanes over typical solid acids and their Pt-promoted catalysts. *Catalysis Today*, 74, 291-297.
- Modhera, B. K., Chakraborty, M., Parikh, P. A. & Jasra, R. V. 2009. n-Hexane Hydroisomerization over Nano-Crystalline Zeolite Beta. *Petroleum Science and Technology*, 27, 1196-1208.
- Mol, J. C. 2004. Industrial applications of olefin metathesis. *Journal of Molecular Catalysis A: Chemical*, 213, 39-45.

- Muegge, B. D. & Massoth, F. E. 1991. Basic studies of deactivation of hydrotreating catalysts with anthracene. *Fuel Processing Technology*, 29, 19-30.
- Nakamura, K., Fujitsuka, M. & Kitajima, M. 1990. Disorder-induced line broadening in first-order Raman scattering from graphite. *Physical Review B*, 41, 12260-12263.
- Nam, I., Seo, J. G., Hwang, S. & Song, I. K. 2010. Deactivation behaviors of hybrid Fischer–Tropsch catalysts in the production of middle distillate from synthesis gas in a dual-bed reactor. *Research on Chemical Intermediates*, 36, 685-692.
- Nelms, S. M. 2005. *Inductively coupled plasma mass spectrometry handbook*, Blackwell ; CRC Press, Oxford (UK); Boca Raton (Florida).
- Okuhara, T. 2004. Skeletal Isomerization of n-Heptane to Clean Gasoline. *Journal of the Japan Petroleum Institute*, 47, 1-10.
- Ono, Y. 2003. A survey of the mechanism in catalytic isomerization of alkanes. *Catalysis Today*, 81, 3-16.
- Park, K.-C. & Ihm, S.-K. 2000. Comparison of Pt/zeolite catalysts for n-hexadecane hydroisomerization. *Applied Catalysis A: General*, 203, 201-209.
- Perego, C. & Ingallina, P. 2002. Recent advances in the industrial alkylation of aromatics: new catalysts and new processes. *Catalysis Today*, 73, 3-22.
- Pérez-Ramírez, J., Berger, R. J., Mul, G., Kapteijn, F. & Moulijn, J. A. 2000. The six-flow reactor technology. *Catalysis Today*, 60, 93-109.
- Pimenta, M. A., Dresselhaus, G., Dresselhaus, M. S., Cancado, L. G., Jorio, A. & Saito, R. 2007. Studying disorder in graphite-based systems by Raman spectroscopy. *Physical Chemistry Chemical Physics*, 9, 1276-1290.

- Pinard, L., Tayeb, K. B., Hamieh, S., Vezin, H., Canaff, C., Maury, S., Delpoux, O. & Pouilloux, Y. 2013. On the involvement of radical “coke” in ethanol conversion to hydrocarbons over HZSM-5 zeolite. *Catalysis Today*, 218-219, 57-64.
- Pradhan, A. R., Wu, J. F., Jong, S. J., Chen, W. H., Tsai, T. C. & Liu, S. B. 1997. Influences of zeolite structure on formation and location of coke: A129Xe and13C CP-MAS NMR study. *Applied Catalysis A: General*, 159, 187-209.
- Qi, G., Xie, Z., Yang, W., Zhong, S., Liu, H., Zhang, C. & Chen, Q. 2007. Behaviors of coke deposition on SAPO-34 catalyst during methanol conversion to light olefins. *Fuel Processing Technology*, 88, 437-441.
- Qian, L. & Yan, Z. F. 2001. Micropore modification of zeolites with transition-metal oxides. *Colloids and Surfaces A: Physicochemical and Engineering Aspects*, 180, 311-316.
- Querini, C. A. & Fung, S. C. 1997. Coke characterization by temperature programmed techniques. *Catalysis Today*, 37, 277-283.
- Rabo, J. A. & Schoonover, M. W. 2001. Early discoveries in zeolite chemistry and catalysis at Union Carbide, and follow-up in industrial catalysis. *Applied Catalysis A: General*, 222, 261-275.
- Ramos, M. J., Gómez, J. P., Dorado, F., Sánchez, P. & Valverde, J. L. 2007. Hydroisomerization of a refinery naphtha stream over platinum zeolite-based catalysts. *Chemical Engineering Journal*, 126, 13-21.
- Rase, H. F. 2000. *Handbook of commercial catalysts : heterogeneous catalysts*, CRC Press USA.
- Regali, F., París, R. S., Aho, A., Boutonnet, M. & Järås, S. 2013. Deactivation of a Pt/Silica–Alumina Catalyst and Effect on Selectivity in the Hydrocracking of n-Hexadecane. *Topics in Catalysis*, 56, 594-601.

- Richardson, S. M., Nagaishi, H. & Gray, M. R. 1996. Initial Coke Deposition on a NiMo/ γ -Al₂O₃ Bitumen Hydroprocessing Catalyst. *Industrial & Engineering Chemistry Research*, 35, 3940-3950.
- Robson, H. 2001. *Verified synthesis of zeolitic materials*, Elsevier Science, Amsterdam.
- Rollmann, L. D. 1977. Systematics of shape selectivity in common zeolites. *Journal of Catalysis*, 47, 113-121.
- Rombi, E., Monaci, R. & Solinas, V. 1999. Kinetics of catalyst deactivation. An example: methylnaphthalene transformation. *Catalysis Today*, 52, 321-330.
- Sadezky, A., Muckenhuber, H., Grothe, H., Niessner, R. & Pöschl, U. 2005. Raman microspectroscopy of soot and related carbonaceous materials: Spectral analysis and structural information. *Carbon*, 43, 1731-1742.
- Sahoo, S. K., Ray, S. S. & Singh, I. D. 2004. Structural characterization of coke on spent hydroprocessing catalysts used for processing of vacuum gas oils. *Applied Catalysis A: General*, 278, 83-91.
- Sánchez-Galofré, O., Segura, Y. & Pérez-Ramírez, J. 2007. Deactivation and regeneration of iron-containing MFI zeolites in propane oxidative dehydrogenation by N₂O. *Journal of Catalysis*, 249, 123-133.
- Satterfield, C. N. 1980. *Heterogeneous catalysis in practice*, McGraw-Hill, New York.
- Sattler, J. J. H. B., Beale, A. M. & Weckhuysen, B. M. 2013. Operando Raman spectroscopy study on the deactivation of Pt/Al₂O₃ and Pt-Sn/Al₂O₃ propane dehydrogenation catalysts. *Physical Chemistry Chemical Physics*, 15, 12095-12103.

- Seo, G., Jeong, H., Jang, D.-L., Cho, D. & Hong, S. 1996. The role of carbonaceous deposits in the skeletal isomerization of 1-butene over ferrierite zeolites. *Catalysis Letters*, 41, 189-194.
- Shamsi, A., Baltrus, J. P. & Spivey, J. J. 2005. Characterization of coke deposited on Pt/alumina catalyst during reforming of liquid hydrocarbons. *Applied Catalysis A: General*, 293, 145-152.
- Shishido, T. & Hattori, H. 1996. Spillover of hydrogen over zirconium oxide promoted by sulfate ion and platinum. *Applied Catalysis A: General*, 146, 157-164.
- Siddiqui, M. R. H., Holmes, S., He, H., Smith, W., Coker, E. N., Atkins, M. P. & Kozhevnikov, I. V. 2000. Coking and regeneration of palladium-doped H3PW12O40/SiO2 catalysts. *Catalysis Letters*, 66, 53-57.
- Sie, S. T. 1996. Miniaturization of hydroprocessing catalyst testing systems: Theory and practice. *AIChE Journal*, 42, 3498-3507.
- Simon-Masseron, A., Marques, J. P., Lopes, J. M., Ribeiro, F. R., Gener, I. & Guisnet, M. 2007. Influence of the Si/Al ratio and crystal size on the acidity and activity of HBEA zeolites. *Applied Catalysis A: General*, 316, 75-82.
- Sing, K. S. W. 1985. Reporting physisorption data for gas/solid systems with special reference to the determination of surface area and porosity (Recommendations 1984). *Pure and Applied Chemistry*.
- Smith, E. & Dent, G. 2013. *Modern Raman spectroscopy: a practical approach*, John Wiley & Sons, England.
- Smith, G. V. & Notheisz, F. 2006. *Heterogeneous catalysis in organic chemistry*, Academic Press, San Diego.
- Soualah, A., Lemberon, J.-L., Pinard, L., Chater, M., Magnoux, P. & Moljord, K. 2010. Hydroconversion of n-decane on Pt/HZSM-5 bifunctional catalysts:

effect of the Si/Al ratio of the zeolite on selectivities. *Reaction Kinetics, Mechanisms and Catalysis*, 101, 209-219.

Soualah, A., Lemberon, J. L., Pinard, L., Chater, M., Magnoux, P. & Moljord, K. 2008. Hydroisomerization of long-chain n-alkanes on bifunctional Pt/zeolite catalysts: Effect of the zeolite structure on the product selectivity and on the reaction mechanism. *Applied Catalysis A: General*, 336, 23-28.

Sparkman, O. D., Penton, Z. E. & Kitson, F. G. 2011. *Gas chromatography and mass spectrometry a practical guide*, Elsevier, Amsterdam; Boston.

Spivey, J. J. & Roberts, G. W. 2004. *Catalysis: Volume 17*, The Royal Society of Chemistry, Cambridge.

Stair, P. C. 2007. The Application of UV Raman Spectroscopy for the Characterization of Catalysts and Catalytic Reactions. *Advances in Catalysis*, 51, 75-98.

Stoltze, P. 2007. *Introduction to Heterogeneous Catalysis, Department of Chemistry and Applied Engineering Science*, Aalborg University, Denmark.

Stucky, G. D. & Dwyer, F. G. 1983. Intrazeolite Chemistry. *ACS Symposium Series*. AMERICAN CHEMICAL SOCIETY.

Subramanian, S. 1992. Temperature -Programmed Reduction of Platinum Group Metals Catalysts. *Platinum Metals Review*, 36, 98-103.

Suryanarayana, C. & Norton, M. G. 2013. *X-ray diffraction: a practical approach*, Springer Science & Business Media, New York.

Taylor, H. E. 2001. *Inductively coupled plasma-mass spectrometry : practices and techniques*, Academic Press, San Diego.

Taylor, R. J. & Petty, R. H. 1994. Selective hydroisomerization of long chain normal paraffins. *Applied Catalysis A: General*, 119, 121-138.

- Thomas, J. M. T. W. J. 1996. *Principles and practice of heterogeneous catalysis*, VCH, Weinheim; New York.
- Thomas, R. 2004. *Practical guide to ICP-MS*, Marcel Dekker Inc., New York, U.S.A.
- Tsai, K.-Y., Wang, I. & Tsai, T.-C. 2011. Zeolite supported platinum catalysts for benzene hydrogenation and naphthene isomerization. *Catalysis Today*, 166, 73-78.
- Uguina, M. A., Serrano, D. P., Van Grieken, R. & Vènes, S. 1993. Adsorption, acid and catalytic changes induced in ZSM-5 by coking with different hydrocarbons. *Applied Catalysis A: General*, 99, 97-113.
- Van de Runstraat, A., Kamp, J. A., Stobbelaar, P. J., van Grondelle, J., Krijnen, S. & van Santen, R. A. 1997. Kinetics of Hydro-isomerization of n-Hexane over Platinum Containing Zeolites. *Journal of Catalysis*, 171, 77-84.
- Van Donk, S., Bitter, J. H. & de Jong, K. P. 2001. Deactivation of solid acid catalysts for butene skeletal isomerisation: on the beneficial and harmful effects of carbonaceous deposits. *Applied Catalysis A: General*, 212, 97-116.
- Van Donk, S., Janssen, A. H., Bitter, J. H. & de Jong, K. P. 2003. Generation, characterization, and impact of mesopores in zeolite catalysts. *Catalysis Reviews*, 45, 297-319.
- Villegas, J. I., Kumar, N., Heikkilä, T., Lehto, V. P., Salmi, T. & Murzin, D. Y. 2006. Isomerization of n-butane to isobutane over Pt-modified Beta and ZSM-5 zeolite catalysts: Catalyst deactivation and regeneration. *Chemical Engineering Journal*, 120, 83-89.
- Walton, K. S. & Snurr, R. Q. 2007. Applicability of the BET Method for Determining Surface Areas of Microporous Metal–Organic Frameworks. *Journal of the American Chemical Society*, 129, 8552-8556.

- Wang, B. 2007. *Zeolite Deactivation During Hydrocarbon Reactions: Characterisation of Coke Precursors and Acidity, Product Distribution*. Ph.D.Thesis, University College London, UK.
- Wang, B. & Manos, G. 2007. A novel thermogravimetric method for coke precursor characterisation. *Journal of Catalysis*, 250, 121-127.
- Wang, J., Tu, X., Hua, W., Yue, Y. & Gao, Z. 2011. Role of the acidity and porosity of MWW-type zeolites in liquid-phase reaction. *Microporous and Mesoporous Materials*, 142, 82-90.
- Weber, R. W., Möller, K. P. & O'Connor, C. T. 2000. The chemical vapour and liquid deposition of tetraethoxysilane on ZSM-5, mordenite and beta. *Microporous and Mesoporous Materials*, 35, 533-543.
- Weitkamp, J. 2000. Zeolites and catalysis. *Solid State Ionics*, 131, 175-188.
- Weitkamp, J., Jacobs, P. A. & Martens, J. A. 1983. Isomerization and hydrocracking of C₉ through C₁₆ n-alkanes on Pt/HZSM-5 zeolite. *Applied Catalysis*, 8, 123-141.
- Weitkamp, J., Raichle, A. & Traa, Y. 2001. Novel zeolite catalysis to create value from surplus aromatics: preparation of C₂+n-alkanes, a high-quality synthetic steamcracker feedstock. *Applied Catalysis A: General*, 222, 277-297.
- Wittcoff, H. A., Reuben, B. G. & Plotkin, J. S. 2004. *Industrial Organic Chemicals*, John Wiley & Sons, Inc., Hoboken; New Jersey.
- Wu, Z. & Stair, P. C. 2006. UV Raman spectroscopic studies of V/ θ -Al₂O₃ catalysts in butane dehydrogenation. *Journal of Catalysis*, 237, 220-229.
- Wulfers, M. J. & Jentoft, F. C. 2013. Identification of carbonaceous deposits formed on H-mordenite during alkane isomerization. *Journal of Catalysis*, 307, 204-213.

- Yaluris, G., Larson, R. B., Kobe, J. M., González, M. R., Fogash, K. B. & Dumesic, J. A. 1996. Selective Poisoning and Deactivation of Acid Sites on Sulfated Zirconia Catalysts for n-Butane Isomerization. *Journal of Catalysis*, 158, 336-342.
- Yang, X., Jentoft, F. C., Jentoft, R. E., Girgsdies, F. & Ressler, T. 2002. Sulfated Zirconia with Ordered Mesopores as an Active Catalyst for n-Butane Isomerization. *Catalysis Letters*, 81, 25-31.
- Yao, J. & Yao, Y. 2016. Investigation of zeolite supported platinum electrocatalyst for electrochemical oxidation of small organic species. *International Journal of Hydrogen Energy*, 41, 14747-14757.
- Zhang, M., Chen, Y., Wang, L., Zhang, Q., Tsang, C.-W. & Liang, C. 2016. Shape Selectivity in Hydroisomerization of Hexadecane over Pt Supported on 10-Ring Zeolites: ZSM-22, ZSM-23, ZSM-35, and ZSM-48. *Industrial & Engineering Chemistry Research*, 55, 6069-6078.
- Zhang, S., Zhang, Y., Tierney, J. W. & Wender, I. 2001. Anion-modified zirconia: effect of metal promotion and hydrogen reduction on hydroisomerization of n-hexadecane and Fischer–Tropsch waxes. *Fuel Processing Technology*, 69, 59-71.
- Zhang, W. & Smirniotis, P. G. 1999. Effect of Zeolite Structure and Acidity on the Product Selectivity and Reaction Mechanism for n-Octane Hydroisomerization and Hydrocracking. *Journal of Catalysis*, 182, 400-416.
- Zhang, X., Chodakowski, M. & Shaw, J. M. 2005. Impact of Multiphase Behavior on Coke Deposition in a Commercial Hydrotreating Catalyst under Sedimentation Conditions. *Energy & Fuels*, 19, 1405-1411.
- Zhao, B. 2008. *High Temperature Behaviours of Asphaltene Aggregates in Heavy Feedstocks and in Mixtures with Diluents*. Ph.D. Thesis, University of Alberta, Canada.

Zheng, S., Heydenrych, H. R., Jentys, A. & Lercher, J. A. 2002. Influence of surface modification on the acid site distribution of HZSM-5. *The Journal of Physical Chemistry B*, 106, 9552-9558.

Zhu, N., Wang, Y., Cheng, D.-g., Chen, F.-q. & Zhan, X.-l. 2009. Experimental evidence for the enhanced cracking activity of n-heptane over steamed ZSM-5/mordenite composite zeolites. *Applied Catalysis A: General*, 362, 26-33.